TECHNISCHE UNIVERSITÄT MÜNCHEN

Lehrstuhl für Experimentelle Genetik

Neurological and molecular biological characterisation of the mutant mouse line Tom40

Ramona Maria Zeh

Vollständiger Abdruck der von der Fakultät Wissenschaftszentrum Weihenstephan für Ernährung, Landnutzung und Umwelt der Technischen Universität München zur Erlangung des akademischen Grades eines

Doktors der Naturwissenschaften

genehmigten Dissertation.

Vorsitzender: Univ.-Prof. Dr. M. Klingenspor
Prüfer der Dissertation:
1. Univ.-Prof. Dr. M. Hrabě de Angelis
2. apl. Prof. Dr. Th. Klopstock
(Ludwig-Maximilians-Universität München)

Die Dissertation wurde am 04.07.2012 bei der Technischen Universität München eingereicht und durch die Fakultät Wissenschaftszentrum Weihenstephan für Ernährung, Landnutzung und Umwelt am 29.01.2013 angenommen.

Was wir wissen, ist ein Tropfen, was wir nicht wissen, ein Ozean.
Sir Isaac Newton (1643-1727)

Table of contents:

Table of figures:

Table directory:

Table of abbreviations:

Å	ångström
actb	actin β
AD	Alzheimer's disease
ALT	alanine-amino-transferase
APOE	apolipoprotein E
AP	alkaline phosphatase
APP	amyloid precursor protein
AST	aspartate-amino-transferase
ATP	adenosine-tri-Phosphate
BNE	blue native electrophoresis
Bp	base pair
BSA	bovine serum albumin
cDNA	complementary DNA
CET	Central European Time
CNE	clear native electrophoresis
cm	centimeter
CO_2	carbon dioxide
DAB	3,3'-Diaminobenzidine
dB	decibel
DEPC	diethyldicarbonat
ddH_2O	double distilled water
DMSO	dimethyl sulfoxide
DNA	desoxyribonucleic acid
DTNB	5, 5'-dithiobis-2-nitrobenzoic acid (Ellman's reagent)
dNTP	desoxyribonucleosidtriphosphate
ECG	electrocardiogram
EDTA	ethylenediaminetetraacetic acid
EGTA	ethylene glycol tetraacetic acid
EOAD	early onset Alzheimer's disease
ES cells	embryonic stem cells
EtOH	ethanol
Δε	extinction coefficient
FAD	familial Alzheimer's disease
FCCP	carbonylcyanide p-trifluoromethoxyphenylhydrazone
G	acceleration of gravity
g	gram
GGTC	German Gene Trap Consortium
GMC	German Mouse Clinic
h	hour
HCG	human chorionic gonadotropin
het	heterozygous
H_2O	water
HPLC	high-performance liquid chromatography
HCl	hydrochloric acid
Hz	Hertz
IDH	isocitrate dehydrogenase
IVC	individually ventilated caging
kb	kilo base pairs
KCN	potassium cyanide
kDa	kilo Dalton (atomic mass unit)
LOAD	late onset Alzheimer's disease
M	molar
$MgCl_2$	magnesium chloride

min	minute
ml	milliliter
mM	milli molar
MMC	mitochondrial Hsp70-associated motor and chaperone protein
mRNA	messenger RNA
msec	millisecond
mtCYTB	mitochondrial encoded cytochrome b gene
mtCOX3	mitochondrial encoded cytochrome oxidase subunit3 gene
mtND1	mitochondrial encoded NADH dehydrogenase 1 gene
mtDNA	mitochondrial DNA
MTP	mitochondrial transition pore
nDNA	nuclear DNA
NFTs	neurofibrillary tangles
NADH	nicotinamide adenine dinucleotide
ng	nanogram
nm	nanometer
nmol	nanomol
PA	polyadenylation site
PAM	presequence activated motor protein
PBS	phosphate-buffered saline
PCR	polymerase chain reaction
PD	Parkinson's disease
PFA	paraformaldehyde
PMSF	phenylmethanesulfonylfluoride
PMSG	pregnant mare's serum gonadotropin
PPI	pre-pulse-inhibition
PQ	Paraquat
RACE	rapid amplification of cDNA ends
RCC	respiratory chain complex
RNFL	retinal nerve fiber layer
RNA	ribonucleic acid
ROS	reactive oxygen species
Rpm	rounds per minute
RT	room temperature
SA	splice acceptor
SAM	sorting and assembly machinery
SCN	suprachiasmatic nucleus
SDH	succinate dehydrogenase
SDHA (-B, -C, -D)	succinate dehydrogenase subunit A (B, C, D)
sec	second
SHIRPA	Smithkline Beecham, MRC Harwell, Imperial College, the Royal London hospital phenotype assessment
SDS	sodium dodecyl sulfate
TBS	Tris-buffered Saline
TOB	topogenesis of mitochondrial outer membrane β-barrel proteins
TCA	tricarboxylic acid cycle
TH	tyrosine hydroxylase
Tim	Translocase of the inner (mitochondrial) membrane
TMPD	N, N, N', N'-Tetramethyl-p-Phenylenediamine
Tom	Translocase of the outer (mitochondrial) membrane
U	enzyme activity (µm/min)
wt	wildtype
X-Gal	bromo-chloro-indolyl-galactopyranoside
µg	microgram
µl	microlitre
µm	micrometer

µM	micro molar
Δψ	membrane potential

Abstract:

The vast majority of mitochondrial proteins is encoded by nuclear genes and then imported into the organelle. The TOM complex mediates the import of all proteins of mitochondria into the intermembrane space and also the insertion of proteins into the outer membrane. TOM40 comprises the main component of the TOM complex as it forms the general import pore. Recent reports showed that in human Alzheimer's disease (AD) brains amyloid precursor protein (APP) accumulates in the TOM40 import channel and thereby inhibits the entry of various nuclear-encoded proteins. Moreover, a variant in the TOM40 gene has been associated with age of onset in AD. The Tom40 mutant mouse line was generated by gene trap mutagenesis using a non-retroviral pT1ßgeo vector. Homozygous *Tom40*-/- mice are not viable, embryos die before E3.5. Heterozygous *Tom40*+/- mice with a 50% reduction of expressed *Tom40* mRNA showed normal development but a reduced life span with a 30% higher mortality after two years. Systemically analysis of mice at different time points during their life time revealed a mild cardiac dysfunction already early in young age and slowly progressing neurological impairments in mutant mice. Young heterozygous *Tom40* mutants showed a subtle heart phenotype in the electrocardiogram (ECG) analysis. A decreased P-wave duration and prolonged Q-T and S-T intervals in the mutants indicate conduction impairments. Electron microscopic images of heart tissue illustrate several alterations concerning structure and arrangement of mutant mitochondria. Despite this alteration, the composition and function of the respiratory chain in the inner mitochondrial membrane was not affected at all in young mutant mice, indicating that the animals were able to compensate the defect to a great extent. With aging, this compensation seemed to fail more and more. Evaluation of basic neurological functions showed no differences in locomotor activity and muscle force but a slight sensorimotor impairment in motor coordination and balance tasks. Motoric nerve conduction velocity (NCV) in the sciatic nerve of mutants was markedly reduced compared to wildtypes, suggesting that there is a peripheral neuropathy already very early in development. There were very subtle alterations in the enzyme activity of mutant brain mitochondria, while the abundance of the respiratory chain complex (RCC) subunits still was normal. However, respirometric analyses of isolated mitochondria revealed a strong genotype-dependant worsening of mitochondrial function in mutants, both in heart and in brain. The same effect could be shown for the motor and the

electrophysiological phenotypes. Irrespective of genome-wide association studies (GWAS) which stated a possible association to AD, there was no evidence for the development of AD specific phenotypes like a memory loss. Tyrosin-hydroxylase (TH) positive neurons in the substantia nigra of aged mutants revealed a reduced number compared to age-matched wildtypes. Since alterations in the abundance of TH-positive neurons and the consequent impairment of the dopaminergic system in the brain are a common phenotype observed in patients suffering of Parkinson's disease (PD), the Tom40 mouse model may serve as model for the development of neurodegenerative diseases like Parkinsonism. Systemic reduction of the main import protein Tom 40 is sufficient to cause cardiac symptoms and progressive neurological impairment.

1 Introduction

1.1 Mitochondria

The term “mitochondria” was introduced by Benda in 1898 for cell organelles that were first described by Kölliker (Von Kölliker, 1856) and later studied by Altmann (Altmann R, 1890). Since the recognition that these small cell organelles are responsible for energy production (Hogeboom GH et al., 1946) they have been intensively studied. Using electron microscopy, it was possible to examine the double-membraned structure consisting of outer and inner membrane with its cristae, characteristically invaginations for surface area amplification, building the compartments matrix and intermembrane space (IMS). (Palade GE, 1956; Sjöstranda FS and Hanzon V, 1954). Referring to the endosymbiont theory mitochondria developed about 1.5 billion years ago from a symbiotic association between a glyolytic proto-eukaryotic cell and an oxidative bacterium (Scheffler IE, 2007). The assembly of mitochondria still reflects their endosymbiontic origin, as these cell organelles for example have a double membrane and β-barrel transmembrane proteins (Dyall SD et al., 2004; Wallace DC, 1994). Additional, they have their own small circular genome (Nass S and Nass MMK, 1963). During evolution, the mitochondrial genome size was reduced to 16569 base pairs, that code for 13 of about 1500 mitochondrial proteins: 22tRNAs, 2rRNAs and 13 polypeptides, which are all components of the respiratory chain (Anderson S et al., 1981; Wallace DC, 1999). Mitochondria comprise highly dynamic cell organelles that can regulate their morphology, distribution, and activity by fusion and fission (Bereiter-Hahn J and Vöth M, 1994; Chan DC, 2006). These processes to be balanced to maintain normal mitochondrial morphology and function; disturbed mitochondrial fusion for example can be followed by neurodegenerative diseases, such as Charcot-Marie-Tooth disease (Züchner S et al., 2004). Fusion in mammals is mainly regulated by the mitofusins Mfn1 and Mfn2 (Santel A and Fuller MT, 2001) and by OPA1 (Delettre C et al., 2000). Fission is mainly controlled by the dynamin-related protein 1 (Drp1) and Fis1 (James DI et al., 2003; Smirnova E et al., 2001b).

Mitochondria are the central part of nearly every metabolic process. Building on the work of Albert Szent-György, Krebs postulated 1937 the tricarboxylic acid (TCA)

cycle which is the key component of the metabolic pathway by which all aerobic living organisms generate energy. The TCA cycle is part of the carbohydrate catabolism. During glycolisis glucose is cleaved to pyruvate ($C_6H_{12}O_6 \rightarrow CH_3COCOO^- + H^+$), a process which happens outside of the mitochondria. After import into mitochondria, pyruvate is converted into acetyl-CoA by decarboxylation. Acetyl-CoA itself enters the Krebs cycle, were it condensates with oxalacetate to build citrate, catalyzed by citrate synthase. In the end, 3 nicotinamide adenine dinucleotide (NADH) molecules, 1 flavin adenine dinucleotide ($FADH_2$) molecule, 2 carbon dioxide (CO_2) molecules and 1 guanosine triphosphate (GTP) result from one cycle (Krebs HA and Weitzman PDJ, 1987; Lowenstein JM, 1969).

Additional, the fatty acid cycle is located within mitochondria (Kennedy EP and Lehninger AL, 1949), a metabolic pathway opening up another important source of energy. By lipolysis, fatty acids are broken down from lipids and beta oxidation splits long carbon chains into acetyl-CoA, which itself can enter the TCA cycle (Nelson DL and Cox MM, 2008; Scheffler IE, 2007). Other important reactions and pathways inside mitochondria include the urea cycle, which was discovered and described by Krebs together with Henseleit in 1932 (Graßhoff G and May M, 2003) and were ammonia is converted to urea, or for example in the heme biosynthesis, the cardiolipin and lipid metabolism, the ubiquinol biosynthesis and the iron sulfur center biosynthesis (Scheffler IE, 2007).

Mitochondria are further involved in thermoregulation: uncoupling protein 1 (UCP1), a protein located in the inner mitochondrial membrane is mainly contained in brown adipose tissue (BAT); it uncouples the oxidation of substrates from energy production and thus is responsible for non-shivering thermogenesis (Argyropoulos G and Harper ME, 2002).

Defects of energy metabolism are involved in a variety of human diseases manifesting preferentially in tissues with high aerobic demand such as brain and muscle. Mitochondrial dysfunction is discussed as a key player in neurodegeneration and aging (Leeuwenburgh C et al., 2011; Petrozzi L et al., 2007; Zeviani M and Di Donato S, 2004).There is also e.g. increasing evidence that impaired mitochondrial function is strongly implicated in the development of insulin resistance and Type-2-diabetes aetiology (Patti M-E and Corvera S, 2010).

Moreover, mitochondria are involved in programmed cell death. Two biochemical cascades lead to apoptosis, on the one hand the extrinsic or death receptor pathway

which is triggered by receptors and their corresponding ligands (for example receptors, which oligomerize in the presence of their ligand) and on the other hand the intrinsic mitochondrial pathway (Brenner C and Kroemer G, 2000; Elmore S, 2007). Mitochondrial membrane permeabilisaton cancels mitochondrial bioenergetic function; proteins from the inter membrane space (IMS) are released to the cytosol where they initiate cell death by several mechanisms (Kroemer G et al., 2007). There is increasing evidence that the extrinsic and the intrinsic pathway are linked with each other (Igney FH and Krammer PH, 2002)

1.2 The mitochondrial respiratory chain

Mitochondria provide cellular energy in form of Adenosine-tri-phosphate (ATP). As stated in Mitchells' chemiosmotic theory in 1961, an electrochemical proton gradient is established with the energy harvested from braking down high-energy molecules like glucose in order drive mitochondrial ATP-production (Mitchell P, 1961). The process of oxidative phosphorylation takes place in the inner mitochondrial membrane. Electrons from NADH are transferred to O_2 across the respiratory chain complexes I-V. The first enzyme complex, the NADH : ubiquinone oxidoreductase (EC 1.6.5.3; NADH dehydrogenase or complex I) was first isolated in 1962 (Hatefi Y et al., 1962) and represents the entry site for the electrons into the respiratory chain. The NADH dehydrogenase is the largest, most complex and best studied enzyme among the complexes of the respiratory chain, consisting in mammals of 46 subunits, of which seven are mitochondria encoded, and comprising a molecular mass of 980kDa (Carroll J et al., 2003; Carroll J et al., 2002; Hirst J et al., 2003; Walker JE et al., 1992; Walker JE et al., 1995). Electrons received by the oxidation of NADH are transferred to the primary electron acceptor flavin mononucleotide (FMN) and subsequently passing eight iron-sulfur (Fe-S) clusters to the final electron acceptor ubiquinone (UQ) (Janssen RJ et al., 2006). UQ is reduced to ubiquinol, and in parallel four protons (H^+) are translocated from the negative charged inner to the positive charged outer membrane, thus producing a proton gradient and the proton-motive force that is used to synthesize ATP (Walker JE et al., 1992; Weiss H and Friedrich T, 1991; Weiss H et al., 1991) . Complex I is discussed to be one of the major sources in the respiratory chain for superoxide formation (Turrens JF and Boveris A, 1980).

The enzyme succinate dehydrogenase (SDH; EC 1.3.5.1; succinate-coenzyme Q reductase (SQR) or Complex II) takes part in the Krebs cycle by converting succinate to fumerate (Ackrell BAC et al., 1992; Kita K et al., 1990). It consists of four nuclear encoded polypeptides. Two are peripheral membrane proteins, a flavoprotein with a covalently bound flavin (Fp, 64-79 kDa; subunit A (SDHA)) and an iron-sulfur protein containing three iron-sulfur clusters (27-31 kDa; subunit B (SDHB)), the other two are integral membrane proteins with a size of 13-18kDA (subunit C (SDHC) containing a heme group) and 11-16kDa (subunit D (SDHD) containing the ubiquinone binding site), both together functioning as anchor (Ackrell BAC, 2000; Hägerhäll C, 1997). Complex II of aerobic organisms share similar structural and catalytic properties to quinol:fumarate oxidoreductases of anaerobic organisms (Ackrell BAC, 2000). Electrons obtained by the oxidation of succinate are delivered into the quinone pool (UQ). The third component of the respiratory chain is the ubiquinol cytochrome c reductase (complex II, EC 1.10.2.2) which consists of 10 are nuclear encoded subunits (for example the cytochrome c1 (cyt c_1) with one covalently bound haem c or the Rieske iron-sulphur protein (ISP) containing a single [Fe_2S_2] cluster) and the mitochondrial encoded cytochrome b, carrying a low- (b_L) and a high-potential (b_H) haem group (Iwata S et al., 1998; Rieske JS, 1976; Schägger H et al., 1986). Peter Mitchell was the first one who described a series of reactions called ubiquinone or Q-Cycle where a lipophilic electron carrier is consecutively oxidized and reduced in order to act as proton pump across a lipid bilayer (Mitchell P, 1975). The reaction mechanism of complex III is a modified version of this principle, with coenzyme Q_{10} acting as mobile electron carrier between complex I / complex II and complex III (Crofts AR, 2004). The enzyme contains two separate ubiquinone binding sites, called Q_o (quinol-oxidising site) and Qi (quinone-reducing site): ubiquinol is oxidized at the Q_o site of the enzyme, one of the resulting electrons is transferred to the Fe-S cluster of the Rieske protein and afterwards to the c haem group of the cytochrome c_1 subunit where it is used to reduce a cytochrome c molecule, while the other reduces first the b_L haem and then the b_H heme, which in turn transfers the electron to the ubiquinone bound at the Qi site and reduces ubiquinone in two cycles to quinol (Crofts AR, 2004; Palsdottir H et al., 2003; Zhang Z et al., 1998). During this process, two protons are taken from the matrix and 4 are released into the IMS (Crofts AR et al., 1999). Complex III is another important source of reactive oxygen species (ROS) (Muller FL et al., 2004).

The large transmembrane cytochrome c oxidase (COX; EC 1.9.3.1; complex IV) is the last enzyme in the electron transport chain; it consists of 3 mtDNA and 10 nuclear DNA (nDNA) gene products (Grossman LI and Lomax MI, 1997; Kadenbach B et al., 1983). It catalyzes the final electron transfer step from cytochrome c to the final acceptor molecular oxygen and transferring 4 protons to the IMS (Branden G et al., 2006; Scheffler IE, 2007). In eukaryotic mitochondria cytochrome c oxidases contain four redox-active metal centres (heme a, heme a_3, CuA, and CuB) with heme a_3 and CuB forming the binuclear reaction centre (Babcock GT and Wikström M, 1992). Reduced cytochrome c, originating from complex III, binds near the CuA binuclear centre where it is oxidized, the reduced CuA binuclear centre transfers the electron to six-coordinate heme a in subunit I, and then to the binuclear reaction centre, where oxygen is reduced to water (Ferguson-Miller S and Babcock GT, 1996; Hosler JP et al., 2006).

The mitochondrial ATP synthase (EC 3.6.3.14; F_1F_O – ATPase) is sometimes described as Complex V of the electron transport chain as it couples the electron transport chain with oxidative phosphorylation by using the established proton gradient and membrane potential to synthesize ATP from adenosine-di-phosphate (ADP) and inorganic phosphate (Pi) (Scheffler IE, 2007). The protein was first isolated and described as “oligomycin sensitive conferral protein” by Tzagoloff and his team (MacLennan DH and Tzagoloff A, 1968; Tzagoloff A et al., 1968). It comprises a rather complex structure, with two main regions (F_1 which rises into the mitochondrial matrix and F_O which is embedded into the inner membrane) consisting of several subunits: the F_O region contains subunits c (building a c-ring in the membrane), a, b, d, F6 and OSCP and the accessory subunits e, f, g and A6L, with subunits b, d, F6 and OSCP forming the peripheral stalk, while the F_1 region is composed of three copies of subunit α, three β, one γ, one δ, and one ε, with subunits γ, δ and ε constituting the central stalk (Galante YM et al., 1979; Hatefi Y, 1985; Jonckheere AI et al., 2011). Subunit a and subunit A6L of the F_O sector are mitochondrial encoded by the *ATP6* and *ATP8* genes (Anderson S et al., 1981). Building of ATP takes place in the F_1 sector. A protonmotive force is established by the proton gradient, consisting of two components: a pH difference between the matrix and the IMS and an electrical membrane potential (Δψm) (Campanella M et al., 2009). Nowadays it is widely accepted that ATP hydrolysis drives the 360° rotation of the centrally located γ subunit relative to the $\alpha_3\beta_3$ complex (Nakamoto RK

et al., 1999). The c-ring is closely attached to the γ subunit. When protons are transferred through the c-ring, they cause a rotation of the ring and additional of the attached subunit. The active site of a β subunit undergoes three conformational changes (Gresser MJ et al., 1982). First, ADP and P_i enter the open and empty active site ("β_E") causing a change in protein conformation ("β_{DP}"). The enzyme again changes its conformation and binds these molecules tightly together ("β_{TP}"). Finally, the active site cycles back to the open state, releases the synthesized ATP (Nakamoto RK et al., 1999).

1.3 Mitochondrial dysfunction, aging and disease

Mitochondrial defects are involved in a variety of diseases and due to their function they can be considered as the main cause for inherited metabolic disorders. One of the first diseases that were understood also on the molecular level was Leber's hereditary optic neuropathy (LHON). MtDNA mutations and the resultant mitochondrial dysfunction are the cause for LHON which leads to a vision (Leber T, 1871). Wallace et al. were the first who identified an guanine (G) to adenine (A) transition at position 11778 of the mitochondrial encoded NADH dehydrogenase subunit 4 of complex I gene, resulting in a conversion of a highly conserved arginine to histidine at codon 340 and this way to a complex I deficiency (Wallace DC et al., 1988). Indeed, it is well known that a complex I deficiency can be detected in various diseases such as Parkinson's disease (PD) (Schapira AH et al., 1990). Additional, complex I as a major source for oxidative stress was discussed to have an extensive influence on cardiac failure by damaging the myocardium (Ide T et al., 1999).
Besides LHON, there are several other diseases known that are caused by mtDNA mutations, like chronic progressive external opthalmoplegia (CPEO) and the Kearns Sayre syndrome (KSS) (Holt IJ et al., 1988). In the mid 90's it was clarified, that not only the mtDNA can be responsible for mitochondrial diseases but also nuclear encoded gene defects affecting the mitochondrial proteome. Mutations in the SDHA were the first nuclear encoded gene defects to cause respiratory chain deficiencies (Bourgeron T et al., 1995). Mutations in this gene were found in a patient suffering of the encephalopathy Leigh syndrome (Parfait B et al., 2000). Nowadays it is well known that mutations in subunits B, C and D cause paraganglioma, generally benign, vascularised tumours in the head and the neck, or phaeochromocytomas (Astuti D et

al., 2001; Baysal BE et al., 2000; Niemann S and Müller U, 2000). Additional, these three genes were suggested to act as tumor suppressor genes (Baysal BE et al., 2001; Rustin P et al., 2002)

Autosomal recessive Friedreich's ataxia is characterized by cerebral ataxia, peripheral neuropathy, hypertrophic cardiomyopathy and sometime diabetes mellitus (Bauer MF et al., 1999). The responsible protein is the nuclear encoded frataxin that seems to be involved in mitochondrial iron transport. A large expansion of GAA repeats in the first intron of the *frataxin* has been identidied as underlying gene defect in most cases (Bit-Avragim N et al., 2001; Campuzano V et al., 1996; Marmolino D, 2011).

Mitochondrial diseases have complex inheritance patterns as they are on the one hand maternally inherited, on the other hand due to the mendelian schema or even in a combination of both (Wallace DC, 1999). Each mitochondrion contains 2-10 copies of mtDNA (Wiesner RJ et al., 1992). The mutation rate of mtDNA is much higher than in nuclear DNA, because of the lack of efficient repair mechanisms, the absence of histone protection and the persistent exposure to oxygen radicals arising from the respiratory chain (Ames BN et al., 1993; Brown MD et al., 1992; Wallace DC et al., 1992). After a mutation, a cell usually contains mutated and non-mutated mtDNA, a state that is also known as heteroplasmy (Wallace DC, 1994). During cell division, the ratio between wildtype and mutant mtDNA can drift towards the one or the other genotype (homoplasmy) by replicative segregation. For heteroplasmic mutations there are distinct thresholds, and clinical manifestation only occurs after exceeding a critical level whereupon this threshold could vary between different organs and tissues (Ames BN et al., 1993; Wallace DC, 1994). To make the whole story even more complex, one mutation can cause different phenotypes and a distinct phenotype can be caused by different mutations.

Somatic mtDNA mutations are not transmitted to the next generation, but they play an important role in aging and cancer development (Wallace DC, 1999). The widely accepted mitochondrial free radical theory of aging (MFRTA) was seriously challenged by various studies with long-living vertebrates and although it is clear that the number of mtDNA damage increases with age and therefore has an influence on mitochondrial dysfunction, it seems that this theory is widely refuted (Lapointe J and Hekimi S, 2010). There were attempts to increase the maximum life-span of mice by feeding them with antioxidants, as for example with coenzyme (Co) Q_{10} (Sohal RS et

al., 2006). However, there were no detectable effects of this treatment on life-span, although the endogenous content of both CoQ_9 and CoQ_{10} were significantly increased. Recent reports suggest a role of mitochondria in aging independently of reactive oxygen species (ROS) formation (Leeuwenburgh C et al., 2011). One example for a current hot topic in aging research is the role of mitochondrial biogenesis. One of the major regulators of this process is the peroxisome-proliferator-activated receptor gamma co activator 1-alpha (PGC-1*α*) and its role in aging and therapy is studied intensely (Wenz T, 2011). Altered mitochondrial biogenesis and function caused by altered PGC-1*α* expression is also involved in the development of metabolic diseases (Lowell BB and Shulman GI, 2005). For example, it has been shown in microarray studies that PGC-1α–responsive genes are down-regulated in obese Caucasians with impaired glucose tolerance and type 2 diabetes (Mootha VK et al., 2003).

1.4 Mouse models for mitochondrial diseases

The mouse is the most popular model organism to study human diseases. In the past years several mitochondrial mouse models were generated in order to identify the underlying pathomechanisms. Most of these models were generated via mutation of nuclear encoded mitochondrial proteins. For example *Ant -/-* mice are used as mouse model for chronic ATP-deficiency (Graham BH et al., 1997). The nuclear encoded adenine nucleotide translocator (ANT) is knocked-out selectively in heart and muscle of these mice, leading to a mitochondrial myopathy and hypertrophic cardiomyopathy. The animals show elevated serum lactate, alanine and succinate levels which go along with an inhibited Krebs cycle and respiratory chain. A result from the impaired ETC is a massive increased ROS production that accounts for massive heart mtDNA damage (Esposito LA et al., 1999).

Tfam-deficient mice serve as a model for the mtDNA depletion syndrome (Larsson NG et al., 1998). Tfam is a nuclear encoded mitochondrial transcription factor and its inactivation in all tissues is embryonic lethal. Heterozygous (het) mice however were viable but with reduced mtDNA copy number and transcription. Homozygous embryos showed massively enlarged, COX negative mitochondria with abnormal cristae. By selectively knocking out Tfam only in heart and muscle tissue, homozygous embryos with morphological and biochemical normal hearts were born

but died three weeks after birth of dilated cardiomyopathy (Wang J et al., 1999). They showed reduced complex I and IV activities and COX deficiency resembling the human phenotype.

Mitochondrial dysfunction is discussed to be causative or at least to have an important impact in neurodegenerative diseases like Parkinson's disease (PD) or Alzheimer's disease (AD). PD has been modeled in animals using the chemical MPTP (1-methyl 4-phenyl-1,2,3,6-tetrahydropyridine), whose metabolite MPP+ inhibits complex I of the respiratory chain (Fornai F et al., 2005). Mice that were exposed to the drug developed PD phenotypes and nigral degeneration with cytoplasmic inclusions of alpha-synuclein and ubiquitin. Complex I inhibition with rotenone had the same effect (Betarbet R et al., 2000), probably caused by oxidative stress (Sherer TB et al., 2003), both of which already has been found in the substantia nigra of PD patients (Schapira AH et al., 1989). Oxidative stress seems to be involved in AD, too. It has been shown for manganese superoxide dismutase (MnSOD) heterozygous mice, a critical antioxidant enzyme, that brain Aβ-amyloid levels and plaque depositions were significantly increased (Li F et al., 2004). Moreover mice with an impaired energy metabolism show elevated β-secretase levels and activity and Aβ levels (Velliquette RA et al., 2005). It has been proven to be challenging to generate mouse models for mutations in the mtDNA, because of the fact that a cell contains hundreds of these organelles (Tyynismaa H and Suomalainen A, 2009). As direct manipulation failed (McGregor A et al., 2001), indirect approaches to damage mtDNA were tested. Transmitochondrial models and mice with increased mtDNA copy number were generated as well as mice with modified nuclear genes to target the mtDNA (Tyynismaa H and Suomalainen A, 2009). Transmitochondrial mito-mice are heteroplasmic, they were generated by isolating mouse cells without mtDNA, fusing them with rmtDNA from somatic tissues, searching for respiration-deficient cybrids and introduced this mtDNA into fertilized eggs (Inoue K et al., 2000). The accumulation of the mutated mtDNA induced mitochondrial dysfunction in various tissues like the heart, muscle or kidney and mice developed severe renal failure and additional anaemia, myopathy, cardiomyopathy, deafness and early death (Nakada K et al., 2001; Nakada K et al., 2004).

1.5 Generation of mutant mice

With the availability of complete DNA sequences for the mouse (Church DM et al., 2009) and human genome as reviewed by Little (Little PFR, 2005), the focus of the studies changed to the annotation of each given gene to its physiological function. Unfortunately, natural mouse mutants are relatively rare (Green MC, 1989). There are various different approaches to introduce mutations into the mammalian genome. One of the most popular phenotype-driven approaches is the ENU mutagenesis where the chemical ethylnitrosourea is used to generate point mutations in spermatogonial stem cells (Russell WL et al., 1979). Some years ago, a large scale approach was started at the Helmholtz Zentrum in Munich to produce and screen ENU derived mouse models in a systemic manner (Hrabé de Angelis MH et al., 2000). Even though there are many advantages, the method faces some limitations, as for example it could be rather tedious to identify the causative gene (Antoch MP et al., 1997; Balling R, 2001; O'Brien TP and Frankel WN, 2004).

Targeted mutagenesis strategies have opened up the possibility to set definied mutations to the genome, to investigate recessive mutations and to create mouse models of human diseases (Capecchi MR, 1989; Smithies O, 1993; Williams RW, 1999). Early attemps were performed by the laboratory of Charles Weissmann who used the chemical N4-hydroxycytidine which induces transition of GC to AT (Flavell RA et al., 1975; Müller W et al., 1978). Nowadays, there is the possibility to create knock-out, knock-in and knock-down mice by targeted mutagenesis (Manis JP, 2007). In knock-out mice coding exons of a gene are replaced or disrupted and therefore the loss of function of a gene can be studied, in knock-in mice a specific mutation can be determined exchanging endogenous with mutated DNA sequences and finally in knock-down mice RNA interference is used to silence genes (Manis JP, 2007).

A widely used genotype-driven approach is the insertional mutagenesis via gene trap. The gene reporter constructs, also called entrapment vectors were originally developed in bacteria (Bedell MA et al., 1996). Gossler et al. pioneered in combining ES cells and insertional mutagenesis in mammalian cells (Gossler A et al., 1989). Friedrich and Soriano were the first ones who mutagenated embryonic stem cells with vectors based on the Moloney leukemia virus (Friedrich G and Soriano P, 1991). Three different classes of trap vectors that can be introduced into the genome either by electroporation or retroviral infection were developed simultaneously: enhancer,

promoter and gene trap vectors. For details see review of Stanford (Stanford WL et al., 2001). Promoterless enhancer traps have to integrate near a cis-acting enhancer element to drive the expression of their reporter gene. They are not suitable for eukaryotes because enhancer sequences are often far away from the regulated gene and enhancers are in general not mutagenic (Gossler A et al., 1989). Promoter traps also consist of a promoterless reporter gene linked to a selectable marker (Friedrich G and Soriano P, 1991; Reddy S et al., 1991; von Melchner H and Ruley HE, 1989). Promoter traps insert into the coding sequence of a gene and thereby generate a fusion transcript. However, the trapping frequency is very low (von Melchner H et al., 1992; von Melchner H and Ruley HE, 1989). Due to the constrictions of the other vector classes, gene trap vectors are the mostly common used tools in eukaryotic genomes. The gene trapping cassette that consists of a promoterless reporter gene and often a selectable genetic marker is flanked by an upstream 3' splice acceptor site (SA) and a downstream polyadenylation (pA) sequence (Gossler A et al., 1989; Skarnes WC et al., 1992). When inserted into an intron of an expressed gene, the gene trap cassette is transcribed from the endogenous promoter and forms a fusion transcript. Friedrich and Soriano generated various mouse lines to proof the mutagenicity of the integrated vector (Friedrich G and Soriano P, 1991). Meanwhile, there exist several laboratories worldwide which perform a large-scale gene trap mutagenesis e.g. the German Gene Trap Consortium (http://tikus.gsf.de/ggtc/aboutus/consortium.php; GGTC) or the European Conditional Mouse Mutagenesis Program (http://www.knockoutmouse.org/about/eucomm; EUCOMM) which is founder member and European cornerstone of the International Knockout Mouse Consortium (IKMC).

1.6 German Mouse Clinic

Given the increasing number of mutant mice the comprehensive phenotyping of those mice is still a crucial step in the evaluation of disease models. The German Mouse Clinic (GMC) offers systemic examination of mouse mutants using a broad standardized phenotypic check-up with more than 550 parameters. The screens in the German Mouse Clinic are designated according to medical disciplines to the areas of behaviour, bone and cartilage development, neurology, clinical chemistry, eye development, immunology, allergy, steroid metabolism, energy metabolism, lung

function, vision and pain perception, molecular phenotyping, cardiovascular analyses and pathology (Fuchs H et al., 2011).
For the next level of mouse phenotyping a Challenge platform is currently established in the GMC. In order to mimic, analyze and understand complex human diseases it is necessary to decipher interactions between genome and environmental factors like nutrition, exercise, air, stress and infection with different standardized experiments (Beckers J et al., 2009). The neurological screen of the GMC established an oxidative stress platform. Oxidative stress is caused by an imbalance between the generation and the scavenging of ROS which are produced as a side product by the mitochondrial respiratory chain during energy metabolism (Keaney JF Jr, 1999).
With the induction of oxidative stress it is possible to mimic acquired mitochondrial dysfunctions by environmental influences. Oxidative stress has an important impact on the development of several human diseases. The herbicide Paraquat (PQ) is known to cause increased ROS formation and hence cause mitochondrial damage due to oxidative stress (Castello PR et al., 2007).

1.7 The mitochondrial import system

The vast majority of mitochondrial proteins is encoded by nuclear genes, synthesized in the cytosol and then imported into the organelle by a complex import machinery as pictured in figure 1 (Hermann JM and Neupert W, 2000; Neupert W, 1997; Schatz G, 1996). The high-molecular weight TOM (translocase of the outer mitochondrial membrane) complex is responsible for the import of almost all mitochondrial precursor proteins to the IMS and also for transport and insertion of outer-membrane proteins (Pfanner N et al., 1997; Rapaport D, 2002). Import into or across the inner membrane is achieved in cooperation with the two TIM (translocase of the inner mitochondrial membrane) complexes TIM22 and TIM23 (Jensen RE and Dunn CD, 2002; Neupert W and Herrmann JM, 2007).

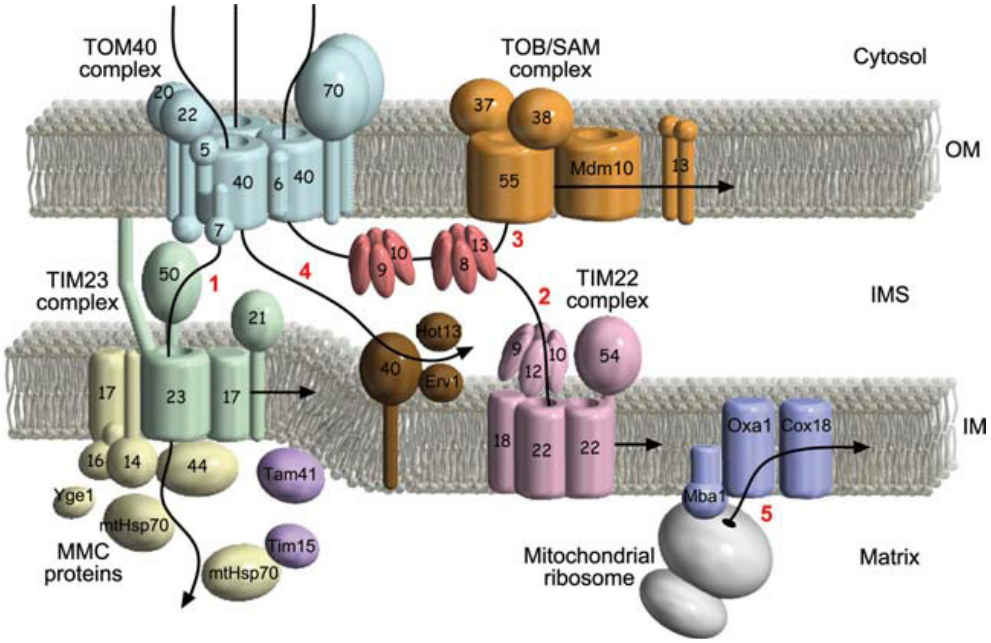

Figure 1: The mitochondrial import system

The components of the outer membrane (OM) are the TOM complex and the TOB/SAM complex, Tim9-Tim10 and Tim8-Tim13 hexamer rings are located in the inter membrane space (IMS) and in the inner membrane (IM) there is TIM23, TIM22, TIM40/MIA40 and OXA (picture is taken from the review by Endo and Yamano, 2009)

The TOM complex consists of seven components, combining the surface receptors Tom70, Tom22 und Tom20 with a translocation pore that is composed of Tom40, Tom5, Tom6 and Tom7 (Hines V et al., 1990; Künkele K et al., 1998; Mayer A et al., 1995a; Moczko M et al., 1993 ; Schneider H et al., 1991 ; Söllner T et al., 1989). Tom40 represents the channel-forming subunit and therefore the main component of the TOM complex that constitutes a 22Å wide, hydrophilic pore (Baker KP et al., 1990; Hill K et al., 1998; Kassenbrock CK et al., 1993; Vestweber D et al., 1989). It has been demonstrated that it plays an active role in sorting the imported proteins (Gabriel K et al., 2003). The small TOM proteins 5,6 and 7 interacts with TOM40, the surface receptors and the precursor proteins (Alconada A et al., 1995; Dembowski M et al., 2001; Hönlinger A et al., 1996; Moczko M et al., 1992; Söllner T et al., 1992). TOM22 seems to be the central part of the receptor complex as it is responsible for the transfer of the precursors from the receptors to the import pore itself (Kiebler M et al., 1993). Precursor proteins with N-terminally targeted presequences and β-barrel outer-membrane proteins are preferentially recognized by Tom20 and Tom22 whereas inner-membrane proteins containing internal targeting signals more likely interact with Tom70 (Ramage L et al., 1993 ; Rehling P et al., 2004; Ryan MT et al., 2000; Söllner T et al., 1989, 1990; Steger HF et al., 1990). After passing the TOM complex, proteins carrying a presequence are bound to the trans receptor site of the

TOM40 pore (Mayer A et al., 1995b). The presequence of the bound precursor protein is recognized by the Tim50 subunit of the presequence translocator TIM23 (Geissler A et al., 2002; Mokranjac D et al., 2003; Yamamoto H et al., 2002). Tim50 interacts with Tim23, whose inner membrane part forms the import channel of the TIM23 complex (Mokranjac D et al., 2009; Tamura Y et al., 2009; Truscott KN et al., 2001). Translocation across the TIM23 complex is an energy-driven process, energy sources are the membrane potential across the inner mitochondrial membrane (Δψ) and ATP in the mitochondrial matrix (Mokranjac D and Neupert W, 2005). The preproteins are afterwards bound to mitochondrial Heat Shock protein 70 (mtHsp70) that is bound to the TIM complex via Tim44 and belongs together with the mitochondrial Hsp70-associated motor and chaperone (MMC) / presequence activated motor (PAM) proteins Tim14 (Pam18), Tim16 (Pam16), Pam17 and Mge1 to the import motor part of the translocase and is responsible for protein unfolding (Endo T and Yamano K, 2009). It has been proven that TIM23 is not a static complex but switches between TOM tethering and PAM binding in a reaction cycle which involves the peripheral subunits Tim21 and Tim17: Tim21 interacts with the TOM complex and promotes inner membrane insertion, while Tim17 is involved in inner membrane sorting and is bound to Pam18 to form the functional TIM-PAM complex (Chacinska A et al., 2005). Inner-membrane proteins containing internal targeting signals, for instance proteins belonging to the solute carrier family and components of the TIM translocases with multiple transmembrane segments are imported via TIM22 (Bauer MF et al., 2000). The 300kDa complex is constituted by three membrane proteins (Tim22, Tim54 and Tim18) and three small Tim proteins (Tim9, Tim10 and Tim12) (Mokranjac D and Neupert W, 2005; Neupert W and Herrmann JM, 2007). After translocation across the outer membrane, the highly hydrophobic proteins are bound by Tim9-Tim10 or Tim8-Tim13 hexamer rings which probably function as chaperones and prevent the precursors from aggregating (Webb C et al., 2006). Tim22, which is homologue to Tim23, mediates the import of carrier proteins into the inner membrane in an Δψ dependant manner (Sirrenberg C et al., 1996). Tim54, which is essential for translocase functionality but not for cell viability, is supposed to be involved in tethering Tim9-Tim10-Tim12 to the TIM22 complex (Kovermann P et al., 2002). The function of Tim18 is still under investigation.

Mitochondrial β-barrel precursors are transferred by Tim9-Tim10 or Tim8-Tim13 to the outer membrane complex topogenesis of mitochondrial outer membrane β-barrel

proteins (TOB) / sorting and assembly machinery (SAM) (Paschen SA et al., 2003; Wiedemann N et al., 2003). The TOB/SAM complex consist of the core subunits Tob55/Sam50, Tom38/Tob38/Sam35 and Mas37/Tom37/Sam37 (Becker T et al., 2008b; Paschen SA et al., 2005). The integral membrane protein Tob55 forms a pore and there is increasing evidence that it assembles β-strands into a barrel structure and thereby forces the insertion into the outer membrane (Endo T and Yamano K, 2009; Kozjak V et al., 2003). The peripheral, cytosol exposed Tob38 was proposed to function as a receptor (Kutik S et al., 2008). While Tob38 is essential for cell growth, a depletion of Mas37 is not deleterious, although it has an influence on correct insertion of β-barrel precursors (Habib SJ et al., 2005; Waizenegger T et al., 2004a). Additional, the mitochondrial morphology and distribution protein Mdm10 was found to be associated with the TOB/SAM complex and contributing to the late TOM complex assembly steps (Meisinger C et al., 2004; Sogo LF and Yaffe MP, 1994). Mim1 or Tom13 is another component of the TOB/SAM complex which has been shown to be involved in the assembly of the TOM complex; it is required for a step after the Tom40 precursor interacted with the TOB complex and depletion results in Tom40 accumulation (Ishikawa D et al., 2004; Waizenegger T et al., 2004b). It has been demonstrated that it not only promotes the insertion and assembly of Tom40 but also of the signal-anchored Tom receptors (Becker T et al., 2008a).
A recently identified pathway is the Oxidase Assembly (OXA) pathway which is used by the mtDNA encoded protein COX2 to get inserted from the mitochondrial matrix into the inner membrane (Bonnefoy N et al., 2009; Neupert W and Herrmann JM, 2007). Another rather new pathway is the TIM40/MIA40 import pathway, with Tim40 introducing disulfide bonds into small proteins in the IMS and this way facilitating their import and folding (Banci L et al., 2009; Chacinska A et al., 2004; Mesecke N et al., 2005).

1.8 The translocase of the outer membrane 40 (Tom40)

Tom40 was previously identified as ISP42 in yeast and it has been demonstrated, that this protein is absolutely essential for cell viability (Baker KP et al., 1990). The same was demonstrated for *Neurospora crassa* by the generation of a *Tom40* null mutant (Taylor RD et al., 2003).

In humans, some studies showed an association between *Tom*40 and an increased risk of developing late-onset Alzheimer's disease (LOAD) (Grupe A et al., 2007; Takei N et al., 2009). *Tom*40 risk alleles seem to be approximately twice as frequent in AD subjects as controls (Potkin SG et al., 2009). Moreover, a variant in the TOM40 gene has been associated with age of onset in AD. There is another study available suggesting that the statistically significant correlation of *Tom40* with Alzheimer's disease arises from linkage disequilibrium to the closely adjacent *APOE* gene (Yu CE et al., 2007). The *Tom40* gene is located only 15kb upstream to *APOE*, a gene whose ε4 allele is a well-characterized genetic risk factor for the development of LOAD (Farrer LA et al., 1997; Gibson GE et al., 2000; Kamboh MI, 2004). Neuropathological features of Alzheimer's disease include intracellular neurofibrillary tangles (NFTs) and extracellular senile plaques within the brain accompanied by extensive neuronal loss (Grundke-Iqbal I et al., 1986; Sisodia SS and Price DL, 1995). The senile plaques are composed of Amyloid-beta protein, a 39-43 amino acid peptide derived from amyloid precursor protein (APP) (Glenner GG and Wong CW, 1984; Masters CL et al., 1985; Selkoe DJ et al., 1987). Mutations in the APP gene together with mutations in the two *Presenilin* genes 1 and 2 (PS1 and PS2) are considered to be the main risk factors for the rare familial form of Alzheimer's disease with an early-onset (FAD or EOAD) which accounts for just 1-2% of all AD cases (Price DL and Sisodia SS, 1998). Devi et al. were able to show that in brains of LOAD patients amyloid precursor protein (APP) accumulates in the TOM40 import channel and thereby inhibits the entry of various nuclear-encoded proteins (Devi L et al., 2006).

The neurological screen of the GMC analyzes several mouse lines with defects in nuclear encoded mitochondrial proteins, especially concerning the import system. Recently, the results of the Tim23 mouse model were published, the first mouse model with an impaired mitochondrial import (Ahting U et al., 2009). Mice showed a markedly decreased life span and a neurological phenotype.

In mice the TOM40 protein was first cloned and characterized as MOM35 by Rivera and colleges (Rivera IL et al., 2000). Since there was no animal model available a *Tom40* knock-out mouse model was created in collaboration with the German Gene Trap Consortium (GGTC) and systemically analyzed in the GMC and with additional collaborators from outside to get further insights about this essential import pathway.

2 Animals and materials

2.1 Compounds

- Acetic acid — Merck, 100058
- Acrylamide/Bis-acrylamide, 30% solution — Sigma, A3449
- ADP (Adenosin5'diphosphate, potassium salt) — Sigma, A 5285
- Ampuwa water — Frisenius-Kabi
- Antimycin A — Sigma, A 867
- Ascorbate sodium salt — Sigma, A 4034
- Boric acid — Sigma, B6768
- 5-Bromo-4-chloro-3-indolyl α-D-galactopyranoside — Sigma, 16555
- BSA, essentially fatty acid free 1 g/l — Sigma, A 6003
- Chloroform — Carl Roth, 6340.2
- Cis-aconitic acid — Aldrich, A3412
- Coomassie Brilliant Blue R-250 — Thermo Fisher Scientific Inc
- Cytochrome c — Sigma, C 7752
- 3,3'-Diaminobenzidine (DAB) — Sigma, D3939
- Diethylpyrocarbonate — Aldrich, 159220-25G
- Dimethyl sulfoxide (DMSO) — Sigma, D4540
- DNTB (5,5′-Dithiobis(2-nitrobenzoic acid)) — Aldrich,D218200
- EDTA — Aldrich, 431788
- EGTA — Aldrich, E 4378
- Ethanol — Merck, Emplura 108543
- FCCP — Sigma, C 2920
- L-Glutamic acid sodium salt — Sigma, G 162
- Glycine — AppliChem, A1067
- Glycerol — Sigma, G5516
- Hydrochloric acid (HCl) — Merck, 109058
- HEPES — Sigma, H 7523
- Isocitric Dehydrogenase (NADP) from porcine heart — Fluka, 58775
- KCl — Merck, 104938
- KCN — Fluka, 6017
- Ketamin 10% — Pharma Partner 797-468
- K-lactobionate — Sigma Aldrich, 153516
- K_2HPO_4 — Merck 105109
- KH_2P0_4 — Merck, 104873
- M2 medium — Sigma, M7167
- L-Malic acid — Sigma, M 1000
- Manganese(II) chloride — Aldrich, 450995
- D-Mannitol — Sigma , M9647 - ACS reagent
- β-Mercaptoethanol — Sigma, M7154
- Methanol — Merck, Emplura 822283

- MgCl2 — Scharlau, MA 0036
- β-Nicotinamide adenine dinucleotide phosphate sodium salt — Sigma, N803
- Nonidet™ P 40 Substitute — Sigma, 74385
- Oxaloacetate — Aldrich, 171263
- Paraformaldehyde (PFA) — Sigma, 16005
- Paraquat dichloride — Fluka, 36541
- Protease Inhibitor Cocktail — Sigma, P8340
- 2-Propanol — Merck, Emplura 818766
- Protein Assay Dye Reagent Concentrate — Biorad, 500-0006
- Rompun 2% injection solution — Bayer
- Rotenone — Sigma, R 8875
- Saline(isotonic) — Fresenius Kabi
- Sodium dodecyl sulphate (SDS) — Sigma, L4390
- Sodium chloride (NaCl) — Sigma, S3014
- Sodium deoxycholate — Sigma-Aldrich, D6750
- Sodium hydroxide (NaOH) — Sigma-Aldrich, S8045
- Sodium phosphate dibasic dehydrate (Na_2HPO_4 *$2H_2O$) — Sigma, 71643
- Succinate disodium salt hexahydrate — Sigma, S 2378
- Sucrose — Roth, 4621.1
- Taurine — Sigma, T 0625
- TMPD — Sigma, T3134
- Tris/HCl — Sigma, T5941
- Triton® X-100 — Sigma, T8787
- Trizma Base — Sigma, T1503
- TRIzol® Reagent — Invitrogen, 15596-026
- Tween 20 — Sigma, 63158
- All primers used for genotyping were distributed by Metabion international AG, Martinsried, Germany
- Used kits:
    - High Pure PCR Template Preparation Kit (Roche, Basel, Switzerland)
    - SequalPrep™ Long PCR Kit with dNTPs (A10498; Invitrogen, Carlsbad, USA)
    - BigDye® Terminator v3.1 Cycle Sequencing Kit (Applied Biosystems, Foster City, USA)
    - *Taq* DNA Polymerase (Qiagen, Germany)
    - QIAamp® DNA Micro kit (Cat.no.: 56304; Qiagen, Germany)
    - SuperScript™ First-Strand Synthesis System (Cat. No: 11904-018, Invitrogen, Carlsabd, USA)
    - DNA Qiagen HotStarTaq DNA Polymerase kit
    - TaqMan® Probe-Based Gene Expression Analysis Kit and Probes (Applied Biosystems, Foster City, USA)
    - QIAGEN RNeasy® MIDI Kit (cat. no.: 75144; Qiagen, Germany)
    - QIAGEN QIAamp®DNA Mini and Blood Mini Kit (cat. no.: 51104; Qiagen, Germany)
    - Restore Plus Western Blot Stripping Buffer (Thermo Fisher Scientific Inc, USA)

2.2 Technical equipment

- 3730 DNA Analyzer (Applied Biosystems, Foster City, California, USA)
- Mastercycler Gradient (Eppendorf, Hamburg, Germaby)
- StepOne™ Real-Time PCR System
- Heidolph DIAX 900
- TissueLyser II system (Qiagen, germany)
- POTTER S Homogenisator (Braun Biotech International, Göttingen, Germany)
- Oroboros *Oxygraph* (Oroboros, Innsbruck, Austria)
- Odyssey® Infrared Imaging System (LI-COR Biotechnologies, USA)
- Vortex genie, Scientific Industries (New York, USA)
- NanoDrop 1000 Spectrophotometer
- Centrifuges
    - Standard tabletop centrifuge (Eppendorf, Hamburg, Germany)
    - Kendro Laborytory products Multifuge 3LR Heraueus (VWR, USA)
    - Biofuge fresco (Heraeus; Hanau, Germany)

- GMC primary screen:
    - Faxitron X-ray Model MX-20 (Specimen Radiography System, Illinois, USA)
    - NTB Digital X-ray Scanner EZ 40 (NTB GmbH, Diepholz, Germany)
    - pDEXA Sabre X-ray Bone Densitometer (Norland Medical Systems Inc., Basingstoke, Hampshire, UK)
    - Open field test apparatus from ActiMot, TSE systems, Bad Homburg, Germany (45.5 x 45.5 x 39.5 cm), illumination: 150lux (periphery), 200lux (centre)
    - Rotarod (Bioseb, Chaville, France)
    - Grip Strength Meter (TSE systems, Germany)
    - Indirect ophthalmoscope (Sigma 150 K, Heine Optotechnik, Herrsching, Germany) in conjunction with a condensing lens (90D lens, Volk, Mentor, OH, USA)
    - “AC Master” (Meditec, Carl Zeiss, Jena, Germany)
    - Hot plate system (TSE systems, Bad Homburg, Germany)
    - Minispec TD-NMR Analyzers (Brucker Optics, Germany)
    - Accu-Chek Aviva glucose analyzer (Roche/Mannheim)
    - Olympus AU 400 autoanalyzer (Olympus, Hamburg, Germany)
    - ABC-Blutbild-Analyzer (Scil Animal Care Company GmbH; Viernheim, Germany)
    - LSRII flow cytometer (Becton Dickinson, USA)
    - Bioplex reader (Biorad, USA)
    - MC4000 Blood Pressure Analysis Systems (Hatteras Instruments Inc., Cary, North Carolina, USA)
    - ECG-auto (EMKA technologies, Paris, France)
    - Lung function: system of Buxco® Electronics (Sharon, Connecticut)
    - GenePix Pro6.1 image processing software (Axon Instruments, USA)

- DigiGait System (Mouse Specifics, Inc., USA)
- Running wheel system (TSE Systems, Bad Homburg, Germany)
- Oculus Pentacam (Oculus GmbH, Wetzlar, Germany)
- Spectralis OCT system (Heidelberg Engineering, Germany)

- Reichert ultramicrotom (Ultraacut E; Fa. Reichert-Jung, Wien, Austria)
- Transmission electron microscope EM 10 CR (Zeiss, Oberkochen, Germany)
- Toennies Neuroscreen (Jaeger-Toennies, Hoechberg, Germany)
- Disposable syringe filter (PTFE membrane), 5996.1 (Carl Roth, Karlsruhe)
- Syringe Omnifi x®-F, 9161406V (B.Braun, Sempach, Switzerland)
- Cryostat (Microm International GmbH, Walldorf, Germany)

2.3 Standard Buffers and Solutions

DEPC-H_2O:

0,2ml Diethylpyrocarbonate
fill-up to 1l with ddH_2O
Stirring over night at 37°C and autoclaved

0,5M EDTA

186.1 g EDTA
700ml ddH_2O and NaOH pellets added until whole EDTA was dissolved
adjusted to pH 8.0 with HCl or NaOH
ddH_2O was added to receive 1 l

5M NaCl

292,2g NaCl
ddH_2O was added to receive 1ml

PBS (10x)

80 g NaCl
2 g KCl
17.8 g Na_2HPO_4 *$2H_2O$
2.72 g KH_2PO_4
dissolved in ddH_2O and adjusted to pH 7.3
ddH_2O was added to receive 1 l

PBS-T (0,05%)

100 ml 10x PBS
500 µl Tween20 (f.c. 0.05%)
900 ml ddH_2O

4% Paraformaldehyde (PFA)

20g PFA dissolved in 400ml 65°C ddH_2O
NaOH pH7.0 was adjusted with NaOH
50ml 10XPBS (pH 7.6) was added and ddH_2O was added to a final volume of 500ml

20% SDS

100g SDS (sodium dodecyl sulfate)
ddH_2O was added to receive 500ml

Tail Buffer

10ml Trizma Base pH 8,0
40ml 0,5M EDTA
4ml 5M NaCl
10ml 20% SDS

TBE-Puffer (10x)

108g Trizma Base
55g boric acid
40ml 0,5M EDTA pH 8,0
ddH_2O was added to receive 1 l

TBS (10x)

80 g NaCl
2 g KCl
30 g Trizma Base
dissolved in ddH_2O and adjusted to pH 7.4
ddH_2O was added to receive 1 l

1M Tris-HCl

121.1 g Trizma Base
dissolved in ddH_2O and adjusted to pH 7.0, 7.5 and 8.0 with HCl
ddH_2O was added to receive 1 l

Western Blot

Gel buffer (Schaeger&Jagow)

3M Tris/HCl pH 8,45
0,3% SDS

1X anode buffer (Schaeger&Jagow)

0,2 M Tris/HCl
Adjust to pH 8,9

1X cathode buffer (nach Schaeger&Jagow)

0,1 M Trizma base
0,1 M Tricin
0,1% SDS
Adjust to pH 8,25

Blot buffer (BioRAD Trans-Blot) (pH 9,2)

5,8g	Trizma base
2,9g	Glycine
3,75 ml	10% SDS
200 ml	MetOH

add ddH_2O to recieve 1l

Staining solutions

Coomassie staining solution		500ml
50%	methanol	250ml
10%	acetic acid	100ml
0,05%	Coomassie Brilliant Blue **R-250**	250mg

ddH_2O was added to recieve 500ml

Destaining solution		500ml
5%	methanol	25ml
7%	acetic acid	35ml

ddH_2O was added to recieve 500ml

$K_3[Fe(CN)_6]$[e] Ferricyanide Potassium 0,5M

8.2g dissolved in 50ml ddH_2O
Aliquoted and stored at -20°C, light protected

$K_4[Fe(CN)_6]^f*3H_2O$ Ferrocyanide Potassium 0,5M

10.5g dissolved in 50ml ddH_2O
Aliquoted and stored at -20°C, light protected

Bromo-chloro-indolyl-galactopyranoside (X-Gal)

50mg/ml 1g dissolved in 20ml DMSO
Aliquoted and stored at -20°C, light protected

Isolation buffers

IB buffer	250ml
215mM mannitol	9.19g
75mM sucrose	6.42g
20mM HEPES	1.19g
1mM EGTA	95.1mg
0.1% BSA	250mg

pH 7.4

M2 buffer	500ml
600mM sucrose	102.57g
5mM EDTA	5ml
1mM PMSF	5µl (100mM PMSF stock)
50mM Tris/HCl (pH 7.5)	3.025g

SET buffer	500ml
250mM sucrose	42.76g
5mM Tris/HCl	303.5mg
2mM EGTA	380.4mg
0.1% BSA	500mg
pH 7.4	

Respirometry and enzyme kinetics

K-lactobionate (0.5M)

35.83g K-lactobionate
Dissolved in 100ml ddH_2O
pH 7.0 with KOH

Miro5 buffer (Oroboros)

110 mM sucrose	37.65 g
20 mM taurine	2.502 g
20 mM Hepes	4.77 g
10 mM K_2HPO_4	1.361 g
60 mM K-lactobionate	120 ml of 0.5 M stock solution
0.5mM EGTA	0.190 g
3mM $MgCl_2$	0.610 g

ddH_2O was added to receive 1l , pH 7.3was adjusted
aliquoted to 10ml and stored at -20°C

Potassium phosphate buffer (100mM, pH7,4)

80.2ml 1M K_2HPO_4 (17.418g in 100ml)
19.8ml 1M KH_2PO_4 (16.609g in 100ml)

Citrate synthase buffer

1ml 1M Tris/HCl
200µl Triton-X
ddH_2O was added to receive 100ml; pH 7,4
buffer was stored in aliquots of 10ml at -20°C

1M $MgCl_2$

95.21g $MgCl_2$ (water free)
Dissolve in 1l ddH_2O

Complex I buffer		final conc.
2.5ml	Potassium phosphate buffer (100mM, pH7,4)	25mM
50µl	1M $MgCl_2$	5mM
25mg	BSA	5mg/ml
30µl	AA (1mg/ml)	3µg/ml
20µl	1M KCN	2mM

ddH_2O was added to recieve 10ml

Complex II/III buffer		
2.5ml	Potassium phosphate buffer (100mM, pH7,4)	25mM
50µl	1M $MgCl_2$	5mM
200µl	succinate	

ddH_2O was added to recieve 10ml

Complex IV buffer		
2.5ml	Potassium phosphate buffer (100mM, pH7,4)	25mM
50µl	1M $MgCl_2$	5mM
30µl	AA (1mg/ml)	3µg/ml

ddH_2O was added to recieve 10ml

Aconitate buffer		final conc.
100µl	Tris/HCl pH8.0	100mM
7.5µl	cis-aconitate (20mM)	0.15mM
10µl	$MnCl_2$ (50mM)	0.5mM
5µl	NADP solution (200mM)	1mM
7.5µl	IDH solution (40 U/ml)	0.3U
5µl	20% TritonX100	0.1%

Finally 850µl ddH_2O were added.

Oxaloacetate (OAA)

50mM OAA 0.0441g in 6.68ml ddH_2O

DNTB (Ellman`s reagent)

100mM DNTB 0.099g in 5ml Tris-HCl pH8.0

Reduced cytochrome C (cyt C)

2mM CytC(equine heart) 0.124 g in 5ml 1,25mM Tris/HCl pH8
Reduction with sodium dithionite powder
Aliquoted and stored at -20°C protected from light

Decylubiquinone

50mM decylubiquinone 0.025g in 1.55ml EtOH (100%)
Aliquoted and stored at -20°C

Aconitate solution

20mM cis-aconitate 0.00348g in 1ml ddH_2O
Preparation immediately before experiment!

Manganese (II) chloride solution

50mM $MnCl_2$ 0.0063g in 1ml ddH_2O

Nicotinamide adenine dinucleotide phosphate (NADP) solution

200mM NADP 0.0153g in 1ml ddH_2O

Preparation immediately before experiment!

Isocitrate dehydrogenase (IDH) solution

40 U/ml 0.001g in 1ml ddH_2O
Preparation immediately before experiment!

20% TritonX100 solution

Add 20ml TritonX100 to 80ml ddH_2O

Substrates

ADP

500mM ADP 0.491 g dissolved in 2ml ddH_2O
Neutralized with 5 N KOH (approx.450 µl), aliquoted into 0.2 ml portions and stored at -80°C

Ascorbate

800mM Ascorbate sodium salt 1.584g dissolved in 10 ml ddH_2O
To prevent autooxidation, pH was adjusted to 6 with ascorbic acid (pH ~2)
Divided into 0.2 ml portions and store frozen at -20 °C protected from light

L-Glutamic acid (glutamate)

2M Glutamate 3.742g dissolved 10 ml ddH_2O
Neutralize with 5 N KOH, divide into 0.5ml portions and stored at -20 °C

L-Malic acid (malate)

800mM malate 1.073g dissolved in 10ml ddH_2O
Neutralized with 10N KOH and divided into 0.5ml portions. Stored at -20 ℃.

Succinate

1M succinate 2.701g dissolved in 10ml ddH_2O
Adjusted pH to 7.0 with 37% HCl, divided into 0.5 ml portions and stored at -20 ℃

TMPD

200mM 47.4mg dissolved in 1ml ddH2O

To prevent autooxidation 0.8M ascorbate were added to a final concentration of 10 mM. Divided into 0.2ml portions and stored at -20 ℃

Inhibitors:

Antimycin A (AA)

1mg/ml AA dissolved in 40ml EtOH (100%)
Aliquoted and stored at -20℃

Rotenone

1mg/ml Rotenone disolved in 40ml EtOH (100%)
Aliquoted and stored at -20℃

KCN

1M KCN 1.3g in 20ml ddH_2O, pH8.0
Aliquoted and stored at -80℃

2.4 Animals

2.4.1 Generation of a Tomm40 knock-out mouse

The ES cell clone W037F03 was generated in collaboration with the GGTC by gene-trap mutagenesis as described (Hansen J et al., 2003; Wiles MV et al., 2000). The non-retroviral pT1*βgeo* gene trap vector, containing a β-galactosidase/neomycin phosphotransferase fusion gene, was electroporated into tbv-2 ES cells (129S2). Gene-trap expressing ES cell clones were selected in 200 µg/ml G418 (GIBCO/BRL), manually picked and expanded. The gene-trap integration site was identified due to the results of 5' Rapid Amplification of cDNA ends (5'RACE)-PCR and the direct sequencing of the PCR products. C57BL/6 blastocysts were injected and resulting male chimeras were bred to C57BL/6 females (Hansen J et al., 2003).

2.4.2 Breeding and housing of animal cohorts

Within the GMC all animals are housed in type II polycarbonate cages in individually ventilated caging (IVC) systems (VentiRack Bioscreen TM, Biozone, Margate, UK) on wood fiber (Altromin, Lage, Germany). In the GMCII rooms where challenge experiments are performed, the used IVC system is provides by Tecniplast (Aero - Mouse IVC Green Line Cages, Tecniplast, Buguggiate (VA) Italy). Cages are changed in every week in Laminar Flow Class II changing stations. Mice get irradiated standard rodent high energy breeding diet (Altromin 1314) and semidemineralized filtered (0.2 µm) water *ad libitum*. Outbred 8-week-old male SPF Swiss mice are used as sentinels. They are housed on a mixture of new and soiled bedding (50:50) from all cages of the IVC rack, and they are exposed to the soiled air. Health monitoring is carried out according to FELASA recommendations (www.felasa.org) by onsite examination of the sentinel mice by certified laboratories (Brielmeier M et al., 2002).

Chimeric mice deriving from a mutated 129S6/SvEvTac ES cell clone were backcrossed into C57BL/6J for several generations. The parental mice for breeding the GMC cohort were backcrossed to C57BL/6J for seven generations. 21 breeding pairs were set, heterozygous females were mated with heterozygous males for four days and then the males were removed from the cages to avoid large age differences

in the offspring. Finally, 40 mutant (20 males, 20 females) and 40 wildtype (wt) animals (20 males, 20 females) entered the primary screen of the GMC (see chapter 3.9).

For breeding the aging cohort, 13 breeding pairs were used to generate at least 37 male (21 wildtype, 16mutant) and 38 female (17 wildtype, 21mutant) mice. Animals were used for secondary screening and cold challenge (see chapters 3.10 and 3.11.2).

For the oxidative stress challenge cohort only the male offspring of fourteen breeding pairs was used. In the end, 13 wildtypes and 15 mutants were used for these experiments (see chapter 3.13.1).

3 Methods

3.1 Determination of the exact integration site of clone W037F03

3.1.1 Preparation of DNA template for sequencing

Genomic DNA of five mice was isolated from mouse tails using a High Pure PCR Template Preparation Kit from Roche. Tails were incubated in 200µl Tissue Lysis Buffer + 40µl Proteinase K on a shaker at 55°C over night. After lysis the samples were mixed with a syringe and 200µl binding buffer plus 100µl absolute isopropanol were added. The tubes were centrifuged with a standard tabletop centrifuge (Eppendorf, Hamburg, Germany) at 13000XG for 5min. The liquid phase was pipeted into the reservoir of the high pure filter tube that was out into a collection tube before. Centrifugation to collect DNA was done at 8000XG. A gradient PCR with annealing temperatures ranging from 52°C-60°C was performed, using Seq-Prep *Taq* DNA Polymerase High Fidelity (Invitrogen: SequalPrep™ Long PCR Kit with dNTPs).
The initial denaturation at 93°C for 3min was followed by 35 cycles with 93°C for 15 sec, 52°C-60°C for 30sec and 68°C for 4min. Final extension was done at 68°C for 7min.
Used primers:
Tom40-I12-E2-R: 5'-GTATctgcgaggggaaaggt-3' and Race-lacZ-R: 5'-CAAGGCGATTAAGTTGGGTAACG-3' (product size: 2262bp) or alternatively EnSA1500-R: 5'-CCTAGGGAAAGGGTCGAGAG-3' (product size: 1644bp). Resulting PCR products were used as template for sequencing.

3.1.2 Sequencing

For sequencing, the product resulting from long range PCR first had to be purified. Contaminants like primers, dNTPs and salts were filtered to waste under vacuum. Therefore, the PCR product first had to be filled up to a volume of 100µl with H_2O (HPLC grade), spun-down and transferred to a NucleoFast clean-up plate (NucleoFast 96 PCR Plates; Macherey-Nagel). The plate was placed on a vacuum manifold. Ultrafiltration was acquired applying a vacuum for 5-10min (20 inches Hg).

The bottom of the plate was dried carefully. For recovery of the PCR product, 30µl water was dropped directly onto the filter and incubated for 10min on a shaker (200rpm). The cleaned-up PCR product then was transferred to a new 96-well plate. The sequencing reaction was performed using BigDye® Terminator v3.1 Cycle Sequencing Kit (Applied Biosystems).

Reaction mastermix:

- 0,5µl BIG DYE Terminator (BDT)
- 1,5µl BIG DYE Buffer
- 1µl forward primer or reverse primer
- 1 µl H_2O (HPLC grade)
- 1µl PCR-product

For precipitation of the substrate 25µl 100% EtOH was added to the sequencing product. After 15min incubation at room temperature (RT) the dark plates were centrifuged at 3000xG for 30min. Supernatant was discarded and 50µl 70% EtOH was added to the wells. Plates were centrifuged at 2000xG for 15min and supernatant was discarded. After air drying for 10min at RT pellet was solved in 50µl AMPUWA-H_2O, transferred to the sequencing plate and sequenced using a 3730 DNA Analyzer (Applied Biosystems, Foster City, California, United States).

3.2 Genotyping

3.2.1 Isolation of tail DNA

For routine genotyping genomic DNA from mouse tails (0.5-1cm) was isolated using a standard protocol: tails were incubated in 700µl tail buffer + 40µl proteinase K (10mg/ml) over night at 55°C. After adding 240µl 5M NaCl, samples were vortexed thoroughly and centrifuged at 13000rpm for 10min. 700µl of the supernatant was put to a new 1,5ml safe-lock tube (Eppendorf, Hamburg, Germany) and 500µl isopropanol was added. Samples were vortexed and centrifuged (13000rpm, 10min). Afterwards, supernatant was discarded and pellet was washed in 1ml EtOH (70%). Samples again were centrifuged (13000rpm, 5min) and supernatant was discarded. After air drying pellets were dissolved in 200µl AMPUWA H_2O over night at room RT. Samples were stored at 4°C.

3.2.2 Routine genotyping

Routine genotyping of the mouse line was done with following primers and conditions:

Wildtype:

Primer 1 (Forward primer) 5'-aatgagcaggtaggcgtgtc-3'
Primer 2 (Reverse primer) 5'-gttcggtgtcctccgagat-3' (product size: 248bp)
Mutant:

Primer 2 (Reverse primer wt): 5'-gttcggtgtcctccgagat -3'
Primer 3 (Reverse primer mut): 5'-CTTCACATCCATGCTGAGGA-3' (product size: 400bp).

Routine genotyping was performed with *Taq* DNA polymerase (Qiagen, Germany) in a 35µl reaction volume:

Component	**Volume / reaction [µl]**	**Final concentration**
primer 1 [10µM]	1	0,3µM
primer 2 [10µM]	1	0,3µM
primer 3 [10µM]	1	0,3µM
25mM $MgCl_2$ solution	2	~2.9mM
10x CoralLoad buffer (contains15 mM $MgCl_2$)	3,5	1x
5x Q-Solution	7	1x
dNTP mix (10mM of each dNTP)	1	~0.3mM of each dNTP
H_2O	15,5	
Taq Polymerase (5units/µl)	0,2	1 unit
Template DNA (10-100ng/µl)	3	

∑ 35 µl

Thermal cycler conditions:

94°C for 2:00 min	
94°C for 0:30 min	40 cycles
55°C for 0:40 min	
72°C for 1:00 min	
72°C for 5:00 min	
10°C for 1:00 min	

PCR products were checked on a 1.5% TBE-agarose gel (120V, 1h).

3.2.3 Embryo and blastocyst genotyping

Heterozygous female mice were injected intraperitoneally (i.p.) with pregnant mares' serum gonadotropin (PMSG) two days before mating to a heterozygous male in order to synchronize the their estrus and additional with the glycoprotein hormone human chorionic gonadotropin (HCG) immediately before mating to induce superovulation (Fowler RE and Edwards RG, 1957). Embryos were dissected at E9.5, lysed and genotyped using routine genotyping conditions (see chapter 2.3.1). Blastocysts were harvested by uterine flushing with M2-Buffer (Sigma) 3.5 days after a vaginal plug was observed and separated individually into 1.5ml safelock tubes (Eppendorf Hamburg, Germany). Blastocyst DNA was purified with the QIAamp® DNA Micro kit. The very small amount of used tissue requires the application of carrier RNA to buffer AL, which enhances the binding of DNA to the column membrane. Thus before starting the purification it was necessary to prepare the also supplied lyophilized carrier RNA (310µg) with 310µl buffer AE to obtain aliquots with a concentration of 1µg/µl that could be stored at -20°C until usage. In this experiment, the use of 1µg carrier RNA per blastocyst was sufficient. Buffers AW1 and AW2 had to be prepared before use with ethanol (96-100%) (Carl Roth) because they were delivered as concentrates. 25ml ethanol (Carl Roth) was added to AW1 and 30ml to AW2. Purification itself was done according to the instruction manual. Briefly, 15µl buffer ATL was carefully dropped into the tube without touching the bottom. After 10µl Proteinase K was added to each sample and they were mixed by pulse-vortexing for 15sec. The tubes then were incubated in a thermomixer (Thermomixer compact, Eppendorf) for 3h at 56°C. 25µl buffer ATL and 50µl buffer AL containing 1µl carrier RNA. 50µl ethanol absolute (Carl Roth) was added to the sample, mixed thoroughly by 15sec pulse vortexing and incubated at room temperature for 5min. To remove drops from the lid, the tubes were shortly spun down. The lysate had to be transferred to QIAamp MiniElute Columns and centrifuged at 6000xG (8000rpm) for 1min. The columns were placed in a clean collection tube and 500µl buffer AW1 was pipeted onto the column membrane. The samples were spun down at 6000xG (8000rpm) for 1min. whereas the filtrate was discarded, the column was again placed in a clean collection tube and 500µl buffer AW2 was added. To get the membrane completely dry, centrifugation at full speed (13000rpm) was done for 3min. Columns were placed in a 1,5ml Eppendorf (Hamburg, Germany) tube. 30µl buffer AE was carefully applied dropwise to the centre of the membrane. After incubation for 1min at

room temperature, the samples were centrifuged at full speed (13000rpm) for 1min. Due to the very small eluation volume, DNA concentrations were not determined. Additional, only wildtype genotyping was performed. Mutant PCR would have been added if necessary (if there would have been samples were no wildtype band would have been visible). For genotyping of blastocyst DNA Qiagen HotStarTaq DNA Polymerase kit was applied.

Reaction mastermix:

Component	**Volume / reaction [µl]**	**Final concentration**
primer 1 [10µM]	1	0,3µM
primer 2 [10µM]	1	0,3µM
25mM $MgCl_2$ solution	1,5	~2.9mM
10x CoralLoad buffer (contains15 mM $MgCl_2$)	2,5	1x
5x Q-Solution	5	1x
dNTP mix (10mM of each dNTP)	0,5	~0.3mM of each dNTP
H_2O	8,2	
Taq Polymerase (5units/µl)	0,3	1 unit
Blastocyst DNA	5	

∑ 25 µl

For each reaction, 20µl mastermix was given to a PCR tube (Greiner Bio-One GmbH, Frickenhausen, Germany) and 5µl template DNA was added. PCR was performed using a thermocycler (Mastercycler Gradient, Eppendorf).

Thermo cycler conditions:

95°C for 15min	Initial incubation to activate HotStarTaq DNA Polymerase
94°C for 0:30 min	35 cycles
54°C for 0:45 min	
72°C for 1:00 min	
72°C for 10:00 min	Final extension
10°C for 1:00 min	

Used primers:

Tom40-wildtyp1-F: 5'- aat gag cag gta ggc gtg tc -3'
Tom40-wildtype1-R : 5'-gtt cgg tgt cct ccg aga t -3' (product size: 248bp)

3.3 Determining expression patterns using LacZ staining

To determine the expression pattern of the Tom40 allele carrying the gene-trap mutation embryos in different stages were dissected of the female Uteri and a LacZ staining was performed. Mutant female mice were treated with PMSG and HCG as described in chapter 2.4.4 and mated to mutant males. Uteri of pregnant females were removed at E9.5, E10.5 and E11.5 and stored in 1xPBS on ice. Embryos were dissected and fixed in 4% PFA for 15min. Then they were washed in Washing Buffer for 10 min. For staining, embryos were incubated in LacZ Staining buffer over night at 30°C protected from light. After washing, they were examined with the binocular and stored in 4% PFA at 4°C.

LacZ Wash	100ml	
1M $MgCl_2$	200µl	(final 0,002M)
5% Deoxycholate	200µl	(final 0,01%)
10% NP40	200µl	(final 0,02%)
Add 1xPBS to 100ml		

LacZ Staining	50ml	
0,5M $K_3Fe(CN)_6$	500µl	(final 0,005M)
0,5M $K_4Fe(CN)_6$	500µl	(final 0,005M)
X-Gal	50mg in 2ml DMF	(final 0,1%)
Add lacZ wash buffer to 50ml		

3.4 mRNA expression analysis

3.4.1 Isolation of mRNA from mouse heart tissue

Total RNA of nitrogen frozen mouse hearts was extracted using the TRIzol (Invitrogen, Karlsruhe, Germany) chloroform standard protocol and purified with QIAGEN RNeasy® MIDI Kit. According to manufactures' instruction, RLT buffer had to be prepared with 1µl β-Mercaptoethanol per 1ml buffer just before needed (only stable for one month after addition of β-Mercaptoethanol). Buffer RPE is supplied as a concentrate, 4 volumes of ethanol absolute (Carl Roth) had to be added before first usage. Kit is suitable for 20-250mg tissue, so whole hearts could be used. The nitrogen frozen tissue was transferred to sterile 15ml BD Falcon™ Blue Max

Centrifuge Tubes filled with 4ml buffer RLT (+β-Mercaptoethanol) and homogenized for 1min with Heidolph DIAX 900 at highest level. Machine was cleaned with 0.1% DEPC water (Diethylpyrocarbonate, Sigma; RNase free water). Homogenized organs were kept on ice and incubated for at least 5min before centrifuging at 4000rpm for 15min at 4°C. Supernatant was transferred to clean 15ml BD Falcon™ Blue Max Centrifuge Tubes. Afterwards 0,2ml chloroform (Carl Roth, Karlsruhe, Germany) per ml supernatant was added, shaken gently for 15sec and centrifuged for 15min at 4000rpm and 4°C. Supernatant again was transferred to clean 15ml falcons. Ethanol absolute (Carl Roth) was added to the sample (same volume like the supernatant), mixed by pipeting and transferred to the RNeasy MIDI column. After a centrifugation step (5min, 4000rpm, room temperature) the flow-through was discarded and 4ml buffer AW1 added. The samples were centrifuged at 4000rpm/5min/room temperature, flow through again discarded and 2,5ml buffer RPE added to the column. After centrifugation at 4000rpm/2min/room temperature, 2,5ml RPE was added for the second time and centrifuged at 4000rpm for 6min (room temperature). To elute, the columns were thereafter placed in a new falcon and 70µl RNase free water was directly dropped onto the filter (carefully, without touching) and incubated for 1min at room temperature. After centrifugation at 4000rpm for 6min at room temperature, the flow through was transferred to a presterilized 1,5ml safelock tube (Eppendorf, Hamburg, Germany). Samples were freezed as quick as possible in liquid nitrogen and stored at -80°C. RNA concentration was determined spectrophotometrically.

3.4.2 cDNA Synthesis

For cDNA synthesis with Invitrogens' SuperScript™ First-Strand Synthesis System, 2µg RNA was implemented. Method was performed following the manufacturers'' instructions.

<u>Mastermix1:</u>

Oligo(dt)12-18 (500ng/ml) Primer (Invitrogen)	1µl
dNTP mix (Fermentas)	1µl

<u>Mastermix 2:</u>

5X First Strand Buffer (Invitrogen)	4µl
0,1M DTT (Invitrogen)	2µl

2µl of mastermix1 was pipeted to a PCR cup; 2µg RNA and RNase free water to an amount of 12µl were added.
For reaction, samples were incubated at 65°C for 5min using a thermocycler (Mastercycler Gradient, Eppendorf) and afterwards kept on ice. 6µl of mastermix 2 were mixed with the sample and incubated for 2min at 42°C. Finally PCR reactions was started by applying 1µl SuperScript® II Reverse Transcriptase to the sample and incubate it in the thermocycler at 42°C for 50min. Reaction inactivated by a final incubation step at 70°C for 15min. cDNA-samples were stored at -20°C.

3.4.3 Real-time quantitative PCR

Real-time quantitative PCR was performed with the TaqMan® Probe-Based Gene Expression Analysis from Applied Biosystems.

Probes:

TaqMan®Gene Expression Assay for Mouse *Tomm40* (20x; Cat. no.: 4331182)
TaqMan®Gene Expression Assay for Mouse *ApoE* (20x; Cat. no.: 4331182)
TaqMan®Gene Expression Assay for Mouse *Actinβ (Actb)* (20x; Cat. no.: 4331182)

All working steps were done in an aura PCR bench. Before starting, the whole equipment inside the bench (pipettes, tips, water, racks, and plates) was irradiated with ultraviolet light for at least 30min.

Reaction Mastermix:

TaqMan Universal Mastermix II, no UNG	10µl
Ctr Primer Probe:	1µl
DEPC-H_2O:	7µl
Template DNA:	2µl

Mastermix was applied to a Micro Amp Fast Optical 96 Well Reaction Plate. Samples were diluted 5ng/µl with DEPC-water; the final cDNA concentration in the reaction well was therefore 10ng. All samples were analyzed by double estimation. Plates were covered with Micro Amp Optical Adhesive Film (PCR compatible DNA/RNA/RNase free) and briefly spun down (Kendro Laborytory products Multifuge 3LR Heraueus). A StepOne™ Real-Time PCR System was used. Data were analyzed by StepOne Software v2.0.

Relative quantification was done using the $2^{-\Delta\Delta C_T}$ method (Livaka KJ and Schmittgen TD, 2001):

$dC_T = C_T$ (Tom40) - C_T (*Actb*)

ØdC_T of all wildtypes was calculated

$\Delta\Delta C_T = dC_T - Ø dC_T$

Relative expression: $2^{-\Delta\Delta C_T}$

3.5 mtDNA copy number and deletion analysis

3.5.1 Extraction of DNA from heart and brain tissue

For extraction of the nucleic acids less than 25mg of nitrogen frozen mouse heart and brain tissue were used for optimal yield. Purification was done using QIAGEN QIAamp®DNA Mini and Blood Mini Kit. Therefore a small slice of mouse heart and brain tissue was placed into presterilized 1,5ml safelock tubes (Eppendorf, Hamburg, Germany) with 180µl ATL-buffer and 20µl Proteinase K. After vortexing, the tubes were incubated on a shaker at 56°C over night for tissue lysis. To remove drops from the lid, the tubes were briefly centrifuged before adding 200µl AL-buffer. To obtain a homogenous solution 15sec pulse-vortexing to mix thoroughly was performed. The samples were incubated at 70°C for 10min and briefly spun-down afterwards. 200µl ethanol absolute (Carl Roth) was added; the sample was again pulse-vortexed for 15sec and briefly centrifuged. The resulting mixture was then transferred to the QIAamp Mini Spin column with collection tube and centrifuged at 6000xG (8000rpm) for 1min. The collection tube with the filtrate was discarded, the column placed in a new collection tube. A volume of 500µl buffer AW1 was added to the column, followed by centrifugation (6000xG (8000rpm) for 1min). The resulting filtrate was discarded; the column was placed in a clean collection tube and 500µl buffer AW2 added. Centrifugation at full speed (13000rpm) was done twice. After the first 3min centrifugation step the used collection tube was discarded and the column put in a new collection tube. The second centrifugation step (1min) had the purpose to avoid possible contamination of the sample with buffer AW2. Finally, the QIAamp Mini Spin column was placed in a clean 1.5ml safelock tube (Eppendorf, Hamburg Germany), 200µl AMPUWA water was added, incubated for 1min at RT and spun down 6000xG (8000rpm) for 1min. This elution step was repeated with another volume of 200µl

AMPUWA water to increase overall DNA yield. Concentrations and quality were measured with a NanoDrop 1000 Spectrophotometer (~30ng/µl with an A_{260}/A_{280} ratio of 1.7-1.9).

3.5.2 Analysis of mtDNA copy number

Heart and brain DNA samples were diluted to 1 ng/µl. Copy number variations of mtDNA molecules were defined by quantifying the mtDNA ND1 *(NADH dehydrogenase 1*) gene copies (He L et al., 2002) relative to the nuclear encoded house keeping gene *Actb* using real-time quantitative PCR (for technical details see chapter 2.3.5). *)*, Additional, *CYTB (cytochrome b)* and *COX3* (cytochrome c oxidase subunit 3) gene copies were also quantified.

A standard curve for each gene was made using DNA extracted from blood of a wildtype C57BL/6J mouse. The following dilutions were used: 1:1, 1:10, 1:100, and 1:1000. dC_T values of the standards were calculated by subtracting (ND1- *Actb,* COX3-*Actb,* and CYTB-*Actb*). Linear equations were produced from the dCT values of the standards (y=mx+b, with m=slope, b=intercept). Samples were analyzed in double estimation. Afterwards, the C_T value specific dC_T values were calculated (in comparison with the standards). Therefore, following formula was used:

i.e. dC_T of ND1-CYTB=(C_TND1-C_T- *Actb*)-(($m_{ND1\text{-- }Actb}$ * C_T ND1)+ $b_{ND1\text{-- }Actb}$)

Copy number was calculated using following formula:

i.e. ND1-CYTB=2^ dC_T of ND1- *Actb*)

Used probes:

Actb: TaqMan®Gene Expression Assay for Mouse *Actb* (20x)

ND1: Custom Taqman(R) Gene Expression Assay Service (20X);

Mouse_ND1_F: GAGCCTCAAACTCCAAATACTCACT
Mouse_ND1 _R: GAACTGATAAAAGGATAATAGCTATGGTTACTTCA
5`- Reporter Dye: 6-carboxy-fluorescein (FAM); TCCAACAGGAATTTCA
3`- Quencher: nonfluorescent quencher (NFQ)

3.5.3 Searching for deletions in the mtDNA

The principle of analyzing the number of mtDNA deletions was described before (Bender A et al., 2006). In brief, mt *ND1 (NADH dehydrogenase 1)*, *CYTB*

(cytochrome b) and COX3 (cytochrome c oxidase subunit3) gene copies were quantified relative to *Actb.* 0.5ng DNA was implemented.

A standard curve for each gene was made using DNA extracted from blood of a wildtype C57BL/6J mouse. The following dilutions were used: 1:1, 1:10, 1:100, and 1:1000. dC_T values of the standards were calculated by subtracting (ND-COX3, ND1-CYTB, ND1- *Actb,* COX3-ND1, COX3-CYTB, COX3-*Actb,* CYTB-ND1, CYTB-COX3, and CYTB-*Actb*). Linear equations were produced from the dCT values of the standards (y=mx+b, with m=slope, b=intercept). Samples were analyzed in double estimation. Afterwards, the C_T value specific dC_T values were calculated (in comparison with the standards). Therefore, following formula was used:

i.e. dC_T of ND1-CYTB=(C_TND1-C_TCYTB)-(($m_{ND1\text{-}CYTB}$ * C_T ND1)+ $b_{ND1\text{-}CYTB}$)

Deletion values were calculated using following formula:

i.e. ND1-CYTB=(1-2^ dC_T of ND1-CYTB))*100

For each animal, the maximum value of all calculated deletion values was taken for comparison with the other animals.

Used probes:

- Cytb: Custom Taqman(R) Gene Expression Assay Service (20x)

  Mouse_cytb-ANY_F GGAACAACCCTAGTCGAATGAATTTG
  Mouse_cytb-ANY_R GGCCGCGATAATAAATGGTAAGATG
  5`- Reporter Dye: FAM TTGACCCGATTCTTCG
  3`- Quencher: NFQ

- Cox3: Custom Taqman(R) Gene Expression Assay Service (20x)

  Mouse_COX3 _F CCTCGTACCAACACATGATCTAGGA 18
  Mouse_COX3 _R AGTGGGACTTCTAGAGGGTTAAGTG 18
  5`- Reporter Dye: FAM TCCAACAGGAATTTCA
  3`- Quencher: NFQ

- *Actb* : TaqMan®Gene Expression Assay for Mouse *Actb* (20x)
- ND1: Custom Taqman(R) Gene Expression Assay Service (20X);

  Mouse_ND1_F: GAGCCTCAAACTCCAAATACTCACT
  Mouse_ND1 _R: GAACTGATAAAAGGATAATAGCTATGGTTACTTCA
  5`- Reporter Dye: 6-carboxy-fluorescein (FAM); TCCAACAGGAATTTCA
  3`- Quencher: nonfluorescent quencher (NFQ)

3.6 Protein extraction from different tissues

Mice were sacrificed by cervical dislocation before organ withdrawal. Organs were either put in ice cold buffer and processed immediately or frozen in liquid nitrogen and stored at -80°C.

3.6.1 Total protein extraction from liver tissue

Frozen tissue (20-402µg) was placed in 2ml safelock tubes (Eppendorf, Hamburg, Germany). 1.5ml SET buffer containing 1% protease inhibitor cocktail (Sigma, P8340) was added and a stainless steel bead (5 mm diameter – QIAGEN). With the TissueLyser II system, samples were simultaneously disrupted through high-speed shaking (two times: 30Hz, 45sec). Homogenates were spun down (800xG, 5min, 4°C), supernatant was aliquoted into new tubes and protein concentration was determined using Bradford assay (see chapter 3.6.4).

3.6.2 Isolation of heart mitochondria

For respirometric measurements in the oxygraph, mouse hearts were dissected, washed in ice-cold 1XTBS and homogenized in 2ml M2 buffer with 3-4strokes using a POTTER S Homogenisator (B. Braun Biotech International, Göttingen, Germany) at 500rpm. Unbroken cells and cell nuclei were spun down at 650xG for 7min at 4°C for three times. Protein concentration of the supernatant was determined using Bradford assay (see chapter 3.6.4).

3.6.3 Isolation of brain mitochondria

Mouse brains were dissected, washed in ice-cold 1XTBS and homogenized in 13ml IB buffer with 3-4strokes using a POTTER S Homogenisator (B. Braun Biotech International, Göttingen, Germany) at 500rpm. Unbroken cells and cell nuclei were spun down at 1300xG for 3min at 4°C for two times. For enzymatic measurements, supernatant was frozen in liquid nitrogen, for respirometric measurements supernatant was centrifuged at 13000xG for 15min. Pellet was dissolved in 500µl Miro5 buffer. Protein concentrations of the samples were determined using Bradford assay (see chapter 3.6.4).

3.6.4 Bradford assay

To determine protein concentrations Bio-Rad Protein Assay was applied. Protein Assay Dye Reagent Concentrate was diluted 1:5 with ddH2O and filtered with a Sterifix® injection filter (B.Braun, Sempach, Switzerland). 1ml of this solution was added to polystyrene cuvettes with 1 cm path length (Biorad, USA). Before measurement, a standard curve using BSA was constructed (0, 1, 2, 4, 6, 8, 10 µg). 1µl protein sample was added to the cuvette, mixed thoroughly and incubated 10min. Measurement at 595nm was done using a spectrophotometer.

3.7 SDS PAGE and Western Analysis

A Tricine-SDS-polyacrylamide gel electrophoresis system developed by Schägger &Jagow (Schägger H and von Jagow G, 1987) was used for analyzing protein expression.

An amount of 20µg protein in 10µl isolation buffer was used. 10µl 5x Laemmlli loading buffer was added.

12% separation gel	component	4% stacking gel
6.6 ml	bis-acrylamide	0.67 ml
6 ml	gel buffer	0.67 ml
2.5 ml	50% glycerol	-
1 ml	ddH_20	3.67 ml
0.05 ml	10% APS	0.04 ml
0.02 ml	TEMED	0.01 ml

The electrophoresis apparatus was set up with cathode buffer inside the negatively charged electrode chamber covering the gel, and anode buffer outside. Samples were denaturized at 70°C for 10min, spun down and loaded to the gel wells together with a prestained molecular marker (Fermentas inc., Maryland, USA). Apparatus was connected to a power source (Biorad, USA); running conditions to separate the protein bands were 50mA/2h.

Then, proteins were transferred to a nitrocellulose membrane by Semi Dry Blotting. Therefore a stack of 6 filter papers (ALDRICH Whatman® cellulose chromatography papers 3MM) was soaked with Blot Buffer and 3 were placed on the anode of a semi dry blotter (Biorad, USA). Nitrocellulose membrane was moistened and put on top of the filter papers. Gel was incubated in Blot Buffer for 10min and placed on top of the

membrane together with the remaining three wet filter papers. Blotter was closed and connected to a power source (200mA, 1h). To check efficiency of transfer gel was stained with Coomassie Brilliant Blue R250 (Thermo Fisher Scientific Inc, USA) over night and destained using an acetic acid solution. Membrane was rinsed with PBS and blocked for 1h either in Odyssey Blocking Buffer (LI-COR Biotechnology, USA) or in 10% milk powder (Sigma, 70166) diluted in PBS-T. Primary antibodies were either diluted in this blocking buffer or in 1% milk powder solution and membranes were incubated over night at 4°C on a shaker. After washing 5x5min with PBS-T, membranes were incubated for 45min in the secondary antibody solution (for Li-COR: IRDye® 800CW – anti mouse; IRDye® 700DX – anti rabbit; both diluted 1:10000 in Odyssey Blocking buffer, protected from light; LI-COR Biotechnology, USA; for analysis by enhanced chemiluminesczence (ECL): Goat anti-Rabbit IgG (H+L), Secondary Antibody, Peroxidase Conjugated (Thermo Scientific Pierce antibodies, 32460) diluted 1:10000 and Goat Anti-Mouse IgG (H+L), Secondary Antibody, Peroxidase Conjugated (Thermo Scientific Pierce antibodies 32430) diluted 1:70000). For Li-COR: Membranes were washed 3x15min in PBS-T and 2x10min in PBS before starting the scanning procedure using the Odyssey® Infrared Imaging System (LI-COR Biotechnologies, USA). Afterwards, membranes were stripped 20min using Restore Plus Western Blot Stripping Buffer (Thermo Fisher Scientific Inc, USA) and reprobed with another primary antibody of a different species. For ECL: Membranes were washed 3x15min in PBS-T (for using the TOMM40 antibody, membranes were washed in 2% milk powder diluted in PBS-T) and 2x10min in PBS. As chemiluminescent substrates for horseradish peroxidase (HRP) the two-component system of Pierce scientific consisting of a stable peroxide solution and an enhanced luminol solution was used (Pierce ECL Plus Western Blotting Substrate 32132). Solutions were mixed 1:1 and incubated on the membrane for 1min (shaking, dark). For detection, the Amersham Hyperfilm ECL (GE Healthcare, 18 × 24 cm, 28-9068-36) was used.

The following antibodies were used:

- Anti-TOMM40 (H-300) (sc-11414; Santa Cruz Biotechnology Inc., USA)
- Anti-TOMM40 (N-15) (sc-11022; Santa Cruz Biotechnology Inc., USA)
- Anti-TOMM40 (C-15) (sc-11025; Santa Cruz Biotechnology Inc., USA)
- Anti-TOMM40 antibody (ab51884; Abcam, Cambridge, UK)
- MitoProfile® Total OXPHOS Rodent WB Antibody Cocktail (Mitosciences, USA) – mouse monoclonal; dilution 1: 1000

- Anti-VDAC1/Porin antibody - mitochondrial Loading control (ab15895; Abcam, Cambridge, UK) – rabbit polyclonal; dilution 1:1000
- Anti-beta Tubulin antibody [DM1B] - Loading Control (ab7287; Abcam, Cambridge, UK) - mouse monoclonal; dilution 1:1000

3.8 Quantification of mitochondrial complexes and isolation of supercomplexes

In order to evaluate import efficiency in mice lacking one TOM40 allele, a quantitative analysis of OXPHOS complexes was performed in different tissues with high energy demand (see Table below).

Table 1: Animals for BNE quantification

Mouse_ID	Age [d]	Strain	Line	Genotype
heart				
30080825	267	C57BL/6J_129/SvJ	TOM40	+/+
30100169	406	C57BL/6J	TOM40	+/-
30100170	406	C57BL/6J	TOM40	+/-
30100615	398	C57BL/6J	TOM40	+/-
30101453	383	C57BL/6J	TOM40	+/+
30111422	259	C57BL/6J_129/SvJ	TOM40	+/+
muscle				
30080825	267	C57BL/6J_129/SvJ	TOM40	+/+
30094744	218	C57BL/6J	TOM40	+/-
30095575	204	C57BL/6J	TOM40	+/-
30126043	207	C57BL/6J	TOM40	+/+
30126044	207	C57BL/6J	TOM40	+/+
30126496	215	C57Bl/6 (129Sv)	TOM40	+/-
brain				
30126043	207	C57BL/6J	TOM40	+/+
30126496	215	C57Bl/6 (129Sv)	TOM40	+/-
30126044	207	C57BL/6J	TOM40	+/+
30126498	215	C57Bl/6 (129Sv)	TOM40	+/-
30084385	332	C57BL/6J	TOM40	+/+
30095575	204	C57BL/6J	TOM40	+/-
liver				
30126043	207	C57BL/6J	TOM40	+/+
30126496	215	C57Bl/6 (129Sv)	TOM40	+/-
30084385	332	C57BL/6J	TOM40	+/+
30095413	167	C57BL/6J_129/SvJ	TOM40	+/+
30126045	218	C57BL/6J	TOM40	+/-
30126042	218	C57BL/6J	TOM40	+/-
Heart of old animals				
30058846	872	C57BL/6J_129/SvJ	TOM40	+/-
30058845	564	C57BL/6J_129/SvJ	TOM40	+/+
30059583	622	C57BL/6J_129/SvJ	TOM40	+/+
30059586	622	C57BL/6J_129/SvJ	TOM40	+/+
30075904	705	C57BL/6J_129/SvJ	TOM40	+/-
30076972	702	C57BL/6J_129/SvJ	TOM40	+/-

All analyses were done by Dr.Ilka Wittigs' work group "Mitochondrial proteome analysis" from the Institute of Molecular Bioenergetics of the University of Frankfurt/Main.

3.8.1 Sample preparation

Preparation of crude mitochondrial membranes and solubilisation of mitochondrial membrane complexes were performed as previously described (Wittig et al. 2006). Briefly, tissue samples from skeletal muscle, brain, liver, and heart were homogenized in 250mM Sucrose, 10mM Tris-Cl pH7.5, 1mM EDTA, 2mM aminocaproic acid using a motor-driven, tightly fitting glass/Teflon Potter-Elvehjem homogenizer. Nuclei and unbroken cells were sedimented 15min at 600xG. The supernatant was divided into aliquots corresponding to the following wet weights: 15mg for skeletal muscle, 10mg for brain and liver, 5mg for heart. Aliquots were centrifuged 10min at 20000xG to obtain a pellet containing mitochondrial membranes. For labelling of mitochondrial proteins with fluorescent dyes, membranes were resuspended in 250mM Sucrose, 20mM phosphate buffer pH7.5, 1mM EDTA and labelled with 10nmol NHS-Fluorescein (Pierce) / 10mg tissue wet weight for 120min on ice, and sedimented again to remove dye excess.
In order to solubilise protein complexes, mitochondrial membranes were resuspended in 50mM NaCl, 50mM imidazole pH7, 1mM EDTA, 2mM aminocaproic acid. Single OXPHOS complexes were solubilised using 20% dodecylmaltoside stock in water (w/v): 2.5µl for heart, 5µl for skeletal muscle, 10µl for liver or brain aliquots. Supercomplexes of the respiratory chain and oligomeric ATP synthase were solubilised by adding the mild detergent digitonin (20% stock in water (w/v)): 5µl for heart, 10µl for skeletal muscle, 20µl for liver or brain aliquots. Samples were centrifuged for 20min at 22,000xG and the protein content of the supernatant was measured. Equal amounts of protein/lane (50 – 100 µg/sample depending on tissue) were mixed with a 5% Coomassie blue G-250 dye stock suspension to obtain a detergent/dye ratio of 8/1.

3.8.2 Native electrophoresis

Blue native electrophoresis (BNE) and clear native electrophoresis (CNE) were performed as described (Wittig & Schägger, 2005, Wittig et al. 2006). Briefly, gels with continuous acrylamid gradients from 3 to 13% and from 4 to 13% were casted using gradient mixers, placed to electrophoresis chambers and supplemented with anode buffer (25 mM Imidazole, pH 7), cathode buffer B for BNE (50 mM Tricine, 7.5mM Imidazole, 0.02% Coomassie blue G-250, pH7) and cathode buffer C for CNE (50 mM Tricine, 7.5 mM Imidazole, pH 7). Equal protein amounts per sample were loaded to allow direct quantification analysis in 1D gels. Electrophoresis was performed at 4-7 °C, 15 mA. Cathode buffer B in BNE was changed to cathode buffer B/10 (50 mM Tricine, 7.5mM Imidazole, 0.002% Coomassie blue G-250, pH7) after the blue front has reached on third of the total gel length. Electrophoresis was continued until the front reached the end of the gel.

3.8.3 2D BN/SDS PAGE

Following separation of mitochondrial OXPHOS complexes by BNE, subunit composition was studied using 2D BN/SDS-PAGE described in Wittig et al. 2006 and Schägger, 2006. Briefly, 1D BN-strips were soaked in 1% SDS for a few minutes and a SDS-gel was casted below. 1D strips were pushed on top of the 2D gel and SDS electrophoresis was performed at room temperature. 2D gels were scanned using a Typhoon scanner (GE Healthcare) to detect Fluorescein (excitation 488nm, emission filter 520 nm*)* and same gels were then stained with silver (Rais et. al. 2004).

3.8.4 Coomassie stain of 1D BN-gels for quantification

Gels were fixed in 50% methanol, 10% acetic acid and stained with 0.025% Coomassie G250 (Serva) in 10% acetic acid. After removal of the dye in 10% acetic acid gels were scanned by an office scanner (Epson perfection 2400 PHOTO) for documentation and densitometry by Quantity One Software (Bio-Rad).

3.8.5 Complex I and V *in-gel* catalytic activity stains

In gel activity stains are used as an additional quantification method of isolated protein complexes by 1D BNE. The *in-gel* NADH: nitrotetrazolium blue (NTB) reductase and ATP hydrolysis assays followed essentially the protocols described by Zerbetto et al. 1997 with some modifications according to Wittig et al., 2007.

Complex I stain: Complex I *in-gel* activity stain was done in 1D BN-gels directly after electrophoresis. NADH is used as electron donor and via complex I nitrotetrazolium blue (NTB) is reduced to formazan, which is purple in colour and stains the position of the native enzyme within the gel. 1D BNE gels were incubated in buffer containing 5mM Tris/HCl, pH7.4, 0.1mg/ml NADH and 2.5mg/ml NTB until the purple colour was developed (approx. 30min). Reaction was stopped with 50% methanol, 10% acetic acid fixing solution for several hours to remove Coomassie. Gels were placed into water and scanned for further densitometric analysis.

ATP hydrolysis assay: Gels were incubated in 35 mM Tris, 270 mM glycine, pH8.3, 14mm $MgSO_4$, 0.2% $Pb(NO_3)_2$, 8mm ATP, pH8.3 until white lead phosphate precipitates developed at positions of ATP synthase (up to 6 hours). The reaction was stopped in 50% methanol for 30 min. Gels were placed into water and scanned for further densitometric analysis.

3.9 Functional Analysis

3.9.1 High-resolution respirometry

Respiratory Chain Complex (RCC) activity measurement of isolated mitochondria from heart tissue was performed by using the OROBOROS^{TM} Oxygraph-2k (with DatLab Software for data acquisition and analysis, Oroboros, *Oxygraph*, Innsbruck, Austria) as a highly sensitive tool to evaluate mitochondrial complex activity by monitoring oxygen kinetics at low oxygen partial pressure (Gnaiger E et al., 2000; Méndez G and Gnaiger E, 1994). The assay medium Miro5 was air-equilibrated for 30-40min before use. All experiments were carried out at 30°C. Calibration of the system, including signal correction for electrode response time, blank controls, internal zero calibration, as well as data acquisition and analyses, was carried out as described (Gnaiger E, 2010). 200µg of the enriched mitochondria were placed into

the 2ml glass chamber. A standard substrate/inhibition titration protocol was applied to measure the different segments of the respiratory chain in defined metabolic states (Kuznetsov AV et al., 2002). Complex I: rotenone-sensitive oxidation of glutamate (10mM) for 1min (shaking, dark) and malate (5mM) in the absence (resting respiration, state 2) and presence (active respiration, state 3) of ADP (50mM), inhibition with 0,5µM rotenone; Complex II: antimycin A-sensitive oxidation of succinate (10mM), inhibition with 2,5µM antimycin A; Complex IV: potassium cyanide-sensitive (KCN) oxidation of ascorbate (2mM) and TMPD (0,5mM), inhibition with 1µM KCN. To determine the effects of aging to mitochondrial function in our animal model we analyzed in addition to young Tom40 mice cohort of aged animals (~700d).

In a second trial, another titration protocol was applied to measure uncoupled respiration (state3u) using the ionophore carbonylcyanide p-trifluoromethoxyphenylhydrazone (FCCP). Respiratory control ratios (RCR) had to be around 2-3 for heart mitochondria and 4-5 for brain mitochondria, lower values suggest damage by the isolation procedure.

3.9.2 Determination of specific enzyme activities in isolated mitochondria

Mitochondria were freeze-thawed to make sure that substrates have full accessibility to the mitochondrial inner membrane. The measurement of the specific activity of the individual complexes of the respiratory chain and citrate synthase as mitochondrial activity marker was performed spectrophotometrically, as described by Sgobbo et al. (Sgobbo P et al., 2007). Aconitase activity was determined as a marker for oxidative damage (Gardner PR, 2002). Therefore an aconitase isocitrate dehydrogenase assay was performed like described in literature with minor modifications (Drapier JC and Hibbs JB Jr, 1996; Hausladen A and Fridovich I, 1996; Rose IA and O'Connell EL, 1967). All assays were performed at 37°C. The volume of reaction was 1 ml in the case of each complex. A hypotonic medium containing 25mM potassium phosphate (pH 7.4) and 5mM $MgCl_2$ was used as assay buffer.

NADH-CoQ oxidoreductase

NADH-CoQ oxidoreductase (complex I) activity was determined by following the rotenone-sensitive initial rate of NADH oxidation at 340nm. Therefore, 200µM NADH

was applied as donor and 65µM decylubiquinone as acceptor. 2,5mg/ml fatty-acid free bovine serum albumin (BSA) (2.5 mg/ml), 2 mM KCN and antimycin A (3 µg/ml) were added to the assay buffer before the assay and 50 µg/ml of protein was used. In the end, the enzymatic activity was inhibited by Rotenone (2 µg/ml).

Calculation of enzyme activity U (µmol/min):

$\Delta\varepsilon_{NADH\ 340nm}$= 6.22 mM^{-1} cm^{-1}

$V_{cuvette}$ = 200µl + sample

d= cuvette thickness (1cm)

- volume activity (U/l) = $((\Delta Abs/min - \Delta Abs/min_{rotenone}) * V_{cuvette}) / (\varepsilon * d * V_{sample})$
- specific activity (U/mg protein) = volume activity/sample concentration
- rotenone sensitivity: $1 - (\Delta Abs/min) / (\Delta Abs/min_{rotenone})$

Succinate-cytochrome *c* oxidoreductase

Succinate-cytochrome *c* oxidoreductase (complex II + III) activity was measured at 550nm as initial rate of antimycin-sensitive cytochrome *c* reduction. Mitochondrial proteins (130 µg/ml) were incubated for 10 min in the assay buffer in the presence of 20 mM succinate before measurement. Rotenone (3 µg/ml), 2 mM KCN and 65 µM decylubiquinone were added to the assay buffer. The reaction was started by the addition of 20 µM ferricytochrome *c*. The enzymatic activity was inhibited by antimycin A (2µg/ml).

Calculation of enzyme activity U (µmol/min):

$\Delta\varepsilon_{cytochrome\ c\ 550nm}$ = 21.1 mM^{-1} cm^{-1}

$V_{cuvette}$ = 200µl + sample

d= cuvette thickness (1cm)

- volume activity (U/l) = $((\Delta Abs/min) * V_{cuvette})\ \varepsilon^{-1}\ d^{-1}\ V_{sample}^{-1}$
- specific activity (U/mg protein) = volume activity/sample concentration
- antimycin A sensitivity: $1 - (\Delta Abs/min) / (\Delta Abs/min_{antimycin})$

Cytochrome c oxidase

Cytochrome c oxidase (complex IV) activity was measured by following the oxidation of ferrocytochrome *c* at 550 using 80 µg/ml of protein. The assay buffer was supplemented with antimycin A (3 µg/ml).

Calculation of enzyme activity U (µmol/min):

$\Delta\varepsilon_{cytochrome\ c\ 550nm}$= 21.1 mM^{-1} cm^{-1}

$V_{cuvette}$ = 200µl + sample

d= cuvette thickness (1cm)

- volume activity (U/l) = ((ΔAbs/min) * $V_{cuvette}$) / (ε*d*V_{sample})

- specific activity (U/mg protein) = volume activity/sample concentration

Citrate synthase

Citrate synthase activity was measured following the reduction of 0.2mM DTNB (5, 5'-dithiobis-(2-nitrobenzoic acid or Ellman's reagent) at 412nm. Proteins (80µg/ml), 0.25mM acetyl-coenzyme A, and 0.2mM DTNB were added to a Tris–HCl buffer (10 mM), pH 7.4, containing 0.2% (v/v) Triton X-100. The reaction was started by the addition of 0.4mM oxalacetate.

Calculation of enzyme activity U (µmol/min):

$\Delta\varepsilon_{DTNB\ 412nm}$= 13.6 mM^{-1} cm^{-1}

$V_{cuvette}$ = 200µl + sample

d= cuvette thickness (1cm)

- volume activity (U/l) = ((ΔAbs/min) * $V_{cuvette}$)/ ε*d*V_{sample}

- specific activity (U/mg protein) = volume activity/sample concentration

Aconitase

Aconitase is a mitochondrial enzyme that converts citrate to isocitrate. Determination of aconitase activity was done indirectly by coupling it to the NADP-linked isocitrate dehydrogenase (IDH). The rate of NADP+ reduction by conversion of isocitrate to α-ketoglutarate was recorded at 340nm. Assay buffer contained 100mM Tris/HCl pH8.0, 0.15mM cis-aconic acid, 0.5mM $MnCl_2$, 1mM NADP+, 0.3U IDH and 0.1% TritonX100. Reaction was started by adding 20µg mitochondria and recorded for 300sec.

Calculation of enzyme activity U (µmol/min):

$\Delta\varepsilon_{NADPH\ 340nm}$= 6.22 mM^{-1} cm^{-1}

$V_{cuvette}$ = 200µl + sample

d= cuvette thickness (1cm)

- volume activity (U/l) = ((ΔAbs/min) * $V_{cuvette}$)/ ε*d*V_{sample}

- specific activity (U/mg protein) = volume activity/sample concentration

3.10 Primary screen within the German mouse clinic

For systemic analysis of the mutant mouse line a cohort of 80 young animals (40 heterozygous mutants, 40 wild-type control littermates) entered the primary screen of the German Mouse Clinic. Mice were tested in the screens Dysmorphology, Behaviour, Neurology, Eye, Nociception, Energy Metabolism, Clinical Chemistry, Immunology, Allergy, Steroid Metabolism, Cardiovascular Function, Lung Function, Molecular Phenotyping, and Pathology. The animals are divided into two groups and enter a standard workflow (Fig. 1; modified after (Brown SD et al., 2005; Fuchs H et al., 2009; Gailus-Durner V et al., 2009; Gailus-Durner V et al., 2005). All standard operation protocols (SOPs) were developed by the EUMORPHIA members and are available at http://www.empress.har.mrc.ac.uk.

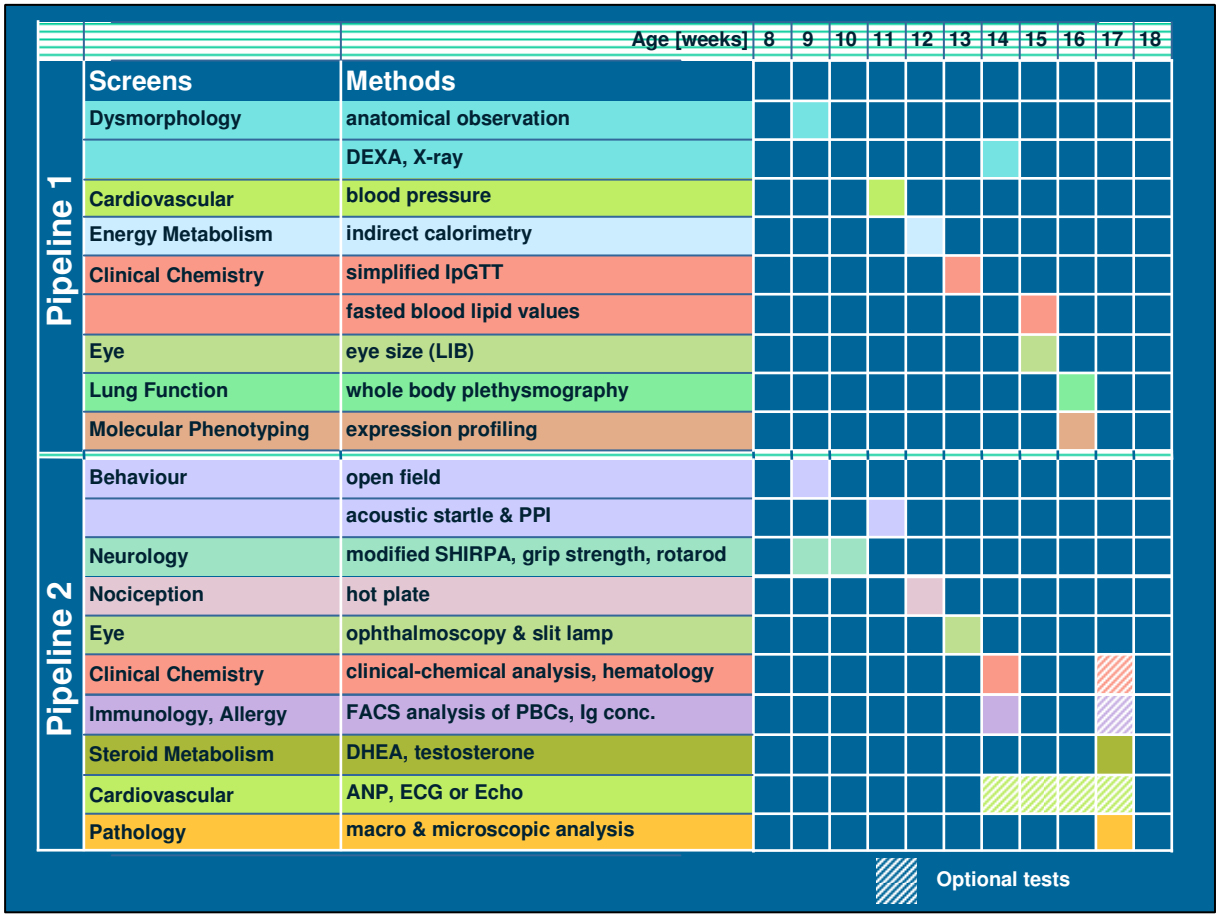

Figure 2: Two pipeline workflow in the GMC

Schematic representation of the two pipeline workflow in the GMC with involved screens and performed experiments.

3.10.1 Dysmorphology, Bone and Cartilage

Passing this module, the animals were screened for abnormal morphology in different organ systems with emphasis on bone and cartilage development and homeostasis. (Fuchs H et al., 2006). Animals were analyzed at different time points: with the age of nine weeks morphological observations were recorded in awaken mice following the protocol of Fuchs et al. (2000). X-ray and bone densitometry analysis (using dual energy X-ray absorption DEXA) were done in anaesthetized animals at an age of 14 weeks. Statistical analysis was done using StatView Software package (SAS cooperation).

3.10.2 Behaviour

The behavioural screen of the GMC addresses the question if the given mutation has behavioural consequences for the mutated mice. Naïve animals were tested in the open field task with the age of 9 weeks. Acoustic startle and Pre-Pulse-Inhibition (PPI) were done two weeks later. Open field task creates an approach-avoidance conflict in mice (exploration of new environment vs. avoidance of open spaces). Therefore it is widely used to assess anxiety-related behaviour in mice (Archer J, 1973; Choleris E et al., 2001; Crawley JN, 2008; Weiss SM et al., 2000).
Mice first were habituated to the experimental room for 30 min. Then they were placed individually into the middle of one side of the arena facing the wall and allowed to explore it freely for 20min. Determination of the animals coordinates was done using light barriers. A corridor of 8cm near the walls was determined by computer software as periphery and the remaining area in the middle as centre.

Table 2: Parameters recorded in the behaviour screen

Behaviour	**Parameters**
Forward locomotor activity	Total distance travelled in arena and periphery
Vertical exploratory activity	Rearings
Speed of movement	Average speed in arena and periphery
Immobility	Resting time in arena, centre and periphery
Anxiety-related behaviour	Latency to enter centre, Percentage time in centre, Percentage centre locomotor activity, Permanence time in centre and periphery, Centre average speed, Number centre en-tries, Centre distance travelled
Habituation	Time courses of distance travelled, rearing frequencies and time spent in centre over the observation period
Equipment: test apparatus from ActiMot, TSE (45.5 x 45.5 x 39.5 cm), illumination: 150lux (periphery), 200lux (centre)	

A detailed description can be found here:
http://www.empress.har.mrc.ac.uk/viewempress/ pdf/ESLIM_007_001.pdf
PPI is routinely applied in animal testing to get information about sensorimotor integration in the brain that is likely to be disturbed in patients with neuropsychiatric diseases like schizophrenia (Geyer MA et al., 2001; Swerdlow NR et al., 1994). The protocol used was based on the SOP on www.eumorphia.org. After a 5-min-acclimation period mice were exposed to five presentations of leader startle pulses with an intensity of 110 dB (excluded from statistical analysis). Four different prepulse intensities (67, 69, 73, 81 dB) were chosen, the startle pulse (110 dB) itself was preceded by each prepulse with a 50 msec inter-stimulus interval. The different trial types were presented to the mice 10 times (random order, organized in 10 blocks, each trial type occurring once per block). Inter-trial intervals varied from 20-30 sec.
Data were statistically analyzed using SPSS software (SPSS Inc, Chicago, USA) with a level of significance at $p<0.05$.

3.10.3 Neurology

As primary observation screen a modified SHIRPA (**S**mithkline Beecham, MRC **H**arwell, **I**mperial College, the **R**oyal London hospital **p**henotype **a**ssessment) protocol was performed (Gailus-Durner V et al., 2005). This protocol is proposed as a rapid, comprehensive and semi-quantitative screening method for qualitative analysis of abnormal phenotypes in a mouse strain (Rogers DC et al., 1997). Each test parameter contributes to an overall assessment in muscle, lower motor neuron, spinocerebellar, sensory and autonomic function. Assessment of each animal at age 10 weeks began with observation of undisturbed behaviour (*Viewing Jar Behaviour*) in a glass cylinder (11 cm in diameter). The mice were then transferred to an arena consisting of a clear Perspex box (420 x 260 x 180 mm) in which a Perspex sheet on the floor is marked with 15 squares. Locomotor activity and motor behaviour within this area was observed (*Behaviour recorded in the Arena*). This was followed by a sequence of manipulations testing reflexes (*Behaviour recorded on or above the arena*). Measurements were completed with the recording of body weight. The last part of the primary screen also involved the analysis of contact righting reflex, and contact righting reflex. A glass cylinder (35 mm diameter, 135 mm length) was used for testing of the contact righting reflex. Throughout the entire procedure, abnormal

behaviour, biting, defecation, and vocalization were recorded. Parameters were rated due to a defined rating scale (see table 4). Between testing, fecal pellets and urination were removed from the viewing jar and arena. All experimental equipment was thoroughly cleaned with Pursept-A and dried prior to testing (Details: http://www.har.mrc.ac.uk/services/%0Bphenotyping/neurology/shirpa.html).

In collaboration with the clinical chemistry screen, serum lactate levels were measured in addition.

Table 3: Parameters recorded in the neurology screen

SHIRPA	Parameter	Rating scale
Muscle/lower motor neuron function	Body position	Inactive=0, active=1, excessive=2
	Gait	Normal=0, abnormal=1
	Positional passivity	Struggle=0, no reaction=3
	Pelvic elevation	Less than 5mm=0, more than 5mm=1
	Tail elevation	Dragging=0, horizontal=1, elevated=2
	Defecation	Present=0, absent=1
	Urination	Present=0, absent=1
Spinocerebellar function	Body position	Inactive=0, active=1, excessive=2
	Gait	Normal=0, abnormal=1
	Pelvic elevation	Less than 5mm=0, more than 5mm=1
	Tail elevation	Dragging=0, horizontal=1, elevated=2
Sensory function	Transfer arousal	Freeze=0, brief=1, immediately=2
	Touch escape	No reaction=0, reaction=1, flees=2
	Gait	Normal=0, abnormal=1
	Pinna reflex	Present=0, absent=1
Autonomic function	Palpebral closure	Open=0, close=1
	Defecation	Present=0, absent=1
	Urination	Present=0, absent=1
Neurological reflexes	Contact righting reflex (CCR)	Present=0, absent=1
	Pinna reflex	Present=0, absent=1
	Corneal reflex	Present=0, absent=1
	Startle reflex	No reaction=0, normal=1, jumping=2
General appearance	Body weight	
	Body position	Inactive=0, active=1, excessive=2
	Transfer arousal	Freeze=0, brief=1, immediately=2
	Vocalization	No=0, yes=1
	Positional passivity	Struggle=0, no reaction=3
	Biting	No=0, yes=1
	Spontaneous activity	
	Locomotor activity	Number of crossed squares
	Abnormal behaviour	

The grip strength meter system determines the grip strength of the limbs, i.e. muscle strength of a mouse. The device exploits the tendency of a mouse to grasp a horizontal metal grid while being pulled by its tail. During the trial set-up, the mouse grasps a special adjustable grid mounted on a force sensor. The mouse is allowed to catch the grid with either 2 or 4 paws. Three trials were undertaken for each mouse

and measurement within one minute. The mean values are used to represent the grip strength of a mouse. All experimental equipment was thoroughly cleaned with Pursept-A and dried prior subsequent tests.
The Rotarod (Bioseb, Chaville, France) was used to get information about the animals fore limb and hind limb motor coordination, balance and motor learning ability (Jones BJ and Roberts DJ, 1968). The device was set up in an environment with minimal distracting stimuli like noise or movement.
The used Rotarod machine was equipped with a computer controlled motor-driven rotating rod. It consists of a rotating spindle and five individual lanes for each mouse. The software allowed pre-programming of session protocols with varying speed. Mice were placed on the Rotarod with head facing the direction of the rotation. During the experiment speed accelerated from 4 to 40rpm within 5min. Infrared beams were used to detect when a mouse fell down to the bottom of the Rotarod. Latency to fall of the rotating rod was measured. Animals were tested for four times with an inter trial interval of 15min. Means were used for subsequent analysis. Weight of all animals was assessed before starting with the first trial.

3.10.4 Eye Screen

In the primary screen, different methods were employed to analyze the eyes of mutant mouse line in comparison to their control littermates. For the examination of the posterior part of both eyes funduscopy (opthalmoscopy) was used. Pupils were dilated with one drop atropine (1%); mice were grasped firmly in one hand and clinically evaluated using a head-worn indirect ophthalmoscope (Sigma 150 K, Heine Optotechnik, Herrsching, Germany) in conjunction with a condensing lens (90D lens, Volk, Mentor, OH, USA) mounted between the ophthalmoscope and the eye.
Slit Lamp Biomicroscopy was performed as described before (Favor J, 1983).
For Laser Interference Biometry mice were anaesthetized with 137 mg Ketamine and 6.6 mg Xylazine per kg body weight and placed in front of the “AC Master” (Meditec, Carl Zeiss, Jena, Germany) equipped with a new technique, optical low coherence interferometry (OLCI), adapted for short measurement distances (Schmucker C and Schaeffel F, 2004). Data were statistically analyzed using MS-Excel. Differences between mouse groups were evaluated with the Student’s t-test. Statistical significance was set at $p<0.05$.

For histology eyes were fixed in Davidson solution for 24h, dehydrated and embedded in plastic medium. With an ultramicrotome transverse 2 µm sections were cut, stained with methylene blue and basic fuchsine and evaluated with a light microscope.

Table 4: Parameters recorded in the eye screen
Funduscopy
qualitative abnormalities of the retinal fundus
qualitative abnormalities optic disc
vessel alterations
development disorders
Slit lamp biomicroscopy
qualitative abnormalities of lens and cornea like opacity
development disorders
Laser interference Biometry
Axial eye length abnormalities
Histology
qualitative retinal lamination
morphology of cell layers and lens
Morphology
qualitative like size and degree of closure

3.10.5 Nociceptive Screen

The responsiveness of the intact somatosensory system to thermal pain was tested using the hot plate test (nociceptive pain). Therefore mice were placed on a metal surface maintained at 52±0.2°C (Hot plate system was made by TSE GMBH, Germany; (Eddy NB and Leimbach D, 1953)). A 20 cm high Plexiglas wall limited the locomotion of the animals to a circular area with a diameter of 28 cm. Test was stopped after one of three behaviours regarded as indicative of nociception was observed: hind paw lick (h.p. licking), hind paw shake/flutter (h.p. shaking) or jumping. Test was not repeated due to profound changes in response latencies. To avoid tissue injury 30 s cut-off time was used. Statistical analysis was performed using a statistical package Statgraphics® (Statistical Graphics Corporation, Rockville, MD). The differences between the groups were compared with ANOVA and LSD test was used as *post hoc*. Statistical significance was set at $p<0.05$.

3.10.6 Metabolic screen

In the metabolic screen of the GMC it is possible to analyze various bioenergetic parameters in. Mechanisms which lead to disturbances in body weight regulation and energy metabolism can be determined. Basal energetic demands are monitored during ad libitum feeding.

In the indirect calorimetry task, high precision CO_2 and O_2 sensors measure the difference in CO_2 and O_2 concentrations in air volumes flowing through control or animal cages. Oxygen consumption over a given period of time can be calculated with air flow through the cage measured in parallel (O2 h^{-1}animal^{-1}). CO2 production is also monitored by the system.

The respiratory exchange ratio (RER) and heat production can be calculated:

- The RER is calculated as the ratio V CO_2 /O_2.
- Heat production (HP) is calculated from V O_2 and RER using the formula: HP [mW] = (4.44 + 1.43 x RER) x VO2 [ml h^{-1}].

The test was performed at room temperature (23°C) with a 12:12 hrs light/dark cycle (lights on 06:30 CET, lights off 18:30 CET). Each mouse was placed individually in the chamber for a period of 21 hours (from 14:00 CET to 11:00 CET next day). They had access to food and water and paper tissue was used as bedding material. Metabolic cuvettes are set up in a ventilated cabinet continuously supplied with an overflow of fresh air from outside.

In addition, body mass before and after gas exchange measurements were taken. Before returning the mice to their home cage rectal body temperature was also determined. Food intake is monitored by weighing and re-weighing the feeder before and after indirect calorimetry.

To determine the body composition of the animals a whole body composition analyzer (Bruker MiniSpec) based on Time Domain Nuclear Magnetic Resonance (TD-NMR) was applied. Lean and fat mass could be determined in awaken mice.

All values are presented as means ± SEM. Two-way-ANOVA (SigmaStat, Jandel Scientific) was used to test for effects of the factors strain and sex. For oxygen consumption a Generalized Linear Model was applied with sex, genotype and body mass as factors to account for the effect of body mass on energy metabolism parameters. The Fisher test was applied for post hoc multiple comparisons.

Table 5: Parameters recorded in the eye screen
Recorded and calculated data during metabolic phenotyping
Oxygen consumption (VO2)
Carbondioxide production (VCO2)
Respiratory exchange ratio (RER)
heat production (HP)
body weight before and after indirect calorimetry
food consumption
rectal temperature

3.10.7 Clinical Chemistry and Haematology

The Clinical-Chemical Screen aims on the detection of haematological changes, defects of various organ systems, and changes in metabolic pathways and electrolyte homeostasis. 21 different clinical-chemical parameters were measured including various enzyme activities, as well as plasma concentrations of specific substrates and electrolytes (see table 8). Additionally, ten basic haematological parameters were determined and the animals were tested for glucose tolerance as well as for fasted blood lipid and glucose values.

For the intraperitoneal glucose-tolerance test, mice were fasted for 16 to 18 hours overnight. In the beginning of the test the body weight was determined. For the determination of the baseline blood glucose level, the tip of the tail was scored using a sterilized scalpel blade and a small drop of blood was analyzed with the Accu-Chek Aviva glucose analyzer (Roche/Mannheim). Thereafter mice were injected intraperitoneally with 2 g of glucose/kg body weight using a 20% glucose solution, a 25 gauge needle and a 1 ml syringe. 15, 30, 60, 90 and 120 minutes after glucose injection, additional blood samples (one drop each) were collected and used to determine blood glucose levels as described before. Repeated bleeding was induced by removing the clot from the first incision and massaging the tail of the mouse. After the experiment was finished, mice were placed in a cage with plentiful supply of water and food. To determine fasted blood lipid and glucose values, mice were fasted for 16 to 18 hours over night before blood collection. Mice were anesthetized with isoflurane and blood was taken by puncturing the retro-orbital sinus with non-heparinised capillaries (1.0 mm in diameter; Neolab; Munich, Germany). The time of sample collection was recorded in a work list. Blood samples of around 300µl volume for the measurement of fasted plasma values were collected in Li-heparin coated

tubes. Blood samples collected from non fasted mice in pipeline II were divided into two portions. The major portion was collected in a heparinised tube (Li-heparin, KABE; Nümbrecht, Germany; Art.No. 078028). The smaller portion was collected (using the same capillary) in an EDTA-coated tube (KABE, Art.No 078035). Each tube was immediately inverted five times to achieve a homogeneous distribution of the anticoagulant. The Li-heparin-coated tubes were stored in a rack at room temperature for two hours and separation of cells and plasma was achieved by a centrifugation step (10 min, 5000 x g; 8°C, Biofuge fresco, Heraeus; Hanau, Germany). Plasma was distributed between the Immunology Screen (30 µl), the Allergy Screen (30µl), the Clinical Chemical Screen (130µl) and the Cardio-Vascular Screen (residual), while the cell pellet was given to the Immunology Screen for FACS-analysis. The plasma sample for the clinical chemical analysis was transferred into an Eppendorf tube and diluted 1:2 with aqua dest. The solution was mixed for a few seconds (Vortex genie, Scientific Industries; New York, USA) to prevent clotting and then centrifuged again for 10 min at 5000 x g at 8°C. In addition, the Clinical Chemical Screen received the EDTA-blood samples for haematological investigations, which were placed on a rotary agitator at room temperature until analysis. The screen was performed using an Olympus AU 400 autoanalyzer and adapted reagents from Olympus (Hamburg, Germany) except creatinine that was measured using an enzymatic kit from Biomed (Oberschleißheim, Germany) and free fatty acids (NEFA) that were measured using a kit from Wako Chemicals GmbH (Neuss, Germany). A volume of 50µl EDTA-blood was used to measure basic haematological parameters with a blood analyzer, which has been carefully validated for the analysis of mouse blood (ABC-Blutbild-Analyzer, Scil Animal Care Company GmbH; Viernheim, Germany). Number and size of red blood cells, white blood cells, and platelets are measured by electrical impedance and haemoglobin by spectrophotometry. Three weeks after the first bleeding a second sample was collected all pipeline II animals. A subset of parameters was retested to check the reproducibility of the first results. From this second bleeding, the steroid screen was provided with plasma samples for their analyses.

Data were statistically analyzed using S-Plus 8.1 with the level of significance set at $p<0.05$, by an applying a linear regression model on the influence of genotype, sex and the interaction of both, and subsequent pair-wise comparisons of the means by T-test using Excel.

Table 6: Parameters recorded in the clinical chemistry screen	
Proteins and plasma enzyme activities	
LDH activity	
Alkaline phosphatase (ALP/ EC 3.1.3.1)	
α-Amylase (EC 3.2.1.1)	
Creatine kinase (EC 2.7.3.2)	
Aspartate-aminotransferase (ASAT/ GOT; EC 2.6.1.1)	
Alanine-aminotransferase (ALAT/ GPT; EC 2.6.1.2)	
Ferritin	
Transferrin	
Total protein	
Albumin	
Plasma concentrations of specific substrates	
Glucose	
Cholesterol	
Triglycerides	
Urea	
Creatinine	
Non-esterified fatty acid (NEFA)	
Plasma concentrations of electrolytes	
Potassium	
Sodium	
Chloride	
Calcium	
Inorganic phosphorus	
Iron	
Basic haematology	
White blood cell count (WBC)	
Red blood cell count (RBC)	
Mean corpuscular volume (MCV)	calculated directly from the cell volume measurements
Hematocrit (HCT)	MCV * RBC
Haemoglobin (HGB)	
Mean corpuscular haemoglobin (MCH)	HGB / RBC
Mean corpuscular haemoglobin concentration (MCHC)	HGB / HCT
Red blood cell distribution width (RDW)	calculated directly from the cell volume measurements
Platelet count (PLT)	
Mean platelet volume (MPV)	calculated directly from the cell volume measurements

3.10.8 Immunology Screen

In primary screen leukocyte populations in peripheral blood and immunoglobulin levels in blood plasma were measured.
Blood samples were taken by the Clinical-Chemical Screen (see chapter 3.10.7).
Peripheral blood leukocytes (PBLs) were isolated from 500 µl blood by erythrocyte lysis with NH4Cl (0.17M) - Tris buffer (pH 7.45) directly in 96-well microtiter plates. After subsequent washing with FACS staining buffer (PBS, 0.5% BSA, 0.02% sodium azide, pH 7.45), PBLs were incubated for 20 min with Fc block (clone 2.4G2, PharMingen, San Diego, USA). Afterwards cells were stained with fluorescence-conjugated monoclonal antibodies (PharMingen). After incubation, propidium iodide was added for the identification of dying/dead cells (Zamai L et al., 1996).
Samples were acquired automatically from 96 well plates with an HTS on a LSRII flow cytometer (Becton Dickinson, USA) until a total number of 30,000 living CD45+ cells was reached for each well. For analysis, intact cells are first identified by their FSC/SSC profile. These cells were gated on the basis of their propidium iodide/PE signal (compensated parameters), allowing the dead cells to be gated out. Living cells were then gated using their SSC/CD45 signal, gating out remaining erythrocytes, thrombocytes and debris (Weaver JL and Broud D, 2002). CD45+ cells were subsequently analyzed by software based analysis (Flowjo, TreeStar Inc, USA).
The plasma levels of IgM, IgG1, IgG2a, IgG2b, IgG3, and IgA were determined simultaneously in the same sample using a bead-based assay with monoclonal anti-mouse antibodies conjugated to beads of different regions (Biorad, USA), and acquired on a Bioplex reader (Biorad). The presence of rheumatoid factor and anti-DNA antibodies was evaluated by indirect ELISA with rabbit IgG (Sigma-Aldrich, Steinheim, Germany) and calf thymus DNA (Sigma-Aldrich), respectively, as antigens and AP-conjugated goat anti-mouse secondary antibody (Sigma-Aldrich). Serum samples from MRL/MpJ-Tnfrsf6lpr mice (Jackson Laboratory, Bar Harbor, USA) were used as positive controls in the autoantibody assays.

3.10.9 Allergy Screen

Mice were screened for alterations in plasma total IgE concentrations. Blood samples were taken by puncturing the retroorbital plexus under isoflurane anaesthesia (see chapter 2.5.7). Plasma was analyzed for total IgE, using a classical immunoassay isotype-specific sandwich ELISA. Briefly, 96-well microtiters were coated with 10 µg/ml anti-mouse-IgE rat monoclonal IgG (clone-PC284, The Binding Site) to detect total IgE. Serum samples were diluted 1:10 and standards for murine IgE (Mouse IgE, k clone C38-2 BD Pharmingen™) were appropriately diluted. As secondary antibodies, biotinylated rat anti-mouse IgE (clone R35-118, BD Pharmingen™) were used followed by incubation with BD OptEIA Reagent Set B (Cat. No. 550534 BD Pharmingen™) Plates were analyzed using a standard micro well ELISA reader at 450 nm. Total murine IgE data are reported in ng/ml, based on a standard curve of purified murine IgE (Alessandrini F et al., 2001).

3.10.10 Steroid Screen

The main focus of the Steroid Screen is the identification of new animal models for human steroid-related diseases therewith supporting the development of their future medical treatment. For primary screening the key steroids dehydroepiandrosterone (DHEA) and testosterone (Labrie F et al., 1995) are extracted from plasma and quantified by ELISA.

Since no steroid ELISA kits are available for mouse samples, human ELISA kits have been adopted. Prior to measurement, steroids had to be extracted from the matrix by liquid/liquid-extraction to avoid mouse plasma matrix effects. 75 µl of plasma were extracted three times in each case with a tenfold excess of *tert*-butylmethylether (TBME). The combined organic extracts were evaporated, dissolved *de novo* in TBME, subdivided equally for the two ELISA tests (DHEA and testosterone) and evaporated again. The material was reconstituted for the respective kit, DHEA in assay buffer, testosterone in steroid free serum.

The steroids were quantified by competitive ELISA according to the manufacturer's protocols (Testosterone ELISA: DRG Instruments GmbH, Catalog No. EIA-1559, DHEA ELISA: AssayDesigns, Catalog No. 901-093). The plates were read in a standard microplate reader at a wavelength of 405 nm (DHEA) and 450 nm (testosterone). The concentrations were calculated upon the calibration from the

respective standard curve and reported in pg/ml (DHEA) and ng/ml (testosterone). The sensitivity of the tests is 2.9 pg/ml for DHEA and 0.083 ng/ml for testosterone.

3.10.11 Cardiovascular screen

The standard primary cardiovascular screen includes tail-cuff blood pressure (BP) analysis, transthoracic echocardiography and heart weight determination. For the Tom40 animal model the workflow was modified: instead of Echocardiography Electrocardiography (ECG) was done.

A non-invasive tail-cuff method using a MC4000 Blood Pressure Analysis Systems (Hatteras Instruments Inc., Cary, North Carolina, USA) was used for measuring the blood pressure in awaken mice. Four animals were re-strained on a pre-warmed metal platform and covered with metal boxes to minimize stress. Tails were looped through a tail-cuff and fixed in a notch containing an optical path with a LED light and a photosensor. Light extension changes caused by the blood flow in the tail artery was measured and transformed into an optical pulse signal. Pulse detection, cuff inflation and pressure evaluation were automated by the system software. First, animals passed five initial inflation runs for habituation, and then 12 measurement runs were performed for each animal in one session. Runs with movement artefacts were excluded. Animals were trained for one day to habituate them to the protocol and the equipment. Measurements are performed on four consecutive days between 8:30 and 11:30 am.

ECG was performed in a faraday cage. Mice were sedated (isoflurane/pressured air inhalation) and three metal bracelets were placed on the joints of the feet together with electrode gel. The position of the electrodes was on the front-paws and the left hind-paw which results in the bipolar standard limb leads I, II and III and the augmented unipolar leads AVF, AVR, AVL. Duration of the measurement was about seven minutes.

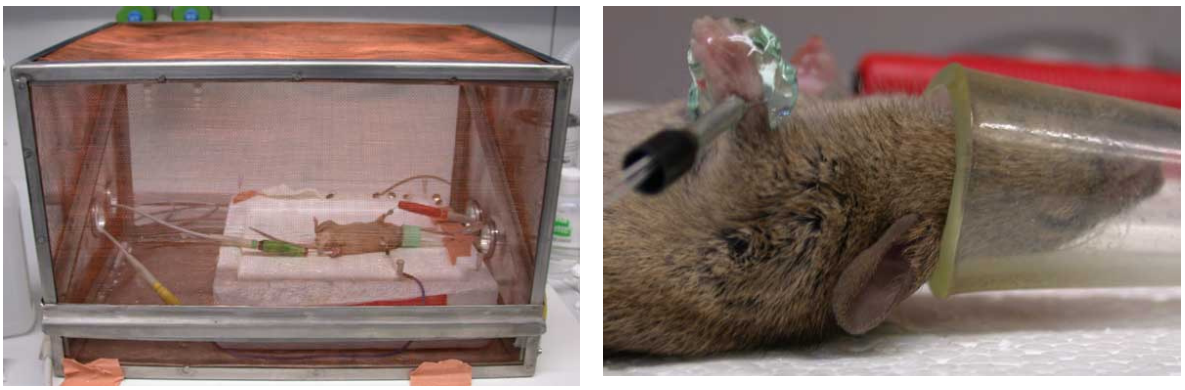

Figure 3: ECG setup in the cardiovascular screen.

A shape analysis of the ECG traces was performed with the software ECG-auto (EMKA technologies, Paris, France). For each animal, intervals and amplitudes were evaluated from five different sets of averaged beats (usually lead II). The parameter Q-T interval is also corrected for the RR interval. Additional, the recordings were screened for arrhythmias, including supraventricular and ventricular extrasystoles and conduction blockages. Sets of five analyzed beats were averaged for one animal. The data were analyzed statistically using Statistica. Analysis of variance (ANOVA) tests are used for multi-factorial analysis of sex and genotype. Post hoc analysis for multiple comparisons included a Duncan's Multiple Range Test & Critical Ranges.

Heart weight was determined in cooperation with the Pathology Screen. Furthermore, body weight and tibia length was measured. Animals were sacrificed using CO_2, weighed and opened from the ventral midline. Blood was removed by cutting the dorsal aorta. Heart was analyzed for abnormalities or excessive fat. For dissection, heart was first removed from the pericardial membrane, and then the major vessels were cut through at the point they enter or exit the atria. The heart weight was obtained wet after blotting the organ on paper towels. The tibia length was determined from the left tibia of the mouse using a ruler.

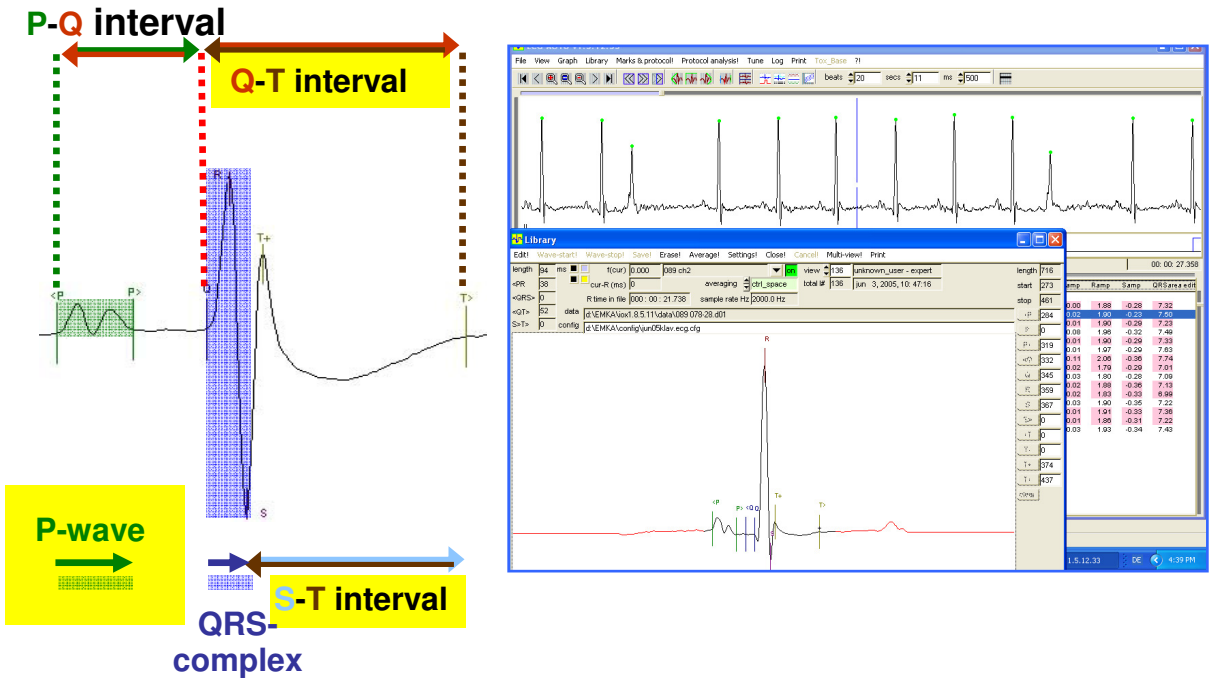

Figure 4: ECG evaluation

Table 7: Parameters recorded in the cardiovascular screen		
Blood pressure		
Systolic Pressure		
Diastolic Pressure		
Mean Arterial Pressure (MAP)		
Pulse		
Electrocardiography		
p-wave duration	Q-Tc	Arrhythmias: • Supraventricular extrasystoles • Ventricular extrasystoles • conduction blockages
P-Q intervals	S-T interval	
QRS complex	J-T interval	
Q-T interval	Q-, R- and S-amplitude	
Heart rate/R-R interval		
Heart Weight Analysis		
Heart Weight		
Body Weight		
Tibia Length		
Heart Weight per Body Weight Ratio		
Heart Weight per Tibia Length Ratio		

3.10.12 Lung Function Screen

Spontaneous breathing patterns during rest and activity were studied in mice from Pipeline 1. Therefore pressure changes which arise from inspiratory and expiratory temperature and humidity fluctuations during breathing were measured in unrestrained animals by a system of Buxco® Electronics (Sharon, Connecticut) according to the principle described by Drorbaugh and Fenn (1955).

These pressure swings are transformed into flow and volume signals so that automated data analysis provides tidal volumes (TV), respiratory rates (f), minute ventilation (MV), inspiratory and expiratory times (Ti, Te), as well as peak inspiratory and peak expiratory flow rates (PIF, PEF). To minimize potential effects of the circadian rhythm measurements were always performed between 8:00am and 11:00am. Measurements were done for 40 min in a quiet room where temperature and humidity were kept constant. Before each measurement, the system was calibrated and the actual barometric pressure, temperature, and humidity were supplied to warrant adequate calculations of flow rates and volumes. Animals were placed into the chamber and data recording was immediately started.

There are three-four typical phases during a measuring period:

First, the animals are stressed (respiratory rate was highest). Usually after 5 min the animals become calmer – *phase of activity* (exploring grooming). Later more and

more phases of rest or even short periods of snoozing occur – *resting phase* (sometimes even to *phases of sleep*).

The frequency histogram of the respiratory rates was determined, and breathing was analyzed during the phases of activity and rest. Beside the directly recorded parameters, mean inspiratory and expiratory flow rates (MEF, MIF) were calculated (ratio of tidal volume and the respective time interval). Additional, the relative duration of inspiration (Ti/TT) was calculated (ratio of inspiratory time to total time required for the breathing cycle). By relating the absolute values to the body weight of the animal specific tidal volumes and minute ventilations (sTV, sMV) could be determined. The mean of all breathing frequencies (mean_f) measured during the 40-minute-period was calculated to assess whether the duration of rest and activity was similar in all mouse strains.

Heart weight was determined in cooperation with the Pathology Screen. Furthermore, body weight and tibia length was measured. Animals were sacrificed using CO_2, weighed and opened from the ventral midline. Blood was removed by cutting the dorsal aorta. Heart was analyzed for abnormalities or excessive fat. For dissection, heart was first removed from the pericardial membrane, and then the major vessels were cut through at the point they enter or exit the atria. The heart weight was obtained wet after blotting the organ on paper towels. The tibia length was determined from the left tibia of the mouse using a ruler.

Table 8: Parameters recorded in the lung screen
Directly recorded data
Tidal volumes (TV)
Respiratory rates (f)
Minute ventilation (MV)
Inspiratory and expiratory times (Ti, Te)
Peak inspiratory and peak expiratory flow rates (PIF, PEF)
Calculated data
Mean inspiratory flow rates (MEF)
Expiratory flow rates (MIF)
Relative duration of inspiration (Ti/TT)
Specific tidal volumes (sTV)
Minute ventilations (sMV)
Mean of all breathing frequencies (mean_f)

3.10.13 Molecular Phenotyping

The aim of the molecular phenotyping screen is the detection of transcriptional affected organs by analyzing RNA expression data. Therefore, organs of mutant mice are collected for subsequent DNA-chip expression profiling analysis. For details see (Horsch M et al., 2008). Briefly, 18weeks old animals were killed by CO_2 asphyxiation between 9am and 12am (minimize influence of circadian rhythm to gene expression). The following nine organs were archived in liquid nitrogen following the established SOPs (Standard operation protocols): spleen, kidney, testis, liver, pancreas, heart, lung, thymus, skeletal muscle and brain. We chose heart and muscle for further analysis.

For preparation of total RNA organs were thawed in Trizol (Sigma) and homogenized using a Polytron homogenizer. Total RNA was obtained according to manufacturer's instructions using RNeasy Midi kits (Qiagen) and RNA concentration was calculated from $OD_{260/280}$ measurement. To check for RNA integrity 1 µg RNA was run on a formaldehyde agarose gel to check for RNA integrity. The RNA was stored at -80°C in RNase free water (Qiagen).

Two chip hybridizations were performed with RNA from heart and muscle of each individual mutant mouse. Chip hybridization was performed against the identical pool of the same organ of reference RNAs (reference RNA pool). For each individual mutant mouse the chip experiments include a colour-flip experiment (in total eight hybridizations/organ).

For reverse transcription 15 µg of total RNA was used. It was indirectly labelled with Cy3 or Cy5 fluorescent dye according a modified TIGR protocol (Hegde P et al., 2000; Horsch M et al., 2008). Labelled cDNA was dissolved in 55 µl hybridization buffer (6x SSC, 0.5% SDS, 5x Denhardt's solution and 50% formamide) and mixed with 55 µl of reference cDNA solution labelled with the second dye. The mixture subsequently was injected on a pre-hybridized microarray in a HS4800 Hybstation (Tecan) and incubated at 42°C for 16 h. After hybridization slides were washed with 3x SSC, 1x SSC, 0.5xSSC and 0.1x SSC at RT, dried with nitrogen and scanned with a GenePix 4000A microarray scanner. The resulting images were analyzed using the GenePix Pro6.1 image processing software (Axon Instruments, USA) (Horsch M et al., 2008).

3.10.14 Pathology Screen

The morphological phenotyping of the animals and immunhistochemistry was done by the pathology screen.

Mice were sacrificed by CO_2 inhalation. The thymus and left lobe of the liver were measured. Blood samples were taken, centrifuged and the serum was saved at –20°C. Tails were preserved at -70°C for further genetic analysis. Following a complete dissection, an x-ray of the complete bone structure was taken, when indicated (Hewlett Packard, Cabinet X-Ray System Faxitron Series). All organs were fixed in 4% buffered formalin and embedded in paraffin for histological examination. Two-µm-thick sections from skin, heart, muscle, lung, brain, cerebellum, thymus, spleen, cervical lymph nodes, thyroid, parathyroid, adrenal gland, stomach, intestine, liver, pancreas, kidney, reproductive organs, and urinary bladder were cut and stained with hematoxylin and eosin (H&E).

Table 9: Parameters recorded in the immunology screen
Organ dissection
Measurement of the thymus
Measurement of the left lobe of the liver
Blood samples
Tail biopsy
Organs were fixed in 4% formalin
H&E staining
Skin, heart, muscle, lung, brain, cerebellum, thymus, spleen, cervical lymph nodes, thyroid, parathyroid, adrenal gland, stomach, intestine, liver, pancreas, kidney, reproductive organs, urinary bladder

3.11 Secondary screen of a second Tom40 cohort

Because of the results of the GMC screen and the fact that many diseases manifest with progressing age, a second Tom40 cohort was generated and analyzed in various screens at different ages. All animals of the aging cohort were tested with the standard neurological primary screen methods (SHIRPA, Rotarod and Grip), young with an age of 4 months and aged with 17months. Beyond that, mice were analyzed in various extra tests that are established in the neurological screen of the GMC (pole test, beam walk and horizontal ladder beam task). Moreover, the Tom40-aging cohort was the first mutant mouse line that was examined using a new installed Running wheel system provided by TSE (TSE Systems, Bad Homburg, Germany). In cooperation with the vestibular screen, animals were checked for gait abnormalities on the DigiGait (age of animals: 10month). The eye screen performed Scheimpflug imaging and optical coherence tomography as secondary screen in aged animals

(~17months). Because of the already mentioned influence of mitochondria in neurodegeneration and aging as well as in several diseases, the behaviour screen offered an extensive memory task battery for young as well as aged Tom40 mice.

3.11.1 Additional neurological tests

3.11.1.1 Pole test

The pole test is used for the assessment of motor coordination (Freitag S et al., 2003; Karl T et al., 2003). The used protocol that was developed by the groups of Matsuura (Matsuura K et al., 1997), Fernagut (Fernagut PO et al., 2003) and Korpi (Korpi ER et al., 1999), with minor modifications. The device is made of a round, metal threaded bar (50 cm high, 1cm diameter; figure 5 C) which was inserted vertically in a platform. Each animal was placed at the top of the bar with its head upwards. The mouse climbed down the pole and its style was rated due to a defined rating scale:

- 5: turns at top half
- 4: turns at under part
- 3: turns half but not complete and walks down sideways
- 2: turns down backwards
- 1: falls down/springs down
- 0: stays on pole

The time the mice needed to turn around completely head down was recorded (T-turn) as well as the time to reach the floor with all 4 paws (T-total). To decrease the effects of vision impairments a small Petri dish with bedding from the home cage was placed at the bottom of the pole to give an olfactory clue towards home cage. Each mouse was habituated to the pole on the day prior to testing. Experiment was repeated five times per session. The best performance of the five descents was chosen for evaluation. If the animal was unable to turn completely downwards, fell or slipped down, the default value of 120 sec was taken into account for T-turn and T-total.

3.11.1.2 Beam walk

Beam walk is commonly used to make conclusions about motor coordination and balance in small rodents (Carter RJ et al., 2001). This method allows monitoring the

sensorimotor system and recovery after cortical or spinal cord injuries (Kunkel-Bagden E et al., 1993). Also in animal models of stroke this experiment was frequently used (Alexis NE et al., 1995). The basic protocol that was used slightly modified was described Rebecca Carter and colleges (Carter RJ et al., 2001). Within this test, animals had to pass a horizontal wooden beam with a length of one meter at which 10cm on both ends were excluded and measurements were taken from the central 80cm part (see figure 5A). Three different types of stripes were used with a medium (13mm) and a large square (20mm) and a round (15mm diameter) cross section. The beam was placed on top of two cages (20cm high, a clean cage on the one hand and the home cage on the other hand), and the animals had to walk towards their home cage. The day before starting the experiment, animals were trained to traverse each beam for at least three times. Weight was recorded immediately before start testing. Experiment itself was repeated three times for each beam type, starting with the widest beam. Animals had to cross the beam in less than 60sec, the number of footslips, time to cross and numbers of falls were noted. Beams were cleaned with Pursept-A after each mouse. As forepaw footslips are very rare in this task, there was a not differentiated between fore and hind paw slipping. All trials were recorded with a video camera. For evaluation, mean and best trials of each parameter were calculated for the different beam types.

3.11.1.3 Ladder

The horizontal ladder beam task was invented by Metz and Whishaw to assess skilled walking in rodents (Metz GA and Whishaw IQ, 2002, 2009). The ladder walk test apparatus consists of two Plexiglas walls (1m X 20cm) that are connected via metal rungs with a diameter of 3mm (see figure 5 B). The width of the alley was adjusted to the animals' size (mice should be not able to turn around easily). An irregular pattern of the metal rungs was used, the distance between the rungs varied from 1 to 5cm. The whole set up was elevated 30cm over the ground with a neutral cage at the beginning and the home cage as refuge at the end. All animals were trained to cross the ladder on one day and tested at the next day. Training and testing was done three times per session.

Time to cross the ladder was recorded and number of fore paw and hind paw slipping was counted. If an animal turned around while traversing the ladder, the trial was aborted and re-started after the animal was placed again at the starting point.

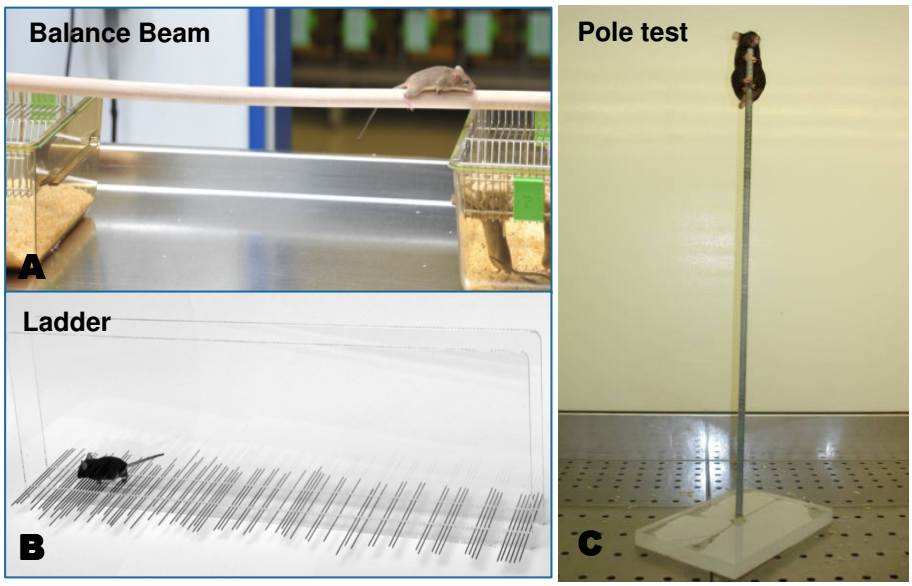

Figure 5: Additional neurological tests
A: Balance beam, B: Ladder walk test apparatus and C: Pole test

3.11.1.4 Gait analyses

Analysis of the gait of 10 month old Tom40 mice was done by the members of the vestibular group that is closely connected to the neurological screen of the GMC.
The DigiGait System (Mouse Specifics, Inc.) consists of a motorized transparent treadmill belt and a high speed camera, which captures the dynamics of the paws and corresponding limbs during mice locomotion. A rectangular transparent chamber is mounted over the tread and serves to keep the mouse within the view of the camera. Light sources are located below and above the mouse to obtain optimal contrast between the paws and body of the mouse. The hind paws and forepaws of mice were painted with red non-toxic paint to enhance visual contrast. Each animal was allowed to run on a clear treadmill belt at speeds of 20 and 35 cm/s. Mice were placed on a stationary treadmill, which was then accelerated to a test speed. For each animal, one trial (500 frames of video) at each speed, in which the animal maintained constant position on the treadmill belt with at least ten complete strides (during at least four seconds but not longer than one minute), was selected for subsequent gait analysis. One complete stride is defined as two consecutive contacts

of a given foot with the treadmill belt. Aberrant strides are excluded from the analysis (jumps, partial steps or “stop and go” walking) (Amende I et al., 2005; Wooley CM et al., 2005). Subsequent examination of different gait parameters was done using DigiGait analysis software which generates “digital paw prints” and dynamic gait signals, representing the temporal record of paw placement relative to the treadmill belt (Fig.6 A). The software automatically quantifies spatial and temporal indices of gait in walking or running animals. Paw placement of each limb is monitored throughout the gait cycle at up to 150 frames per second with a spatial resolution of more than 5 000 pixels per cm^2. Numerous postural and kinematic metrics of gait dynamics is determined by dissecting the time each limb is spent in various position of walking phase (Fig. 6 B).

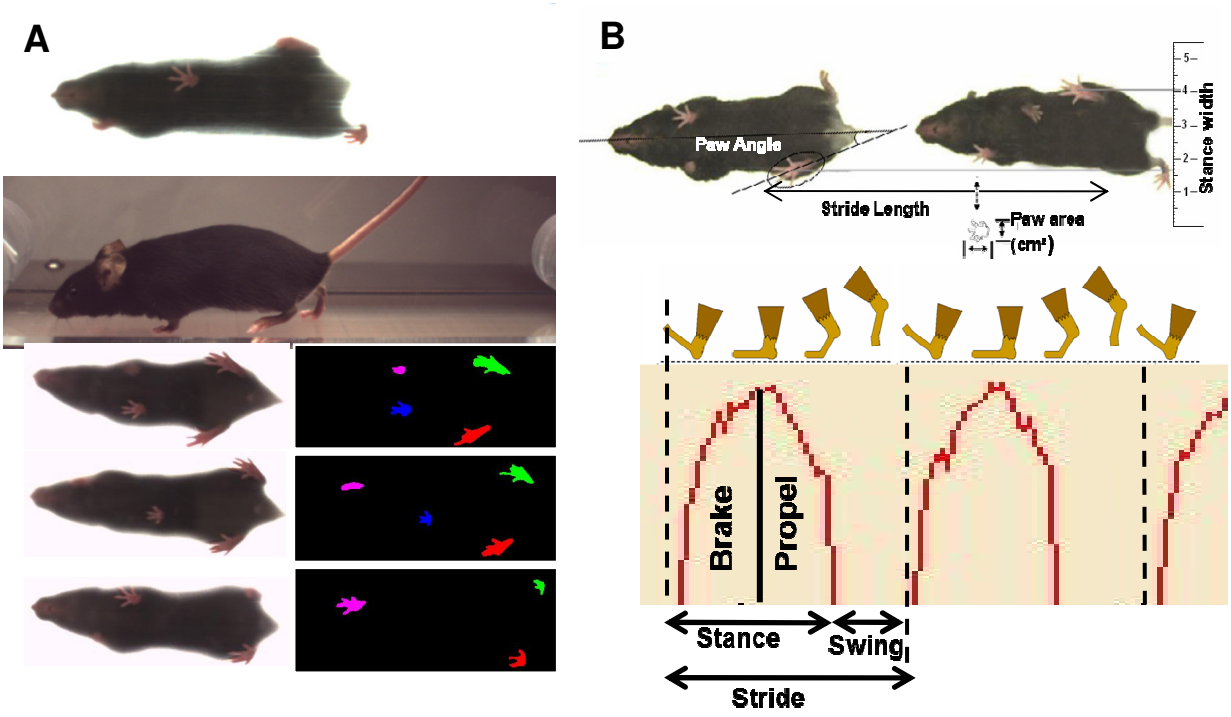

Figure 6: Gait analysis using the DigiGait system

A: Mice walk on a motorized transparent treadmill belt. Below there is a video camera mounted to capture the image of the ventral side of the animals. DigiGait™ software generates „digital paw prints“and dynamic gait signals.. This represents the temporal record of paw placement relative to the treadmill belt. B: Gait cycle components: durations of stance, swing, stride, propel, and brake are measured for every single paw. For statistical analysis, the means of fore/hind limbs are calculated and used for data interpretation 37 gait parameters are calculated from at least 11 strides

The gait signal of each limb comprises the stride duration, which includes the stance duration when the paw of a limb is in contact with the walking surface. Stance duration is subdivided into braking duration (increasing paw contact over time) and propulsion duration (decreasing paw contact area over time). A spreadsheet-ready

format with more then 30 gait indices, including stance, swing, braking, propulsion, and stride is used for further statistical analysis. The DigiGait software determines treadmill contacts of individual paws and then uses this to derive more than 30 different indices including time-domain gait parameters (stride, stance and swing time). For statistical analysis, at least 10 strides for each limb are to be included for a valid data set. Only strides recorded when the mice are walking in a fixed position relative to the camera are used. Values for each parameter are calculated using the average of all valid strides for each of the four paws.

For statistical analysis of data, the mean values for pairs of fore- and hind limbs were used. Due to strong influence of body weight and body length on the gait performance, those factors are also included into the model in order to find out their combined effects on the data. Multifactor analysis of variance (ANOVA) is performed to determine the statistical significance among the groups.

Table 10: Parameters recorded during gait analysis

Gait index	Description
Stride length	The spatial length that a paw traverses through a given stride
Stride	Time duration of the one complete stride for one paw.
Swing	Time duration of the swing phase (no contact of paw with the belt)
% Swing/Stride	Percent of the total stride duration that the paw is in the air.
Stance	Time duration of the stance phase (paw contact with belt), is equal to the sum of braking duration and propulsion duration.
% Stance/Stride	Percent of the total stride duration that the paw is in any contact with the belt.
Stance width	Width between both forelimbs and between both hind limbs.
Brake	Time duration of the braking phase (initial paw contact to maximum paw contact)
%Brake/Stride	% of the total stride duration that the paw is in the braking phase.
%Brake/Stance	% of the stance phase that the paw is in the braking phase.
Propel	Time duration of the propulsion phase (maximum paw contact to just before the swing phase)
%Propel/Stride	% of the total stride duration that the paw is in the propulsion phase.
%Propel/Stance	% of the stance phase (paw contact) that the paw is in propulsion phase (paw coming off of belt).
Hind limb shared stance	Time both paws contact the belt. Also known as “double support”.
Paw angle	The angle that the paw makes with the long axis of the direction of animal motion.
Max dA/dT	Maximal rate of change of paw area in contact with the treadmill belt during the braking phase.

3.11.1.5 Running wheels

To offer mice the possibility of voluntary running in their home cage, a TSE running wheel system for small laboratory animals was established in the neurological screen of the GMC. In cooperation with TSE systems the wheels had to be adjusted for the use in the standard GMCII IVC-rack system (Tecniplast, Aero - Mouse IVC Green Line, Buguggiate (VA) Italy). They provided a system consisting of a control unit with integrated electronic brake and a wheel drum (diameter drum 115mm, width drum: 40 mm, diameter stainless steel grid rods:4mm, distance between rods: 8.9mm centre to centre). Control unit was connected with a data cable to a computer. A second cable connected the wheel to a brake control device. Brake strength could be gradually regulated from 1 to 10. Wheel and control unit were fixed on a metal mask that should prevent the mouse climbing on the control unit and bite through the cables. Data were acquired by Phenomaster Software. Left and right rotations were counted, as well as number of runs, time that was spent on the rod [min], average and maximum speed [m/s] and maximal continuous run length [sec]. The program calculated from the number of wheel rotations the distance the mice covered. The recording interval was set to 5min. 14 - 16 months old mice were weighed before the experiment and put individually to the running wheel cages. For two weeks, animals were allowed to use the running wheels voluntary and without restrictions, in the third weeks, workload control was enabled by activating the brake and thereby raise running resistance of the wheel. Two different brake intensities were chosen for this experiment (5 and 7). Cages were changed once a week, animals were weighted and wheels were cleaned with water and Pursept-A. To document changes in body composition due to the lasting exercise, 3 wildtype and 3 heterozygous animals were examined with the Mini Spec of the metabolic screen (see chapter 2.5.6).

Figure 7: Running wheel integrated in an IVC cage

3.11.2 Memory tasks

The Behaviour Screen (Dr. Sabine Hölter, Institute for Developmental Genetics) used two different tests to get information about the animals` cognitive abilities: social discrimination and object recognition.
Social Discrimination and the Object Recognition task were performed as previously described (Feil et al., 2009; Pham et al., 2010). In the Social Discrimination test olfactory stimuli that are used of small rodents for social communication are used. The mouse was exposed for 4 min to an unknown conspecific (an ovariectomized female was used for this purpose). After an inter-exposure interval of 2 hours they were presented to two mice, the familiar mouse from the first task together with another, novel animal (simultaneous discrimination task). If the tested animal is able to remember the first mouse it will spend more time in olfactory investigation of the second unfamiliar one.
The Object Recognition task works the same way, it is a simultaneous discrimination task and consists of three 5 min sample trials with an intertrial interval of 15 min, and two test trials, 3 hours and 24 hours after the end of the third sample trial.
Like in the Social discrimination task, a mouse with an intact recognition memory will spend significant more time investigating the new object then the familiar one. A recognition index was calculated: index = investigation time novel / (investigation time familiar + investigation time novel). All data were analyzed using the Observer 4.1 Software (Noldus, Wageningen, Netherlands).

3.11.3 Quantification of dopaminergic neurons in the brains of aged mice

This experiment was performed in cooperation with Dr. Daniela M. Vogt Weisenhorn and her team from the institute of developmental genetics (IDG). Animals (n=5 for each genotype) were asphyxiated with CO_2, the thoracic cavity was opened via scissors to dissect the heart and a blunt needle was inserted through the left ventricle into the ascending aorta. Then, the right atrium was opened by a small cut. A pump was used to rinse the vessels with PBS. This was done until the liver became pale. For perfusion 4% precooled, fresh diluted PFA/PBS was pumped through the animal for 4-6 min until its body got stiff. Afterwards mice were decapitated and the brains were carefully dissected removing bones and meninges. Brains were postfixed in 4% PFA/PBS for 1-4h at 4°C and equilibrated in 20% sucrose in 1x PBS at 4°C

overnight. Frozen sections were generated on the cryostat (Microm International GmbH, Walldorf, Germany). The tissue was fast frozen at -50°C on an object holder with freezing medium. Horizontal sections of 40 µm thickness were cut with an object temperature of -14°C to -16°C, and a blade temperature 2°C below the temperature of the object. Series of 12 were collected free-floating in cryoprotection solution and stored at -20°C. For 3,3'-Diaminobenzidine (DAB) staining sections were taken out of the cryo protection solution and washed overnight in 1x PBS at RT. Then they were treated according to the following protocol.

step	time	solution	remarks
wash	3 x 10 min	1x PBS	
incubate	10 min	0.1% H_2O_2 1x PBS	
wash	2 x 10 min	0.1% Triton-X/PBS (1x)	
blocking	2 h	2% fetal calf serum in 0.1% Triton-X/PBS	RT
1st antibody	over night	1st antibody in 0,1% Triton-X/PBS	4°C
wash	6 x 10 min	0.1% Triton-X/PBS	
2nd antibody	45 min	2nd antibody (1:300), 0.1% Triton-X/PBS	RT
wash	6 x 10 min	0.1% Triton-X/PBS	
intensifying	45 min	ABC (1:300) in 0.1% Triton-X/PBS	RT, keep dark
wash	4 x 10 min	0.1% Triton-X/PBS	
wash	2 x 10 min	0.1M Tris-HCl	
DAB-staining	2-20 min	0.05% DAB, 0.02% H_2O_2 in Tris-HCl; prepare fresh and put on sections immediately	keep dark
wash	10 min	Tris-HCl	
wash	10 min	1x PBS	

After immunohistochemistry, sections were mounted on slides out of 1x PBS, air dried, embedded in Roti-Histokitt II, covered carefully with cover slips to avoid air bubbles, and dried over night under the hood.

1st Antibody: polyclonal rabbit anti-tyrosine hydroxylase (TH) from Chemicon (Chemicon International; AB152); 1:1000

2nd Antibody: Biotinylated Goat Anti-Rabbit IgG Antibody (Vectastain ABC Elite kit, Vector Laboratories)

ABC-solution: from Vectastain (Vectastain ABC Elite kit, Vector Laboratories)

For stereological quantification of dopaminergic neurons, the mounted sections were observed under the stereo microscope. Out of the twelve series originating from one mouse brain, two series with an interval of six were chosen randomly for every brain. Stained cells of the substantia nigra were counted blind using the Stereo Investigator software, descending from dorsal to ventral. The following settings were used:

Serial section manager

block advance	40 µm
mounted sections thickness	25 µm
evaluation interval	6
Z axis value	0

Optical fractionator

x-value	150 µm
y-value	150 µm
desired sampling sites	10 (or lower value as given by the program for most dorsal sections with small substantia nigra area)
fixed distance	3 µm
optical dissector height	20 µm
mounted section height	25 µm

Numbers of cells per brain were calculated by Stereo Investigator software and recorded. Statistical analysis were performed using GraphPad Prism software.

3.11.4 Secondary eye screen in aged mice

Secondary screening was done by Dr. Oliver Puk from the eye screen in the GMC. 20 aged Tom40 mice (5 males and 5 females per genotype, age: ~500 days) were analyzed by Scheimpflug imaging technique (Puk O et al., 2009). This method is used within the eye screen of the GMC for objective cataract quantification (Fuchs H et al., 2011). Additional, the retina of three mutant and three wildtype males was imaged using optical coherence tomography (OCT).

For Schleimpflug imaging, anaesthetized mice were placed in front of the Oculus Pentacam (Oculus GmbH, Wetzlar, Germany) on a polystyrene platform in a darkened environment. Eyes were treated with 1% Atropine prior to scanning and dried to avoid reflections. The vertical blue examination slit (475 nm) was orientated in the centre of the eye ball. Fine adjustment of the optimal distance between the eye of the mouse and the camera was done by moving the joystick as proposed by the fine positioning arrows (disappeared when position was considered to be optimal) given by the Pentacam software. Due to the small size of a mouse eye scanning had

to be started manually. The opacification pattern was properly reflected by the automatically generated densitometry diagram.
OCT analysis was done as described by Fischer and his co-workers (Fischer MD et al., 2009). In brief, it is possible to get sectional images of the retina *in vivo* by investigating interferences that are triggered by varying degrees of light reflection (Spraul CW et al., 1998) Membrane-rich layers appear dark (i.e. nerve fibers or synapses) in contrast to light layers that contain only a few membranes.
Animals were sedated with a Ketavet-Xylazin narcosis (5ml NaCl, 1ml Ketavet, 250µl xylazine) and eyes were treated with 1% atropine. Sectional images of the retina were taken with a Spectralis OCT. Simultaneously Fundus was imaged using a confocal scanning laser optahlmoscopy (SLO). Method is described in Fischer et al . 2009. Due to his protocol, a contact lens (optical lens, 100diopter) with Methocel® was placed on the eye of the mouse. To make OCT images in mice possible, the Spectralis OCT system had to be expanded with an additional Volk 78 D magnifying glass. Afterwards, sectionalk images of the retina were reworked with Adobe® Photoshop®.

3.12 Transmission Electron Microscopy

In order to get information about possible morphological differences between wildtype and mutant mitochondria Transmission Electron Microscopy of heart tissue mitochondria was performed in collaboration with the pathology screen of the GMC. One male and one female animal of each genotype (age: ~3month) were used for this experiment. Animals were killed using CO_2 asphyxiation, hearts were dissected and fixed over night in 2,5% Glutaraldehyd in Cacodylatpuffer (0,2M pH 7,4; Fa.SCIENCE SERVICES). Samples were washed three times in Cacodylatbuffer for 20min and fixed again in a Dalton's chrome osmium fixative for 1-2hours:

$K_2Cr_20_7$ (Potassium dichromate) solution (5%) pH 7,2	100 ml
NaCl (3,4 %)	100 ml
OsO_4-solution (2%)	200 ml

Afterwards samples were washed in ddH_2O (double distilled water) for 30min.

Dehydration was performed using an ascending alcohol series:

50% EtOH
70% EtOH (15-20 min each)
90% EtOH
96% EtOH
100% EtOH (3times, 15-20min each)

Propylenoxide (two times, 30min each)

Tissue was embedded in Epon (ready for use) -/- Propylenoxid 1:1 for one hour.

250ml Epon (ready for use) solution consist of:

DDSA (Dodecenylsuccinic anhydride)	61,5g
MNA (Methyl norbornene 1,3-dicarboxylic acid)	81,5g
Glyidether 100 (Epon 812)	130,5g
2, 4, 6-Tris (dymenthylaminomethyl)-phenol	3,75ml

After incubating over night in Epon (ready to use) samples were transferred to Epon-filled capsules. Once the tissues had sunken to the ground they were incubated at 60°C for 24-48 hours for polymerization.

Semifine sections (~1µm thickness) were sliced using a Reichert ultramicrotom (Ultraacut E; Fa. Reichert-Jung, Wien, Austria) and stained with toluidine blue:

Toluidin blue	1g
1% Natriumbicarbonat	60 ml
Glycerol	40 ml

Thereafter, 60-70nm thick ultrafine sections were cut, collected on copper grids and contrasted with 0.5 % aqueous uranyl acetate and 3 % aqueous lead citrate.

Sections were studied with a transmission electron microscope EM 10 CR (Fa. Zeiss, Oberkochen, Germany).

3.13 Nerve Conduction Velocity (NCV) Studies

NCV studies are commonly used to evaluate the function of nerves. The method was established in the neurological screen for mice using a Neuroscreen setup provided

by Toennies (Jaeger-Toennies, Hoechberg, Germany). As theoretical and methodical background following literature was used:

- Manual for nerve conduction study and surface anatomy for needle electromyography, 4-th edition. (Hang J. Lee and Joel DeLisa, 2004)
- Clinical electromyography, 3-rd edition (Shin J Oh, 2002)
- EMG, NLG: Elektromyography, Nervenleitungsuntersuchungen, 2nd edition. (Bischoff C et al., 2008)
- Electrophysiology of sensory and sensorimotor processing in mice under general anaesthesia (Ellrich J and Wesselak M, 2003)

After starting Neuroscreen, the recording electrodes had to be plugged in to the amplifier: ground electrode in the middle plug and connection cable for Active and Reference electrodes. The stimulating electrodes were connected to the “Patient” plug at the Neuroscreen workstation via adaptor for reference and active electrodes.
Before starting the measurement, mouse data had to be registered in the Neuroscreen program (ID – mouse ID, Name – strain/mutant line, first name – wt/mut, date of birth – date of birth, sex – male/female). Body/skin temperature of the animal was also determined. Mice were anaesthetized by IP injection of a Ketamine-Xylazine mixture (Ketamine, 80-100 mg/kg; Xylazine, 10-20 mg/kg). The animal was carefully monitored until unconsciousness ensues to the point of loss of the pedal reflex (toe-pinch). Eyes were covered with an ointment (Bepanthen Nasen- und Augensalbe) to protect them from drying-out. The anaesthetized mouse was put onto a corkboard for recording and electrodes were mounted to the right positions.
For evaluating motoric NCV the sciatic nerve was stimulated, electrode placement was done as follows (see figure 8 and 9):

1. Recording electrodes (connected via adaptor to the amplifier) were placed between digits as following:
    a. Reference electrode (red) was pierced between first and second digit.
    b. Active electrode (black) was pierced between second and third digit.
2. Ground electrode (green) was placed on the side of the mouse.
3. Stimulating electrodes were placed on the mouse limb on the ankle for recording of the first signal. The second signal was recorded by stimulating the nerve near the knee (approximately 1cm above the first stimulating point) and the third one near the hip at the sciatic notch.

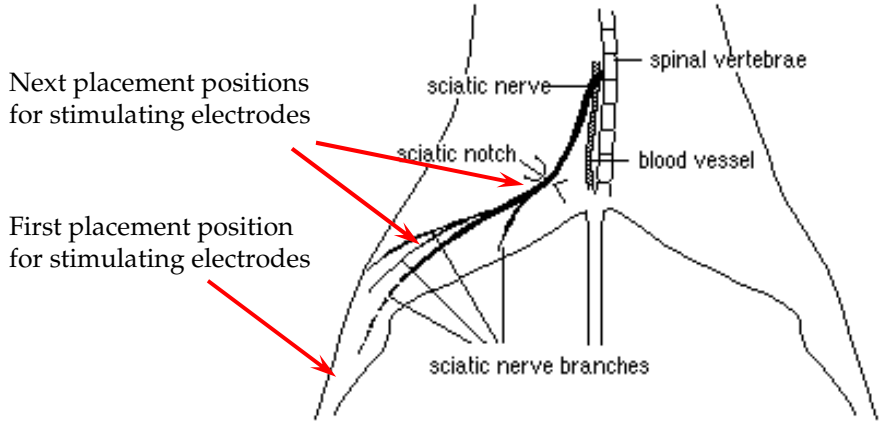

Figure 8: Placement of the electrodes

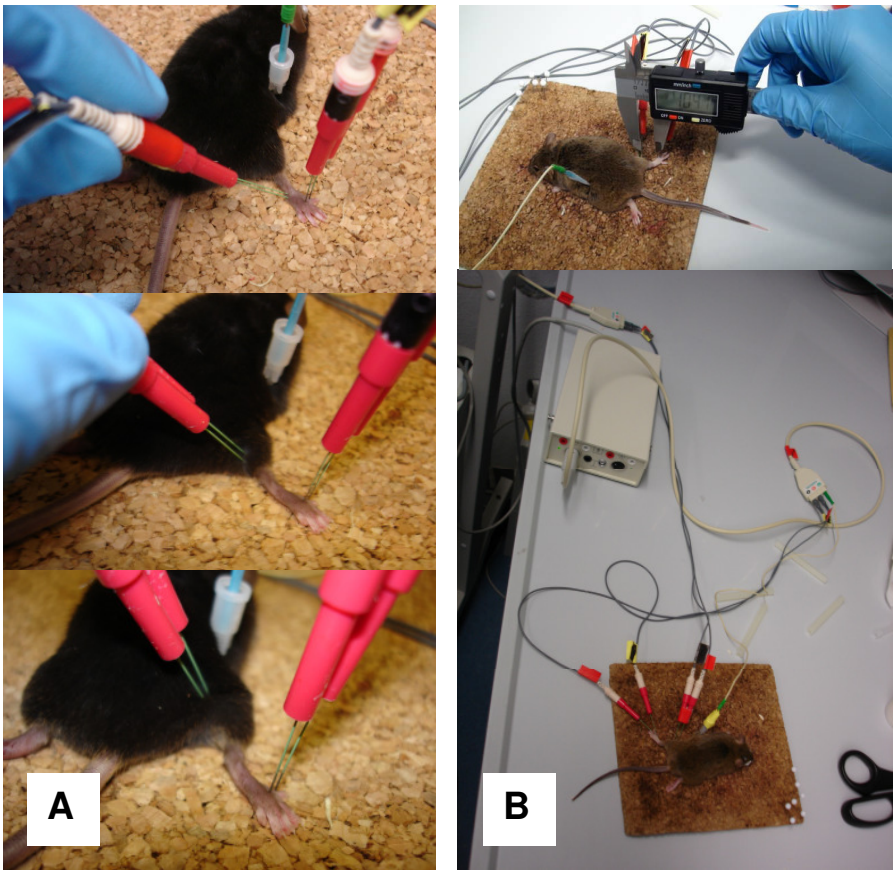

Figure 9: Motoric NCV measurement

A: Placement of the electrodes (three points measurement)
B: Determining the distance between the measurement points and experimental set-up

For nerve stimulation, an electrical impulse was applied using a foot pedal. The intensity of stimulus was gradually increased until supramaximal stimulation was achieved. The stimulation occurred within the time base of 1 msec. After reaching the supramaximal stimulation on the first stimulation position, the stimulation electrodes were transferred to the second stimulation site and the distance in between was

noticed (cm). Stimulation at the second point was performed as described and electrodes were placed at the last stimulation point at the sciatic notch. The distance between stimulation point 2 and 3 was noticed. NCV was measured on both feet. For waking up, mice were placed on a heating plate (37℃).

For data analysis, the cursors for latencies and amplitudes should be corrected, since the program does not put the always correctly. NCV was calculated by the Neuroscreen program (see figure 10)

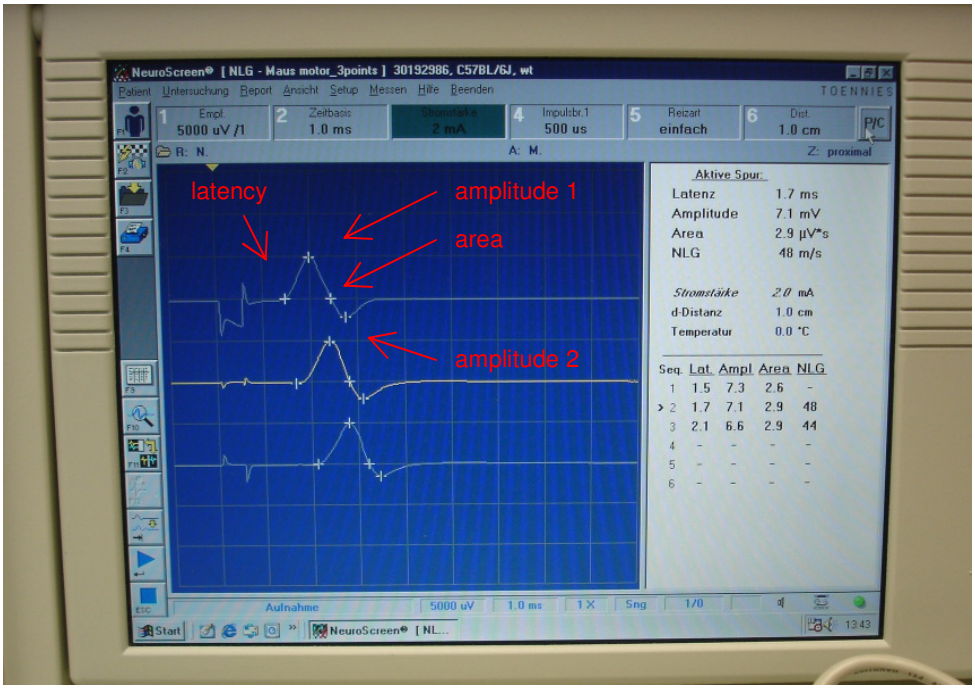

Figure 10: Neuroscreen: NCV measurement in mice (motoric, three points)

3.14 Challenge experiments

The cold challenge was done with mice of the aging cohort. Animals were ~6month old when they entered the metabolic challenge platform. As the final examination of the oxidative stress platform is lethal, a separately cohort of mice was bred (only males entered the challenge). Animals were ~14 weeks old when challenge started.

3.14.1 Paraquat challenge to produce oxidative stress

To mimic the environmental influence of endogenous induced oxidative stress for the pathology of diseases, the herbicide Paraquat was used. Prior to the challenge phase, the cohort was tested in various neurological standard experiments (Grip strength, Rotarod, Beam walk, Ladder). Before treatment, body weight and general health was checked. 6 wildtype animals and 9 mutant animals were injected imp. with 15mg/kg Paraquat dichloride (Fluka PESTANAL®) for eight weeks with an injection interval of 5-6 days. Additional, a control cohort (6 wildtypes, 6 mutants) was treated with Saline (100µl/10g body weight). One day after injection, the body weight was recorded again.

After eight weeks treatment, animals were examined neurologically. Final, animals were sedated with isoflurane and blood was collected as described before (see chapter 3.9.7). In cooperation with the clinical chemistry, various parameters in blood plasma were analyzed (Proteins and plasma enzyme activities: Alkaline phosphatase (AP), α-Amylase (α-Amy), creatine kinase (CK), aspartate-amino-transferase (AST), alanine-amino-transferase (ALT), lactate dehydrogenase activity (LDH), transferrin, Total protein (TP), Albumin; Plasma concentrations of specific substrates: glucose (Gluc), cholesterol (Chol), triglycerides (TG), urea (HST), uric acid (HS), creatinine (Crea), enzymatic determination of creatinine amount (E-Crea); Plasma concentrations of electrolytes: Potassium (K^+), Sodium (Na^+), Chloride (Cl^-), Calcium (Ca^{2+}), Inorganic phosphorus (Phos), Iron). Animals were sacrificed by cervical dislocation and following organs were dissected, frozen in nitrogen and stored at -80°C: brain, heart, muscle, liver.

Organs were used for measuring of aconitase and citrate synthase activity (see chapter 3.9.2).

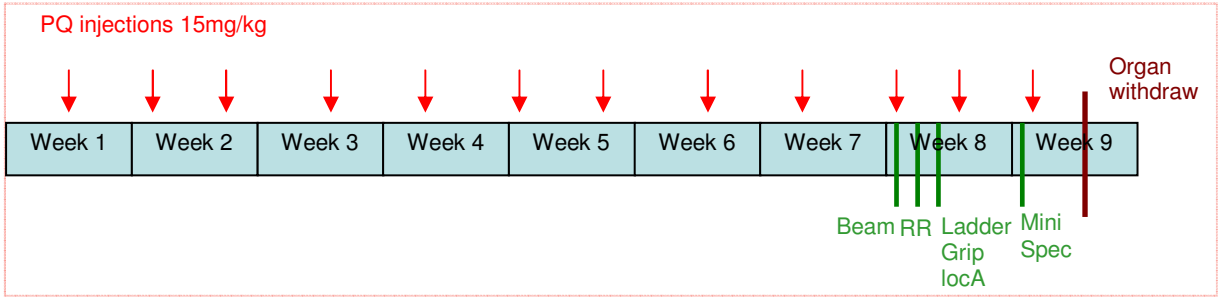

Figure 11: Experimental workflow of the Paraquat challenge

3.14.2 Cold challenge

The cold challenge was done by members of the metabolic screen. In a preliminary study that was done in parallel to the GMC primary screen two wildtype and two mutant male Tom40 mice were tested in a challenge experiment combining fasting and a mild cold challenge (see figure 12).

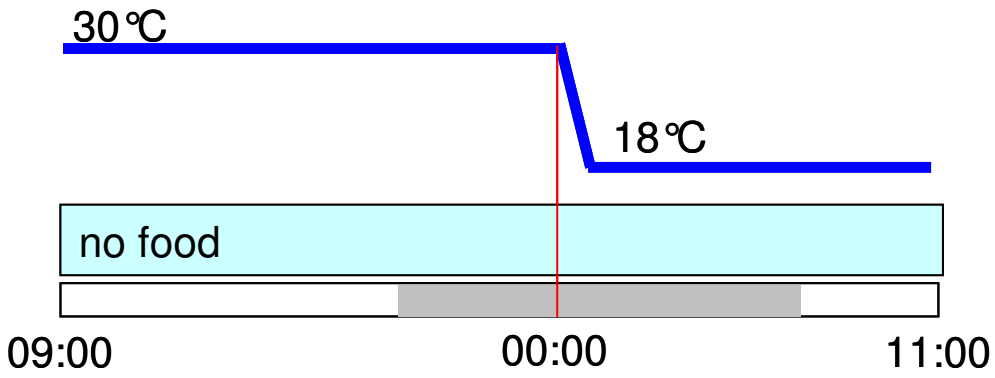

Figure 12: Pilot study: combined fasting and mild cold

As secondary screen, an acute cold challenge experiment was performed using short exposure to low ambient temperature to analyze the ability of the mutants to cope with cold (Fig. 13).

Figure 13: Experimental workflow of the secondary test.

A cohort of nine adult Tom40 control (+/+) females and ten mutant (+/-) females, as well as ten control (+/+) and ten mutant (+/-) males entered the Metabolic Screen at an age of 25-27 weeks. For metabolic measurements mice were transferred to respirometric cages that matched regular home cages in size. Body mass was measured and rectal body temperature was taken prior to the measurement which started at 8:15 a.m. (CET). Mice were transferred to a climatic chamber ventilated with compressed air with a chamber temperature of 30±1°C. At this temperature mice

are in thermoneutrality (Meyer CW et al., 2004). At 10:30 a.m. (CET) chamber temperature was set to 5°C. Cooling down of the chamber lasted 1.5 h. Afterwards gas exchange of the mice was monitored for 5 h. After the experiment mice were weighed and rectal body temperature was measured. Mice had no access to food during the trial because basal metabolic rate (BMR) by definition is determined in post absorptive mice in thermoneutrality whereas resting metabolic rate (RMR) was determined at 5°C. For details concerning indirect calorimetry see chapter 2.6.6.

3.15 Statistics

If not otherwise stated, differences between the genotypes and sexes were evaluated statistically using Two Way ANOVA or student's t-test using SigmaStat Software.
Tables summarizing the data will show mean ± standard error of the mean. Significant differences are indicated stepwise from 0.05, 0.01, 0.001 to 0.0001.
For more complex data, linear model were used to account for different covariates: Grip strength trial results were compared between genotypes, controlling for the effects of sex and weight, by fitting linear mixed effect models (Pinheiro JC and Bates DM, 2000). repeated measurements like the rotarod analysis were analyzed using the mixed effects model, with sex, genotype, body mass, trial number and/or age as factors to influence the performance (S-Plus).
The p-value for the genotype effect within the specific model found for the data indicates the significance of the statistical test of interest. Interaction effects are considered and included in the model, if necessary.
In each model, the parameter of interest is the coefficient of the genotype effect. A significance test or a confidence interval for this coefficient can be extracted from the model fitted.
Ladder and beam walk data contain dependencies, which resemble the rotarod data. Nerve conduction velocity data were analyzed in the same manner than grip data.
In the cardiovascular screen, the data were analyzed statistically using Statistica. Analysis of variance (ANOVA) tests were used for multi-factorial analysis of sex and genotype. Post hoc analysis for multiple comparisons included a Duncan's Multiple Range Test & Critical Ranges.
Statistical analysis of nociception data was performed using a statistical package Statgraphics® (Statistical Graphics Corporation, Rockville, MD). The differences

between the groups were compared with ANOVA and LSD test was used as *post hoc*. Statistical significance was assumed at $p<0.05$.

In the metabolic screen a Two-way-ANOVA (SigmaStat, Jandel Scientific) was used to test for effects of the factors strain and sex. For oxygen consumption a Generalized Linear Model was applied with sex, genotype and body mass as factors to account for the effect of body mass on energy metabolism parameters. The Fisher test was applied for post hoc multiple comparisons.

Clinical chemistry data were statistically analyzed using S-Plus 8.1 with the level of significance set at $p<0.05$, by an applying a linear regression model on the influence of genotype, sex and the interaction of both, and subsequent pair-wise comparisons of the means by T-test using Excel. Data of the following parameters were transformed to the reciprocal value before analysis to achieve normal distribution: ALT, AST, LDH, triglycerides and iron.

TIGR software package for Microarray analysis (Saeed AI et al., 2003) was used for normalization (MIDAS: Microarray Data Analysis System (Quackenbush J, 2002) and identification of genes with significant differential regulation (SAM, Significance Analysis of Microarray (Tusher VG et al., 2001).

For *in silico* analysis of differentially expressed genes EASE, a module of the DAVID database assigning genes to Gene Ontology (GO) functional categories was employed. EASE analysis including a Bonferroni multiplicity correlation evaluated the set of differentially expressed genes for over-representation of two categories of GO terms: Biological processes and molecular functions (Dennis G Jr et al., 2003).

4 Results:

4.1 Integration site of the pT1βgeo gene trap vector

The murine *Tom40* gene (NM_001109748) is located on chromosome 7, contains 10 exons and encodes a transcript of 1350 base-pairs (UCSC Genome Browser Assembly July 2007 (NCBI37/mm9) chr.7:20286667-20300605).

Long range gradient PCR using genomic DNA of mutant animals with the two different primer combinations revealed products of ~1.5kb and ~2.2kb size at temperatures from 58-60°C (Fig. 14).

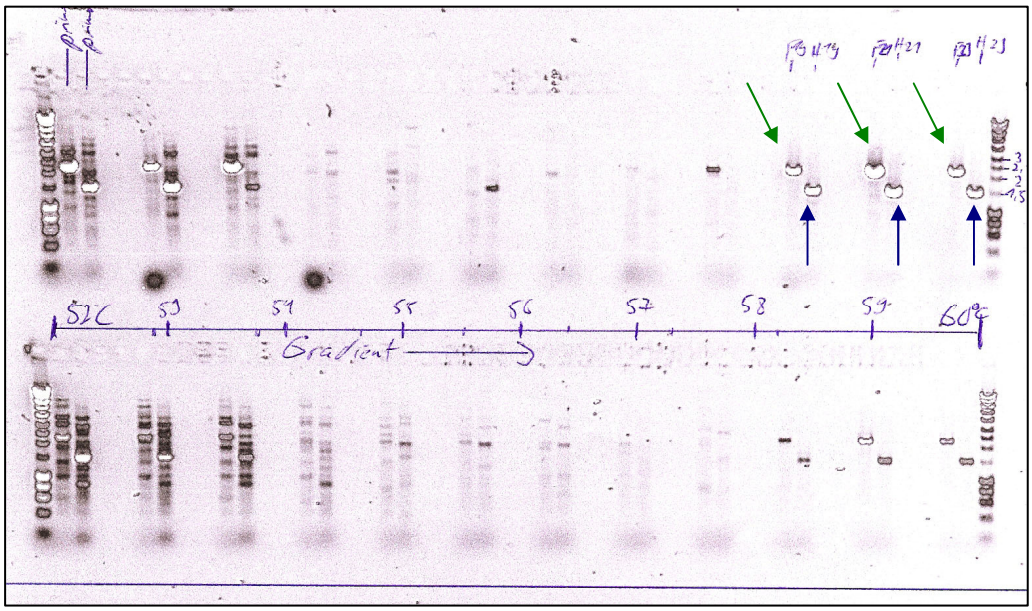

Figure 14: Results of the long range PCR

Sequencing these PCR products showed that the pT1βgeo gene trap vector integrated at position 2030096 on the antistrand, in front of exon1 of the *Tom40* gene (Fig.15). This in turn means that the consensus sequence of the vector has been inserted into the promoter region of the Tom40 gene. Reciprocal crosses of *Tom40 +/-* mice with wild type C57BL/6J mice demonstrated that the *Tom40* mutation is transmitted through the maternal as well as the paternal germline.

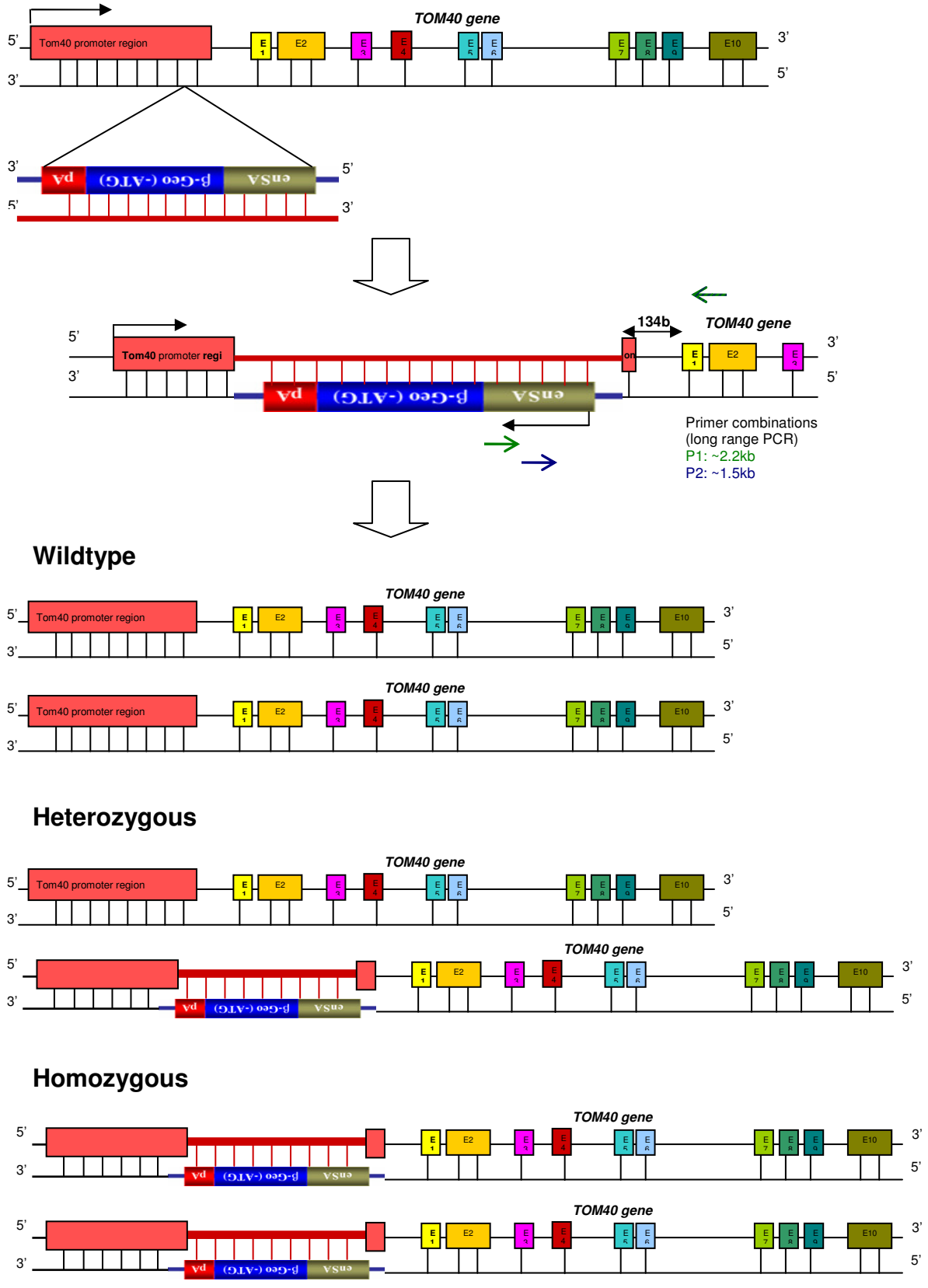

Figure 15: Integration site and possible genotypes

The pT1βgeo vector has inserted at genomic position 2030096 on the (+)-strand, whereas the Tom40 gene is located on the (-)-strand of chromosome 7. Thereby, the promoter region of the Tom40 gene was affected.

4.2 Genotyping

Genotyping of the offspring of *Tom40 +/- inter se* crossed mice revealed, that no homozygous mutants were born. To address the question in which embryonic stage the *Tom40*-/- mutants die, 40 embryos at E9.5 was determined (Fig.16 shows a representative picture of 23 genotyped embryos). As there were no homozygous mutants in this stage of development, 92 3.5 days old blastocysts were isolated and genotyped (only wildtype conditions). Nevertheless, in this embryonic stage no -/- mutants could be found too, arguing that homozygous *Tom40*-/- embryos do not survive until E3.5.

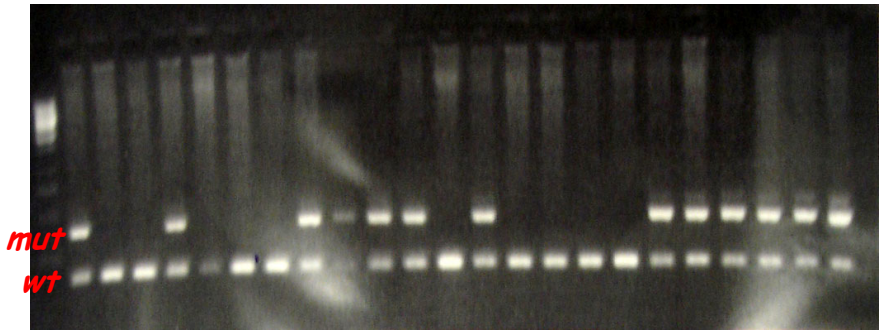

Figure 16: Embryo genotyping

Embryo genotyping was done using standard Tom40 genotyping conditions. Size of resulting PCR products: wt: 248bp, mut: 400bp

4.3 Reduced Tom40 mRNA expression in heterozygous mice

To address the question if the mutation in the promoter region of the Tom40 gene causes altered Tom40 expression, *Tom40* mRNA and protein expression levels were determined. Real-time quantitative PCR revealed a ~50%-reduction of *Tom40* mRNA in heart tissue of heterozygous animals (Fig.17A; n: wt=12, mut=20; students t-test: $p<0.001$, ***). Since the gene coding for APOE which is involved in LOAD (Farrer LA et al., 1997; Gibson GE et al., 2000) is in close proximity to *Tom40*, the expression of *ApoE* gene was analyzed to exclude that the mutation has additional effects on other closely located genes. The expression level of this gene doesn't differ between mutant and wildtype mice (Fig.17B; n: wt=9, mut=11; students t-test: $p=0.434$, n.s.) although there was a slight tendency.

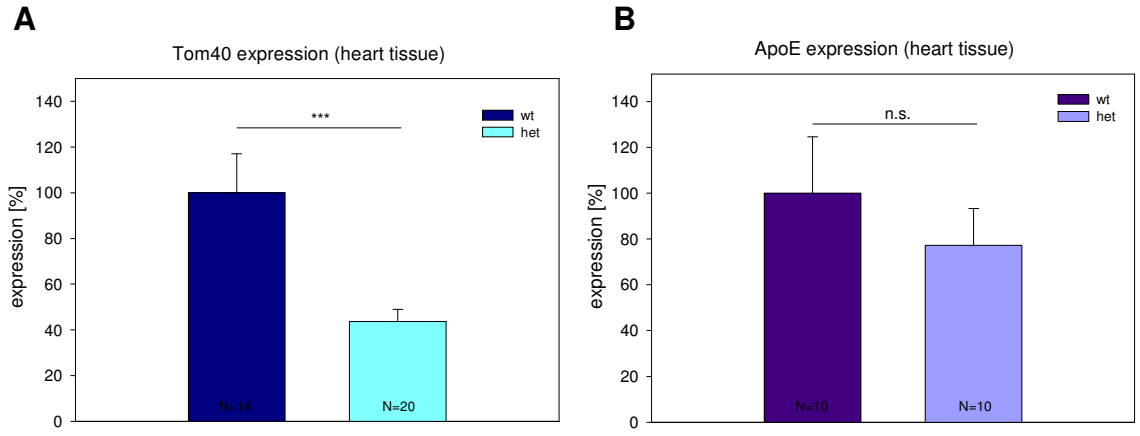

Figure 17: *Tom40* and *ApoE* mRNA expression in heart tissue

A: In heterozygous animals Tom40 expression is reduced to ~50% compared to wildtype controls (t-test, $p<0.001$, ***). Data are given as means and standard error of means (SEM). B: There are no genotype specific differences in ApoE expression comparing mutant Tom40 heterozygous mice to wildtype controls (t-test, $p>0.05$, n.s.). Data are given as means, error bars as standard error of means (SEM).

4.4 Western Blot: Evaluation of protein expression

To analyse protein expression in different tissues a suitable antibody was needed. Unfortunately, although several Tom40 antibodies were commercially available, none of those were described by the manufacturer to be approproaite for mouse tissue lysate. Therefore several antibodies were tested in varying conditions.

Anti-TOMM40 antibody (H3000):

TOM40 is, as the name implies, a 40kDa protein but it was not possible to detect a signal at 40kDa but at 80kDa using the ECL method. this could represent a dimer of the TOM40 protein, but neither by using different protein isolation and subsequent sample preparation protocols nor by running other gel systems resulted in 40kDa bands. However, looking at the signal at 80kDa revealed no visible differences between wildtypes and mutants (Fig.18A). Anti-VDAC was used as mitochondrial loading control (Fig.18B).

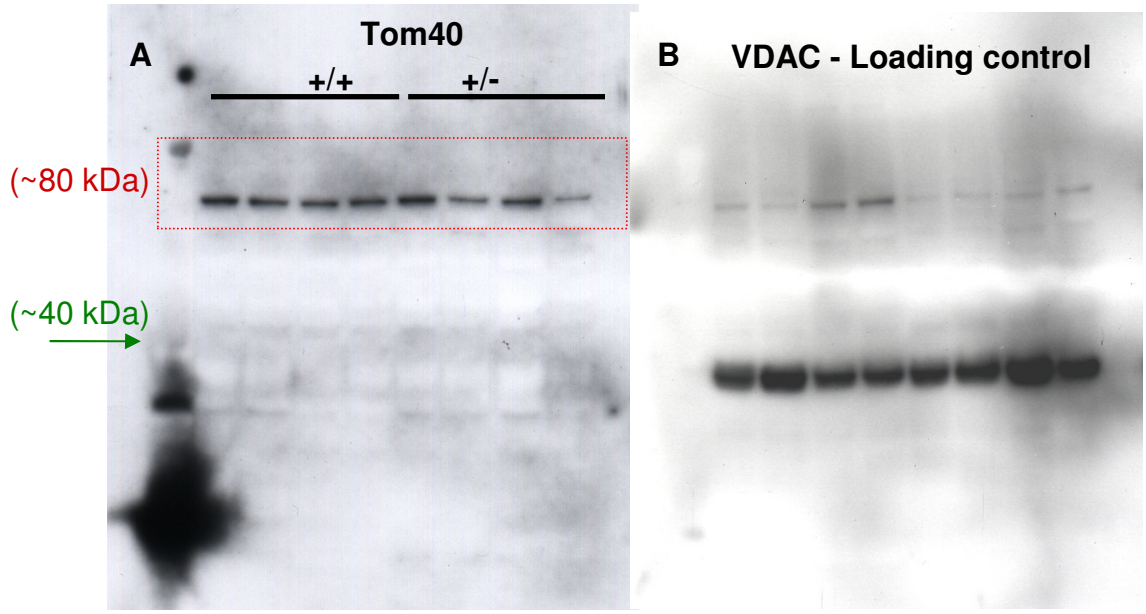

Figure 18: TOM4*0* and VDAC expression in heart tissue (anti-TOMM40 H300)

A: There was a signal detected at 80kDa, pointing towards dimerization of the TOM40 protein. It was not possible to tease out a protein band at 40kDa which would have been the proposed (and in human cell culture for this antibody confirmed) size of the TOM40 protein; B: Anti-VDAC was used as mitochondrial loading control.

Anti-TOMM40 antibody (N-15 and C-15):

These antibodies were directed against some epitopes mapping near the N- respectively the C-terminus of Tom40 of human origin. It was not possible to detect any specific band.

Anti-TOMM40 antibody (abcam):

The use of this antibody has lead to the most promising result with one band with a size of about 40kDa. For loading control an anti-β-tubulin antibody was used and resulted in a signal at 55kDa At first glance there was the impression that TOM40 expression in mutant mice was slightly reduced (Fig.19). Unfortunately, this result was hardly reproducible and therefore it was not possible to make a quantitative analysis of the expression level.

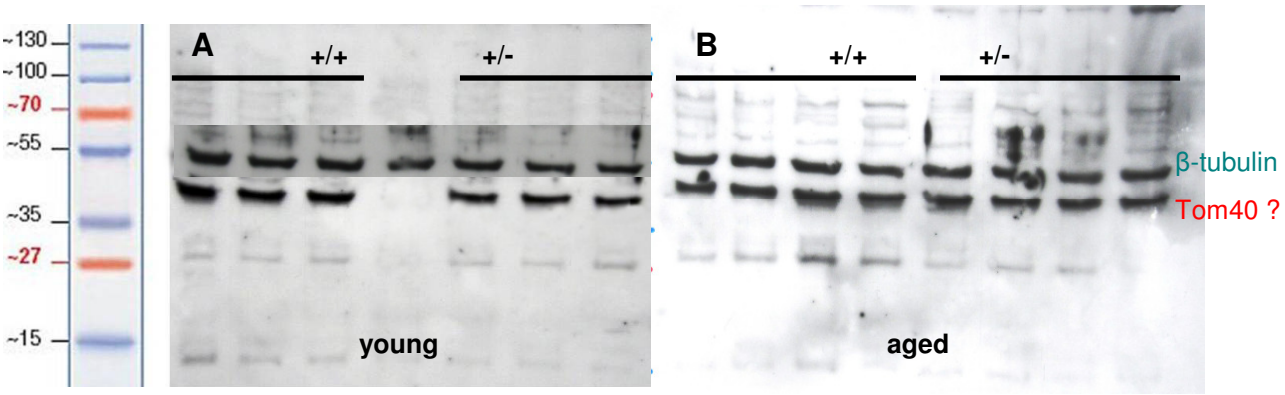

Figure 19: Anti-TOMM40 antibody (Abacm) and anti-β-tubulin as loading control

Heart protein lysates of young (A) and old (B) Tom40 wt and het animals were used for western blotting. After rinsing the membranes with PBS-T charged with 5% milk a band at 40kDa was left using the anti-TOMM40 antibody produced by abcam. Anti-β-tubulin antibody was added in a second work step, producing a distinct band at 55kDa. It seems that TOM40 expression is slightly reduced in heterozygous animals, but this was not quantifiable using ECL.

MitoProfile® Total OXPHOS Rodent WB Antibody Cocktail

For a first investigation of the respiratory chain complexes an antibody cocktail from mitosciences was used, one each against CI subunit NDUFB8, CII-30kDa, CIII-Core protein 2 , CIV subunit I and CV alpha subunit. There were no indications that there were differences between the genotypes (Fig.20). Nevertheless a detailed analysis was done subsequently using BNE (see chapter 3.8).

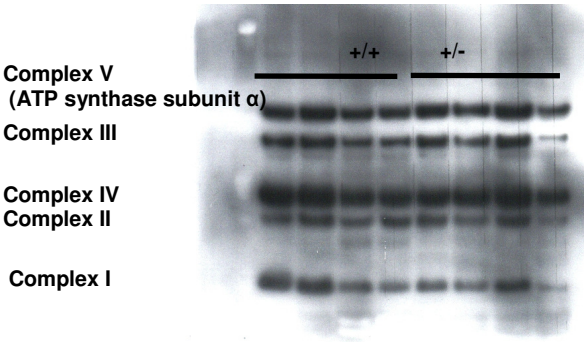

Figure 20: MitoProfile® Total OXPHOS Rodent WB Antibody Cocktail

Targets of the antibodies: complex I subunit NDUFB8 - "CI-20" ~ 20kD, complex II subunit 30kDa - "CII-30" ~ 30kD, complex III subunit Core 2 - "CIII-core2" ~ 47kD, complex IV subunit I - "CIV-I" ~ 39kD, ATP synthase subunit alpha - "CV-alpha" ~ 53kD; there were no obvious alterations in the heart of young animals.

LiCOR infrared imaging

As ECL faces some limitations as for example a narrow quantifiable linear range, all antibodies were tested for compatibility to the LiCor system which uses infrared fluorophores and overcomes these problems (Schutz-Geschwender et al., 2004). MitoProfile® Total OXPHOS Rodent WB Antibody Cocktail, anti-VDAC/Porin antibody and anti-β-tubulin antibody worked very well under the LiCOR conditions (Fig.21).

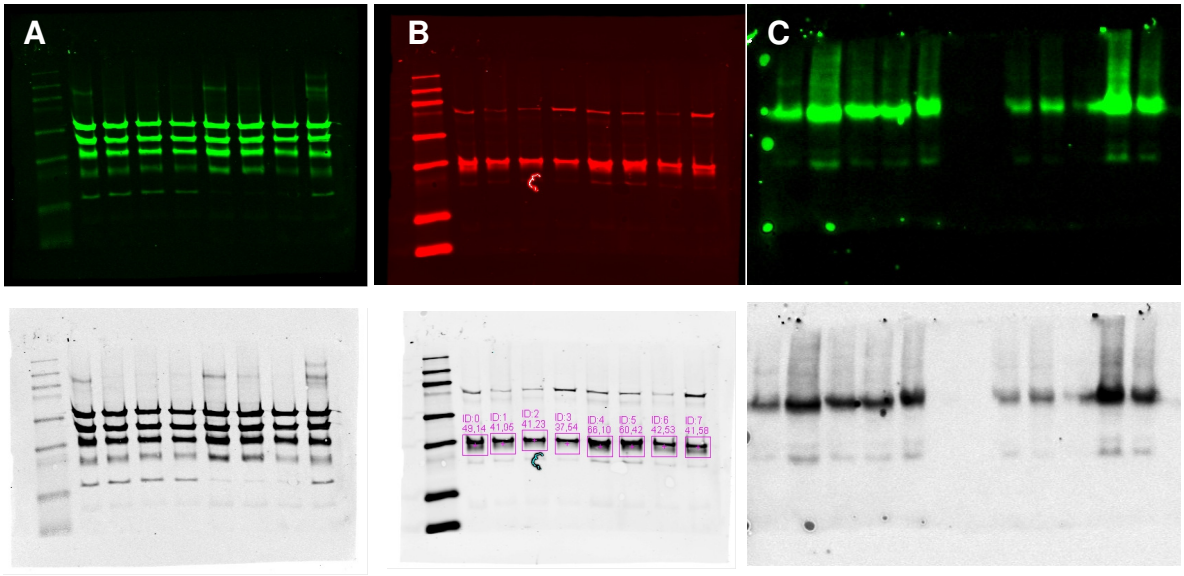

Figure 21: Using IRDye secondary antibodies

A: MitoProfile® Total OXPHOS Rodent WB Antibody Cocktail
B: Anti-VDAC/Porin antibody
C: Anti-β-tubulin antibody

It was not possible to determine optimal conditions for Abcams' anti-TOMM40 antibody. Washing the membranes with PBS-T lead to numerous unspecific bands of all sizes. Adding milk or BSA was not possible because of the resulting strong background. Washing with the LiCOR blocking buffer diluted 1:10 with PBS-T resulted once in a 40kDa band (Fig.22). Unfortunately also this was irreproducible.

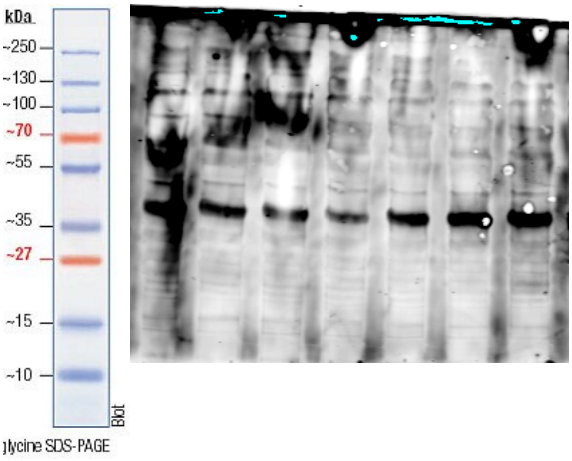

Figure 22: Anti-TOMM40 antibody using the LiCOR system

Primary antibody: anti-TOMM40 (abcam) VD 1:1000, secondary antibody: IRDye 700DX – anti rabbit dilution 1:10000; Washing steps were done with a 1:10 dilution of Odyssey Blocking buffer and PBS-T (0.05%). This was just a test blot and unfortunately it was irreproducible.

4.5 Quantification of mitochondrial complexes and isolation of supercomplexes

First a survey of OXPHOS complexes was carried out using BNE in collaboration with Ilka Wittig. Prepared mitochondrial membranes from heart (Fig.23 and 27), skeletal muscle (Fig.24), liver (Fig.25) and brain (Fig.26) were solubilised with the detergent dodecylmaltoside and OXPHOS complexes were isolated by BNE. Densitometric quantification of Coomassie stained protein complexes and in-gel complex I activity stains did not detect any drastic changes in the abundance (Fig.23-27). A slight but significant reduction of complex III in heterozygous mice was detected only in brain (Fig.26). Complex II was not detectable by the staining methods used.

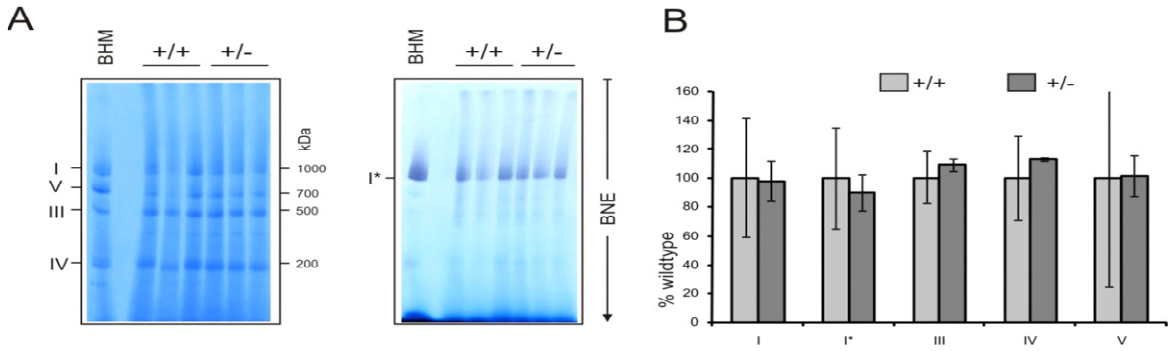

Figure 23: Quantification of OXPHOS complexes from heart tissue.

A, protein complexes were isolated by BNE (4 to 13% acrylamide gradient gels) and stained with Coomassie (left panel) or in-gel complex I activity stain (right panel). B, Complexes were quantified by densitometry (n=3). Assignment of complexes: I, complex I; I*, complex I activity stain; III, complex III; IV, complex IV; V, complex V. +/+, mice with both TOM40 wildtype alleles; +/-, mice lacking one TOM40 allele, BHM, bovine heart mitochondria as ladder.

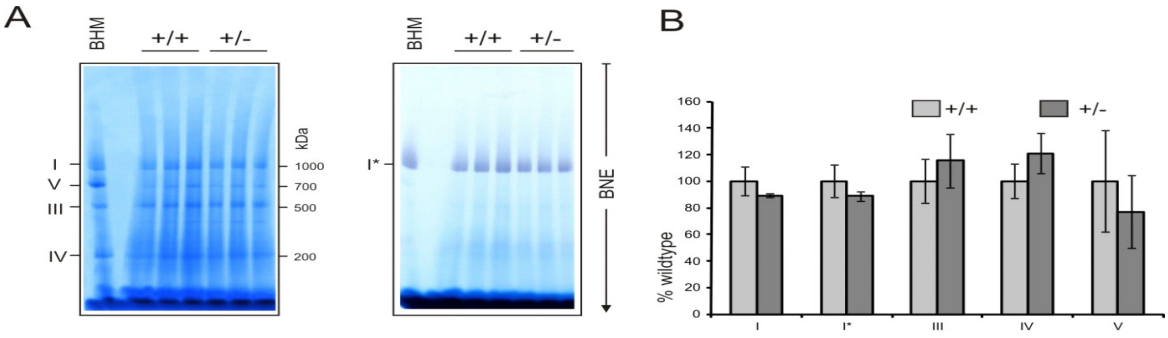

Figure 24: Quantification of OXPHOS complexes from skeletal muscle.

A, protein complexes were isolated by BNE (4 to 13% acrylamide gradient gels) and stained with Coomassie (left panel) or in-gel complex I activity stain (right panel). B, Complexes were quantified by densitometry (n=3). Assignment of complexes: I, complex I; I*, complex I activity stain; III, complex III; IV, complex IV; V, complex V. +/+, mice with both TOM40 wildtype alleles; +/-, mice lacking one TOM40 allele, BHM, bovine heart mitochondria as ladder.

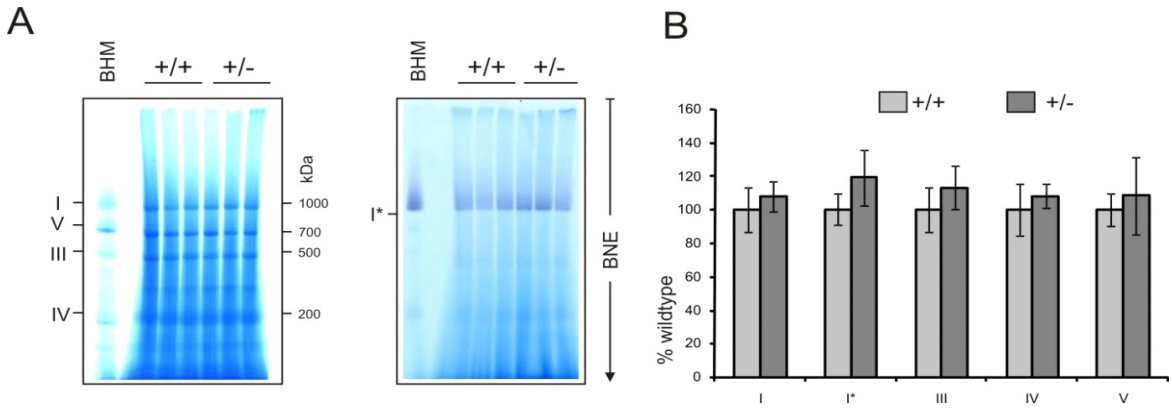

Figure 25: Quantification of OXPHOS complexes from liver.

A, protein complexes were isolated by BNE (4 to 13% acrylamide gradient gels) and stained with Coomassie (left panel) or in-gel complex I activity stain (right panel). B, Complexes were quantified by densitometry (n=3). Assignment of complexes: I, complex I; I*, complex I activity stain; III, complex III; IV, complex IV; V, complex V. +/+, mice with both TOM40 wildtype alleles; +/-, mice lacking one TOM40 allele, BHM, bovine heart mitochondria as ladder.

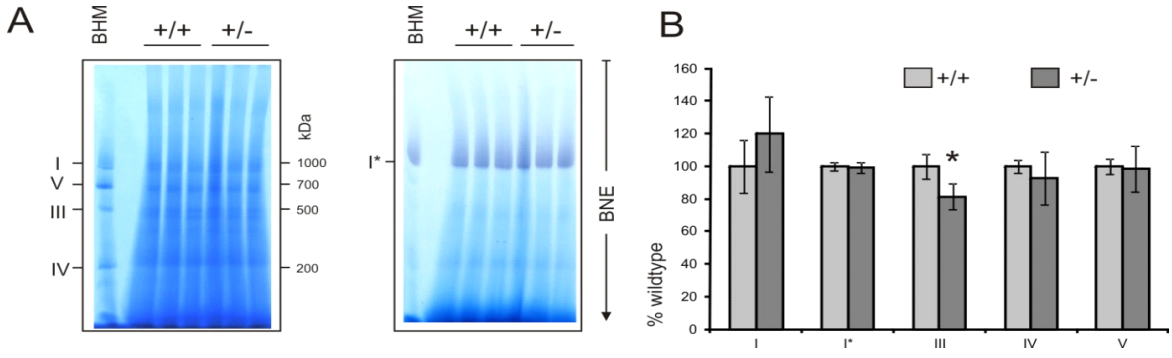

Figure 26: Quantification of OXPHOS complexes from brain.

A: protein complexes were isolated by BNE (4 to 13% acrylamide gradient gels) and stained with Coomassie (left panel) or in-gel complex I activity stain (right panel). B: Complexes were quantified by densitometry (n=3). Assignment of complexes: I, complex I; I*, complex I activity stain; III, complex III; IV, complex IV; V, complex V. +/+, mice with both TOM40 wildtype alleles; +/-, mice lacking one TOM40 allele, * significant (t-test: $p<0.05$), BHM, bovine heart mitochondria as ladder.

Quantitative analysis of old heart tissue could also not detect any dose dependent effects of heterozygous deletion mutant (Fig.27).

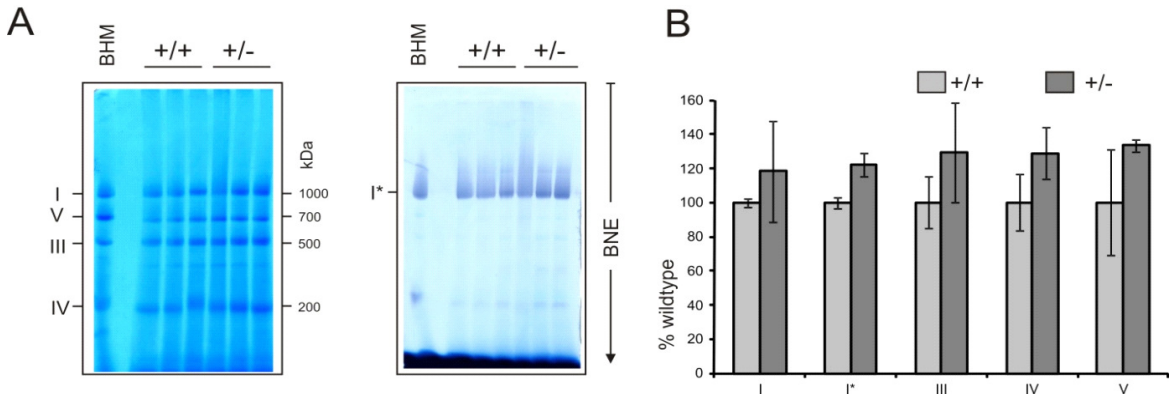

Figure 27: Quantification of OXPHOS complexes from old heart tissue.

A, protein complexes were isolated by BNE (4 to 13% acrylamide gradient gels) and stained with Coomassie (left panel) or in-gel complex I activity stain (right panel). B, Complexes were quantified by densitometry (n=3). Assignment of complexes: I, complex I; I*, complex I activity stain; III, complex III; IV, complex IV; V, complex V. +/+, mice with both TOM40 wildtype alleles; +/-, mice lacking one TOM40 allele, BHM, bovine heart mitochondria as ladder.

In order to study assembly/stability of respirasomes in the heterozygous TOM40 deletion strain, formation of supercomplexes was analyzed in 2D BN/SDS gels. Tissue homogenates from heart (Fig.28), skeletal muscle (Fig.29), liver (Fig.30A and B) and brain (Fig.30C and D) were solubilised with the mild detergent digitonin to isolate supercomplexes by BNE. For enhanced detection of subunits sensitive fluorescence labelling for the 2D BN/SDS PAGE was used. The same gels were also stained with silver. In all tissues respirasomes were detected at wildtype levels indicating that the lack of one TOM40 allele did not affect assembly/stability of supercomplexes. Interestingly supercomplex stability seemed to be enhanced in old heart tissue. 2D gels detected only low amounts of supercomplexes in mitochondria of young hearts.

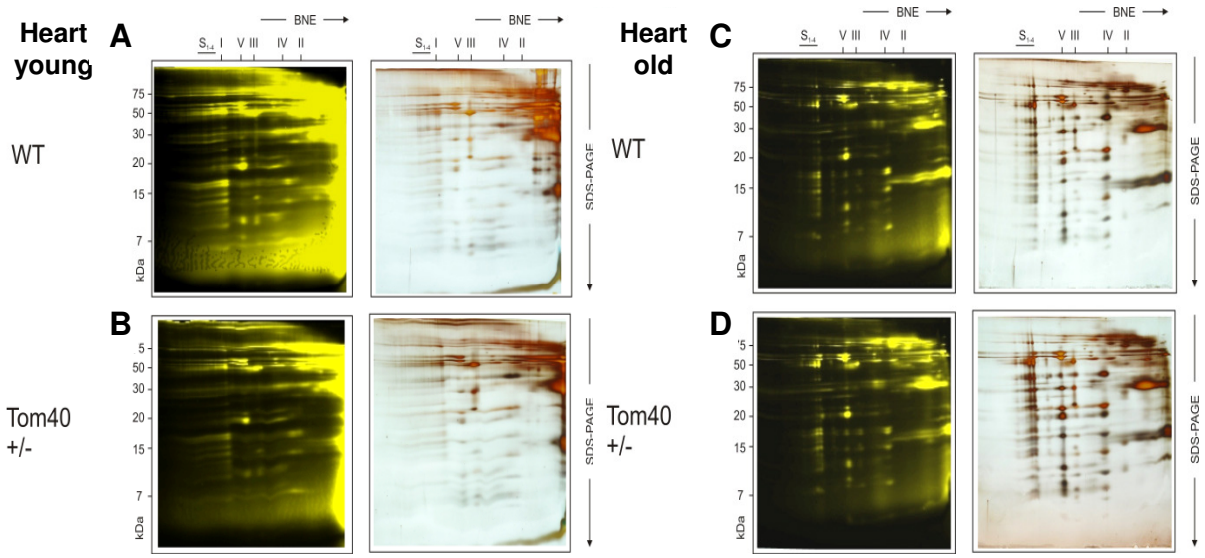

Figure 28: Isolation of respiratory supercomplexes from young heart tissue.

Young hearts: homogenates from heart tissue were solubilzed with digitonin and protein complexes and subunit composition by 2D BN/SDS PAGE is shown as fluorescence scan (left panel) and silver stain (right panel) from A, wildtype and B, TOM40 +/- mice. Assignment of complexes: S, supercomplexes containing complex I, III and IV with the stoichiometry of I1III2IV0-4; I, complex I; III, complex III; IV, complex IV; V, complex V. Old hearts: homogenates from old heart tissue were solubilzed with digitonin and protein complexes and subunit composition by 2D BN/SDS PAGE is shown as fluorescence scan (left panel) and silver stain (right panel) from C, wildtype and D, TOM40 +/- mice. Assignment of complexes: S, supercomplexes containing complex I, III and IV with the stoichiometry of I1III2IV0-4; III, complex III; IV, complex IV; V, complex V.

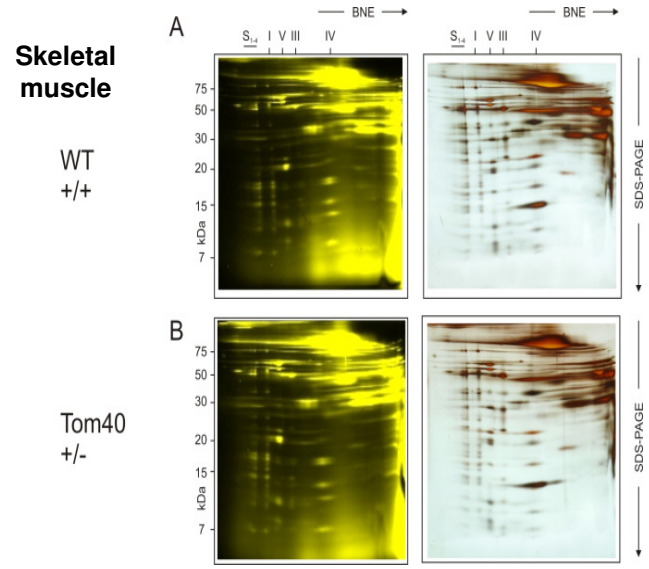

Figure 29: Isolation of respiratory supercomplexes from skeletal muscle.

Homogenates from skeletal muscle were solubilzed with digitonin and protein complexes and subunit composition by 2D BN/SDS PAGE is shown as fluorescence scan (left panel) and silver stain (right panel) from A, wildtype and B, TOM40 +/- mice. Assignment of complexes: S, supercomplexes containing complex I, III and IV with the stoichiometry of I1III2IV0-4; I, complex I; III, complex III; IV, complex IV; V, complex V.

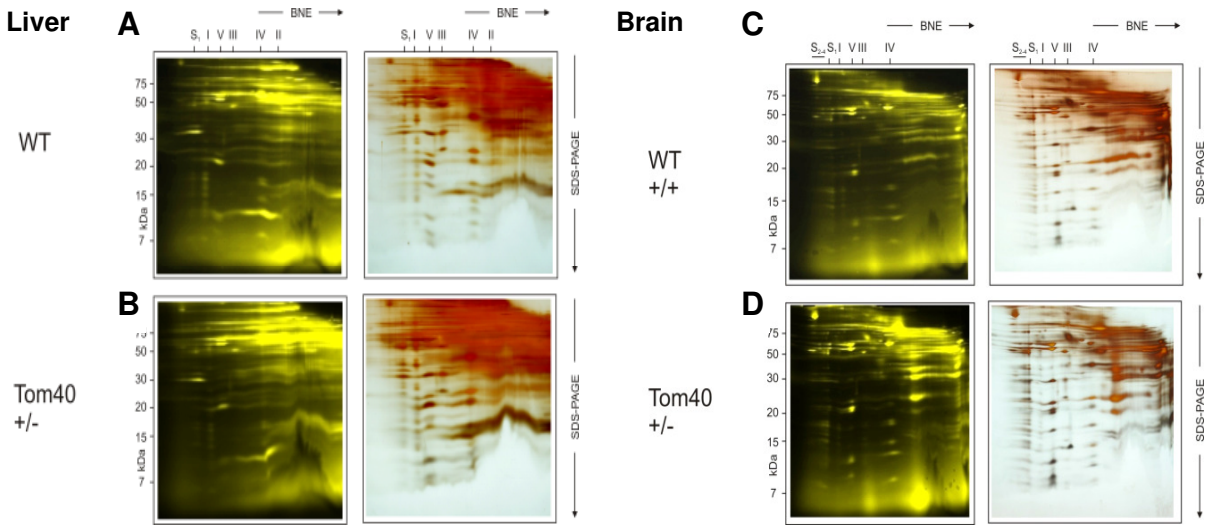

Figure 30: Isolation of respiratory supercomplexes from liver and brain

Homogenates from liver tissue were solubilzed with digitonin and protein complexes and subunit composition by 2D BN/SDS PAGE is shown as fluorescence scan (left panel) and silver stain (right panel) from liver A: wildtype and B: TOM40 +/- mice and brain C: wildtype and D: TOM40 +/- mice . Assignment of complexes: S, supercomplexes containing complex I, III and IV with the stoichiometry of I1III2IV0-4; I, complex I; III, complex III; IV, complex IV; V, complex V.

Next the formation of the complex V homo-oligomers was analyzed using the mild detergent digitonin and instead of BNE conditions of clear-native electrophoresis were used to prevent disassembly of oligomers. ATP synthase was stained by ATP hydrolysis assay (Fig.31). All tissues showed wildtype amounts of dimeric and oligomeric complex V. Again like respirasomes, supercomplexes of ATP synthase seems to be more stable or in higher abundance in old than in young heart tissue.

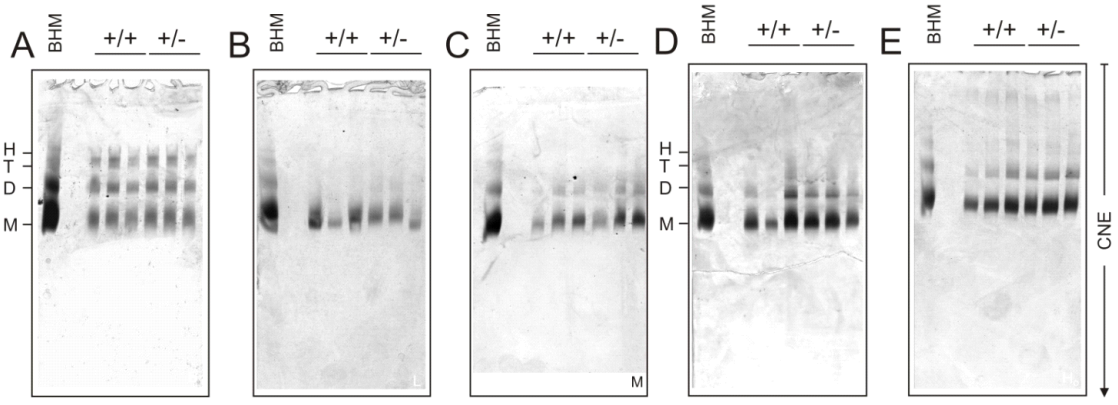

Figure 31: Isolation of oligomeric ATP synthase

A, brain, B, liver, C, muscle, D, heart from young and E, old mice. Tissue homogenates were solubilzed with digitonin and protein complexes were isolated by CNE (3 to 13% acrylamide gradient gels). ATP synthase was stained with in-gel ATP hydrolysis assay. Assignments: M, monomeric; D, dimeric; T, tetrameric, H, hexameric ATP synthase; BHM, bovine heart mitochondria as ladder. Gels are shown as inverted gray scale scans.

4.6 MtDNA copy number and deletion analysis

To check for the influence of the mutation on amount/number of mitochondria and integrity of mitochondrial DNA copy numer and percentage of deletions were analysed (heart: wt n=8, age: 199d, het n=11, age 279d; brain: wt n=10, age: 160d, het n=10, age: 222d). There were no significant differences in copy number and deletion percentage neither in heart nor in brain tissue of *Tom40* mutant and wildtype animals (Fig.32).

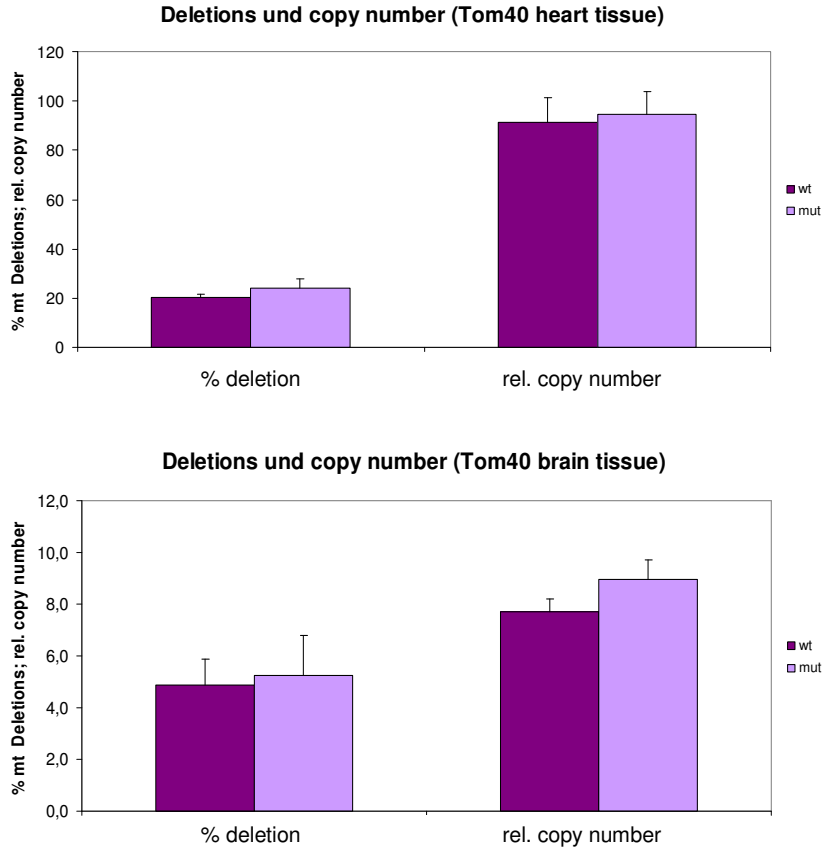

Figure 32: mtDNA copy number and deletion analysis

There were no differences between mutants and wildtypes (students t-test: p>0.05, n.s.)

4.7 Expression pattern

Staining of the embryos of Tom40 mutant mothers to get information about the expression pattern of the gene with the inserted vector did not work. There was no staining visible in none of the tested animals. As a positive control Dll1LacZ control mice were used (Fig.33). The blue pattern is very intensive in these embryos, arguing that the method itself was working.

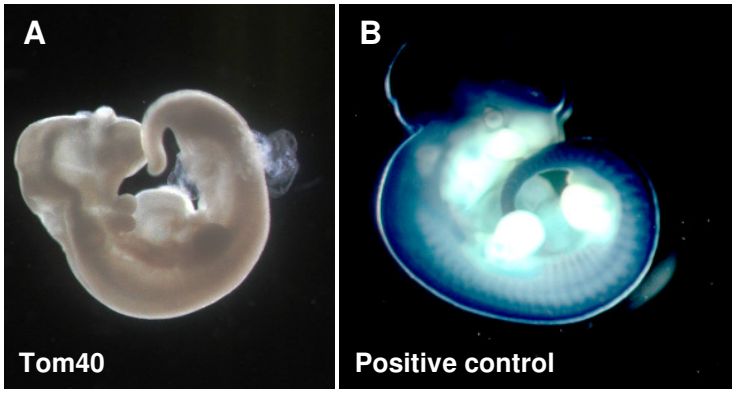

Figure 33: LacZ staining
Tom40 offspring at E9.5 (a) and a positive Dll1LacZ control mice (b) at E14.5

4.8 Functional analysis of Tom40+/- mitochondria

In order to monitor the effect of the loss of one functional allele of *Tom40* on mitochondrial function we analyzed the oxygen consumption of the respiratory chain complexes in response to stimulation with their substrates and their subsequent inhibition. For this experiment freshly isolated heart and brain mitochondria were used.

Heart mitochondria: Heart mitochondria of adult mice and also aged ones were analysed (wt young: n=11, age=164d; het young: n=11, age=205d; wt aged: n=8, age=704d; het aged: n=8, age=712d) There were no differences in the RCC activity of adult animals despite a tendency towards a reduction in Complex II-III (statistics CI: Mann-Whitney Rank Sum Test $p>0.05$, n.s.; statistics CII-III: t-test $p=0.072$, n.s.; statistics CIV: t-test $p>0.05$, n.s.). In the aged group, however, several effects could be observed (Fig.34). RCC activity of complex II-III and complex IV states that mutant mitochondria perform much worse than aged wildtypes (Comparison of young and old mitochondria of wildtype and mutant animals: Two way ANOVA: CI: $p>0.05$, n.s., CII-III: there is a statistically significant interaction of age and genotype $p<0.001$, ***, CIV: there is a statistically significant influence of the age $p<0.001$, ***, and a statistically significant interaction of age and genotype $p<0.05$, *). Complex IV of old animals was affected in wildtypes as well as in mutants. The impairment nevertheless was more pronounced in mutant mitochondria (t-test $p<0.05$, *). In contrast, the combined recording of Complex II and III activity revealed that only in mutant mitochondria oxygen consumption was dramatically lowered compared to old

wildtypes (t-test p<0.01, **). The complex II-III activity of aged wildtype mitochondria ranges on the same level as visible in the young group. The values of Complex I showed high variation, so that it was not possible to conclude whether there is the same tendency than in the other complexes or not.

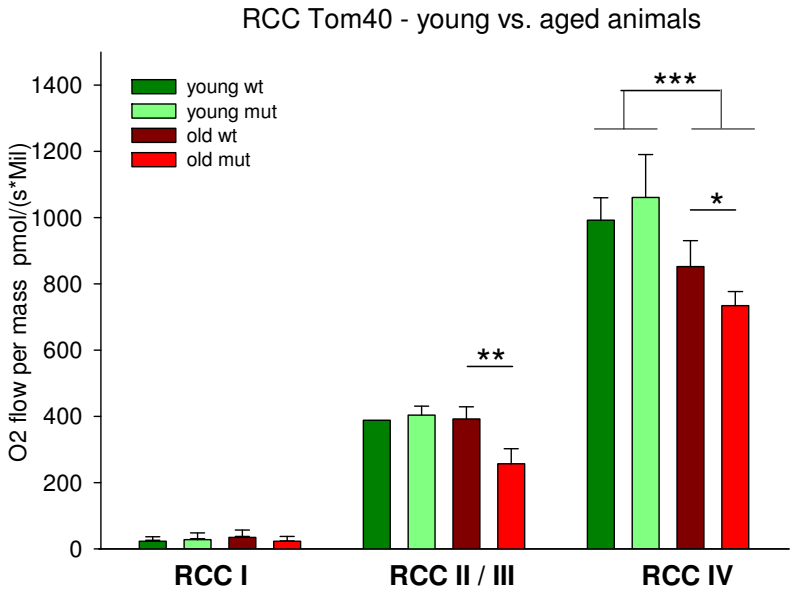

Figure 34: RCC activity of isolated heart mitochondria

There were no genotype specific differences in young animals. Analysis of complex IV revealed a pronounced aging effect (ANOVA p<o.oo1, ***). Additional, in aged animals there was a significant genotype-effect comparing the oxygen flow of mutant and wildtype mitochondria (ANOVA: interaction age x genotype p<0.05; genotype: t-test p<0.05, *). Aging had no effect on complex II-III of wildtype animals but on mutant mitochondria which perform much worse (ANOVA: Interaction age X genotype p<0.001, ***; genotype: t-test p<0.01, **).

Brain mitochondria: There were no statistically significant differences in the RCC activity of aged animals but trends towards a lowered activity in mutant brain mitochondria (Fig.35; wt aged: n=18, age=708d; het aged: n=12, age=770d; statistics CI and CIV: t-test p>0.05, n.s.; statistics CII-III: t-test p=0.056, n.s.).

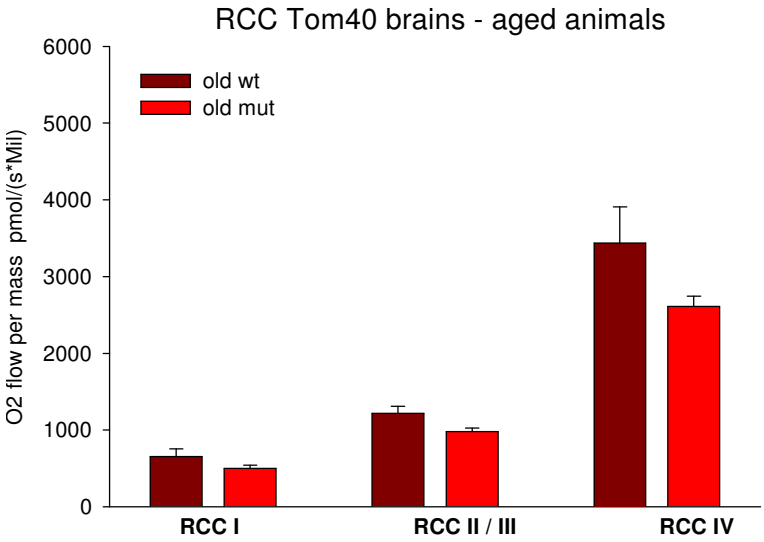

Figure 35: RCC activity of isolated brain mitochondria

There were no significant differences in the RCC activity of aged brain mitochondria, but there was a trend towards a lowered activity in mutants.

4.9 Uncoupling of heart mitochondria

In addition, the uncoupling ability of freshly isolated heart mitochondria was determined. There were no significant differences between wildtype and mutant heart mitochondria of young animals concerning their ability to uncouple the respiratory chain (wt: n=25, age=150d; het n=26, age=215d; t-test, p>0.05, n.s.). Neither absolute vales (Fig.36A) nor values normalized to citrate synthase activity (Fig.36 B) differed between the genotypes.

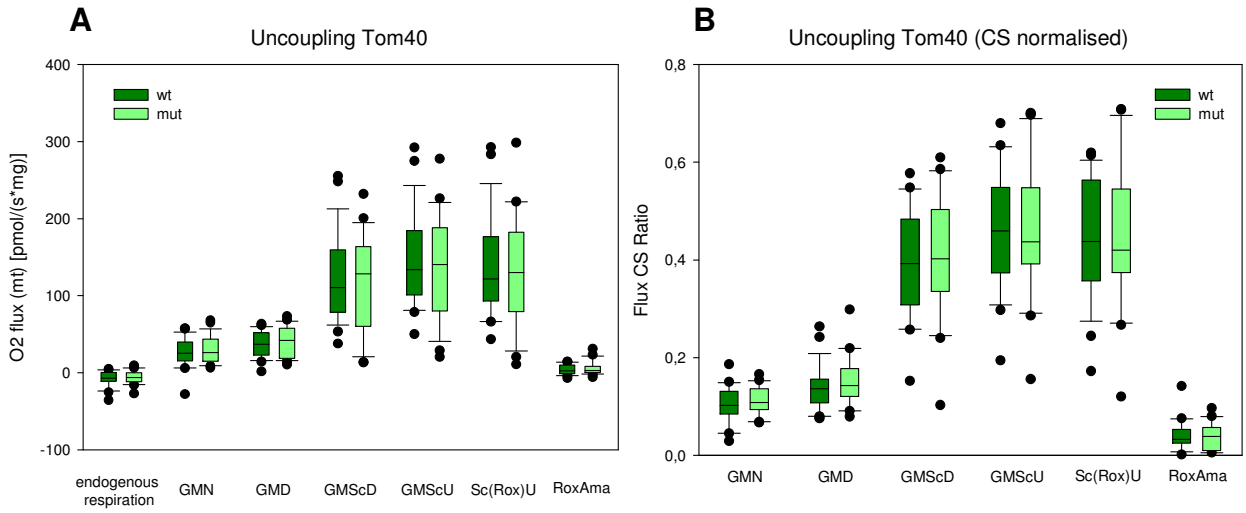

Figure 36: Uncoupling of heart mitochondria isolated from young animals

There were no genotype specific differences neither looking at the absolute values (A) nor looking at citrate synthase activity normalized values (B). states: GMN: glutamate+malate (LEAK; no adenylates added, state 4), GMD: +ADP (stimulated respiration, coupled, state 3), GMScD: +succinate, GMScU: +FCCP (uncoupled), Sc(Rox)U: +Rotenone (inhibition of CI), RoxAma: +Antimycin A

In addition, data were normalized to maximum flux in controls which was the uncoupled and not inhibited GMScU state (flux control ratio). However, there also were no significant differences between mutant and controls (Fig.37).

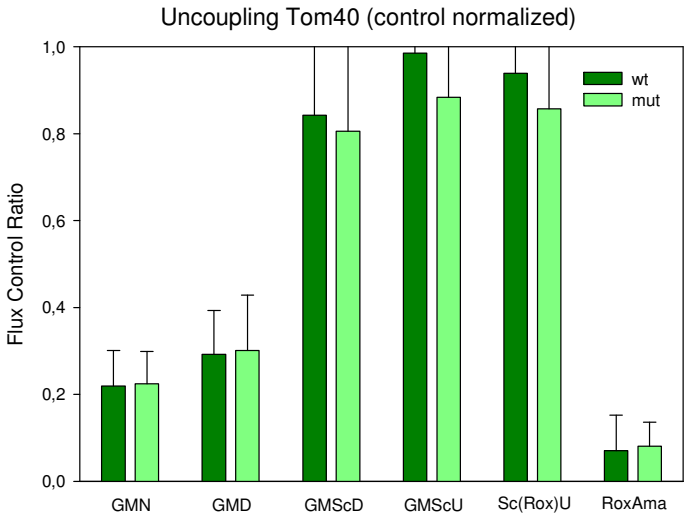

Figure 37: Uncoupling of heart mitochondria: flux control ratio

There were no genotype specific differences after normalizing data to the maximum oxygen flux measured in control mitochondria. states: GMN: glutamate+malate (LEAK; no adenylates added, state 4), GMD: +ADP (stimulated respiration, coupled, state 3), GMScD: +succinate, GMScU: +FCCP (uncoupled), Sc(Rox)U: +Rotenone (inhibition of CI), RoxAma: +Antimycin A

4.10 Enzyme activity

Activity of respiratory chain complex enzymes can also be analysed in lysates of frozen tissue. Therefore heart mitochondria of young and old animals were tested for complex I, II-III and IV, as well as for citrate synthase. For the investigation of brain mitochondria only aged animals were used. Complex I and IV and the citrate synthase were analyzed.

Heart mitochondria: Evaluating the specific activity of the key enzymes of the single complexes and also of the citrate synthase revealed no significant alterations in mutant mice (Fig.38; wt young: n=6, age=167d; het young n=11, age=176d; wt aged: n=9, age=704d; het aged: n=7, age=711d). Complex II-III enzyme activity was slightly reduced in aged mitochondria (Two Way ANOVA: p=0.079). Normalized to CS this subtle difference disappeared.

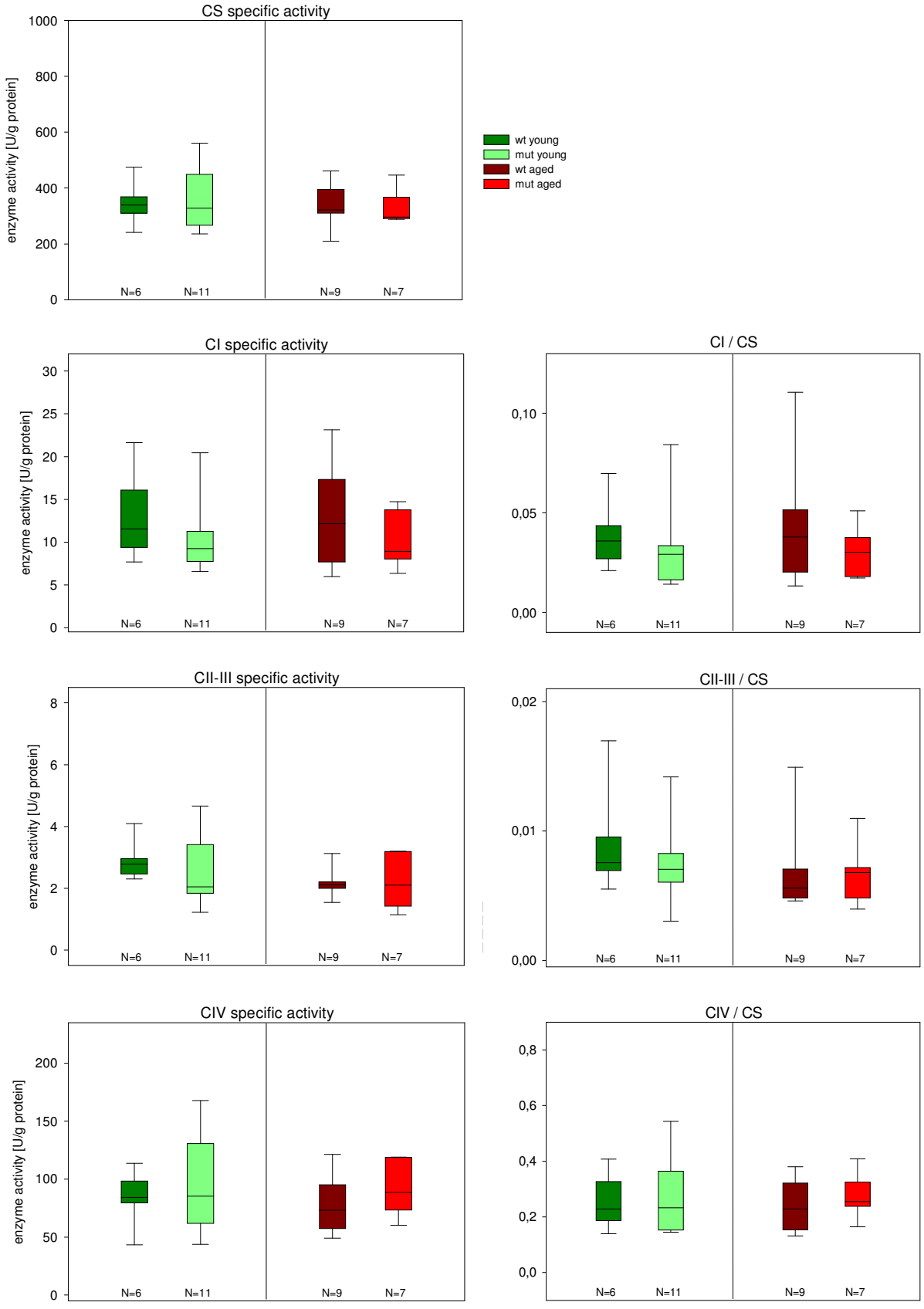

Figure 38: Enzyme activities (heart tissue of young and old mice)

No genotype specific differences in none of the tested tissue lysates.

Brain mitochondria: The specific activity means of complex I were suggestive of lower values in mutant animals (Fig.39A; wt: n=6, age=562d; het: n=6, age 683d). Due to a very high variance in wildtypes no significance could be reached. After normalization of CI specific activity to CS activity, a trend towards reduced activity in mutant animals could be observed (Fig.39B; t-test: p=0.066). Examining CIV specific activity revealed a highly significant difference between mutant and wildtype mitochondria (t-test: p<0.001), however this difference diminished after CS normalization (p=0.093). The citrate synthase activity was not differing between mutants and controls. Correlating CI to CIV activity resulted in lowered values in mutant animals compared to wildtypes (t-test: p<0.05, *).

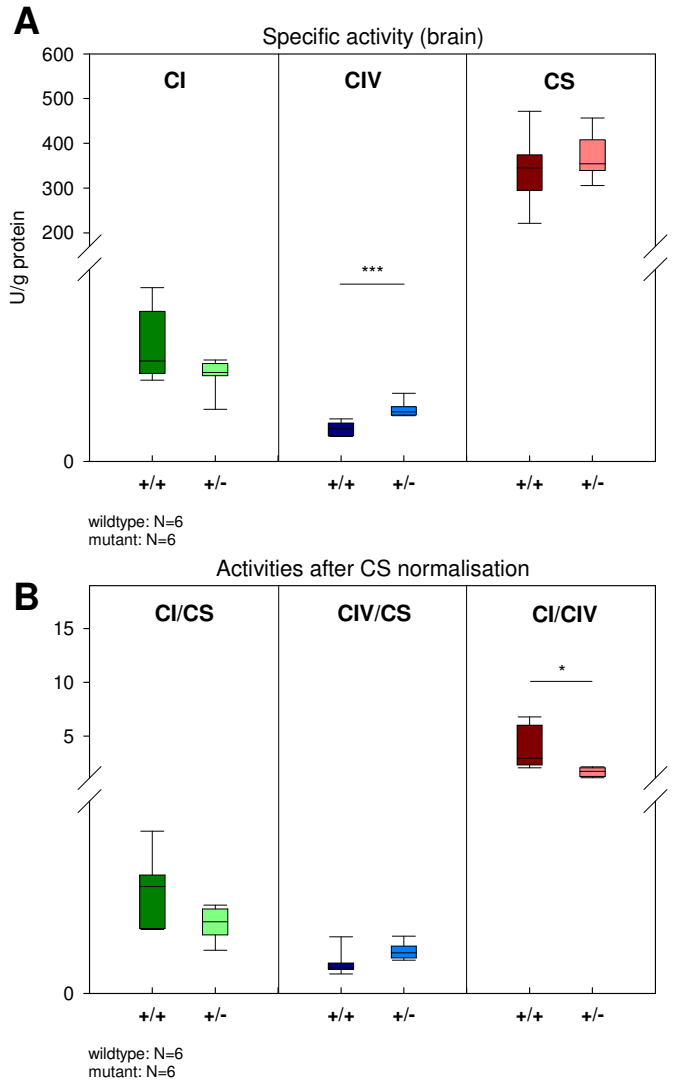

Figure 39: Enzyme activities (brain tissue of aged mice)

A: Specific activity of CI (left) CIV (middle) and CS (right): CIV activity was significantly higher in mutant brain mitochondria than in controls (t-test: p<0.001, ***).
B: Activity after normalization: CI/CS (left), CIV/CS (middle) and CI/CIV (right): CI/CIV was significantly lower in mutants than in wildtypes (t-test: p<0.05, *).

4.11 Results of the GMC screen

A cohort of young Tom40 animals entered the GMC primary screen and was analysed by the respective specialists from each screen.

4.11.1 *Tom40* mutants show minor alterations in dysmorphology

The Tom40 mutant mouse line was analyzed in the Dysmorphology, Bone and Cartilage module of the German Mouse Clinic. In the clickbox test, a retarded reaction in mutants and controls was observed (table 11).

Table 11: Results from clickbox test (hearing test; eight-week old mice)
Number of mice exhibiting a particular score range. Data are given as means.

Score	Male		Female	
	Control	Mutant	Control	Mutant
0	-	-	2	-
1	4	1	2	-
2	5	6	5	7
3	1	3	1	3
4	-	-	-	-
5	-	-	-	-
Mean Score	***1.70***	***2.20***	***1.50***	***2.30***
Kruskal-Wallis ANOVA on Ranks: n.s.				

0: no reaction at all,
1: no Preyer reflex,
2: retarded reaction,
3: normal reaction,
4: strong reaction,
5: particularly strong reaction

In the morphological investigation via visual inspection and X-ray analysis, also no genotype-specific differences were found. In the DEXA analysis, fat mass and fat content were significantly increased in female mutants. The sex differences that were observed are common in many mouse strains, and thus are not abnormal (unpublished data).

4.11.2 Heterozygous *Tom40*+/- mice show behavioural alterations

Behavioural analysis revealed significant differences between mutants and wildtypes regarding PPI (Fig.40; Significant genotype effect revealed by Two-way ANOVA: PPI(67dB): p=0.020; PPI(69dB): p=0.014; PPI(73dB): p=0.001; PPI(81dB): p=0.004; Global: p=0.002). In females PPI was significantly increased at all intensities and globally (t-test, $p<0.05$, *). Males show the same tendencies with a significant difference at 73 dB prepulse (PP) intensity (t-test, $p<0.05$, *).

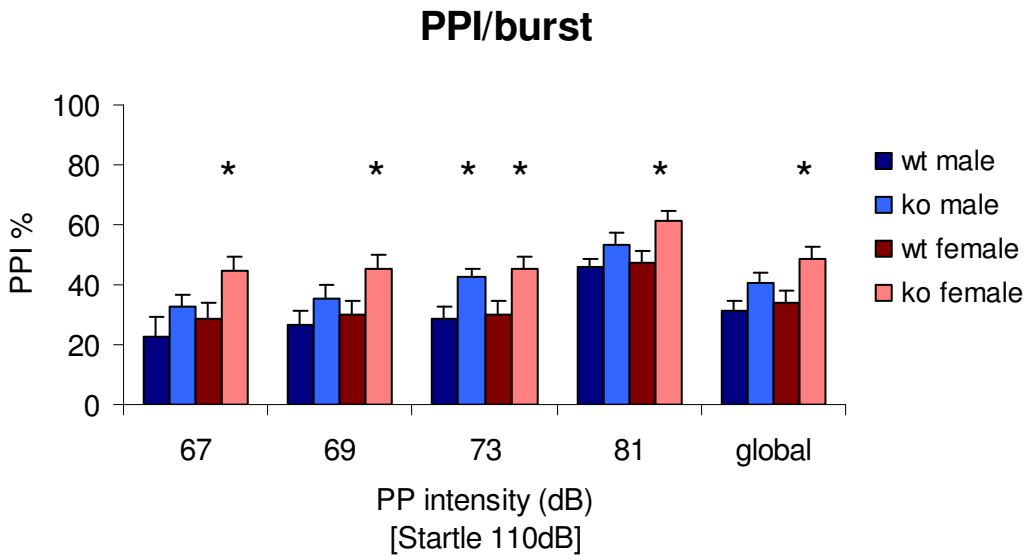

Figure 40: Results of PPI

PPI results at a startle intensity of 110 dB and prepulse intensities of 67, 69, 73 and 81 dB. "Global" is the mean PPI value of all 4 prepulse intensities. *p<0.05 vs. control

There was no significant genotype effect on **acoustic startle reactivity** (Fig.41). A significant sex difference with females showing generally a weaker reaction than males was detected (Multivariate tests, p<0.05, *). Values of mutant animals of both sexes were slightly lower than values of their wildtype littermates (Multivariate tests, p>0.05, n.s.).

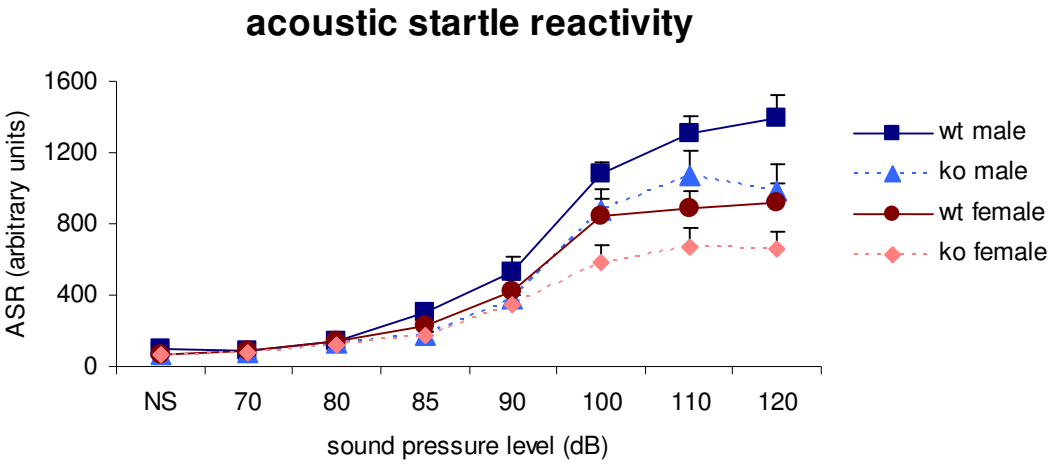

Figure 41: Acoustic startle response

Measured at background noise (NS) and sound pressure intensities of 70 - 120 dB.

Behavioural analysis of spontaneous activity in a novel environment, using the Open Field test, revealed no significant genotype effects (data not shown). This included no change in locomotor activity, exploratory or anxiety-related behaviour.

4.11.3 No obvious neurological phenotype in young mice visible

Primary phenotypic characterization of young heterozygous *Tom40* mice revealed no obvious neurological differences between mutants and wildtypes comparing the mean values on the Rotarod (Fig.42). Statistical evaluation revealed a significant interaction between body weight, trial number and genotype (Linear mixed effects model: $p<0.05$, *).

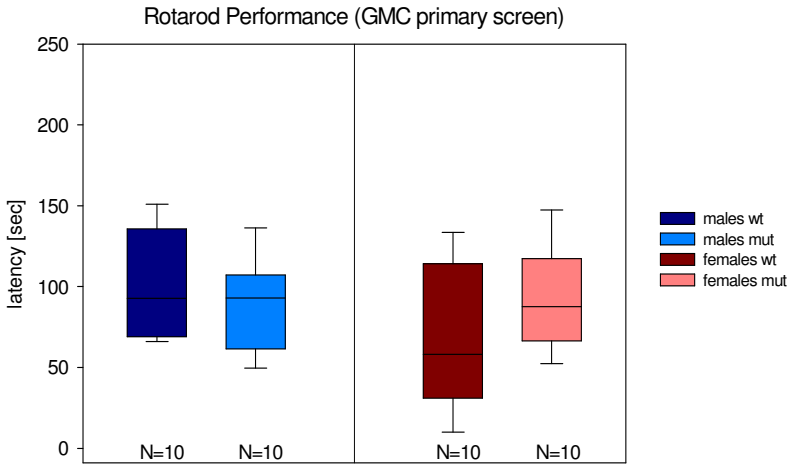

Figure 42: Mean latency to fall of the rod (primary screen)
There was no significant different difference between the genotypes but an interaction of body weight x trial number x genotype (Linear mixed effects model: $p<0.05$, *).

Examining males and females separately revealed a significant interaction of genotype and body weight on Rotarod performance (Fig.43; Linear mixed effects model: $p<0.05$, *): heavier mutants fell off the rotating rod earlier than lighter ones.

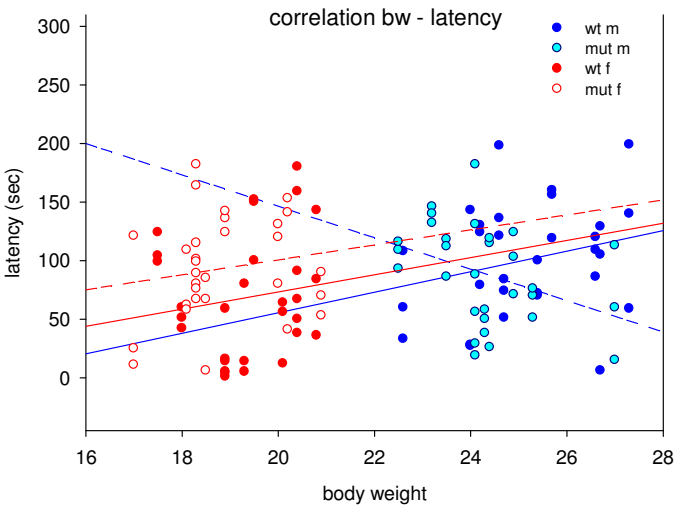

Figure 43: Correlation body weight x latency to fall of the rod
Males: significant interaction between body weight and genotype ($p<0.05$, *)

In addition there was a significant genotype x trial interaction in males: While wildtype mice showed a learning curve, mutant mice didn't (Fig.44; Linear mixed effects model: $p<0.05$, *). Female mice of both genotypes showed an improvement with ongoing trials ($p<0.01$, **).

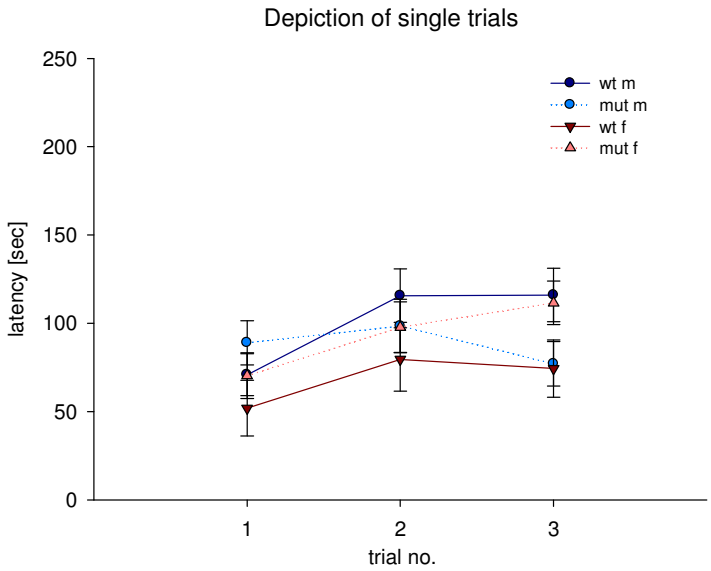

Figure 44: Depiction of Rotarod single trials (GMC primary screen)
Males: significant interaction between trial number and genotype ($p<0.05$, *): while control mice improve, mutant males got worse.
Females: significant trial effect ($p<0.01$, **): improvement with trial.

All SHIRPA parameters were without significant findings. Serum lactate levels revealed a typical sex-specific difference between males and females (Two Way ANOVA: $p<0.001$, ***) but no differences between mutants and controls (Table 12).

The locomotor activity was higher in female mutants than in female controls, but lower in male mutants than in male controls (Table 12). This is reflected by a significant interaction of sex and genotype was found (Two Way ANOVA: p<0.01, **). However, only the activity reduction in males reached significance (t-test p<0.01, **).

Table 12: Body Weight, Locomotor activity (SHIRPA) and serum lactate levels
Data are presented as mean ± standard error of mean.

	Males (m)		Females (f)		Post hoc (genotype)		2-Way-ANOVA		
	wt	het	wt	het	m	f	Sex	Geno-type	Inter-action
Para-meter	(n=10)	(n=10)	(n=10)	(n=10)	*p-value*	*p-value*	*p-value*	*p-value*	*p-value*
bw (g)	24.71 ± 0.42	23.61 ± 0.37	19.43 ± 0.31	18.87 ± 0.38	***<0.05***	*n.s.*	***<0.001***	***<0.05***	*n.s.*
Loc A (no. of squares)	28.5 ± 1.65	21.6 ± 2.50	23.7 ± 1.37	28.1 ± 1.35	***<0.01***	*n.s.*	*n.s.*	*n.s.*	***<0.01***
Serum lactate	13.48 ± 0.30	12.71 ± 0.46	11.64 ± 0.40	11.53 ± 0.55	*n.s.*	*n.s.*	***<0.001***	*n.s.*	*n.s.*

There was a body weight differences between the sexes (Two Way ANOVA: p<0.001, ***) and between the genotypes (p<0.05, *). While in pipeline I of the primary screen mutants showed significantly increased body weight compared to controls (Fig.45A, weight data were taken from the dysmorphological screen, age of the mice: 14 weeks; t-test p<0.05, *, for both sexes), in pipeline II the body weight of male mutants was significantly decreased (Fig.45B, data were taken from the neurological screen, age of the mice: 10 weeks; t-test p<0.05, *).

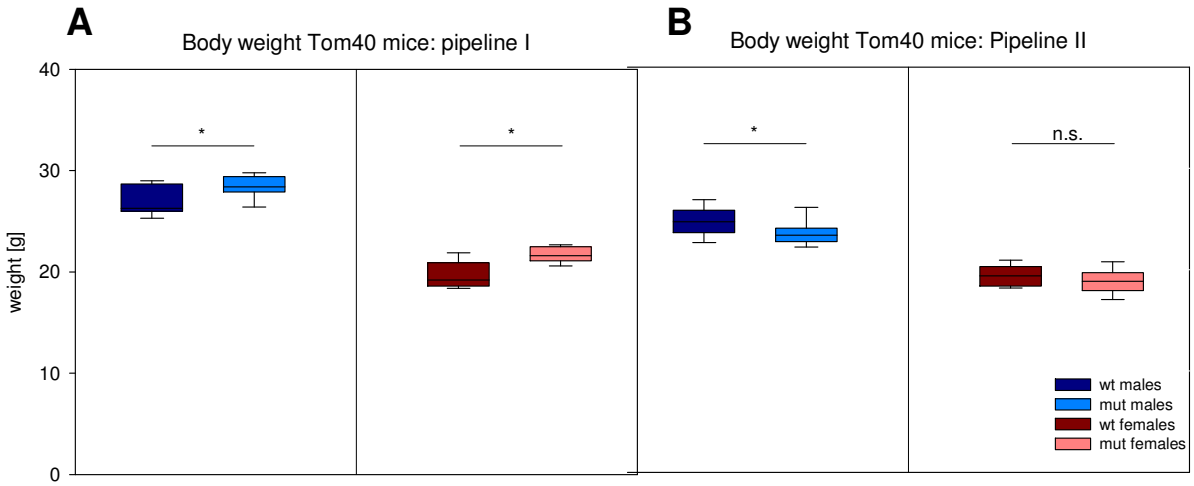

Figure 45: Body weight Tom40 primary screen cohort
A: Pipeline I: significant body weight increase in mutants of both sexes (Two Way ANOVA: p<0.05, *)
B: Pipeline II: significant body weight decrease in mutant male mice (Two Way ANOVA: p<0.05, *)

Comparing the grip strength of two and four paws did not reveal impairments (Fig.46; Linear mixed effects model: p>0.05, n.s. for both, 2 and 4-paws measurement). In the four paws measurement there was a trend towards higher values in mutant animals (p=0.0636).

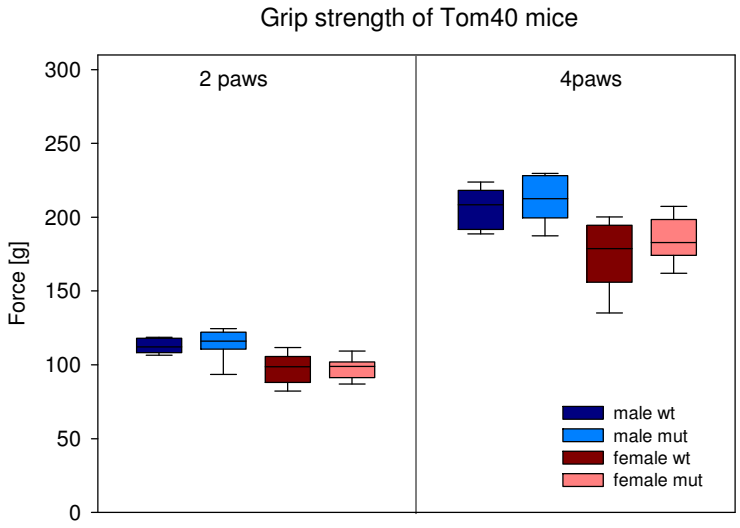

Figure 46: Grip strength, two paws and all paws (GMC primary screen)
No significant differences.

4.11.4 There is no eye-phenotype in young mice

All mice were first examined by Slit Lamp Biomicroscopy. There were no abnormalities of the anterior eye segment associated with the Tom40 mutation. The small nuclear flecks observed in the lens represent a strain specific problem rather than a consequence of the altered genotypic situation. The same was found for the posterior eye segment by funduscopical investigations. Laser Interference Biometry data indicated typical sex differences among normalized (for body length) eye sizes of both groups, but only among absolute axial lengths of the controls. Mutants and controls did not differ significantly in both parameters.

4.11.5 *Tom40* +/- mutants don't differ in nociception

The first reaction on the hotplate for evaluation of thermal nociception presented by the animals was "hind paw shaking", the second one "paw licking". We did not find any difference in the recorded latencies between the genotypes. We detected a slight difference between the sexes in the first reaction, but only in the controls (wt males 1st sign of pain=7.73±0.75, 2nd reaction=11.01±1.28; wt females 1st sign of

pain=10±0.8, 2nd reaction=12.83±1.3; mut males 1st sign of pain=8.43±0.75, 2nd reaction=13.4±1.28; mut females:1st sign of pain=9.78±0.8, 2nd reaction=14.98±1.3; ANOVA: 1st sign of pain: genotype; p = 0.706, sex p = 0.018, genotype*sex; p = 0.584; 2nd reaction: genotype; p = 0.085, sex; p = 0.192 , genotype*sex; p = 0.926).

4.11.6 Young *Tom40* mutants show no metabolic phenotype

Due to a technical problem no carbon dioxide production could be monitored. Only few genotype effects on energy metabolism parameters could be detected in *Tom40*-mutant mice under *ad libitum* conditions. Mutant mice were heavier than controls but no shift in body composition could be detected by NMR scans. Energy expenditure, body temperature and locomotor activity did not differ between mutant and control mice.

Table 13: Metabolic Parameters
Data are presented as mean ± standard error of mean.

Parameter	Control		Mutant		2 – Way – ANOVA *(*GLM: genotype*sex+bm)*			
	male (n=10)	female (n=10)	male (n=9)	female (n=10)	*p genotype*	*p sex*	*p geno*sex*	*p bm*
Body mass (g)	21.1 ± 0.7	21.9 ± 0.3	26.9 ± 0.9	28.9 ± 0.4	0.035	**<0.001**	0.322	n/a
Fat mass (g)	5.4 ± 0.4	5.5 ± 0.2	5.9 ± 0.3	6.3 ± 0.2	0.512	**0.001**	0.833	**<0.001**
Lean mass (g)	12.5 ± 0.3	13.1 ± 0.2	16.9 ± 0.6	18.1 ± 0.2	0.323	**<0.001**	0.738	**<0.000**

4.11.7 Clinical chemistry results

No genotype-related differences in glucose clearance were detected in the IpGTT comparing heterozygous mice with controls (Fig.47).

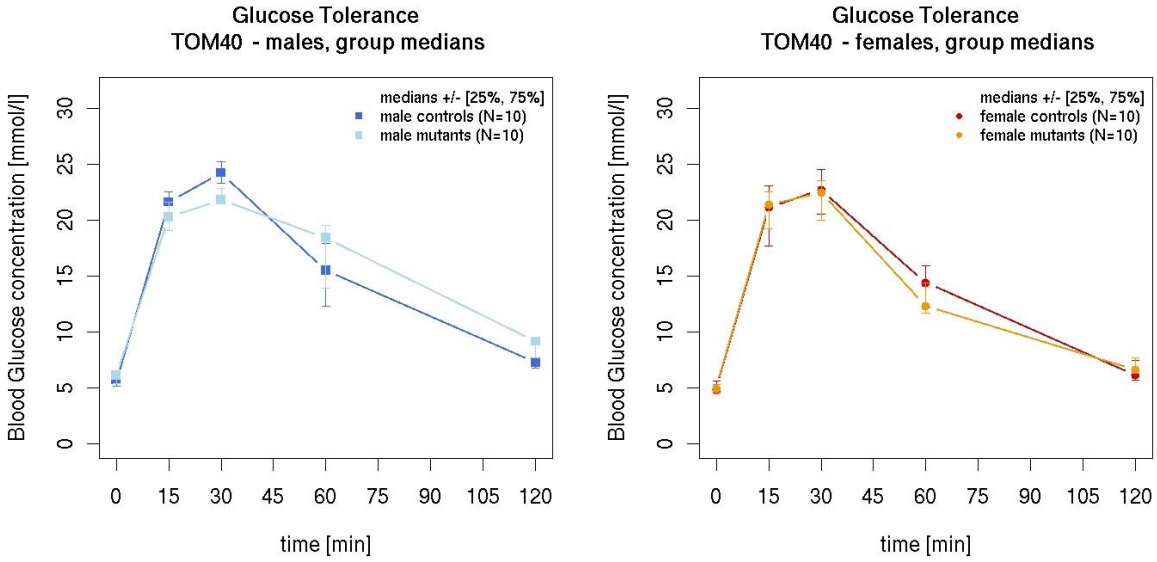

Figure 47: IpGTT of male (A) and female (B) *Tom40*-mutant mice and controls
No genotype-specific differences.

The analysis of plasma samples collected from overnight fasted mice revealed only mild genotype-related differences in HDL-cholesterol level, which was slightly higher in mutant mice, and free fatty acid concentration, which was slightly lower in mutants compared to controls (table 16, appendix). None of these findings was significant after Holm correction.

In the first sample there was an influence of the genotype on plasma cholesterol and triglyceride concentrations as well as LDH activity, which were slightly decreased in mutant animals, while ALP activity was increased in mutants (ANOVA, $p<0.05$, *, see table 14). Additionally there were slightly lower total protein and glucose values in heterozygous males compared to controls.

Nevertheless none of these differences were confirmed by the second measurement (table 17 appendix), except the effect on ALP activity in mutants and the slightly lower glucose concentration in mutant males. All differences were small and not considered to be significant after Holm correction.

In the peripheral blood cell count a genotype-related effect on platelet count was found in *Tom40*-mutant mice, which was slightly lower in heterozygous *Tom40*-mutant mice (wt: male=1473 ± 40.5, female=1189 ± 54.5; mut: male=1268 ± 46.9,

female=1152 ± 45. 6; ANOVA: genotype p<0.05, sex p<0.001, interaction p=0.084; t-test: males: p<0,01, females n.s.). However, again this difference was very small and after multiple testing adjustment of the significance level not considered to be significant. Therefore it is likely that this change is an accidental finding. Sex-related differences were found for many parameters.

Table 14: Clinical-chemical parameters, 1st sample.
Data are presented as mean ± standard error of mean.

Parameter	Control (A)		Mutant (B)		A~B	A~B	ANOVA		
	Male	Female	Male	Female	Male	Female	genotype	sex	inter.
	(n=10)	(n=10)	(n=10)	(n=9)	*p*	*p*	*p*	*p*	*p*
Sodium [mmol/l]	142 ± 0.67	137.2 ± 0.44	142 ± 0.67	136.7 ± 0.67	n.s.	n.s.	n.s.	p<0.001	n.s.
Potassium [mmol/l]	3.94 ± 0.15	3.92 ± 0.15	4.09 ± 0.11	3.84 ± 0.16	n.s.	n.s.	n.s.	n.s.	n.s.
Calcium [mmol/l]	2.32 ± 0.01	2.24 ± 0.02	2.33 ± 0.01	2.28 ± 0.02	n.s.	n.s.	n.s.	p<0.001	n.s.
Chloride [mmol/l]	111.3 ± 0.69	108.7 ± 0.48	110.9 ± 0.48	109 ± 0.34	n.s.	n.s.	n.s.	p<0.001	n.s.
inorg. phos. [mmol/l]	1.46 ± 0.11	1.34 ± 0.11	1.36 ± 0.07	1.27 ± 0.12	n.s.	n.s.	n.s.	n.s.	n.s.
Total Protein [g/dl]	5.66 ± 0.08	5.18 ± 0.11	5.4 ± 0.06	5.29 ± 0.13	p<0.05	n.s.	n.s.	p<0.01	n.s.
Albumin [g/dl]	2.34 ± 0.052	2.38 ± 0.036	2.32 ± 0.033	2.333 ± 0.033	n.s.	n.s.	n.s.	n.s.	n.s.
Creatinine [mg/dl]	0.12 ± 0.01	0.12 ± 0	0.11 ± 0.01	0.12 ± 0	n.s.	n.s.	n.s.	n.s.	n.s.
Urea [mg/dl]	75.8 ± 2.82	71.3 ± 2.75	75 ± 3.63	67.9 ± 2.53	n.s.	n.s.	n.s.	p=0.06	n.s.
Cholesterol [mg/dl]	107.5 ± 3.36	78.8 ± 2.17	100.7 ± 4.54	71.3 ± 3.52	n.s.	n.s.	p<0.05	p<0.001	n.s.
Triglycerides [mg/dl]	162 ± 10.7	107 ± 9.5	137 ± 14.8	87 ± 7.9	n.s.	n.s.	p<0.05	p<0.001	n.s.
LDH [U/l]	449 ± 81.45	355.4 ± 87.89	285.2 ± 7.03	245.4 ± 32.64	n.s.	n.s.	p<0.05	n.s.	n.s.
ALT [U/l]	38.4 ± 6.98	29.2 ± 3.73	40.2 ± 12.73	33.3 ± 7.5	n.s.	n.s.	n.s.	n.s.	n.s.
AST [U/l]	61 ± 14.53	54 ± 3.65	54 ± 10.95	61.1 ± 5.26	n.s.	n.s.	n.s.	n.s.	n.s.
ALP [U/l]	98.2 ± 3.38	141.6 ± 7	108.6 ± 1.98	154.7 ± 6.08	p<0.05	n.s.	p<0.05	p<0.001	n.s.
α-Amylase [U/l]	577 ± 14.2	1301 ± 751.4	582 ± 36.5	449 ± 16	n.s.	n.s.	n.s.	n.s.	n.s.
Glucose [mg/dl]	192.7 ± 8.6	216.4 ± 14.6	158.2 ± 13	205.8 ± 8.4	p<0.05	n.s.	n.s.	p<0.01	n.s.
Ferritin [ng/ml]	23.5 ± 1.27	26.8 ± 0.94	49.3 ± 26.76	25.9 ± 1.83	n.s.	n.s.	n.s.	n.s.	n.s.
Transferrin [mg/dl]	133.2 ± 1.85	131.8 ± 0.92	132.9 ± 1.55	129.4 ± 1.44	n.s.	n.s.	n.s.	n.s.	n.s.
Iron [µg/dl]	110.4 ± 5.53	134.2 ± 11.52	106.8 ± 3.3	119.3 ± 6.39	n.s.	n.s.	n.s.	p<0.05	n.s.

4.11.8 Immunology: subtle differences in male mutants

Flow cytometric analysis of *Tom40*-mutant mice in the primary Immunology Screen revealed a genotype-related immune phenotype in male mutants. On a statistical significance level of $p<0.05$ a significantly higher frequency of T cells was found in both subsets of CD4+ and CD8+ T cells. A positive correlation between the frequencies of CD4 and CD8 T cells is observed also in wild-type mice (own observations and Petkova et al. (2008)). The increase in T cells did not go together with statistically significant changes in other leukocyte subsets. In order to investigate, whether the change in the frequency of T cells is caused by peripheral proliferation or primary production of naïve T cells, we analyzed the pattern of T cell subsets based on the expression on CD25, CD44, CD62L and Ly6C. We observed only slight differences in the expression pattern in the CD4 and CD8 T cell cluster which were not found to be statistically significant (permutation test, 10000 permutations).

4.11.9 No differences in allergy parameters

The analysis of total IgE levels in plasma of Tom40 mice did not reveal statistically significant differences between mutant and control mice (wt males=27±42, females= 72±70; mut males=34±60, females 35±40).

4.11.10 No differences in steroid metabolism

The analysis of DHEA and testosterone concentrations in plasma of *Tom40*-mutant mice revealed no statistically significant differences between mutants and controls. In both groups of mutant and control animals, the testosterone levels were significantly higher in males than in females.

4.11.11 Heterozygous Tom40+/- mice show a cardiac phenotype

The basal cardiovascular functions were investigated in the primary screen by non-invasive blood pressure measurement over four days, six lead surface ECG, and determination of heart weight.
In blood pressure analysis (Fig. 48) no genotype specific differences were found.

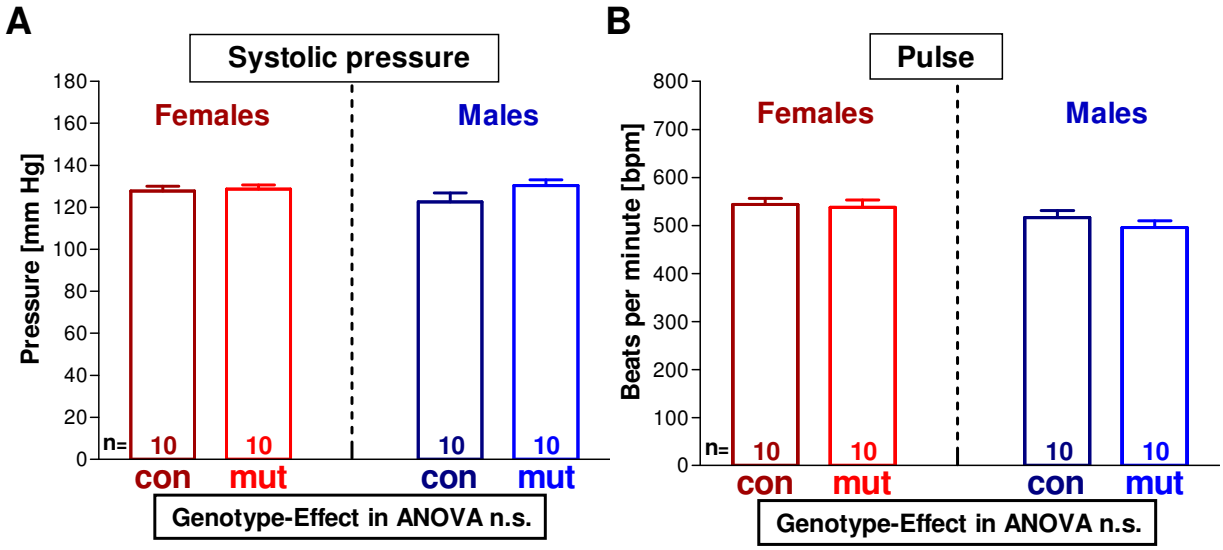

Figure 48: Blood pressure parameters systolic pressure (A) and pulse (B)
No genotype-specific difference.

The ECG analysis revealed a genotype-specific shortening of P-wave duration mainly in female mutants (Fig.49A, ANOVA: Genotype effect $p<0.05$,*). The P-wave represents the depolarization through the myocardium of the atria. In addition, the *Tom40*-mutant mice showed an increased QT interval and QTc, the QT interval corrected for heart rate (Fig.49C). The QT interval represents the electrical events during the systole comprising the depolarization and repolarization of the ventricle. Therefore, it is dependent of the frequency and usually normalized for heart rate (QT interval corrected). In contrast to QT, the ST interval is a measurement for repolarization only, although both intervals merge and the transition is not very well defined in mice (Danik S et al., 2002). Also the ST interval was increased in *Tom40*-mutant animals (Fig.49B). No difference was seen in the QRS complex duration, which suggests that the repolarization is more affected than the depolarization. These effects were more pronounced in the male mice than in the female mice. Subtle effects (lower S amplitude, trend to lower R amplitude and trend to interaction of sex and genotype in Q amplitude) were seen in the different components of the QRS amplitude, which can supply information about the excitable mass of the heart. In the more indicative parameter of the QRS amplitude no significant alteration was seen.

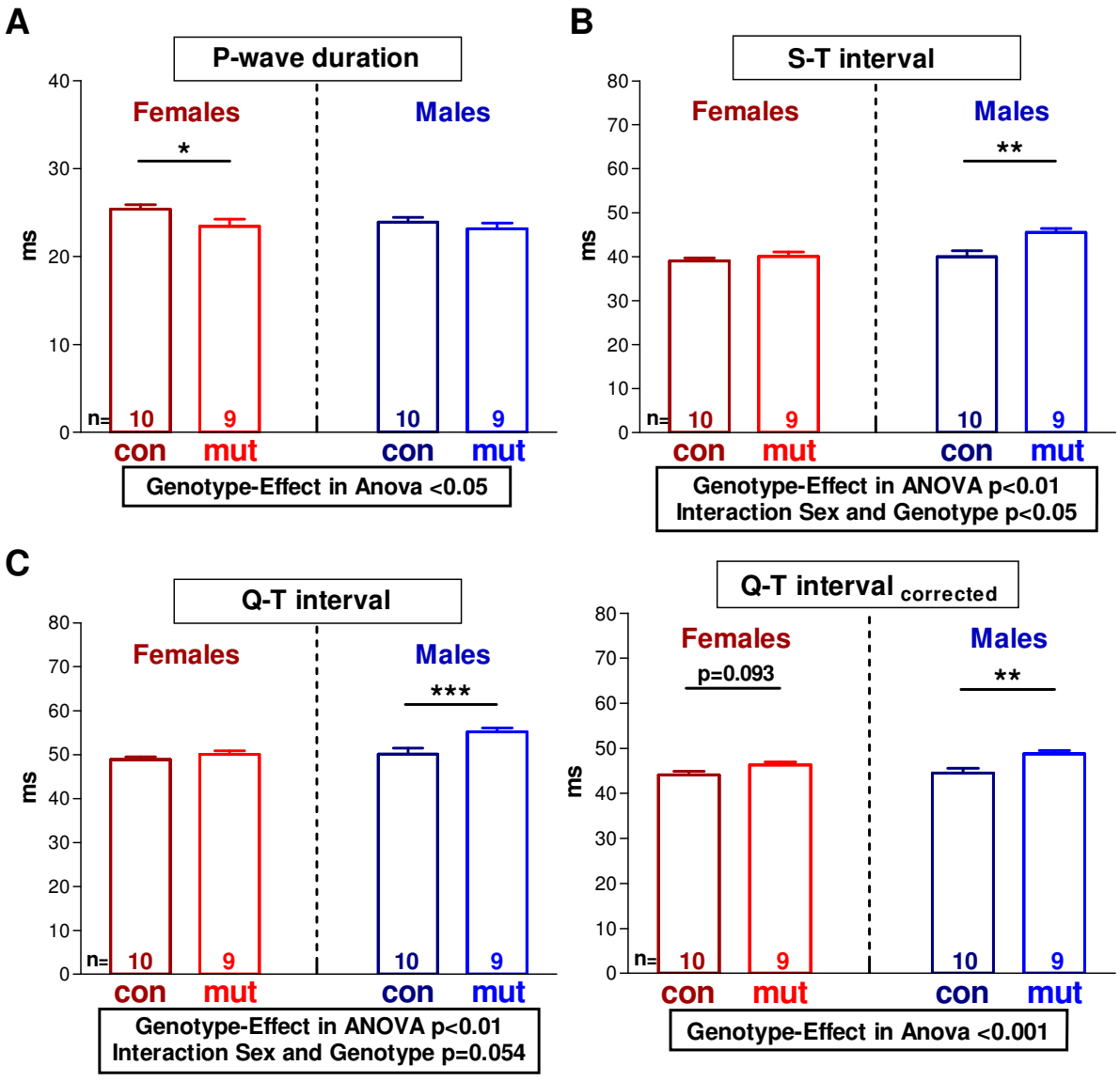

Figure 49: Results of ECG analysis

A: The P-wave duration in mutant mice revealed a slight but significant genotype-specific de-crease mainly in the female mutants (ANOVA p<0.05, *; post-hoc: males p<0.05, *). B: In the S-T interval a genotype-specific increase mainly in male mutants was found (ANOVA: sex p<0.01,**, genotype p<0.01,**, interaction sex-genotype p<0.05,*; post-hoc: males p<0.01, **) C: The Q-T interval genotype-specifically increased which was more pronounced in the male mutants.(ANOVA: genotype p<0.01, **, sex p<0.01, **, Interaction sex-genotype p=0.054; Post hoc: males p>0.001, ***). Correction to heart rate resulted in a reduction of sex differences but sustained genotype-specific increase (ANOVA: genotype p<0.001, ***; post hoc: males p>0.01, ***, females p=0.093, n.s.).

In heart weight analysis (Fig.50) no genotype-specific differences were found com-paring mutant to control mice.

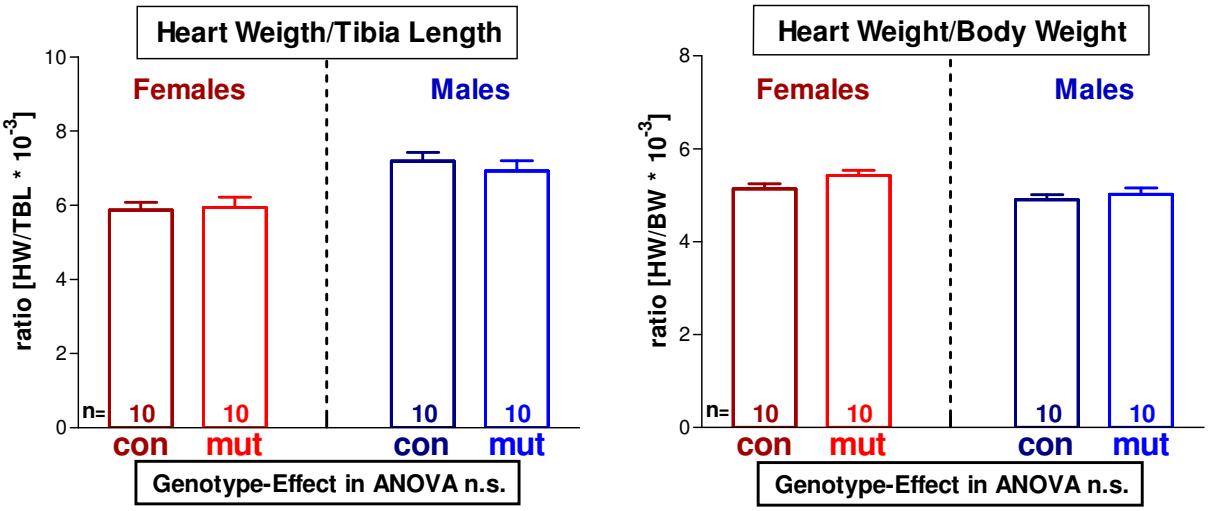

Figure 50: Normalized Heart weight

Heart weight revealed no genotype-specific difference comparing mutant with control mice, neither normalized to tibia length nor normalized to body weight.

4.11.12 No genotype-specific changes in lung function

There were minor significant differences between male groups with higher tidal volumes (TV) in mutants (t-test $p<0.05$, *), secondary causing an increase in inspiratory flows (PIF, MIF; t-test $p<0.05$, *). However, specific values for TV are comparable. No differences at all were observed between female groups.

4.11.13 Molecular phenotyping of brain and liver tissue

Brain and liver were chosen for the Tom40 mutant mouse line for expression profiling analysis. These two organs were selected due to expected phenotypes in tissues with high energetic demands such as brain and skeletal muscle. The statistical analysis of eight experiments of each selected organ from four *Tom40*-mutant mice identified no significant differentially expressed genes. Expression levels between mutant and wild type tissue were similar in these organs.

4.11.14 Pathology: primary screen without findings

A total of 39 mice were analyzed macroscopically. Histological analysis of all organs was performed in 24 mice: 12 heterozygous *Tom40*-mutant (six females, six males) and 12 control mice (six females, six male).

All the analyzed organs appeared normal and none of the heterozygous *Tom40*-deficient mice showed a genotype-specific morphological phenotype (i.e. heart tissue (Fig.51) and muscle tissue (Fig.52)).

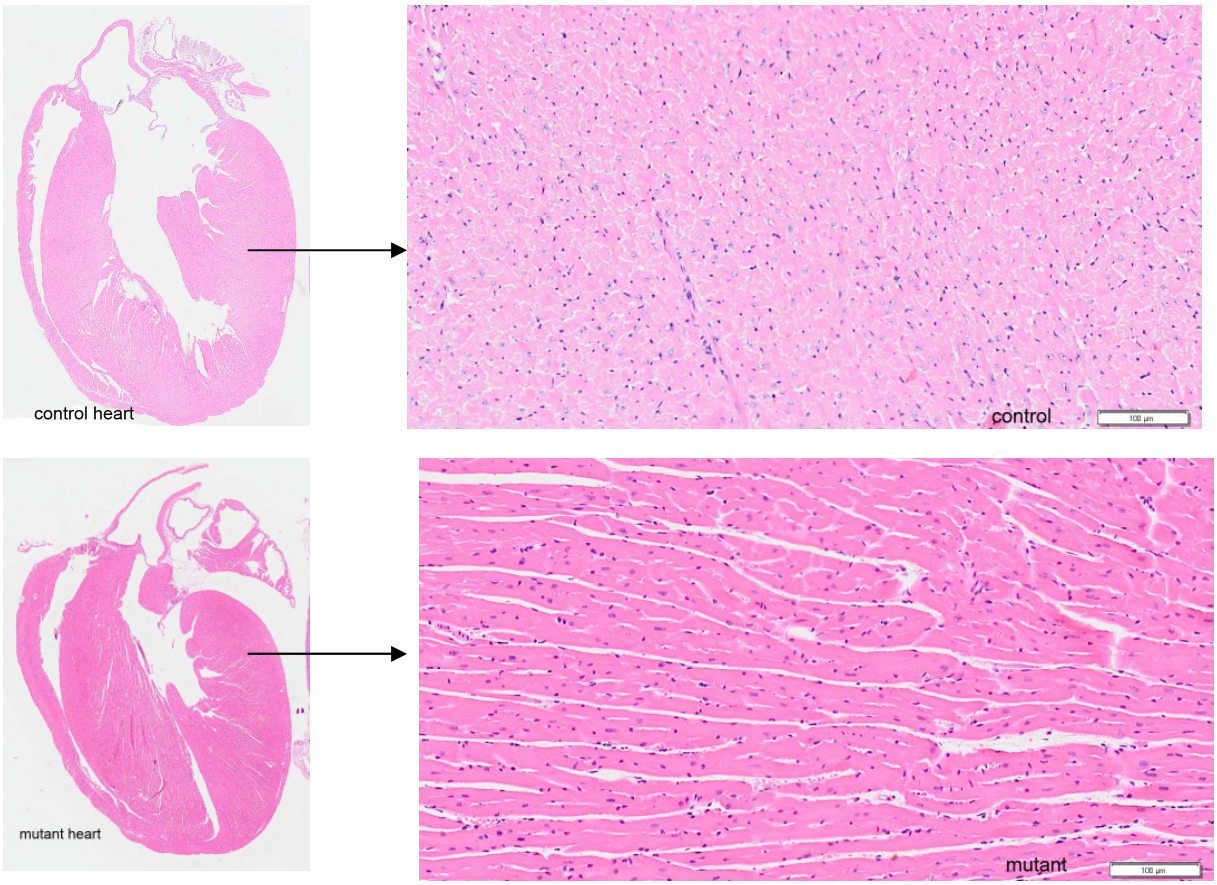

Figure 51: H&E staining of mutant and wildtype heart tissue.
No genotype-specific changes.

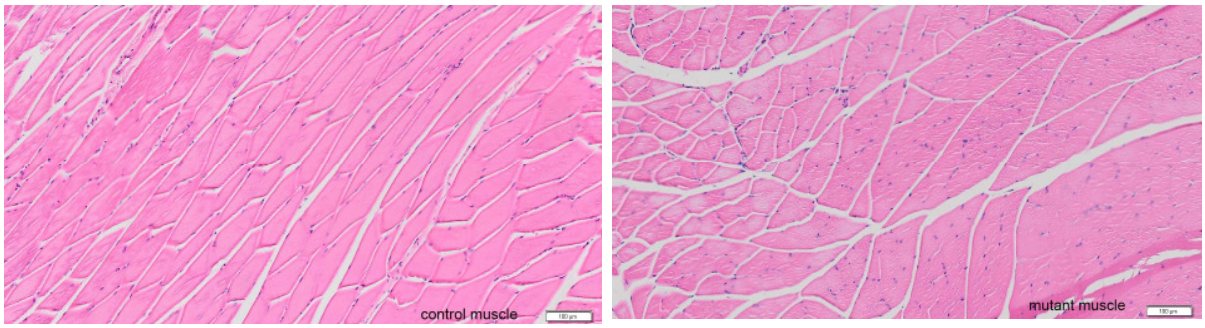

Figure 52: H&E staining of mutant and wildtype muscle tissue.
No genotype-specific changes.

4.12 Transmission Electron Microscopy

Although the primary screening did not reveal alterations in heart pathology further analysis was performed because of the cardiovascular phenotype. A marked difference between mutant and control animals already was detectable when looking at the semifine sections of the prepared heart tissue prepared for transmission Electron Microscopy (Fig.53). While control heart muscle showed a very clear organization and structure mutant heart tissue seemed to be much more unstructured and distorted.

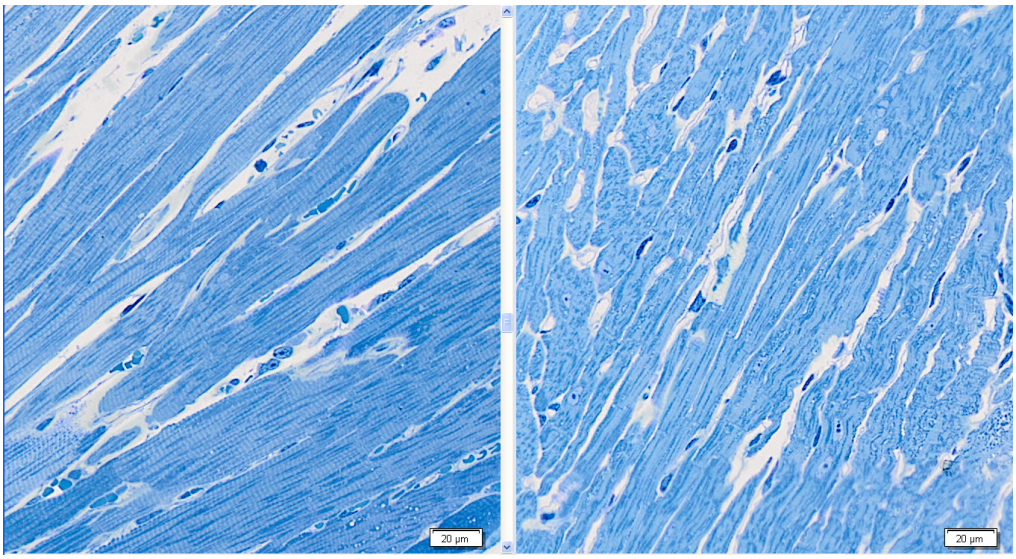

Figure 53: Semifine sections of heart tissue of control and mutant mice.

In the TEM analysis the altered morphology in mutant mice was clearly visible: normal morphology of the myocardium as seen in the control mice consist in one or two rows of mitochondria of regular size distributed in parallel to the myofibrils (Fig.54). In turn, one interesting finding in heart muscle of the mutant mouse was the presence of mitochondria's aggregates with irregular size und form, surrounded groups of myofibrils. This is apparently associated with distortion of the myofibrils. It is important to consider that these changes were not generalized and areas with normal morphology were observed in the mutant mice, too (Fig.54).

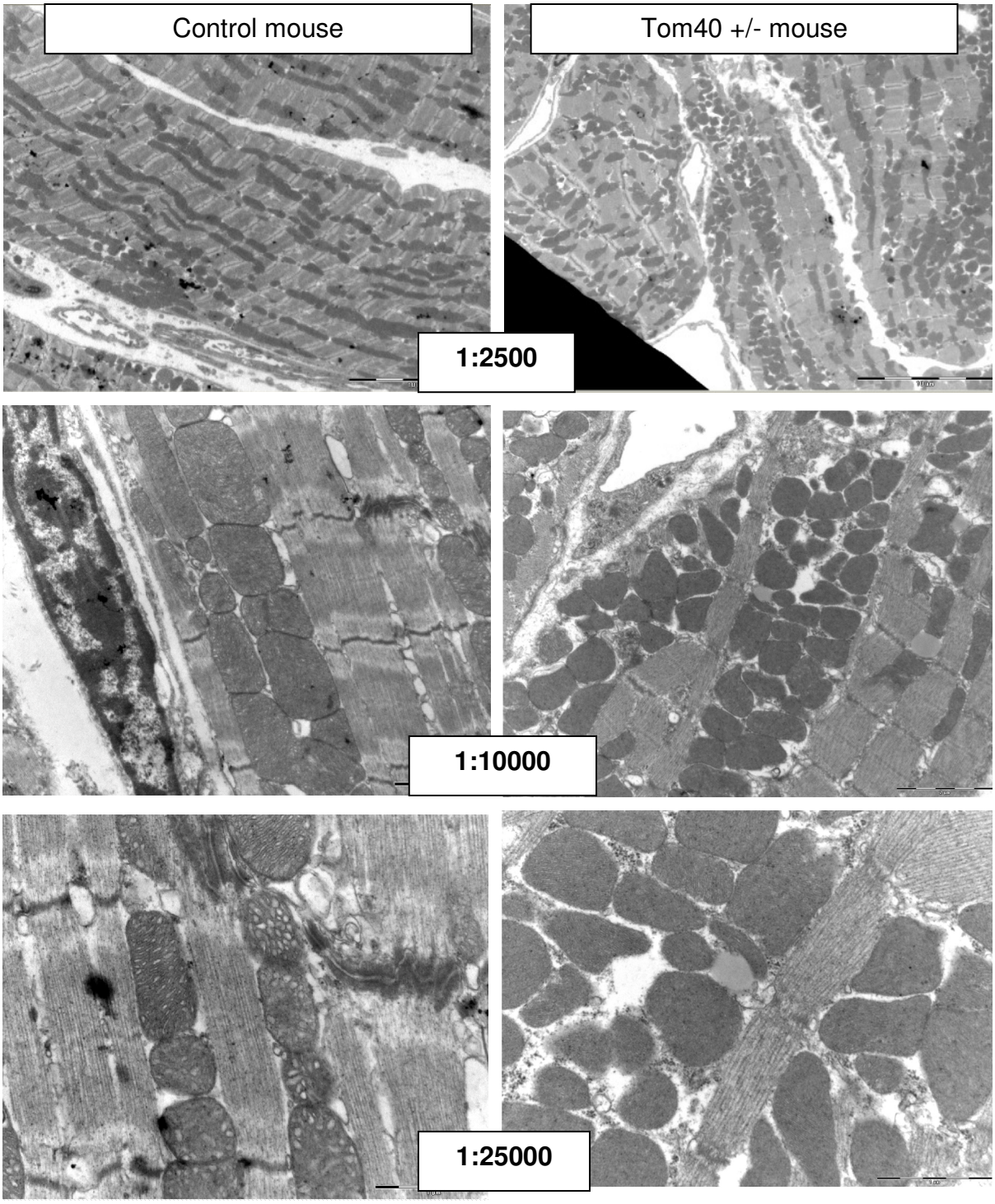

Figure 54: Heart from control and *Tom40* +/- mouse at different amplifications

The pictures depict clearly the apparently distortion of the myofibrils and presence of mitochondrial aggregates with irregular size und form observed in the mutant mouse.

Concerning the ultra structural anatomy of the mitochondria differences between mutant and control mice were observed (Fig.55). Mutant mitochondria appeared darker and their inner structure seemed to be condensed with less space between

the cristae. Increase of fibrous or adipose tissue between the myofibrils was not observed. In addition, no differences in the striated morphology of cardiac muscle between Tom40- mutant and control mice were observed.

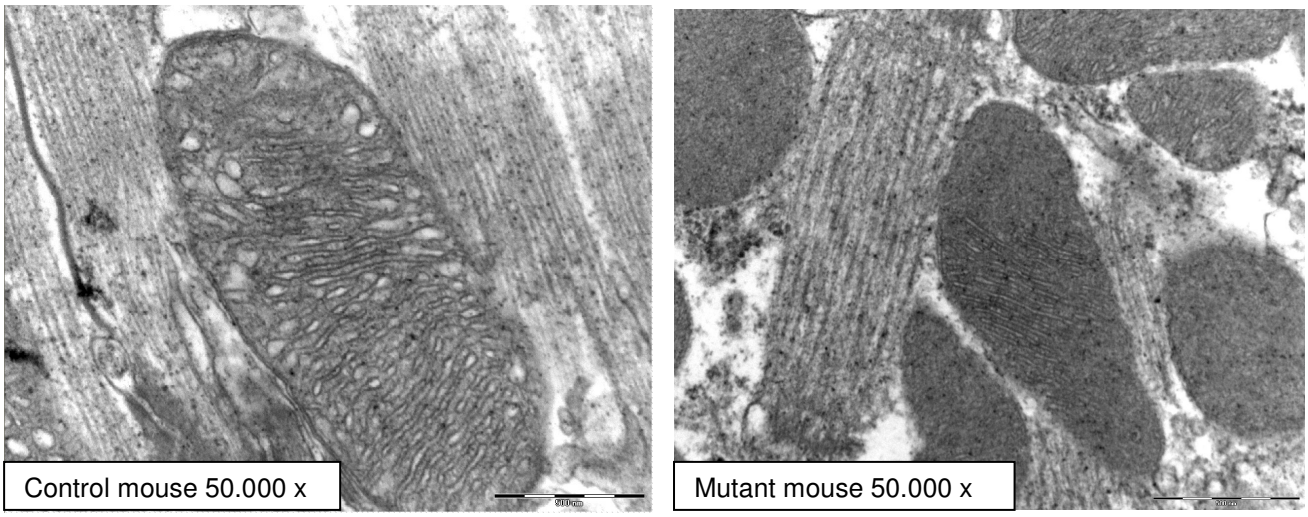

Figure 55: Ultrastructure of mitochondria in wildtype and mutant animals.
No differences between control and mutant mice were observed.

4.13 Secondary screening of an aging cohort

4.13.1 Survival of the aging cohort animals

Animals were bred and kept in the animal facilities for more than 24 month. For the survival curve only those mice were used that died naturally (i.e. if they were found dead or if they were fatally ill and had to be sacrificed). Of 75 born mice investigated (38 *Tom40*+/+, 47 *Tom40*+/-) two mutant mice died within the first year, while all wildtypes survived. In the second year 12 mutant mice died, whereas there where only 5 dead wildtype *Tom40*+/+ mice. Statistical analysis showed that the survival curves for the genotypes are significant different (Fig.56; Logrank Test: $p<0.01$, **).
After two years 89.5% of the wildtype mice cohort still was alive (males: 90.5%, females: 88.2%) whereas in the mutant cohort only 59.5% were left (males: 68.8%, females: 52.4%).

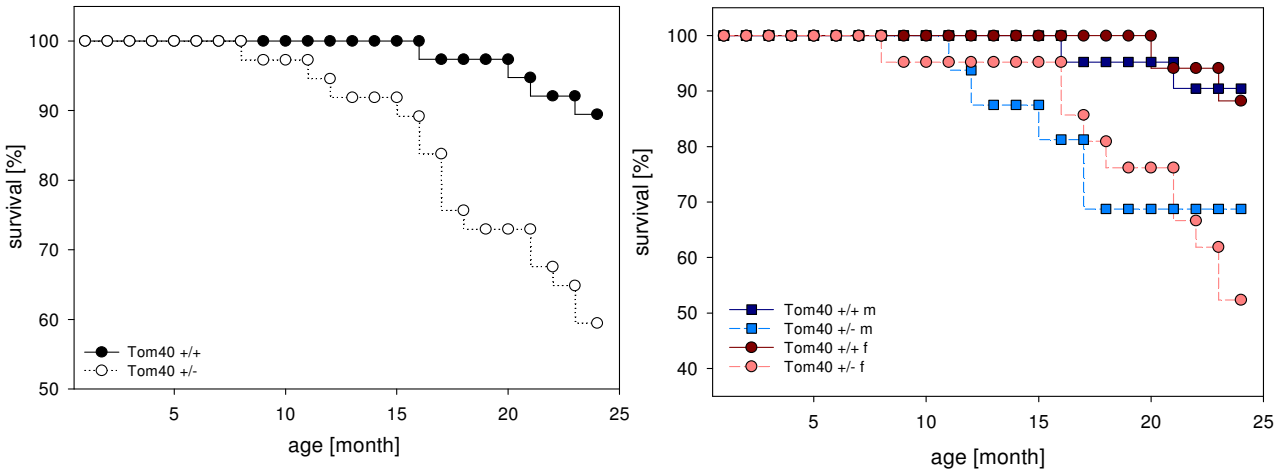

Figure 56: Kaplan-Meyer survival curves of *Tom40+/+* and *Tom40+/-* mice

Mutant animals seem to die earlier than their wildtype littermate. Mortality after two years is about 40% in heterozygous Tom40 mutant mice and 10% in controls.

4.13.2 Neurological screening of the aging cohort

4.13.2.1 Grip strength of aged animals

Analysis of muscle force revealed no genotype-specific difference between mutant Tom40-heterozygous mice and controls when they were old (Fig.57; males: wt n=20, het n=13; females: wt n=17, het n=18; Linear mixed effects model, p>0.05, n.s.).

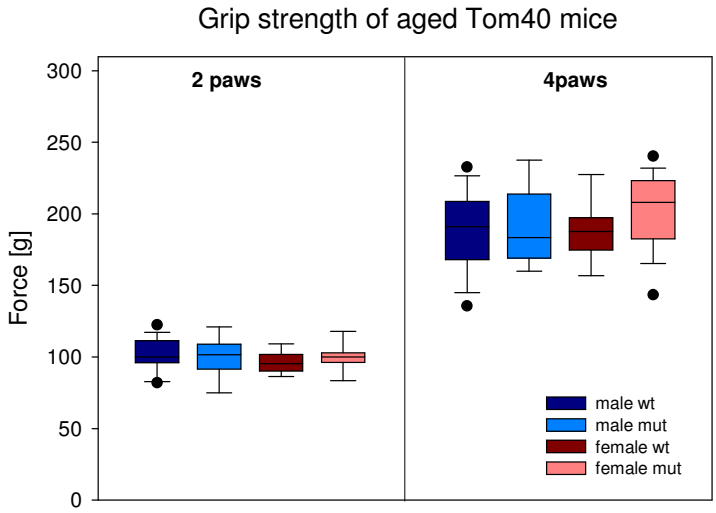

Figure 57: Grip strength of the aged Tom40 cohort

No genotype-specific changes, neither looking at the fore paws nor looking at all paws.

4.13.2.2 Rotarod

The ability of *Tom40* mutant mice to cope with the Rotarod was examined at different time points: the aging cohort was first tested when animals were 6month old and tested again after 2years. Like in primary screen of the GMC no obvious phenotype was detectable in young animals (compare with chapter 4.11.3). In aged animals, there was a significant genotype-effect more pronounced in male mice concerning the latency to fall of the rod (Fig.58; young animals: males: wt n=21, het n=16; females: wt n=17, het n=21; aged animals: males wt n=16, het n=10; females: wt n=16, het n=19; Linear mixed effects model: genotype $p<0.01$, **; only males $p<0.01$, **; females $p>0.05$, n.s.).

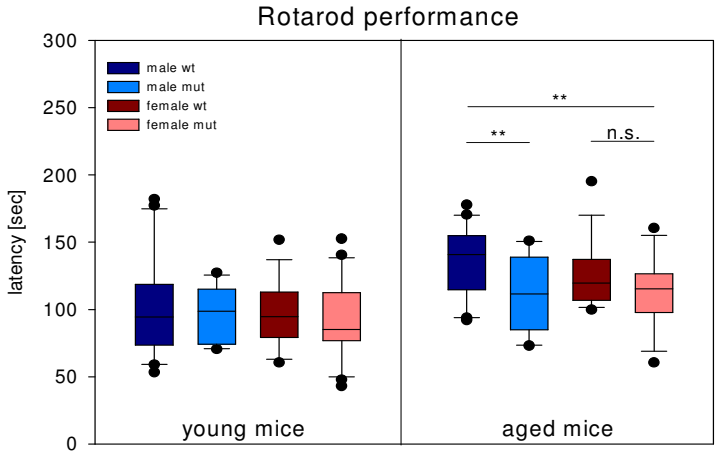

Figure 58: Rotarod analysis of young and aged *Tom40* mice

In young animals there were no genotype-specific effects. In aged mice, there was a significant difference in the latency to fall of the rod: mutant mice perform worse than controls (Linear mixed effects model: $p<0.01$, **). This is more pronounced in male animals than in females.

The depiction of single trials revealed a significant effect on the single trials in female mice: animals improved with time (Fig.59; Mixed effects model: $p<0.001$, ***, males $p=0.0795$, n.s., females $p<0.001$, ***).

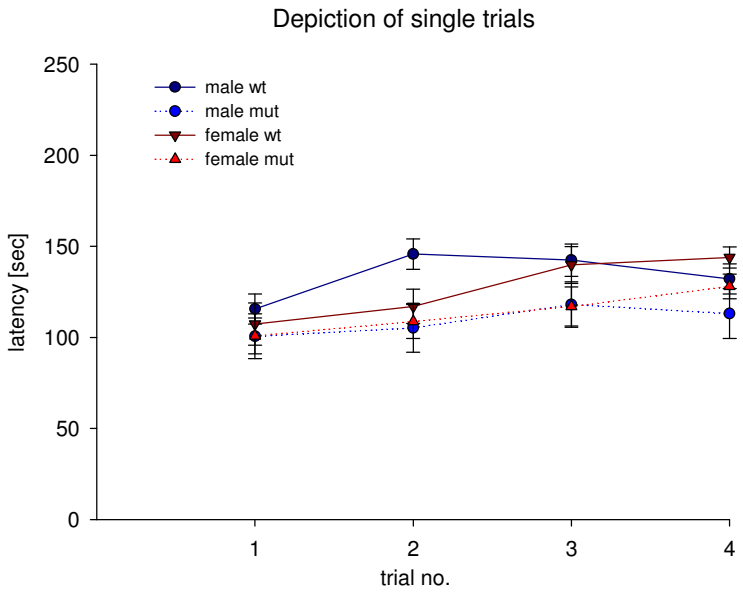

Figure 59: Single trial analysis of the aged cohort

Female animals of both genotypes improve with time (Linear mixed effects model: p<0.001, ***)

The longterm Rotarod task was performed with young animals (Fig.60A; age: 3 month; males: wt n=13, het n=15; females: wt n=18, het n=15) as well as with aged ones (Fig.60B; age: 17month; males wt n=16, het n=10; females: wt n=16, het n=19). Within the young cohort, there were interactions between body weight x speed (Linear mixed effects model: p<0.05, *): heavier animals had more problems to cope with the higher speeds, more pronounced in male mice. An Interaction sex x speed (p<0.05, *).. indicated a greater decline in performance with increasing speed in male mice than in females, even so also in females a speed effect could be observed (p<0.001, ***).

Aged animals showed a significant influence off speed on their performance, too: the faster the earlier mice fell off the rod (Fig.60B; Linear mixed effects: p<0.001, ***). Additional, there was a significant effect of the body weight with heavier animals performing worse (p<0.05, *). There was no statistically significant difference between the genotypes, but at least a tendency towards mutants performing worse than wildtypes (p=0.0552, n.s.).

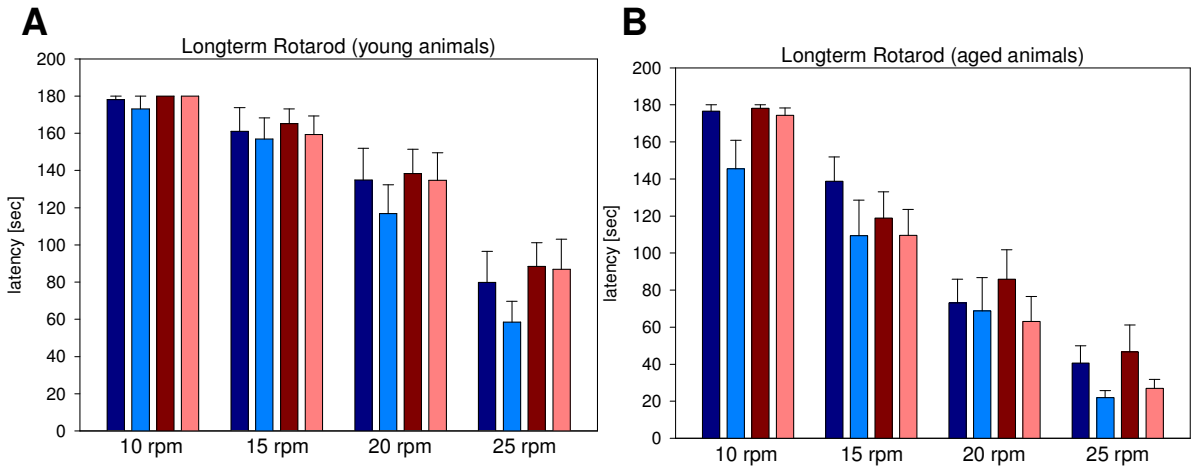

Figure 60: Longterm Rotarod performance

A: Young animals – significant interaction of body weight x speed (Linear mixed effects model: p<0.05, *) and sex x speed (p<0.05, *). Males: interaction body weight x speed (p<0.05, *), females: highly significant influence of speed (p<0.001, ***); B: Aged animals – No genotype-specific differences but at least a tendency towards mutants performing worse than wildtypes (p=0.0552).There was a strong effect of speed (p<0.001, ***) and also a moderate effect of body weight (p<0.05, *) on Rotarod performance. Data are given as means and SEM.

4.13.2.3 Pole test

In aged animals there was a sex-specific difference in performance: males needed more time to turn around (Fig.61; males wt n=19, het n=11; females: wt n=18, het n=19; Linear mixed effects model: p<0.05, *) and also to climb down (p<0.01, **).

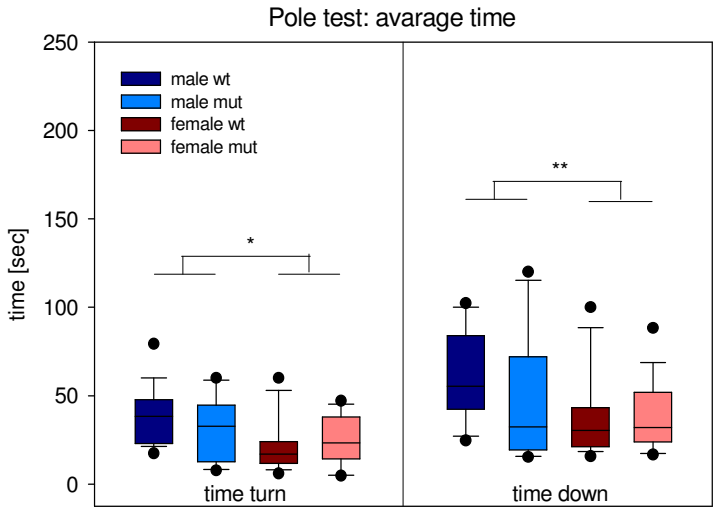

Figure 61: Pole test of aged animals

There was a sex specific difference: males performed worse than females (Linear mixed effects model: turn - p<0.05, *, down – p<0.01, **). Males: wt n=19, mut=11; females: wt n=17, mut=18;

Depiction of single trials revealed a highly significant trial effect considering the time needed to turn around (Fig.62A; p<0.001, ***, for both, males and females: p<0.001, ***) and to go down (Fig.62B; p<0.001, ***; males p<0.001, ***; females p<0.01, **).

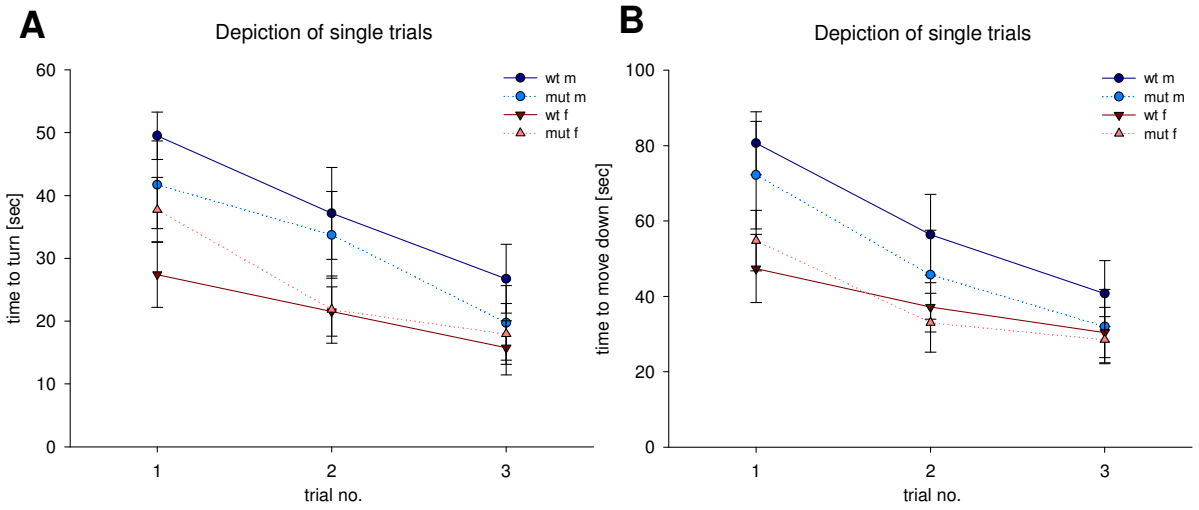

Figure 62: Pole test of aged animals – depiction of single trials

There was a highly significant trial effect in the time to turn as well as in the time to go down the pole (Linear mixed effects model: p<0.001, ***).

Examining the style of the animals to climb down the pole again revealed a sex specific difference (Fig.63; Linear mixed effects model: p<0.01, **): females performed better and reached therefore higher ratings than their male littermates. There was no genotype specific difference.

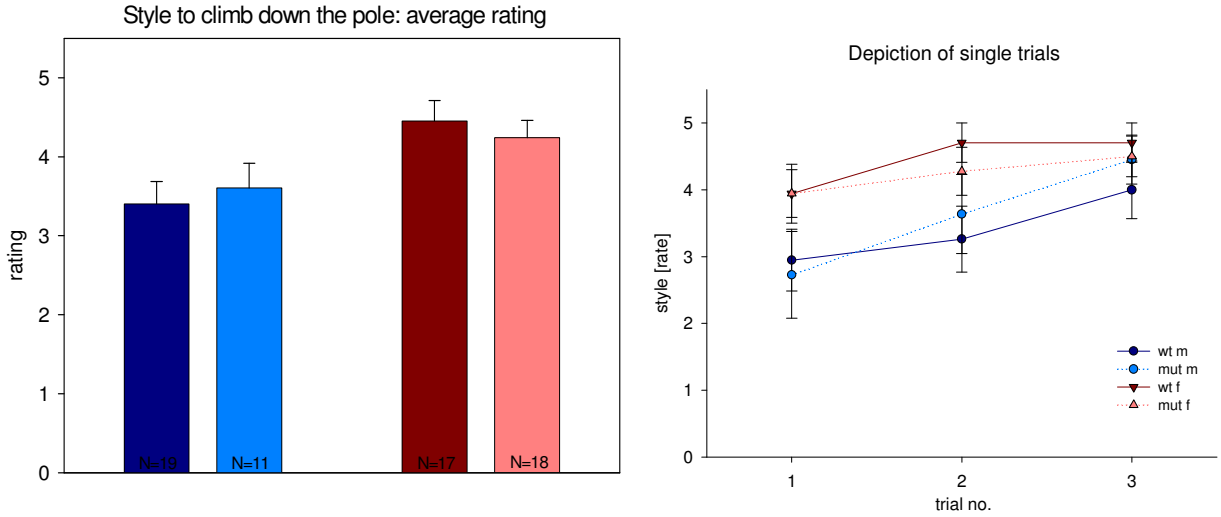

Figure 63: Pole test of aged animals – analyzing the style to climb down the pole

Looking at the style to climb down the pole which was rated due to a defined rating scale, female animals performed better than male animals 8p<0.01, **). There was a highly significant trial effect (Linear mixed effects model: p<0.001, ***, more pronounced in males, p<0.01, **, than in females, p<0.05, *). Data are given as means ± SEM.

Analysis of the single trials showed a learning effect in all animals (Fig.63; $p<0.001$, ***), more pronounced in males ($p<0.01$, **) than in females ($p<0.05$, *). That was caused by the fact that many females already started with the highest rating rendering an improvement impossible.

4.13.2.4 Beam walk

Beam walk was tested in young as well as in aged mice. Besides the number of footslips, the time needed to cross the beam was measured. As the performance is strongly related to body mass, mice were weighed before the test.

Young cohort

The measured body weights were not different between genotypes: for male wildtypes 25.2±0.668g (n=13), malemutants 25.1±0.462g (n=15). Female wildtypes 19.1±0.173g (n=19) and female mutants 19.0±0.343g (n=15).

In the young cohort, there was a subtle genotype x body weight x sex interaction on the 20mm beam (Linear mixed effects model: $p<0.05$, *). Evaluating the sexes separately from each other revealed that mutant male mice performed worse than controls (Fig.64A: Linear mixed effects model: $p<0.05$, *). Evaluating the body weight x genotype x sex interaction revealed that male mutants performed better with increasing body weight while female mutants perform worse with increasing body weight. The results of the 15mm beam showed a tendency in mutants to perform worse but without reaching a significant level (Fig.64B). On the 13mm beam, mutant mice showed significantly more foot slips than wildtypes (Fig.64C; Linear mixed effects model: genotype effect $p<0.05$, *). This was more pronounced in females ($p<0.05$, *).

Examining the single trials of the 20mm beam walk task to get information about the motor learning ability of the animals revealed a significant trial effect, more pronounced in male mice ($p<0.05$, *): animals improved with practice. There were no effects analyzing the single trials of the 15mm and 13mmm beam walk experiments. Mice hardly made mistakes in the first trial (~1-2 footslips), that is why there was not a real possibility to improve performance.

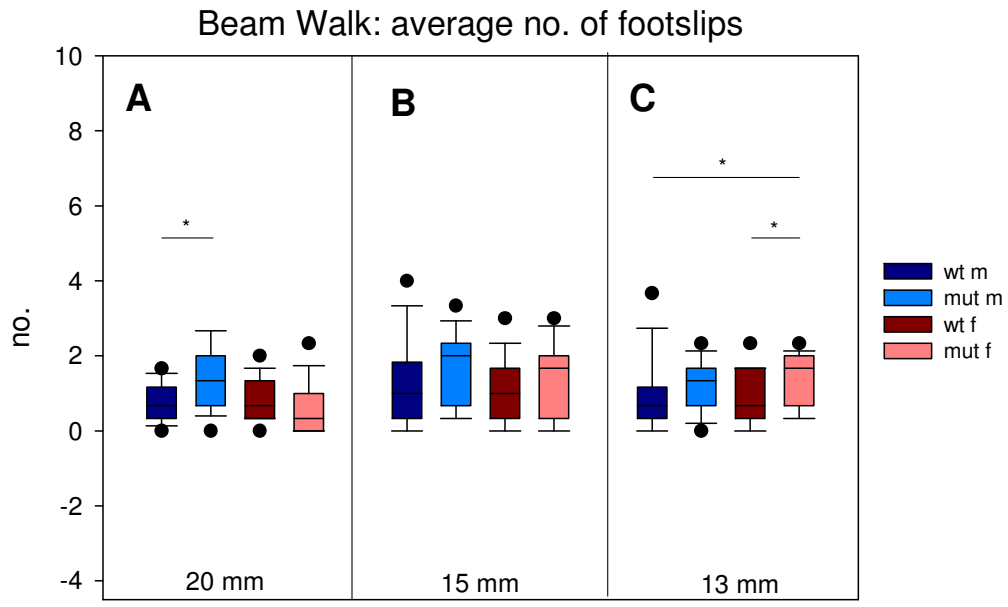

Figure 64: Beam walk results of the young cohort – average number of foot slips

A: 20mm beam performance – genotype effect in male mice (Linear mixed effects model: $p<0.05$, *); B: 15mm beam performance – no genotype-specific differences; C: 13mm beam performance – genotype-specific difference with mutant animals showing significant more footslips than controls ($p<0.05$, *, more pronounced in female mice)

The time to cross the beam was also recorded in this experiment. On the 20mm beam there was no genotype-specific difference between mutant and wildtype mice (Fig.65A; Linear mixed effects model: $p>0.05$, n.s.). Nevertheless, there was a significant effect of trial number on the time the experimental animals needed to cross the beam (Linear mixed effects model: $p<0.01$, **). The same was true for the time to cross the 15mm beam: There was no genotype-specific effect on mutant *Tom40* heterozygous mice (Fig.65B) but there was a significant improvement over time (Linear mixed effects model, $p<0.01$, **).

There was no genotype effect on the time to cross the 13mm beam (Fig.65C) but there was a significant interaction between sex x genotype x body weight x trial number (Linear mixed effects model: $p<0.01$; **). Interactions are sometimes hard to interprete; therefore sexes were analyzed separately to get more information. In male animals, there was a significant influence of trial number on crossing time ($p<0.01$, ***). Males of both genotypes got slower with practice, maybe due to boredom or the need to explore. In females, there was a significant interaction between genotype x body weight x trial number ($p<0.01$, **). Mutant females did not improve or worsen with trials, while wildtypes needed longer in the end than in the beginning. It occured that female wildtypes spent more time with exploring the environment in the later

trials, while mutants just walked across the beam. Analyzing the body weight x genotype interaction showed that female wildtype mice worsened with increasing weight while mutants improved.

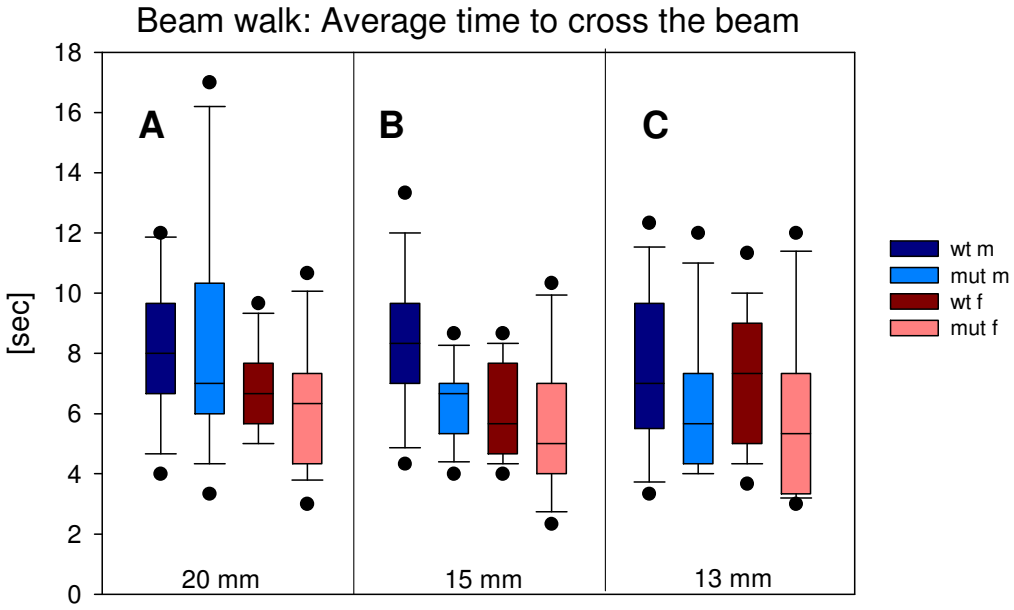

Figure 65: Beam walk results of the young cohort – average time to cross the beam
Time to cross beam (A: 20mm, B: 15mm, C: 13mm) – no genotype-specific differences

.

Aged cohort

Body weight was determined before the experiment: male wildtypes: 34.2±0.520g (n=20), male mutants: 34.5±0.932g (n=13), female wildtypes: 27.3±0.844g (n=17) and female mutants: 27.5±0.685 (n=18).

In the aged mice, there was a significant interaction of sex x body weight x trial number on the number of footslips on the 20mm beam (Linear mixed effects model: $p<0.05$, *). In male animals there was an interaction of body weight and trial number ($p<0.01$, **) with heavier animals improving less than lighter ones. In female mice there was a strong genotype-effect apparent (Fig.66A; Linear mixed effects model: $p<0.01$, **) and number of foot slips were additional significantly influenced by the trial number ($p<0.01$, **).

Evaluating the performance on the 15mm beam revealed a statistically significant interaction of body weight and trial number (Linear mixed effects model: $p<0.05$, *).

Heavier animals improved less than their lighter heavier littermates. There were no genotype-specific effects detectable (Fig.66B). In females there was a highly significant effect of trial number (Linear mixed effects model: p<0.001, ***): the more often animals crossed the beam, the less footslips were counted.

Analyzing the mice on the 13mm beam revealed various effects: besides an effect of sex (Males performed worse than females; Fig.66C; Linear mixed effects model: p<0.001, ***) and of trial number: animals improved over time (Linear mixed effects model: p<0.05, *) there was a strong genotype-effect: mutants showed generally more foot slips than controls (Fig.66C; Linear mixed effects model: p<0.01, **). In males performance was an affected by trial number (Linear mixed effects model: p<0.05, *) and by genotype (Linear mixed effects model: p<0.05, *). Number of foot slips in females did not differ significantly between the genotypes. There was a significant influence of body weight on performance (Linear mixed effects model: p<0.05, *).

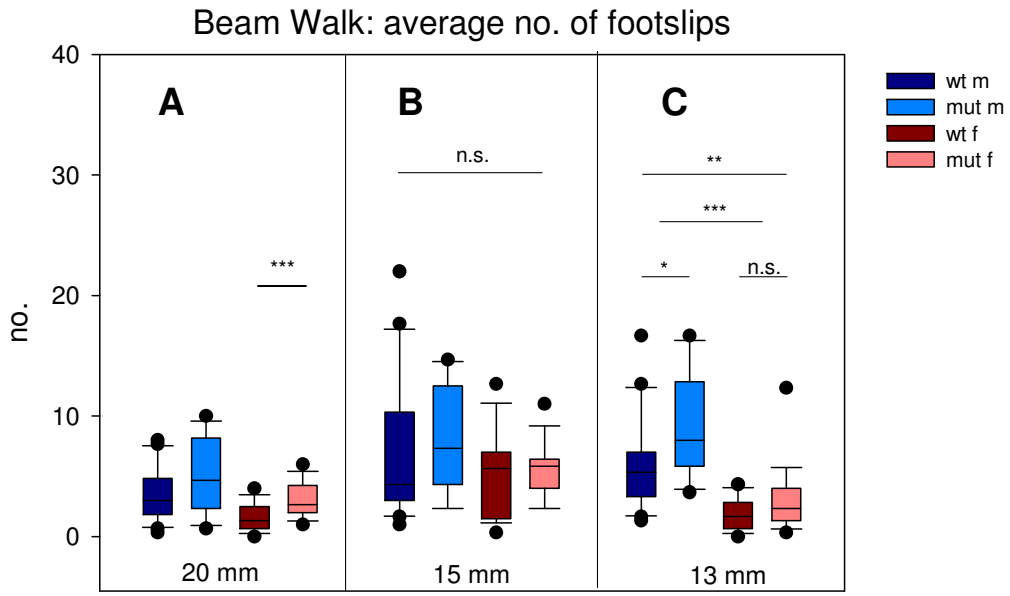

Figure 66: Beam walk results of the aged cohort – average number of foot slips

A: 20mm beam performance –interaction of sex x body weight x trial number (Linear mixed effects model: p<0.05, *); males: interaction body weight x trial number (p<0.01, **) but no genotype specific difference; females: marked genotype specific difference with heterozygous animals showing significantly more footslips than controls (p<0.001, ***).
B: 15mm beam performance – no genotype-specific differences
C: 13mm beam performance – sex-specific difference with male animals showing significant more footslips than females (p<0.001,** *) and genotype specific difference with mutants performing significantly worse than controls (p<0.01, **). This was more pronounced in males (p<0.05, *) than in females (p>0.05, n.s.)

The time to cross the 20mm beam was significantly influenced by genotype (Linear mixed effects mode: $p<0.01$, **): mutant animals needed significantly longer to cross the beam (Fig.67A). There was also a trend towards a sex difference ($p=0.087$). Statistical analysis revealed an interaction between trial number and body weight in males ($p<0.05$, *). In females, there was a significant genotype-effect for this parameter: control mice needed less time to reach the home cage at the target point (Linear mixed effects model: $p<0.05$, *).

The time to cross the 15mm beam was significantly influenced by an interaction of body weight x trial number (Linear mixed effects model: $p<0.01$, **) and sex x trial number (Linear mixed effects model: $p<0.001$, ***). In male mice, there was a significant interaction of body x weight and trial number (Linear mixed effects model: $p<0.05$, *). Heavier animals improved less over trials. In female mice there was a body weight influence stating that heavier animals performed worse (Linear mixed effects model: $p<0.05$, *) and additional a strong effect of the trial number: the often they practiced the longer animals of both genotypes needed to cross the apparatus (Linear mixed effects model: $p<0.001$, ***). Again, this is mainly caused by explorative behaviour after the animals got familiar with the test conditions. However, there was no effect of the genotype on this parameter detectable.

Looking at the time needed to cross the 13mm beam, a significant interaction of genotype and trial number appeared (Linear mixed effects model: $p<0.05$, *). The more often mutant mice crossed the beam, the longer they needed. Separating the sexes showed again an interaction between trial number and genotype in males (Linear mixed effects model: $p<0.05$, *) whereas in there was just an influence of trial number ($p<0.001$, ***).

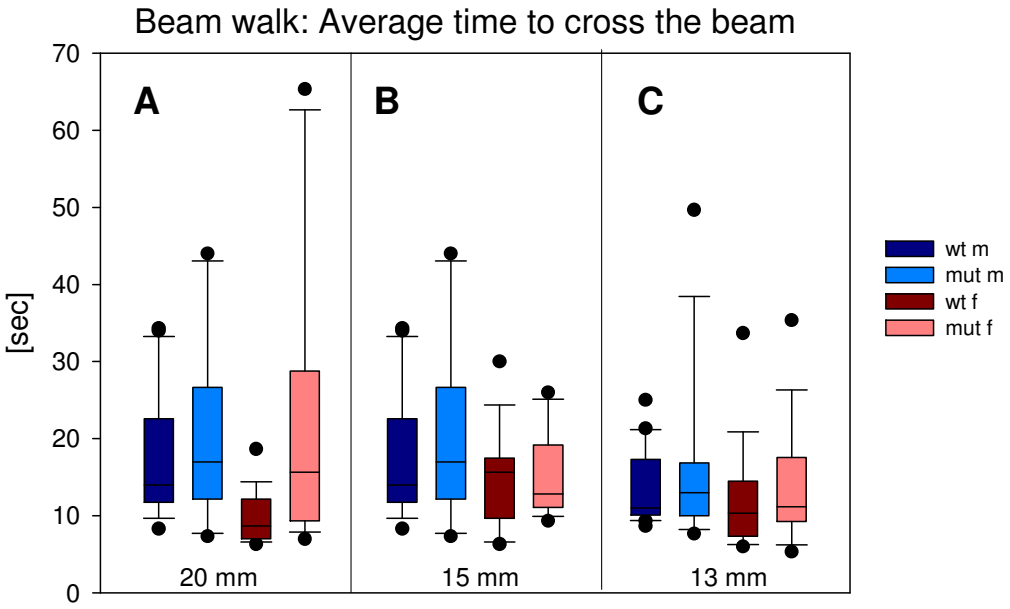

Figure 67: Beam walk results of the aged cohort – average number of foot slips

A: 20mm beam - time to cross the beam: genotype effect p<0.01, **, in females: p<0.05, * (Linear mixed effects model); B: 15mm beam – time to cross beam: no genotype-specific differences; C: 13mm beam – time to cross beam: genotype-specific changes, neither looking at the fore paws nor looking at all paws.

4.13.2.5 Ladder walk

Besides the number of fore- and hind paw footslips, the time needed to cross the ladder was measured. Mice were weighed before the test.

Young cohort

Measured body weights were for males: wildtype 25.2±0.773g (n=13) and mutant 25.1±0.421g (n=15). For females following weights were measured: wildtype 19.4±0.156g (n=19) and mutant 19.4±0.305g (n=15).

Analyzing forepaws data revealed a significant genotype-specific difference between mutant Tom40 mice and wildtypes (Fig.68A; Linear mixed effects model: p<0.01, **). Mutants showed significant higher slipping numbers than controls (p<0.05 for both sexes). Looking at the hind paws, there was a significant sex x genotype interaction (Linear mixed effects model: p<0.01, **). Male mutants performed worse than controls (p<0.05, *), whereas female mutants didn't (Fig.68B). Taking the number of

footslips of all paws together resulted in a significant sex x genotype interaction (Linear mixed effects model: p<0.05, *). In male mice there was a significant genotype effect with mutants slipping more often from the metal grids than wildtypes (Fig.68C; p<0.01, **). In both sexes, there was a significant improvement with trial number (p<0.001, ***).

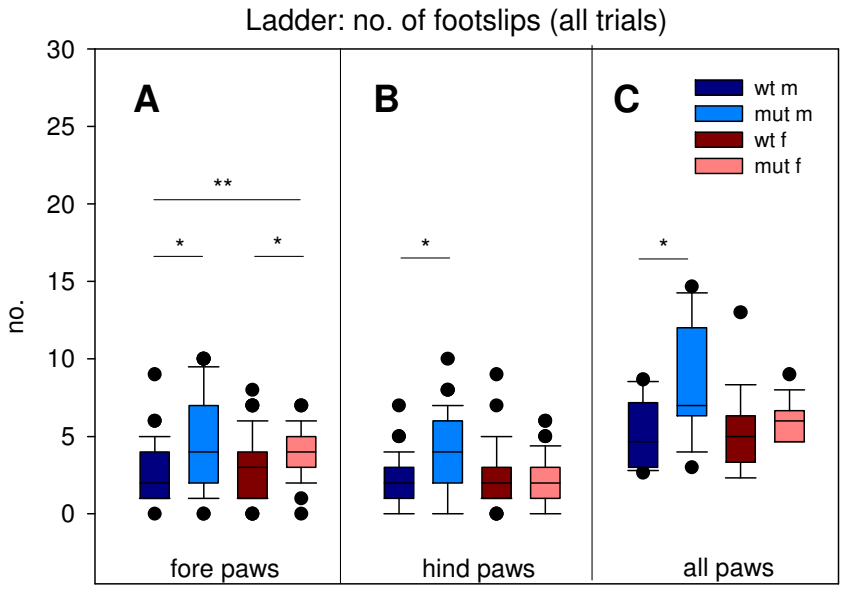

Figure 68: Ladder walk results of the young cohort – all trials

A: Forepaws: mutants perform worse (Linear mixed effects model: genotype p<0.01, **; sex: p<0.05 *). B: Hind paws: genotype effect in male mice (Linear mixed effects model: p<0.05, *). C: All paws: there was a sex x genotype interaction (Linear mixed effects model: p<0.05, *). Males: significant genotype effect with mutants slipping more often from the grids than wildtype mice (p<0.01, **). In both sexes, there was a significant improve with trial number (p<0.001, ***).

There were no significant differences in the time to cross the ladder (Fig.69).

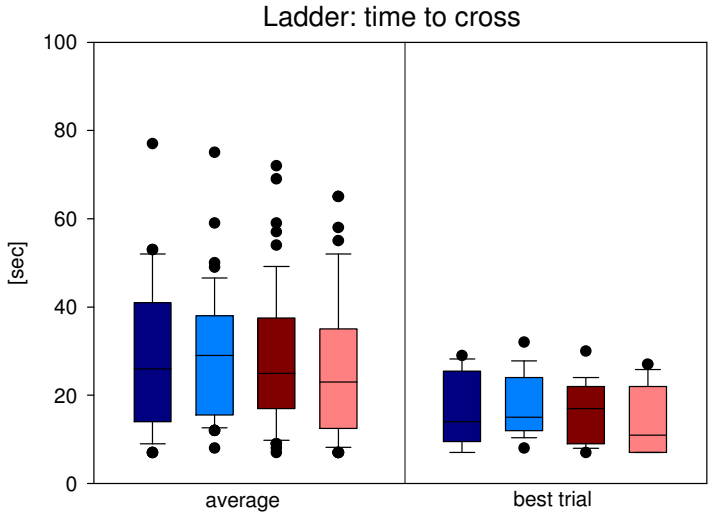

Figure 69: Ladder walk results of the young cohort – time to cross the ladder

There were no genotype-specific differences between mutants and controls.

Evaluation of the single trials revealed a highly significant influence of trial number on forepaws data (Linear mixed effects model: $p<0.001$, ***) and on time to cross the ladder ($p<0.001$, ***): animals improved with trial number. Hind paws data was influenced by a genotype x trial number interaction ($p<0.05$, *): only mutants improved.

Aged cohort

Following body weights were measured for males: wildtype 34.1±0.449g (n=20) and mutant 33.1±0.706g (n=13); for females following weights were measured: wildtype 27.4±0.690g (n=17) and mutant 27.8±0.985g (n=18).

Looking at the number of slips of the forepaws, a significant interaction of sex x body weight x trial number (Linear mixed effects model: $p<0.05$, *) and of genotype x sex x trial number (Linear mixed effects model: $p<0.01$, **) was detected. Sexes then were analyzed separately, revealing a significant interaction of genotype and trial number ($p<0.05$, *) as well as of body weight and trial number ($p<0.05$, *) in males. Mutants showed no signs of improving over time. Heavier animals improved less than their lighter littermates. In females there was a significant interaction of genotype and trial number ($p<0.05$, *). Female wildtype animals showed already in the beginning rarely fore paws footslips. This could be considered as reason for that there is not a real learning curve.

Statistically evaluation of the hind paw data revealed a significant effect of trial number (Linear mixed effects model: $p<0.001$, ***) and body weight ($p<0.01$, **). Additional there was a strong genotype-specific effect, with mutants showing clearly more foot slips than control animals (Fig.70B; $p<0.001$, ***). This was true for males as well as for females. Mutants and wildtypes of both sexes showed an improvement over time more pronounced in females ($p<0.01$, **). Heavier animals had more problems to cross the ladder walk.

Taking fore- and hind paw results together the clear genotype effect got even more pronounced (Fig.70C). There was an interaction of trial number x body weight x sex (Linear mixed effects model: $p<0.05$, *) and trial number x genotype x sex ($p<0.05$, *). Looking only at the males, there was a strong genotype-specific difference (Linear mixed effects model: $p<0.001$, ***) and also a significant trial-effect with animals improving over time ($p<0.01$, **). The same was detected for female animals (Linear mixed effects model: genotype $p<0.001$, ***; trial number $p<0.001$, ***). Additional there was a body weight effect ($p<0.01$, **) in females demonstrating that heavier

animals performed worse, in males this was not significant (p=0.0865). Elucidating the time mice needed to cross the ladder revealed no genotype-specific differences (Fig.71A). There was a highly significant trial effect detectable (Linear mixed effects model: p<0.001, ***) demonstrating that all groups got faster with practicing.

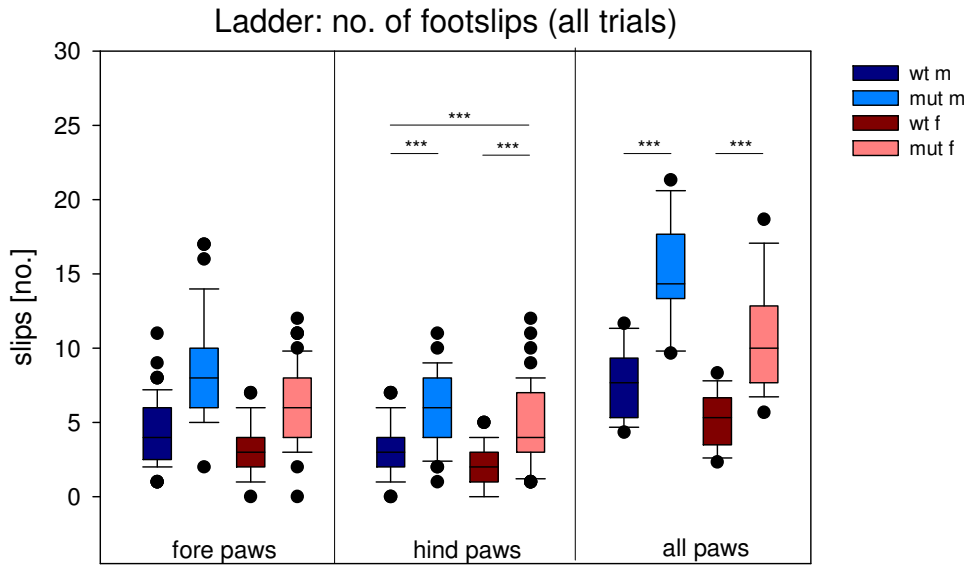

Figure 70: Ladder walk results of the aged cohort – all trials

A: Forepaws: interaction of genotype x sex x trial number (Linear mixed effects model: p<0.01, **); B: Hind paws: strong genotype effect (Linear mixed effects model: p<0.001, ***); C: All paws: interaction of genotype x sex x trial number (Linear mixed effects model: p<0.05, *). Genotype-specific difference in males and females: p<0.001, ***;

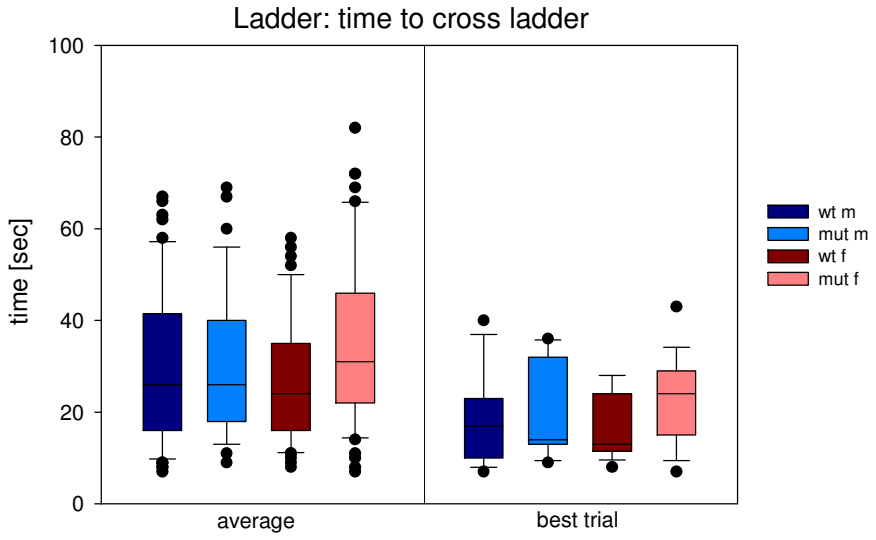

Figure 71: Ladder walk results of the aged cohort – time to cross the ladder

There were no genotype-specific differences between mutants and controls.

4.13.2.6 Locomotor activity

There were no genotype specific differences concerning lotomotor activity of aged *Tom40* heterozygous mice compared to their wildtype littermates (Two Way ANOVA: $p>0.05$, n.s.; data males: wt – n=20 locA=20±1.2, mut – n=13 locA=20±1.3; data females: wt – n=17 locA= 18±1.6, mut – n=19 locA=17±1.2).

4.13.2.7 Running wheels

The voluntary running of the animals was investigated for a three weeks period. The first cohort consisted of 9 animals of each genotype, the second cohort of 6 per genotype. After two weeks free running, wheels were restricted: animals of the first cohort had to deal with a resistance intensity of 5 and animals of the second cohort with a resistance intensity of 7. Looking at the covered distances by animals from the first cohort covered, a clear training effect was visible in the first two weeks in both genotypes (Fig.72A). After starting the restriction of the wheels, mutant animals were not longer able to improve their performance and therefore stagnated by ~14km maximal covered distance per day while controls were not impaired by the brake and improved to 16km. Statistical evaluation of data revealed a highly significant triple interaction of genotype x body weight x day (Linear mixed effects model: $p<0.001$, ***). It was evident that mutant mice were slightly heavier than controls just at the beginning (wt= 27.1g, het=28.8 g). After three weeks exercise the body weight of control mice was 24.5g and of mutants 26.1g. Both genotypes lost nearly the same amount of weight (wt: 9.5%, mut: 9.3%). After starting with the restriction, the slightly higher body weight of mutants seemed to have a greater influence on performance than during the free running trials.

The second cohort, which was restricted with a higher intensity, showed for both genotypes an explicit worsening after brake activation (Linear mixed effects model: day x restriction $p<0.01$, **). While the first two weeks of exercise led to a massive increase in covered km per day ($p<0.001$, ***) performance afterwards dropped to values animals showed in the beginning (Fig.72B).

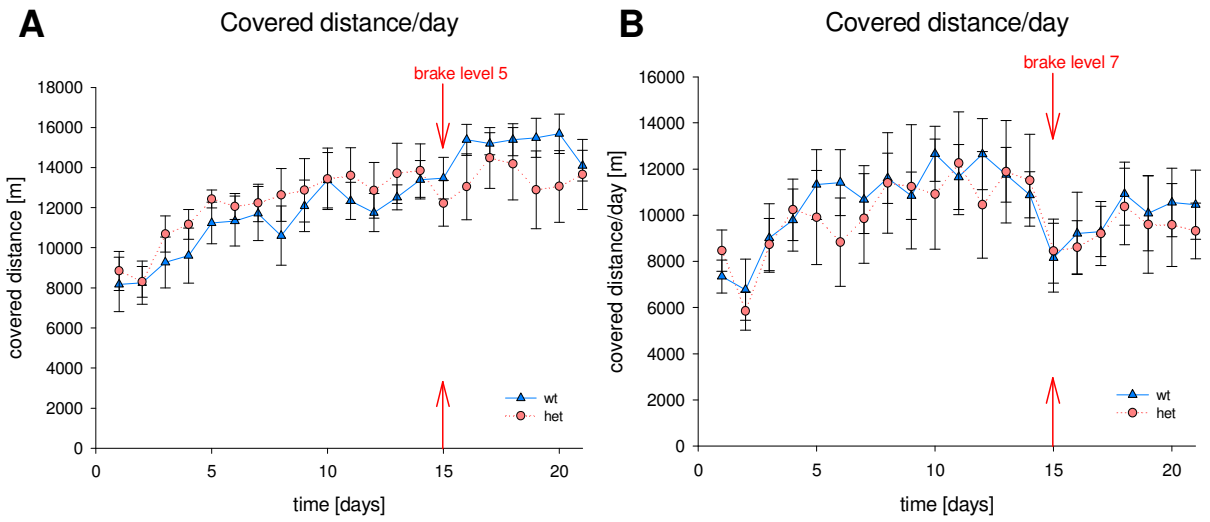

Figure 72: Covered distance per day

A: Cohort 1 with a wheel restriction of intensity 5 after two weeks training: interaction of genotype x body weight x day (Linear mixed effects model: $p<0.001$, ***). By separating training from restriction phase it got obvious that this interaction was apparent in the unrestricted phase. Afterwards there was a genotype x body weight interaction left ($p<0.05$, *). B: Cohort 2 with a wheel restriction of intensity 7 after two weeks training: interaction day x restriction (Linear mixed effects model: $p<0.01$, **). During training there was a significant improvement ($p<0.001$, ***).

In a next step data of both cohorts were analyzed together. There was an obvious training effect from the 1st (blue) to the 2nd week (red) for both genotypes (Fig.74). Within the 3rd week (green) a differentiation between the different brake intensities became necessary. Wildtypes from the level 5 cohort were not impaired by the brake, they even further improved. However mutants showed a strong variation from also not being affected to severely impaired. At level 7 both genotypes were affected equally.

Another parameter that was analyzed was the maximal length an animal was able to run non-stop. In the first cohort a significant interaction between genotype x body weight x brake x day was determined by statistical evaluation (Fig.73 A; Linear mixed effects model: $p<0.05$, *). Analyzing the training phase separately, a significant genotype x body weight x day interaction was detected ($p<0.05$, *). The heavier mutants showed equal or even subtle higher values than wildtypes, both genotypes nevertheless had a clear-cut learning-curve with longer durations after two weeks than in the beginning. After start of restriction, both genotypes showed worse performance than before. This, however, was much more pronounced in the still heavier mutant animals than in controls (Linear mixed effects model: genotype x body weight interaction $p<0.01$, **; genotype x day interaction $p<0.05$, *). Data from animals from the second cohort also showed a significant genotype x body weight x

brake x day interaction (p<0.01, **). During training phase there was a significant body weight x day interaction (p<0.05, *) on performance but no influence of genotype. After restricting the wheels, there was a statistically significant interaction of genotype x body weight x day on performance (p<0.05, *). Wildtypes from this cohort were in the beginning slightly but not significantly heavier than mutant animals (wt=27.9g, mut=27.1g). After three weeks exercise body weight of the wildtype females had dropped to 25.2g, mutants had a weight of 25.9g meaning that wildtypes lost 9.6% of their body weight and mutants just 5.1%. There was a training effect comparing week 1 with week 2 and a clear effect of restriction on mutant animals of the level5 cohort while there was no influence on the controls. At restriction level 7 animals of both genotypes were affected in an equal manner (Fig 73B).

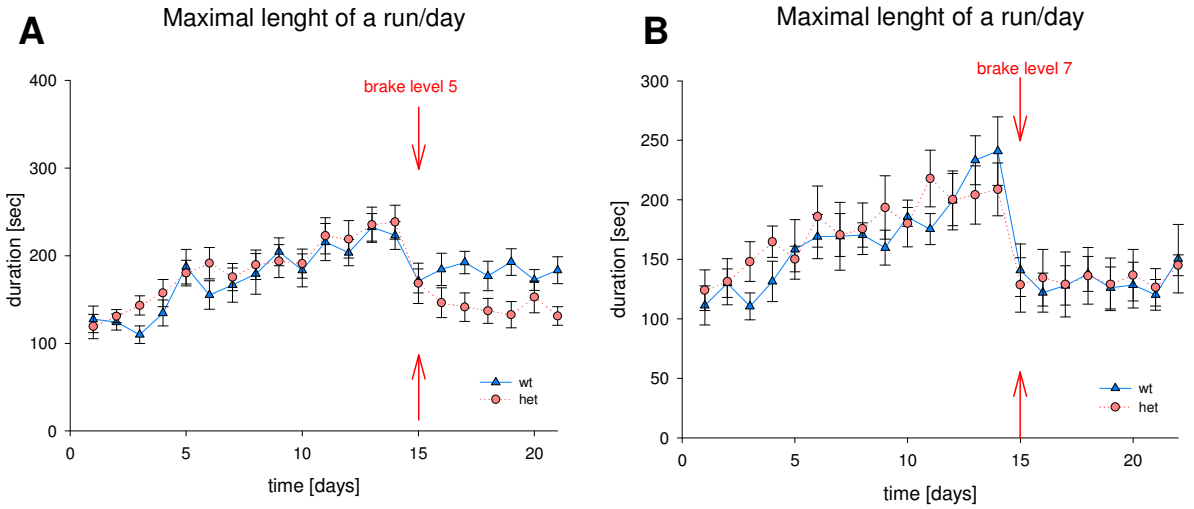

Figure 73: Maximal run length per day

A: Cohort 1 with a wheel restriction of intensity 5 after two weeks training: interaction of genotype x body weight x day x brake (Linear mixed effects model: p<0.05, *). Separating training from restriction phase for the training phase a significantly increasing performance of both genotypes was verified (p<0.05, *). Heavier mutants showed the same improvement as lighter controls. After engaging the brake, mutants showed much worse performance than controls, they still were heavier than wildtype mice (Linear mixed effects model: genotype x body weight interaction p<0.01, **; genotype x day interaction p<0.05, *; B: Cohort 2 with a wheel restriction of intensity 7 after two weeks training: interaction of genotype x body weight x brake x day (p<0.01, **). There was a significant body weight x day interaction (p<0.05, *) in the first two weeks of training. After restricting the wheels, there was a statistically significant interaction of genotype x body weight x day on performance (p<0.05, *).

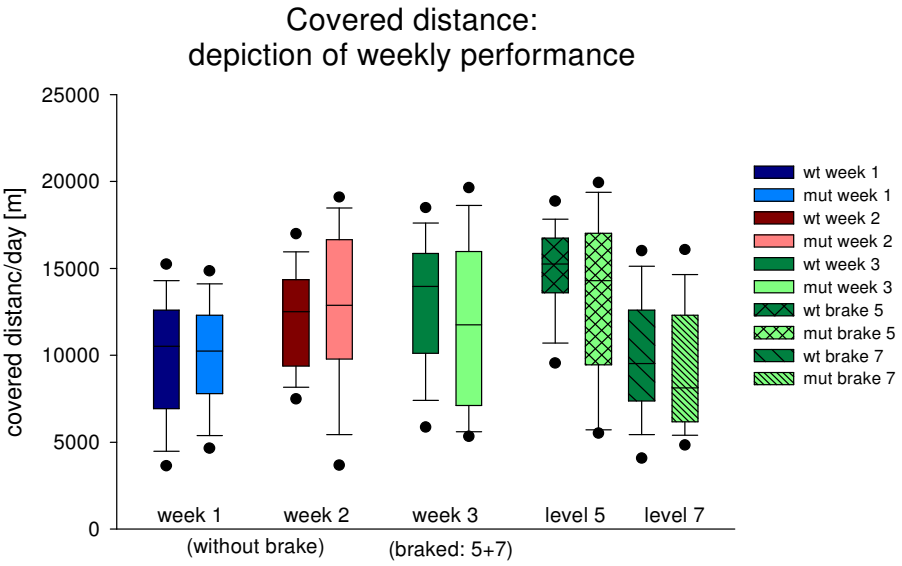

Figure 74: Covered distance : depiction of the weeks

Additional the parameter average duration of a non-stop run was analyzed, there was a highly significant interaction of genotype x body weight x brake x day in cohort 1 (Fig.75A; Linear mixed effects model $p<0.01$, **). Animals of both genotypes improved average run duration during the training phase. Then after restriction, there was a clear reduction in the heavier mutant mice whereas controls were not affected.
In cohort 2 there was a genotype x body weight x brake interaction, too (Fig.75B; $p<0.001$, ***). In contrast to cohort 1, all mice from cohort 2 showed shorter run durations after the level 7 restriction, no matter if mutant or wildtype, subsequent to the highly significant improvement over time in the training phase (day effect: $p<0.01$, *). There was a genotype x body weight interaction with slightly heavier mutants performing as worse than lighter wildtype mice ($p<0.01$, **).
Analyzing data per week revealed that there was a marked training effect with a duration increase if comparing week 1 with week 2 (Fig.76). In week three there was a difference between the genotype in cohort 1 with mutants performing worse, whereas in cohort 2 mutants seemed to be better than their wildtype littermates.

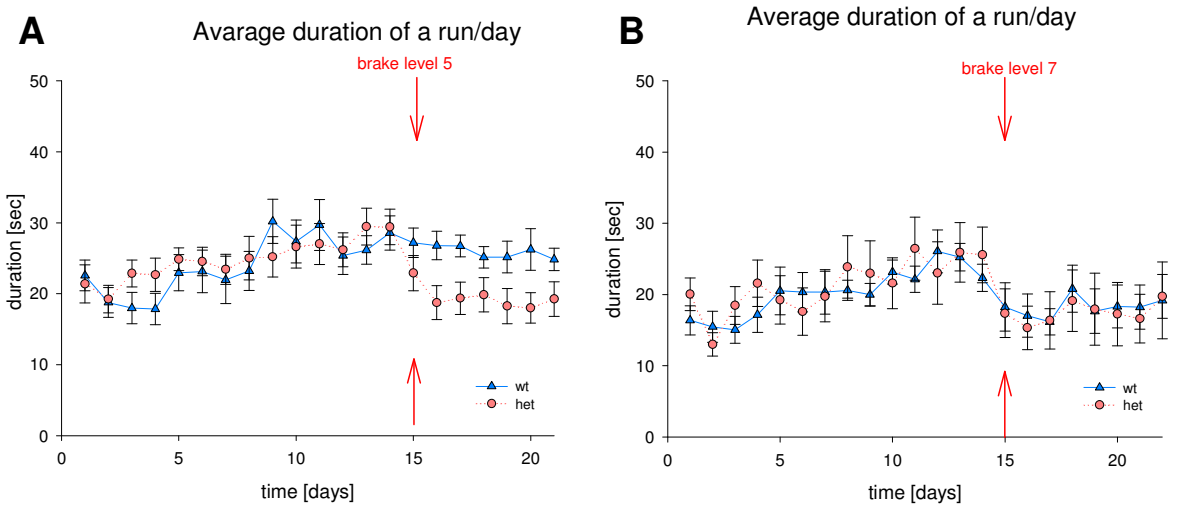

Figure 75: Average run length per day

A: Cohort 1 with a wheel restriction of intensity 5 after two weeks training: interaction of genotype x body weight x brake x day (Linear mixed effects model: p<0.01, **); B: Cohort 2 with a wheel restriction of intensity 7 after two weeks training: interaction of genotype x body weight x brake x day (p<0.001, ***). Training phase: day effect p<0.01, **. In the restriction phase there was a genotype x body weight interaction: mutants with more body weight showed an equal average run time like lighter wildtype mice.

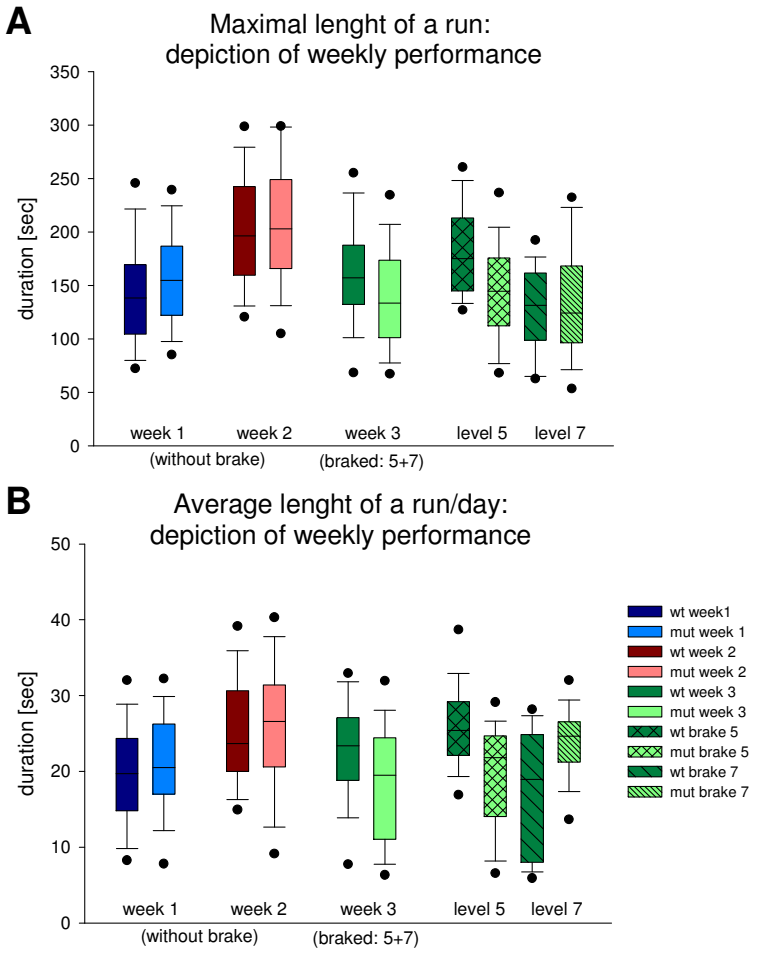

Figure 76: Maximal (A) and average (B) length of a run : depiction of the weeks

Besides distance and run time, speed was recorded during the running wheels experiment. The maximum speed mice reached was recorded per day as well as the average speed. In cohort 1 there was a significant interaction of genotype x day x brake for maximum speed (Linear mixed effects model: p<0.05, *). Before restriction, there was a speeding-up with increasing test duration in both genotypes. Wildtypes showed a lower maximum speed than mutants although they were not as heavy (Fig.77A; genotype x body weight x day interaction, p<0.05, *). After restriction, there was no difference between the genotypes anymore; mutants first slightly decreased their maximum speed and then both genotypes showed the same velocity increase with time (day effect: p<0.001, ***). In cohort 2 statistical analyses revealed a significant genotype x body weight x brake interaction (Fig.77B; Linear mixed effects model: p<0.05, *). Slightly heavier mutants and controls showed nearly the same improvement with time before restriction. Analyzing the unrestricted phase alone revealed a highly significant day effect (p<0.001, ***), all animals were able to increase their maximum speed. At the first day of restriction, a marked dropping of performance occurred. Afterwards both genotypes slightly increased their speed again. Examining the data per week revealed that there was a training effect comparable to distance and run duration. The maximum speed increased within the training period (Fig.79A). After restriction there was impairment.

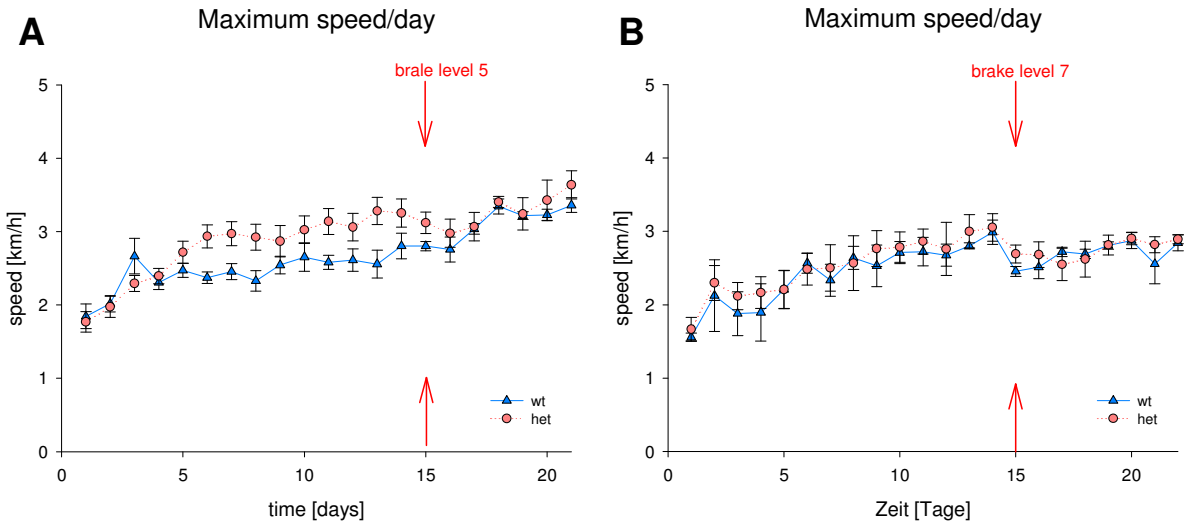

Figure 77: Maximum speed per day

A: Cohort 1 with a wheel restriction of intensity 5 after two weeks training: interaction of genotype x brake x day (Linear mixed effects model: p<0.05, *). Training: genotype x body weight x day interaction: p<0.05, *; restricted wheels: day p<0.001, ***; B: Cohort 2 with a higher wheel restriction. after two weeks training: interaction of genotype x body weight x brake (p<0.05, *); Training: there was a highly significant influence of day on performance p<0.001, ***.

Statistical analysis of the average speed showed a genotype x body weight x day x brake interaction in cohort 1 and cohort 2 (Fig.78; Linear mixed effects model: p<0.01, **, for both cohorts). There was a genotype x weight x day interaction for the free training phase for cohort 1 (Fig.78A; p<0.001, ***) and also for cohort 2 (Fig.78B; p<0.05, *). In the restricted phase, there was a genotype x weight x day interaction for both cohorts (cohort 1: p<0.05, *, and cohort 2: p<0.01, **). Mutants had a slightly higher average speed than wildtypes before restriction. Afterwards they showed the same values than controls.

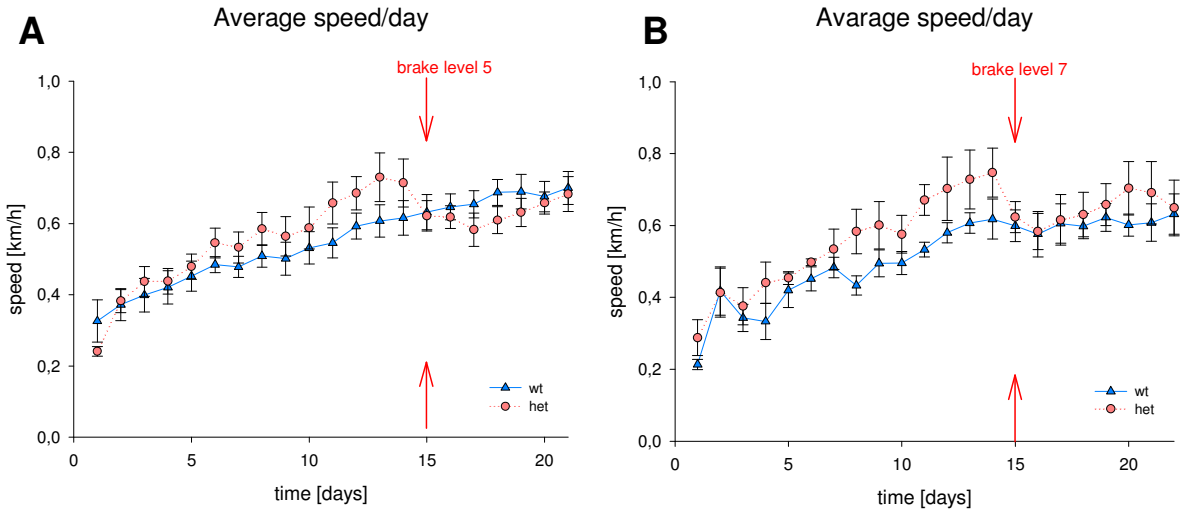

Figure 78: Average speed per day

A: Cohort 1 with a moderate wheel after two weeks training: interaction of genotype x body weight x brake x day (Linear mixed effects model: p<0.01, **). Training: genotype x body weight x day interaction: p<0.01, ***; restricted wheels: genotype x body weight x day p<0.05, *; B: Cohort 2 with a high wheel restriction after two weeks training: interaction of genotype x body weight x brake x day (p<0.01, **). Training: there was a significant interaction between: genotype x body weight x day: p<0.01, **;

The graphic presentation of the single week data showed an obvious training effect was obvious regarding week 1 and 2 (Fig.79B). The average speed of both genotypes increased, more pronounced in mutants. In week 3 there was no effect of restriction visible, neither in cohort 1 nor in cohort 2.

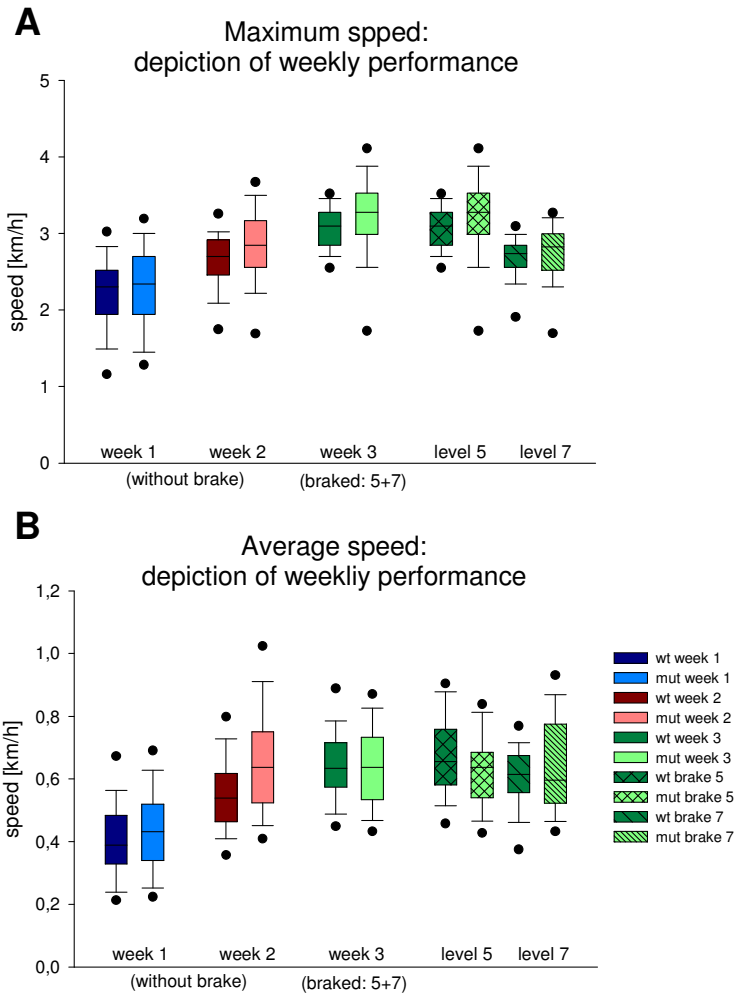

Figure 79: Maximal (A) and average (B) speed : depiction of the weeks

The experiment also allowed an evaluation of the circadian activity rhythm of the animals, and no shifting or difference between the genotypes was found (Fig.79). Measurements were started in the late afternoon. Activity increased during the dark phase with a maximum in the middle of the night. During the light phase, animals were asleep and there was hardly activity visible.

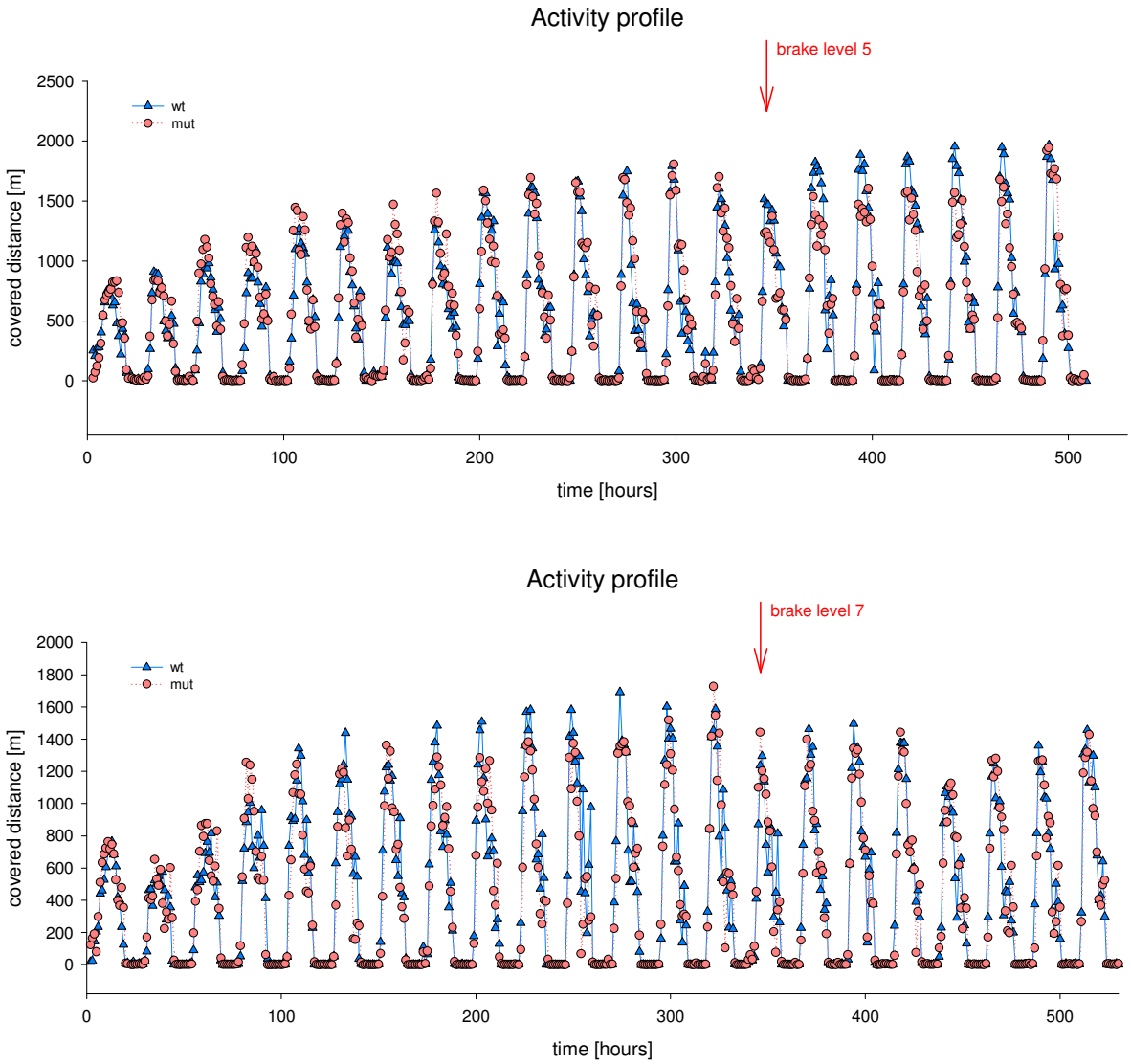

Figure 80: Circadian activity rhythm of both cohorts.

Taken together, there were some effects in mutant mice after restricting the wheels with a medium resistance intensity. Both genotypes showed a drop in the parameter “maximal length of a run per day” but this was more pronounced in mutants. In contast to wildtypes, also the average duration of the runs decreased significantly in mutant mice.

4.13.2.8 Gait analysis

Animals were tested twice in their life time. The first time the animals had an age of six month and both sexes were analyzed. The second time, only females were available for testing. The mice were 26 month old and especially mutants had to be treated very carefully because of a previously observed stress intolerance (some mutants evolved seizures and died just because of handling stress).

Young *Tom40* females were lighter and shorter than the males. There weren't any significant differences in the gait of the mutants compared to the controls. Mutant females were slightly heavier and larger and most of the significant differences showed an interaction with the body weight respectively sex (see table 15). No obvious gait abnormalities were observed in the mutants compared to the controls. Some parameters were increased, but the findings were small and only detectable at one distinct speed. For this reason they might be findings by chance.

In aged animals, there were some alterations in mutants, but again, findings were subtle and mostly restricted to one speed. Additional it was not possible to test the animals at higher speeds because of their age and the concomitant inability to cope with faster running.

Table 15: Altered gait parameters

		Tom40 young						Tom40 old (females only)			
		15cm/s	interact	25cm/s	interact	35cm/s	interact	10cm/s	interact	15cm/s	interact
Propel	FP									↓(**)	**BW**
	HP										
% Propel /Stride	FP			↑(**)	sex	↑(**)	sex				
	HP										
%Propel /Stance	FP										
	HP									↓(*)	**BW**
Stance width	FP									↓(*)	
	HP										
Step width variability	FP							↓(*)			
	HP										
Step angle variability	FP										
	HP			↑(**)				↓(**)			
Step Angle CV	FP										
	HP			↑(**)				↓(**)			
Paw area variability at peak stance	FP							↓(T)		↓(T)	
	HP										
Overlap Distance	FP			↑(*)	sex						
	HP										

4.13.3 Mini Spec of aged animals

Body composition of aged animals was determined with the aid of the metabolic screen (see chapter 3.10.6) without finding any genotype-specific alterations. There was a highly significant sex difference concerning body weight (Fig 81; Two Way ANOVA: p<0.001, ***). The same was detected for lean mass. There were no significant differences at all in fat mass.

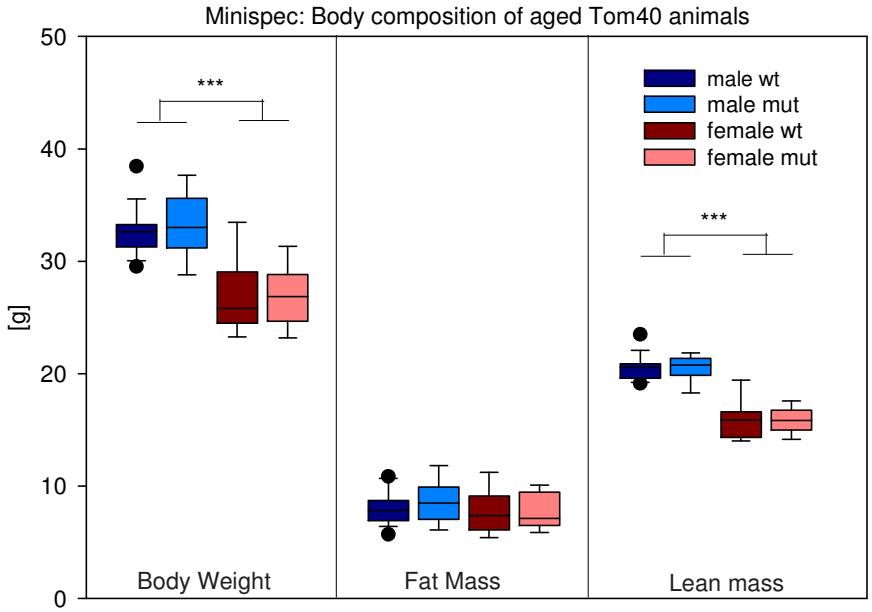

Figure 81: Body composition of aged *Tom40* heterozygous and wildtype mice

There was a sex specific difference in body weight and lean mass with heavier males than females (Two Way ANOVA: p<0.001, ***) while fat mass was equal in both sexes. There was no genotype – specific difference in one of the analyzed parameters.

4.13.4 Eye screen

For secondary screen, 5 male and 5 female aged mice were analyzed by a Schleimpflug-camera. Additional three males of each genotype were tested with OCT. All pictures of the Schleimpflug-experiment show a circular carteract which is typical for aged C57Bl/6J mice (Fig.82A). OCT also did not reveal genotype-specific chances between mutant and control animals (Fig.82B).

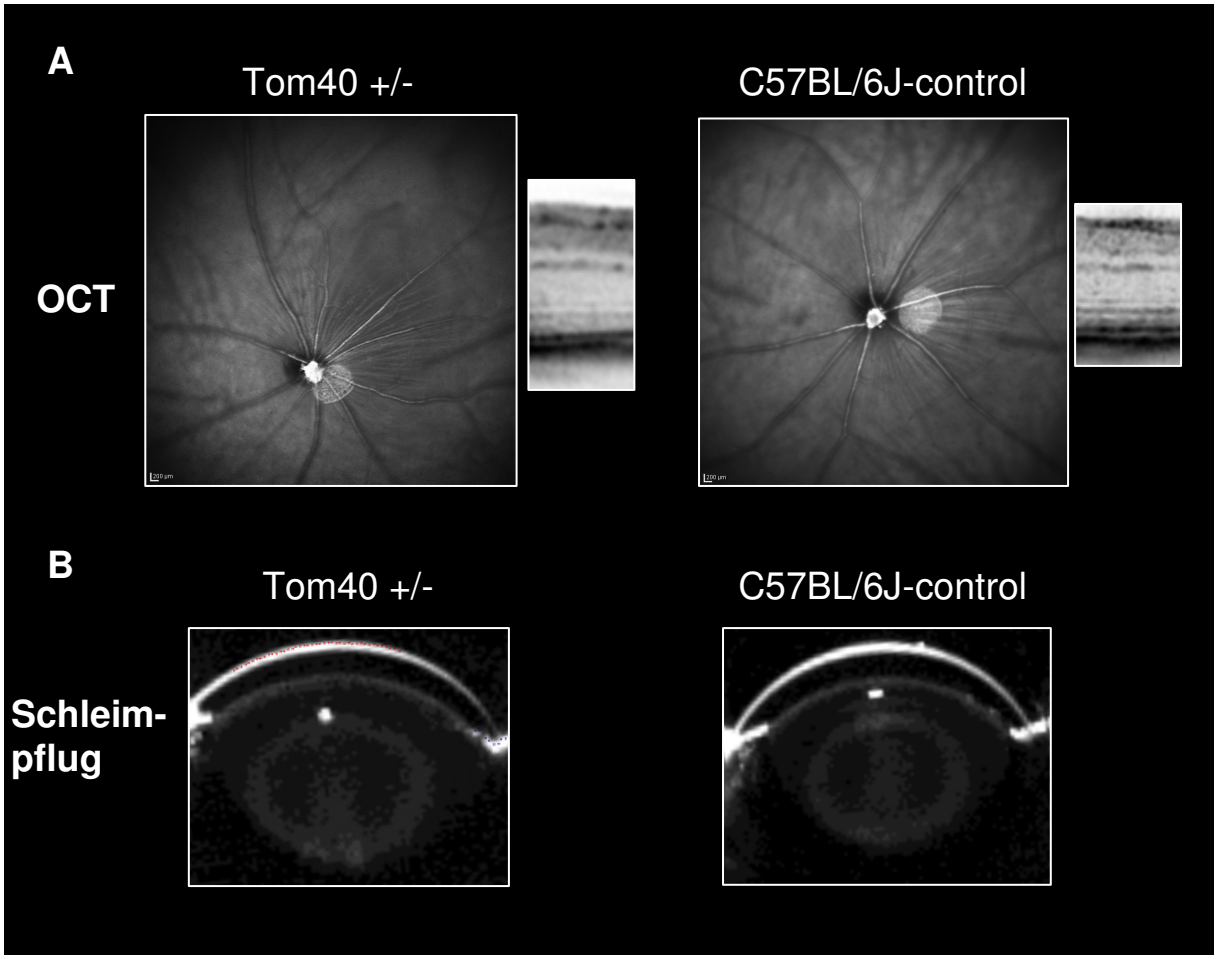

Figure 82: OCT (A) and Schleimpflug (B) analysis

No genotype-specific differences between aged wildtype and mutant animals were detectable.

4.13.5 Investigation of memory

Social discrimination

There was no genotype specific difference between heterozygous *Tom40* mice and controls concerning investigation time of the new animal in the sample phase or the familiar animal in the test phase test phase (Fig.83A males, B females) or the social recognition index (=unfamiliar object / (unfamiliar + familiar object); see Fig.87C) in the test phase (Two Way ANOVA: $p>0.05$, n.s.). Analysis of the test phase revealed that there was a trend in control mice towards different investigation time of the familiar and the unfamiliar object (t-test: $p=0.055017$, n.s.).

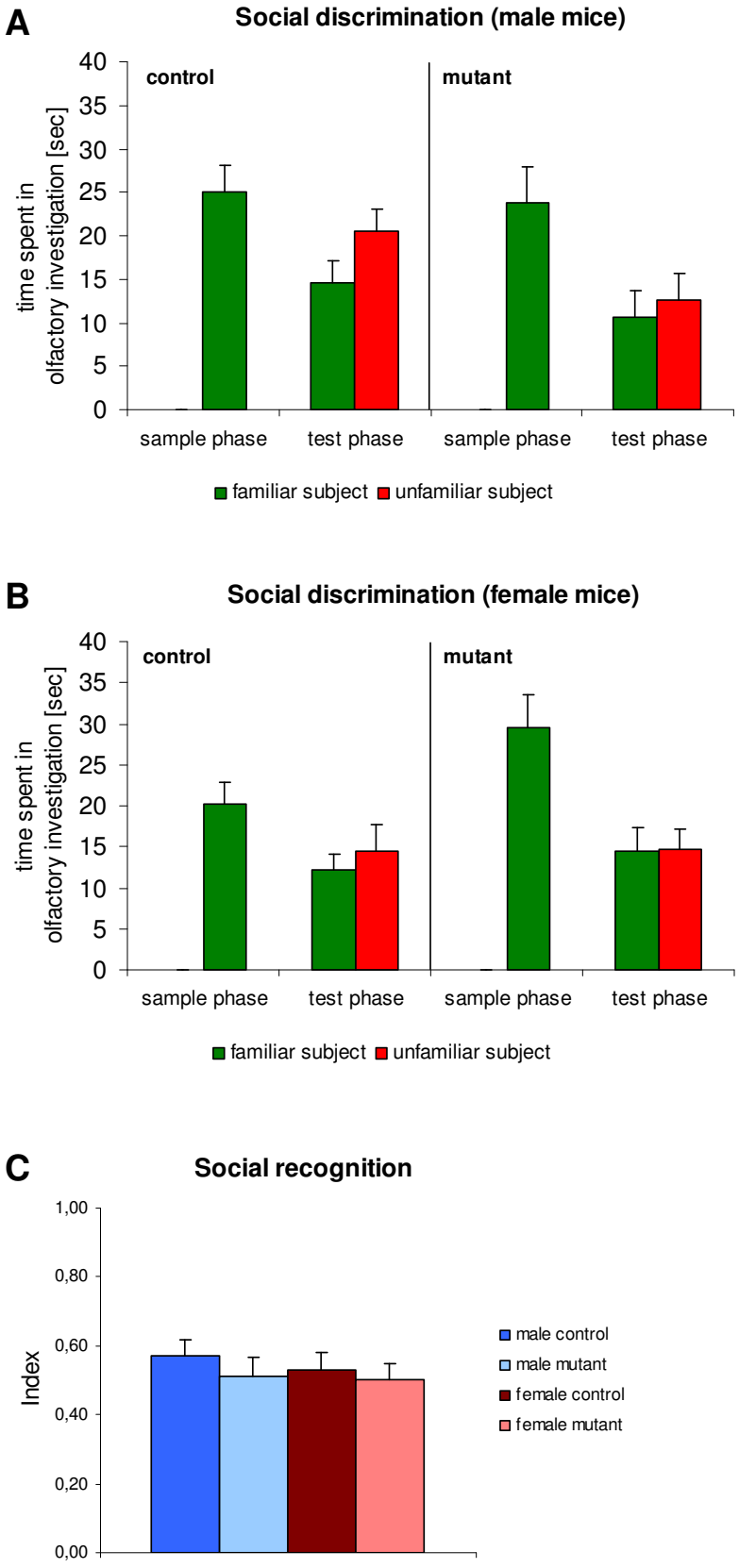

Figure 83: Social discrimination (A+B) and recognition (C) of aged mice

There were no genotype-specific differences between Tom40 heterozygous and wildtype mice.

Object recognition

The object recognition task was only performed with male mice.

There was no genotype specific difference between mutant and wildtype animals, neither concerning total number nor duration of investigations or latency to first observation during sample phase (Fig.84; Two Way ANOVA, n.s.). There was a significant effect of sample number (total number / duration / % duration: $p<0.001$, ***; latency: $p<0.05$, *).

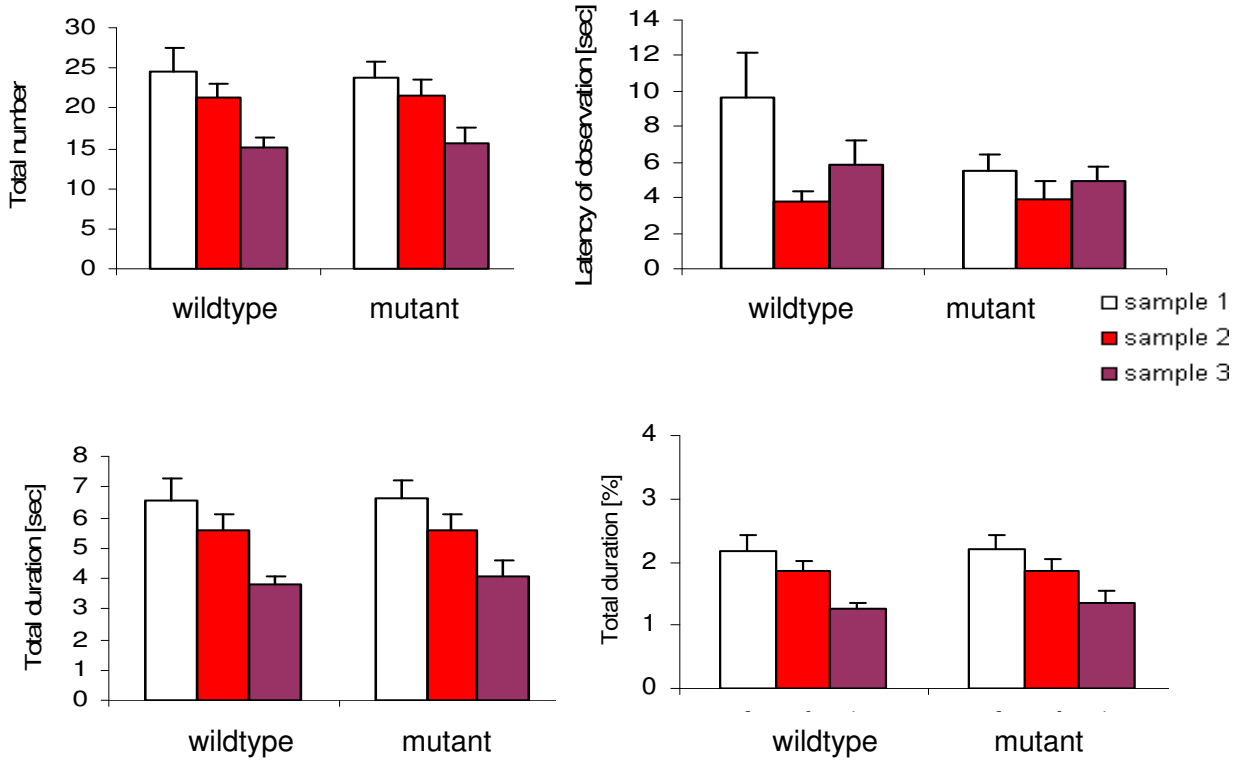

Figure 84: Object recognition – sample phase

There were no genotype-specific differences between Tom40 heterozygous and wildtype mice.

In the test phases 3h and 24h after training the animals were confronted with the familiar object from the sample phase and simultaneously with an unfamiliar object.

In the 3h session, wildtype and mutant mice were able to remember the familiar object and investigated the unfamiliar significantly more often (Fig.85 A; t-test: wildtype $p<0.01$, **; mutant $p=0.0586$, n.s.) and for a longer time (Fig.85 C; t-test: wildtype $p<0.05$, *; mutant $p=0.0542$, n.s.). Nevertheless, animals of both genotypes were not very motivated to investigate the objects, the active investigation duration within the whole 5min test interval was below 1% in all groups with a alight tendency

towards longer investigation of the unfamiliar object (Fig.85 D; t-test: wildtype $p<0.05$, *; mutant $p=0.0544$, n.s.).

The latency of observation was significant different in wildtype mice (Fig.85 B; t-test $p<0.05$, *): the unfamiliar object was investigated much earlier than the familiar object. This could not be found in mutant animals.

However, there were no statistically significant genotype-specific differences between mutants and wildtypes.

After 24h there still was the tendency that the animals were able to remember the familiar object, but a level of significance could not be reached for any of the examined parameters (Fig.86). There was a weak genotype effect concerning the total numbers of investigations of the unfamiliar object (Fig.86 A; Two Way ANOVA: $p<0.05$, *) and a tendency in the total duration of investigation (Fig.86 C; Two Way ANOVA: $p=0.066$, n.s.). Nonetheless, differences were very small as both genotypes hardly spent time in investigating any object.

.

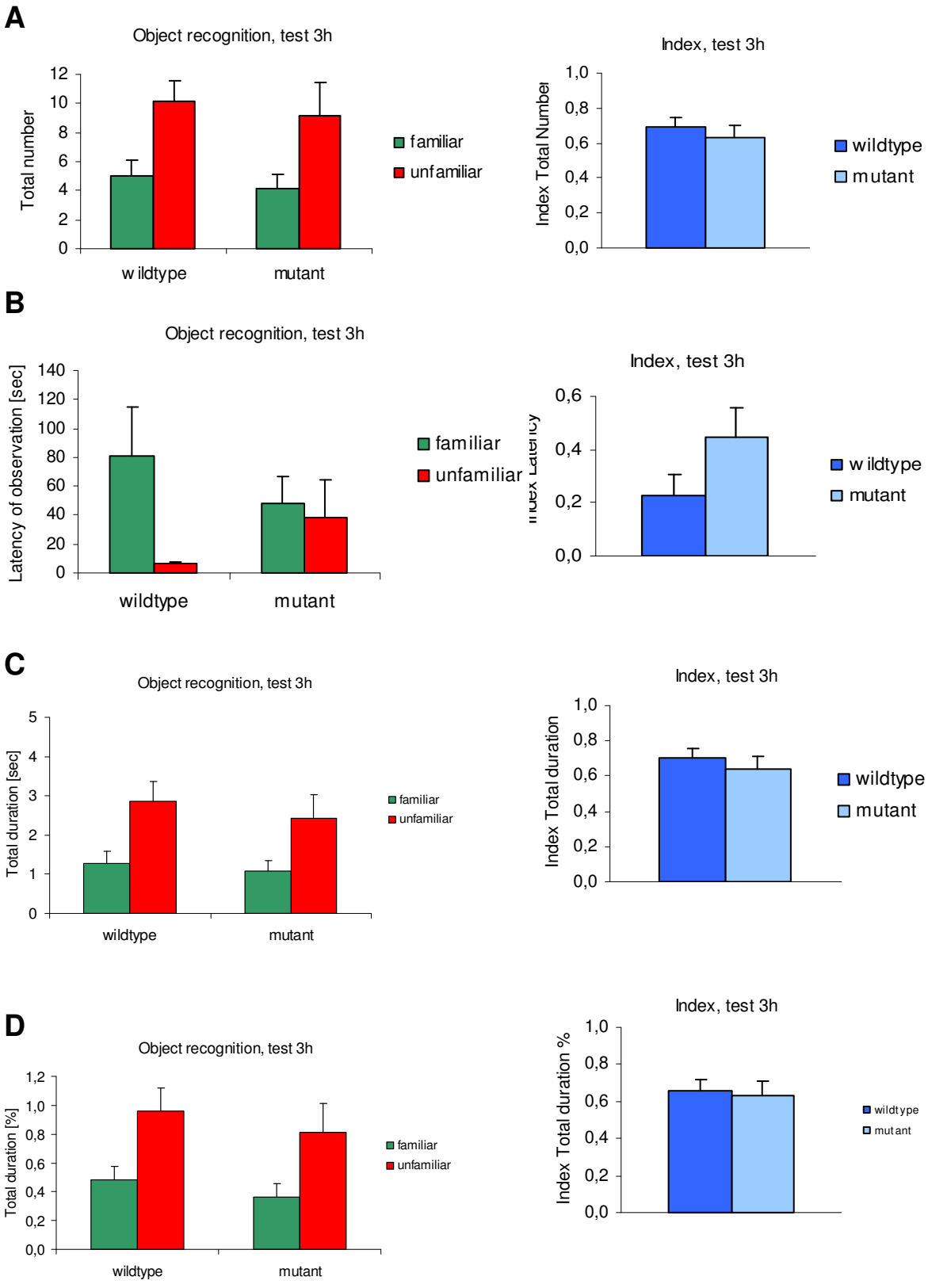

Figure 85: Object recognition – test phase (24h)

There were no genotype-specific differences between Tom40 heterozygous and wildtype mice

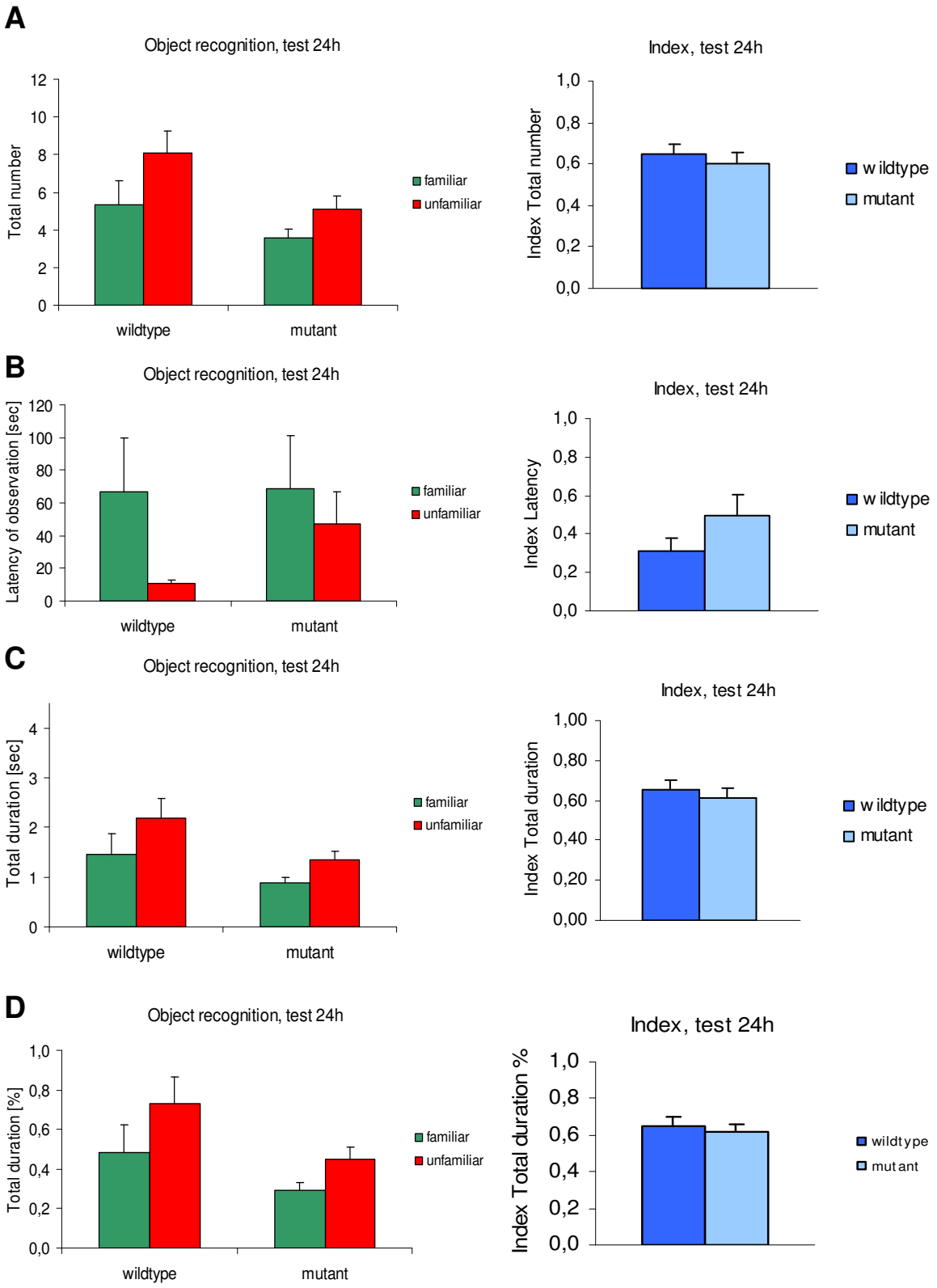

Figure 86: Object recognition – test phase (24h)

There were no genotype-specific differences between Tom40 heterozygous and wildtype mice.

4.13.6 Counting dopaminergic neurons

The number of TH-positive neurons counted in wildtypes was by trend higher than in mutants. Due to the small sample size (n=5 per genotype) and high fluctuations in the wildtype group, the results did not reach the level of significance (Fig.91; Graph Pad Prism, t-test p=0.144, n.s.)

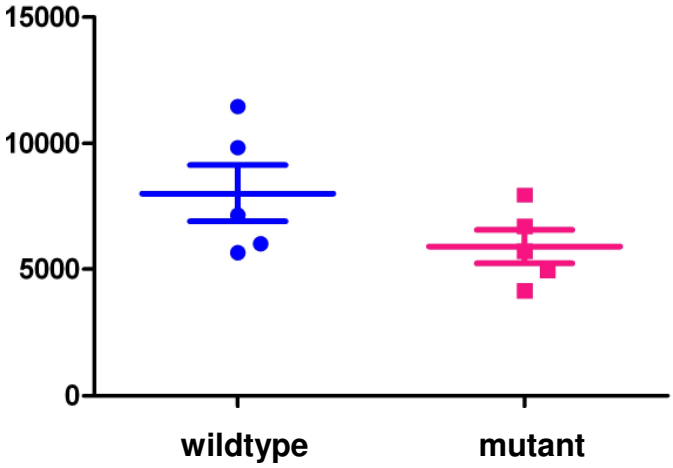

Figure 87: TH-positive neurons in aged *Tom40* +/- and wildtype mice
There were no genotype-specific differences between Tom40 heterozygous and wildtype mice.

4.14 NCV studies

Motoric NCV was measured in a group of aged (wt: 672d, mut: 731d) and young (wt: 216d, mut: 232d) animals. The number of evaluated aged mice remained quite low due to a high vulnerability to narcosis. There was a clear-cut effect of age and of genotype (Linear mixed effects model: $p<0.001$, ***). The motoric nerves of aged mice conducted electrical stimuli significant slower than the young one (Fig.88). Additional there was a genotype-effect in the young as well the aged group, with mutants showing marked worse performance.

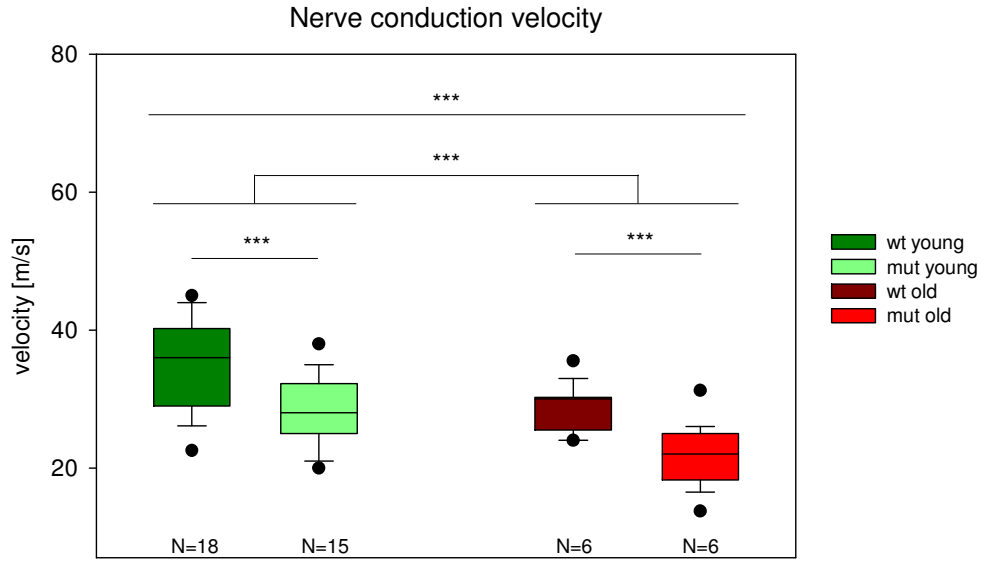

Figure 88: Motoric NCV of young and aged mutant mice

Electrophysical analyses were performed in the scatiatic nerve of both hind legs using a three point measurement technique. Therefore four measured values of each animal were received. There was a significant aging effect (Linear mixed effects model: $p<0.001$, ***) and a significant genotype effect (Linear mixed effects model: $p<0.001$, ***). The velocity reduction in mutants is visible in aged as well as in young mice (Linear mixed effects model: $p<0.001$, ***).

4.15 Challenge experiments

4.15.1 Paraquat challenge

Animals were challenged for 8 weeks with 2-3 times treatment per week (injection every three days). Phenotyping was done before and after challenge.

Body weight

Body weight was measured just before injection and one day after. There was a significant effect of treatment (Linear mixed effects model: significant interaction of genotype x treatment x day: $p<0.01$, **): Paraquat treated animals were in the end lighter than saline treated animals (Fig.89). Wildtype mice lost slightly more body weight than mutant animals due to the PQ treatment.

After eight weeks treatment, saline treated animals reached approximately 105% of their starting body weight while PQ treated mice achieved only 95% (Fig.89 C).

Figure 89: Weight curve during treatment

A-C: There was a significant treatment x genotype x day effect apparent: PQ treated animals were lighter at the end of the challenge than animals of the control groups. Wildtypes seemed to be slightly more affected than mutants (Linear mixed effects model: significant interaction of treatment x genotype x day: $p<0.01$, **).

Grip strength

Analysis of muscle force of the animals before treatment revealed no differences between the groups neither looking at the fore paws nor looking at all paws (Fig.90 A; Linear mixed effects model: $p>0.05$, n.s.). Measuring the grip strength after the PQ challenge again revealed a subtle increase in muscle force in the all paws measurement of treated animals compared to saline treated mice (Fig.90 B; Linear mixed effects model: $p<0.05$,*).

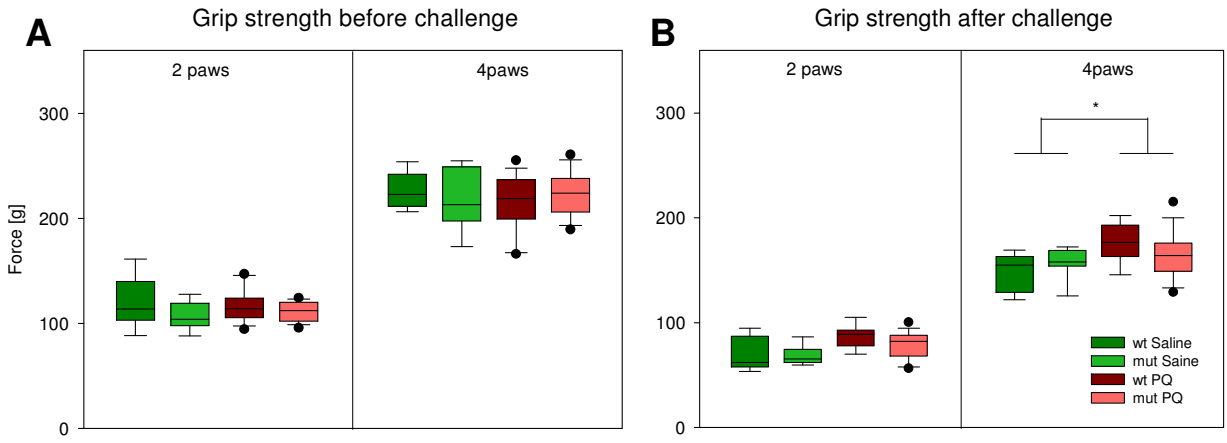

Figure 90: Grip strength before (A) and after challenge (B)

A: Before: There were no significant differences between the four experimental groups. B: After: There was a statistical significant treatment effect in the four paws muscle force (Linear mixed effects model: $p<0.05$, *)

Locomotor activity

The locomotor performance of the animals was not changed after treatment. There was no effect of treatment or of genotype on number of crossed squares (Two Way ANOVA, n.s.)

Rotarod performance

Determining the Rotarod performance of the animals before the challenge (see Fig.91A) showed an interaction between body weight x genotype x treatment (Linear mixed effects model: $p<0.05$, *). As mice were not treated yet, treatment in this experimental phase means differences caused by group assignment. Evaluating only the saline group, there was an effect of trial on performance: mice improved with trial number (Fig.92A; Linear mixed effects model: $p<0.001$, ***). Within the PQ group there was a significant interaction of body weight x genotype (Fig. 93; Linear mixed effects model: $p<0.05$, *). After finishing challenge the Rotarod performances of both treatment groups were quite similar 42 before: there was no effect of treatment concerning the mean latency to fall of the rod (Fig.91B; Linear mixed effects model: $p>0.05$, n.s.). Depiction of single trials revealed a treatment X trial number interaction (Linear mixed effects model: $p<0.01$, **): while there was a significant trial effect in saline treated animals ($p<0.05$, *) no improvement was detectable in PQ treated mice (Fig.92 B).

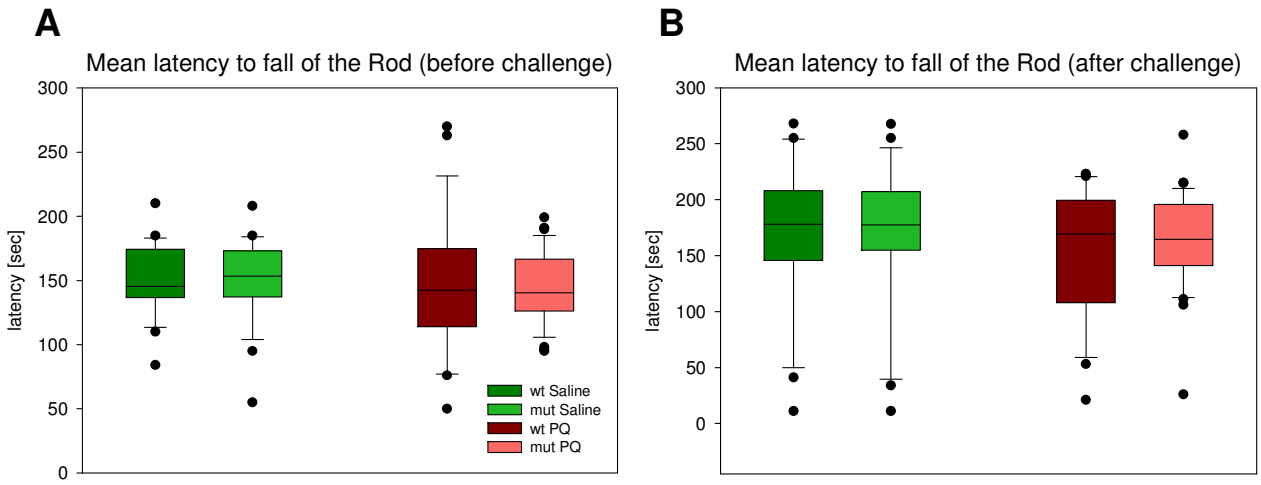

Figure 91: Mean latency to fall of the rod before (A) and after (B) challenge

A: There was a significant interaction between body weight x genotype x treatment before start of the challenge (Linear mixed effects model: $p<0.05$, *). B: There was no genotype specific difference concerning the mean latency of 4trials after challenge.

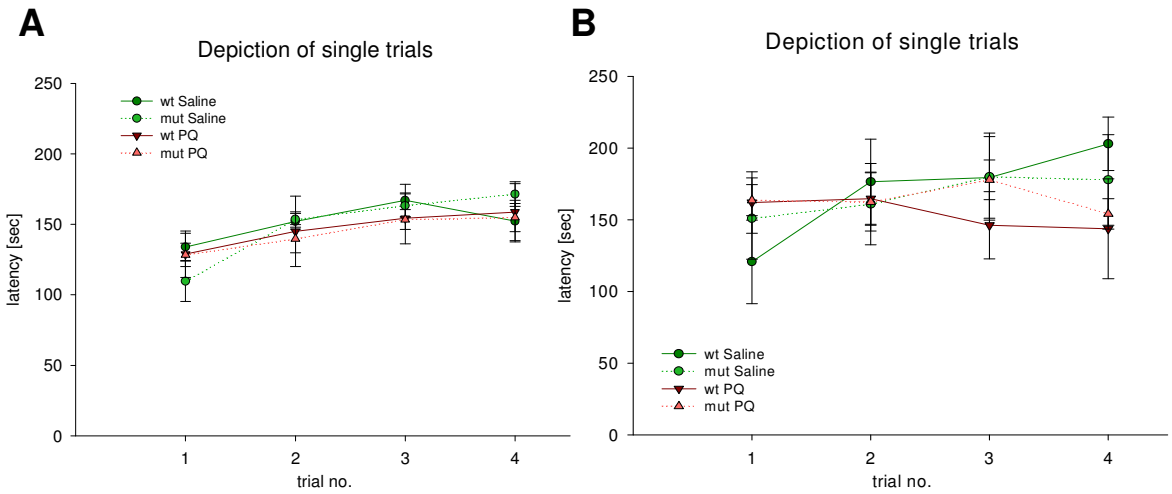

Figure 92: Single trials before (A) and after (B) challenge

A: There were a significant trial effect in the saline group (Linear mixed effects model: $p<0.001$, ***) and an interaction of body weight x genotype in the PQ group ($p<0.05$, *). B: There was a significant treatment x trial interaction (Linear mixed effects model: $p<0.01$, **): saline treated animals showed an improvement with trial ($p<0.05$, *) while Paraquat treated did not.

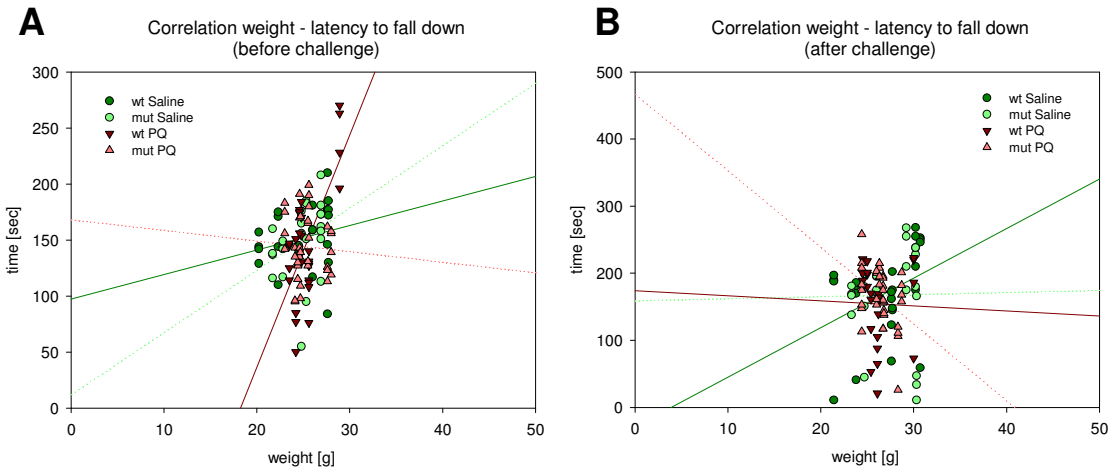

Figure 93: Body weight x latency before (A) and after (B) the challenge

A: There was a significant interaction of body weight and genotype on performance of PQ treated animals: While wildtype mice showed a higher latency with increasing body weight, heavier mutant mice fell off the rod earlier ($p<0.05$, *). B: There was no significant correlation between body weight and genotype detectable after challenge.

In addition, all animals were analyzed using the longterm Rotarod protocol. Before start of the challenge there was a significant interaction between genotype x speed x treatment group (Linear mixed effects model: $p<0.05$, *). To simplify the interpretation of the results, treatment groups were regarded individually. In the saline group, there was an interaction of genotype and speed ($p<0.05$, *) while in the future PQ group an interaction of body weight and speed was found ($p<0.05$, *). Mutants in the saline group performed worse than wildtypes at 20rpm and especially at 25 rpm (Fig.94A). PQ animals performed generally worse than saline animals, although no treatment had been done so far.

After challenge there still was a genotype x treatment x speed interaction (Linear mixed effects model; $p<0.05$, *). However in the saline group, the only finding was a significant influence of speed (Fig.94B; $p<0.01$, **), while in the PQ treated group a significant body weight x speed interaction was detected. The heavier the animals were, the more problems they had at higher velocities ($p<0.05$, *).

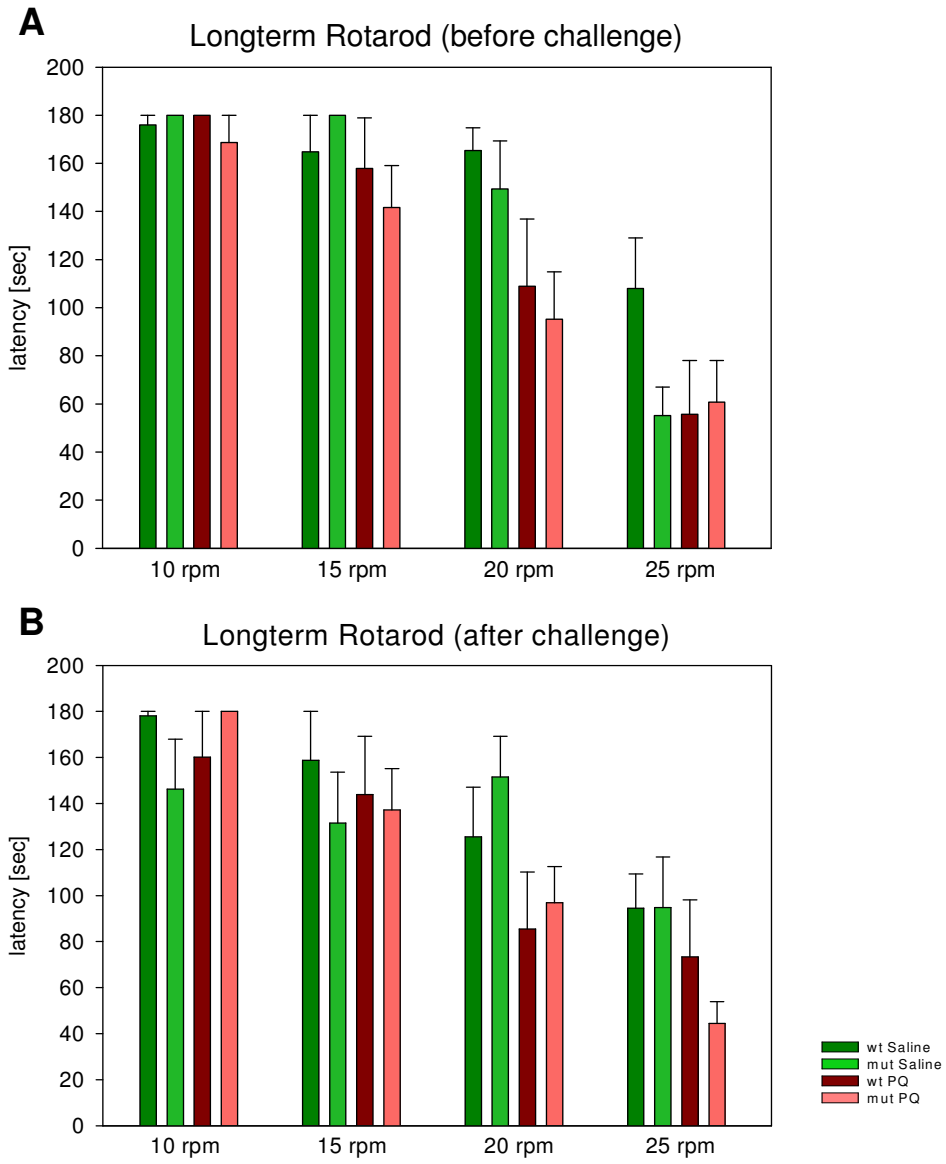

Figure 94: Longterm Rotarod performance before (A) and after (B) challenge

A: Before challenge, there was a significant genotype x speed x treatment (Linear mixed effects model: $p<0.05$, *): analyzing the data from animals from the saline group revealed a significant genotype x speed interaction ($p<0.05$, *) with mutants performing worse at higher velocities; for the PQ group a body weight x group interaction was found ($p<0.05$, *). B: After treatment there was a genotype x treatment x speed interaction found ($p<0.05$, *) saline treated animals showed a worsening with increasing speed ($p<0.01$, **) while in Paraquat treated animals a significant body weight x speed interaction could be found ($p<0.05$, *). Data are given as means and SEM.

Beam walk

Beam walk performance was measured before and after the challenge on three different beams: 13mm and 20mm (square) and 15mm diameter (round). There were already multiple effects in untreated mice. However, those differences were quite small and thus were hypothezised to be increased after challenge.

On the 20mm beam, there was a significant genotype-specific difference between heterozygous and control mice: Mutants showed more foot slips than wildtype mice (Fig.95A; Linear mixed effects model: $p<0.05$, *; Saline group: n.s., PQ group: $p<0.05$, *; treatment: $p=0.0787$, n.s.). This was more pronounced in the future PQ-group than in the saline group. Again, a distinctive improvement with trial number could be observed ($p<0.05$, *). On the 15mm beam no significant differences were detectable. Evaluating the data from the 13mm beam assured a subtle interaction of trial number x body weight x genotype ($p<0.05$, *). By analyzing the treatment groups individually it got obvious that this triple interaction was apparent within the PQ group. In the saline cohort a slight body weight x trial number interaction could be detected ($p<0.05$, *).

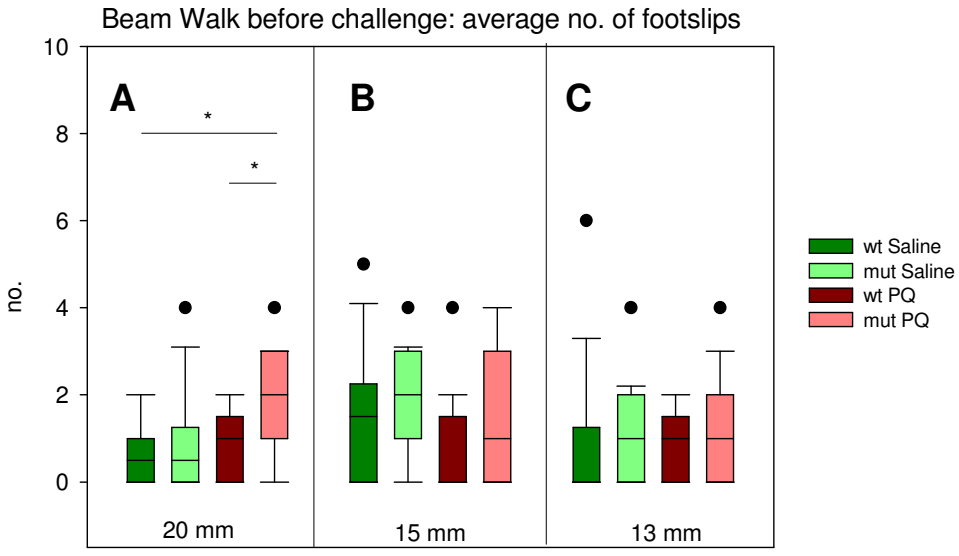

Figure 95: Beam walk before challenge – number of footslips

A: 20mm beam performance – genotype effect mainly due to the results of the PQ group (Linear mixed effects model: $p<0.05$, *); B: 15mm beam performance – no genotype-specific differences; C: 13mm beam performance – no treatment or genotype effects, but a subtle interaction of trial number x body weight x genotype ($p<0.05$, *);

Regarding the time required to cross the beam, there was an obvious treatment effect already before the challenge: animals assigned to the PQ group needed longer

to cross the 20mm diameter beam than animals in the saline group (Fig.96A; Linear mixed effects model: p<0.01, **).

Additional, there was a subtle but hardly significant trial effect: the more often animals tried to cross the beam, the faster this was achieved (Linear mixed effects model: p<0.05, *). On the 15mm beam slightly lowered times to cross the beam in mutant mice of both treatment groups were found (p<0.05, *). A complex interaction of body weight x treatment x genotype x trial number was detected on the 13mm beam (p<0.05, *). There was a strong trial number effect in the saline groups (p<0.01, **), while data of the PQ groups showed a genotype x body weight x trial number interaction (p<0.05, *).

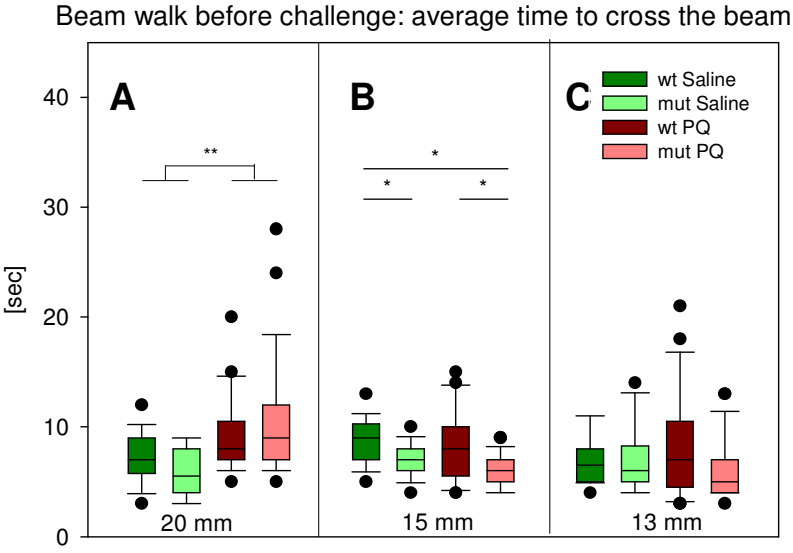

Figure 96: Beam walk before challenge – time to cross the beam

A: 20mm beam performance – global treatment effect (Linear mixed effects model: p<0.05, *);
B: 15mm beam performance – genotype effect (p<0.05, *): mutants are faster in crossing the beam than wildtypes; C: 13mm beam performance – no treatment or genotype effects, but a subtle interaction of trial number x body weight x genotype (p<0.05, *)

After challenge, there were still multiple differences between the groups, but again the differences were very small and it looked like if treatment did not worsen the performance of the animals. In detail, there were some trends on the 20mm diameter beam. The number of footslips was by trend higher in mutant (p=0.0803) and in heavier animals (p=0.0859) but there was no effect of treatment (Fig.97A; Linear mixed effects model, p>0.05, n.s.). Examining the performance of the different groups on the 15mm beam revealed a genotype x body weight x treatment

interaction (Linear mixed effects model: p<0.05, *). Individual evaluation of the treatment groups showed that there was a subtle interaction of body weight and genotype in the control groups with heavier mutants performing worse while there was no increase in foot slip number with increasing body weight in wildtype animals (p<0.05, *). Within the PQ groups there was a genotype specific difference: mutants perform worse than wildtypes (Fig.97B; p<0.05, *). However again, there was no treatment effect. It was quite the same with the performance on the 13mm beam: there was a significant genotype x body weight (Linear mixed effects model: p<0.01, **) and additional a subtle body weight x treatment interaction (p<0.05, *) with heavier mutant animals showing more footslips, mainly in the saline cohort.

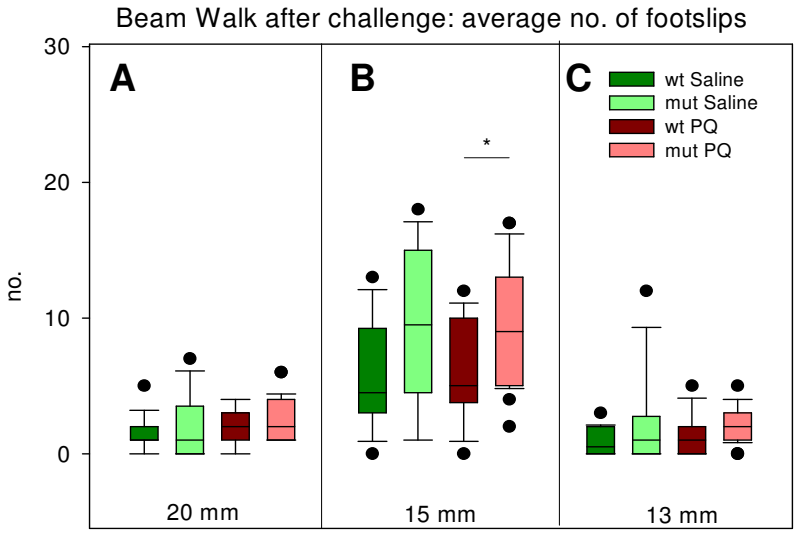

Figure 97: Beam walk after challenge – average number of footslips

A: No genotype specific differences (trend p=0.0803) or treatment effects.
B: Significant genotype x body weight x treatment interaction (p<0.05, *). Within the PQ cohort there was a significant genotype effect with heterozygous mice performing worse than controls (p<0.05, *).
C: No genotype specific changes, no treatment effects.

Utilizing the single trials verified that all animals were able to improve their performance regardless of which beam type was used. There was a significant influence of trial number on the 20mm beam (p<0.05, *), more pronounced in the saline group (p<0.01, **). Examining data of the 15mm beam demonstrated highly significant trial effects for both treatment groups (p<0.001, ***). There was no improvement on the 13mm beam due to the fact that already in the first trial animals hardly showed foot slips and therefore improving was not really possible.

Investigating the time to cross the 20mm beam showed no treatment or genotype effect but a highly significant influence of trial number: animals of all groups

significantly got faster with increasing trial number (Linear mixed effects model: p<0.001, ***). This improvement was also visible on the 15mm beam (p<0.01, **; more pronounced in the PQ treated groups p<0.05, *). On the 13mm beam there was a significant interaction of body weight and genotype influencing the crossing time (p<0.05, *).

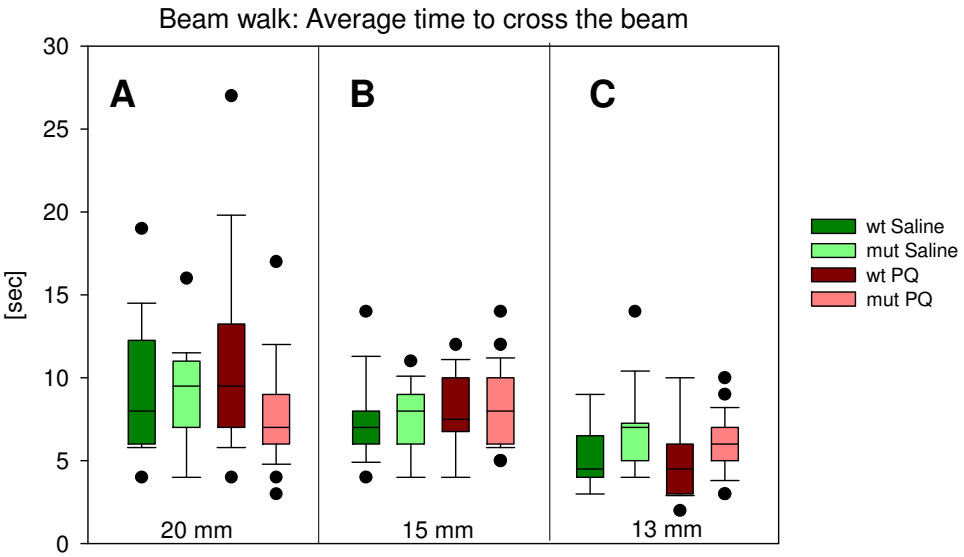

Figure 98: Beam walk performance after challenge – time to cross the beam
No genotype or treatment effects on all tested beam types.

Ladder walk

Statistical evaluation of the results gained from phenotyping the mice on the ladder walk resulted in a significant interaction of genotype x body weight x treatment group x trial number for the parameter fore paw slips (Fig.99A: Linear mixed effects model: p<0.01, **). Animals divided up to the saline group showed a significant improvement with trial number (Linear mixed effects model: p<0.001, ***). Evaluation of the results gained from animals divided up to the PQ treatment groups revealed a complex interaction of body weight x trial number x genotype (p<0.05, *).

A genotype and a trial number effect was found analyzing the hind paw data (Linear mixed effects model: genotype p<0.05, *, and trial number p<0.001, ***): mutant animals performed significantly worse than wildtypes (Fig.99B). All groups improved with trial number.

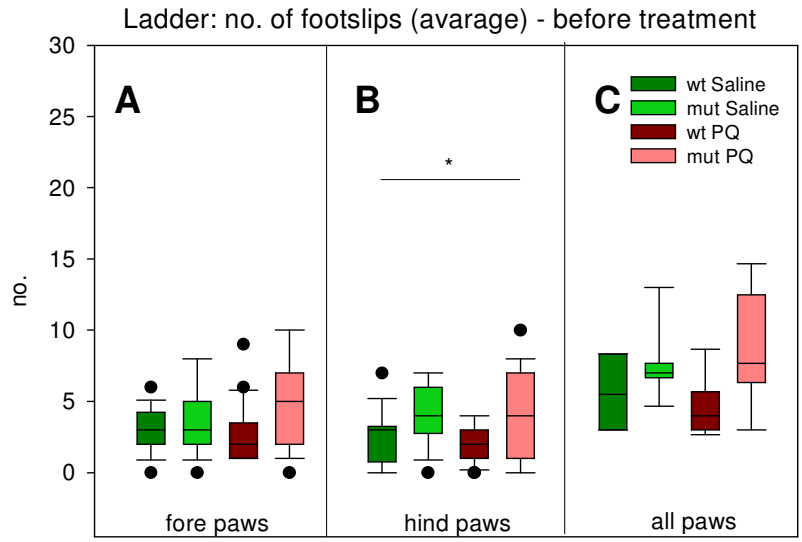

Figure 99: Ladder walk performance before challenge – Number of footslips

A: fore paws – significant interaction of genotype x body weight x treatment group x trial number (Linear mixed effects model: p<0.01, **): animals from the saline groups showed an trial effect (p<0.001, ***) with better performance in later trials while animals from the PQ groups showed a genotype x body weight x trial number interaction (p<0.05, *); B: hind paws – significant genotype effect (p<0.05, *), C: all paws taken together

Analyzing the animals' performance on the ladder after treatment revealed strong genotype specific differences for both parameters, fore paw (Fig.100A; Linear mixed effects model: p<0.001, ***) and hind paw slipping (Fig.100B; p<0.001, ***). Separate analysis of the individual treatment groups showed a genotype specific difference in the parameter fore paws in saline treated animals (p<0.01, **) while there was just a trend in PQ treated mice (p=0.0511, n.s.): mutants slipped more often from the metal grids than wildtypes. Graphic illustration of the hind paw results showed the same phenotype for the hind paws. Statistical analysis of the gained data revealed a significant genotype specific difference with worse performing mutants of the PQ group (p<0.01, **), while wildtype data did not reach the level of significance.

Evaluating the time needed to cross the ladder highlighted an interaction of trial number and treatment (Linear mixed effects model: p<0.01, **). Animals from the saline group showed a highly significant trial effect (p<0.001, ***), while in the PQ group this was just a trend (p=0.072, n.s.).

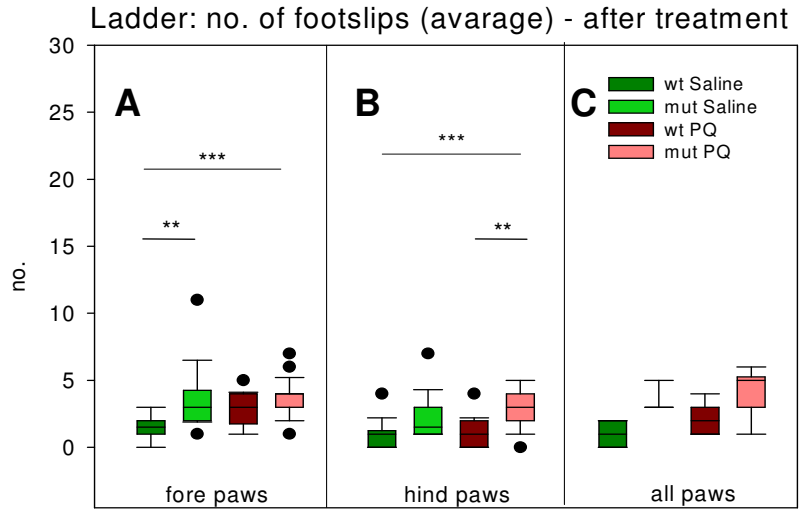

Figure 100: Ladder walk performance after challenge – Number of footslips

A: fore paws – significant genotype effect (Linear mixed effects model: p<0.001, ***), more pronounced in the saline group (p<0.01, **): mutants show more footslips than wildtypes; B: hind paws – significant genotype effect (Linear mixed effects model: p<0.001, ***), more pronounced in the PQ treated group (p<0.01, **): mutants show more footslips than wildtypes; C: all paws taken together

After challenge, Paraquat treated mutant mice needed significantly more time to cross the ladder than both of the saline treated groups and PQ treated wildtypes (Fig.101B; Linear mixed effects model: p<0.05, *).

In addition, there was a significant influence of trial number on the fore paw data (Linear mixed effects model: p<0.001, ***; Saline: p<0.05, *, PQ: p<0.001, ***), but not on hind paw data. Time to cross the beam was significantly influenced by the trial number in PQ treated animals (Linear mixed effects model: p<0.05, *).

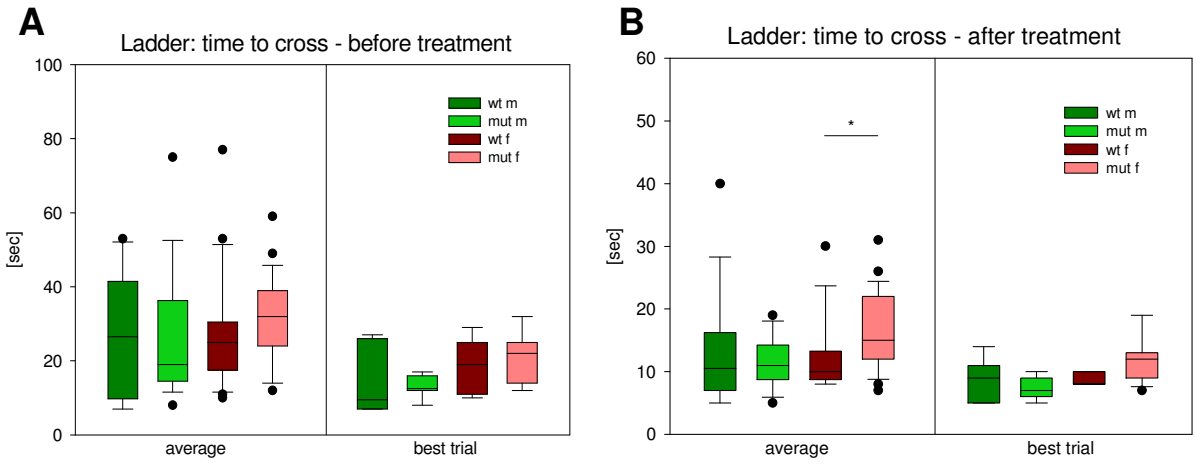

Figure 101: Ladder walk before (A) and after (B) challenge – Time to cross the ladder

A: average time to cross the ladder – interaction of trial number and treatment (Linear mixed effects model: p<0.01, **). Animals from the saline group showed a highly significant trial effect (p<0.001, ***) while in the PQ group this was just a trend (p=0.072, n.s.); B: average time to cross the ladder – mutant PQ treated animals spent more time to cross the ladder than the other groups (Linear mixed effects model: p<0.05, *);

Body composition

Mini Spec was measured by the metabolic screen one week before the last injection. There were no significant differences in body composition between the groups, neither concerning body weight nor fat or lean mass at this time point (Fig.102; Two Way ANOVA: n.s.).

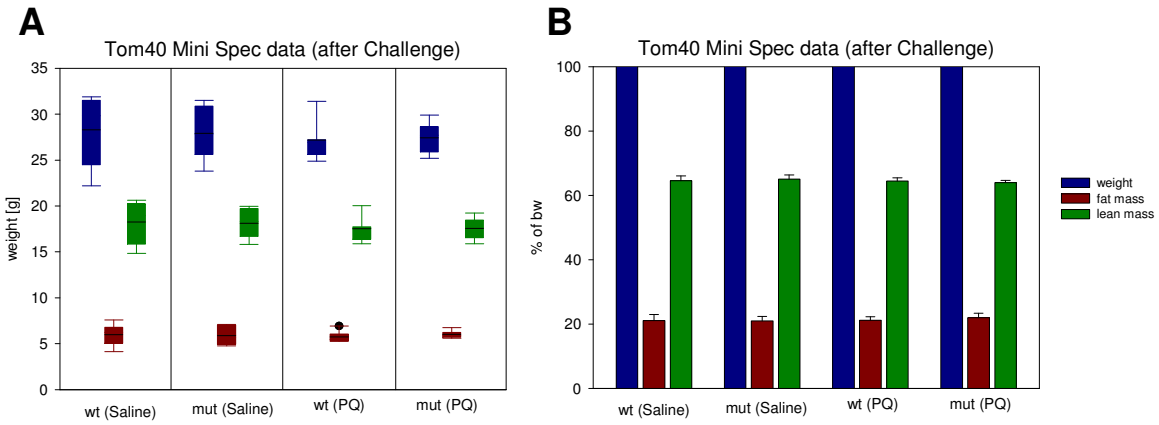

Figure 102: Body composition after treatment

A: Body weight, lean mass and fat mass, absolute values; B: Body composition with body weight set to 100% and lean or fat mass pro rata. There was neither a significant effect between treatment groups nor between the genotypes.

Clinical chemistry

Blood samples were taken just before organ withdrawal and analyzed by the clinical chemistry screen. The only genotype-specific difference that could be detected was a reduction of urea in treated wildtype mice (Fig.103; t-test: $p<0.01$, **). Values of treated mutant mice in contrast were similar to these in untreated animals and untreated wildtypes additional did not differ from mutants. Beyond, there were some parameters changed between treated and untreated mice (Tab.23 appendix): Cholesterol was significantly lowered in PQ challenged animals compared the control groups (Fig.103; Two Way ANOVA: $p<0.01$, **). However, there was no effect of genotype. Triglycerides (TG) values were also reduced in treated animals (Fig.103; Two Way ANOVA: $p<0.01$, **), whereas Transferrin was not altered.

There was a significant treatment effect concerning plasma iron levels (Two Way ANOVA: $p<0.05$, *): Treated animals showed slightly increased values compared to non-treated animals (Fig.104). Neither genotype nor treatment had an effect on Creatinine or uric acid.

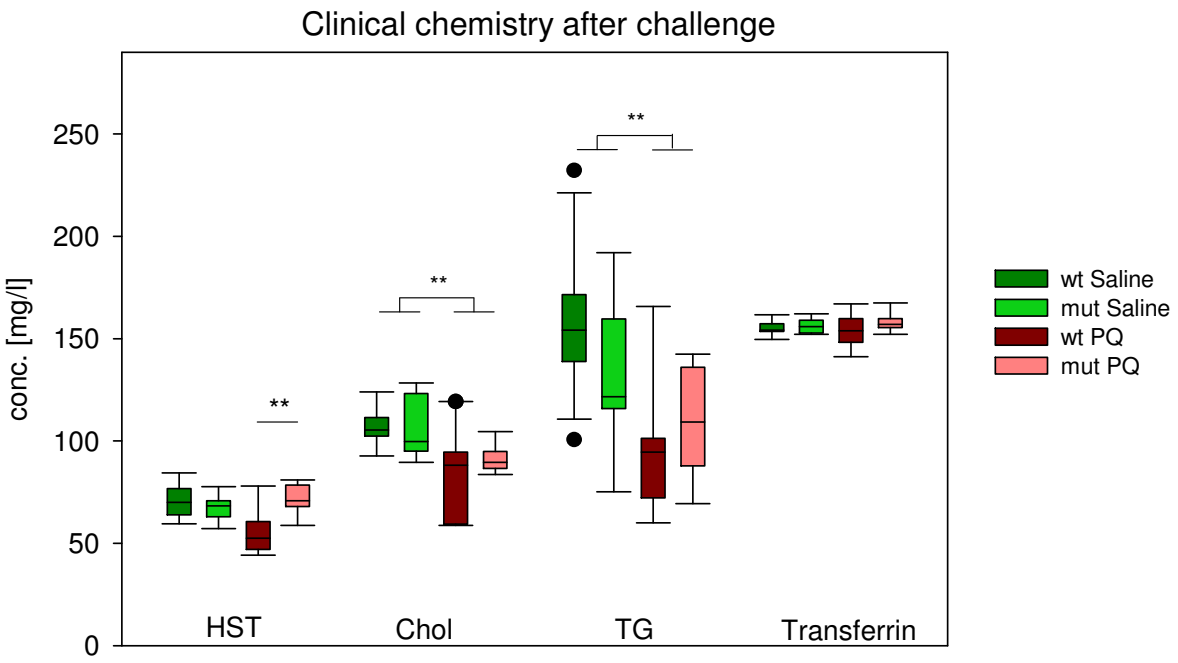

Figure 103: Urea (HST), cholesterol (Chol), triglycerides (TG), transferrin

Concentration was determined in mg/l. Urea was significantly reduced in wildtype PQ treated mice (t-test: $p<0.01$, **). Cholesterol levels were lowered in treated mice as well as triglycerides (Two Way ANOVA: $p<0.01$, **). However, Transferrin was not changed.

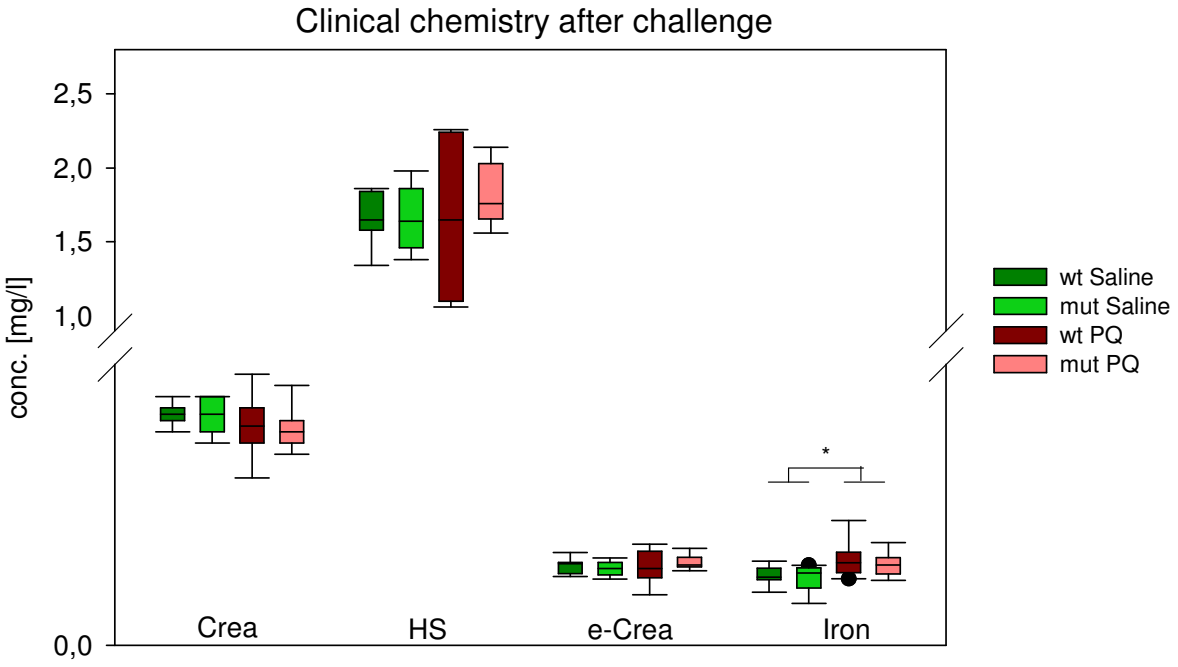

Figure 104: Creatinine (Crea), uric acid (HS), enzymatic creatinine (e-crea), iron

Concentration was determined in mg/l. Iron was significantly increased in treated mice 8Two Way ANOVA: $p<0.05$, *) while creatinine, uric acid and enzymatic determination of creatinine amount was not altered significantly.

There were no significant differences for total protein (TP), albumin and serum glucose levels (Fig.105) as well as for the electrolytes sodium (Na), potassium (K),

calcium (Ca), chloride (Cl), and inorganic phosphate (Phos) (Fig.106). There was a noticeable variation in treated wildtypes for most parameters. Activity of the enzymes AP, ALP and AST was not altered significantly (Fig.107), although ALT activity was slightly reduced in treated mice whereas for AST a subtle increase was found. There were no statistical significant changes in CK and LDH activity but α-amylase activity was slightly reduced in treated mice (Fig.108; Two Way ANOVA: $p<0.05$, *). LDH seemed to be slightly reduced in treated mice, CK values fluctuated greatly in (for some animals they even reached pathological values).

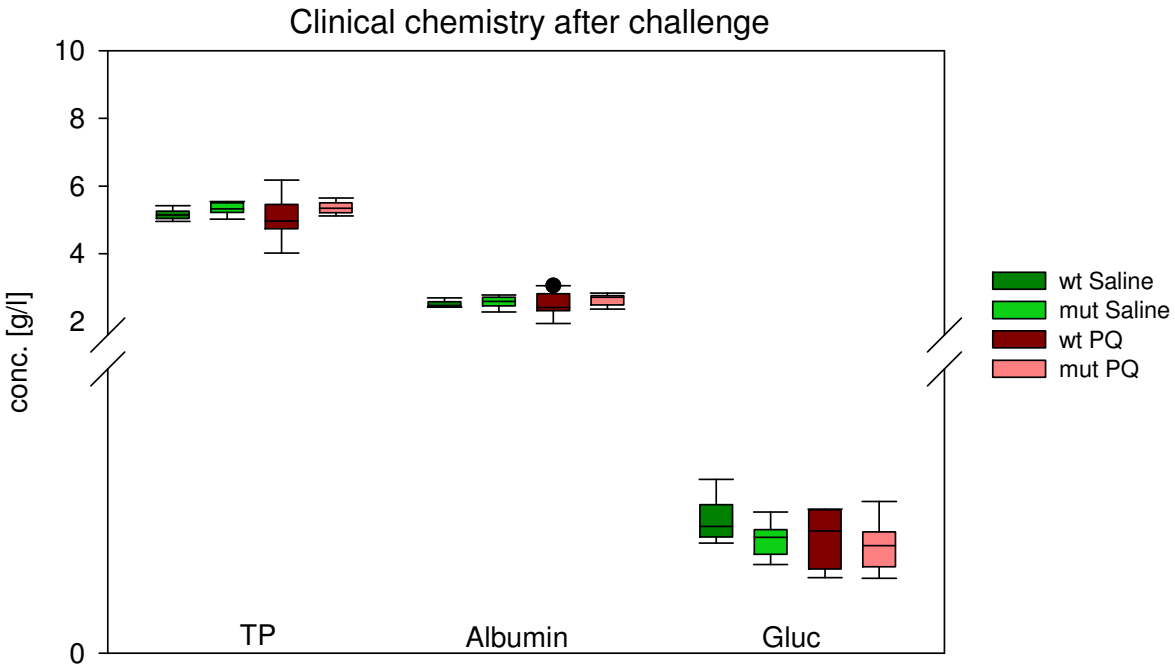

Figure 105: Total protein (TP), albumin and glucose (Gluc)
There were no significant genotype- or treatment-effects.

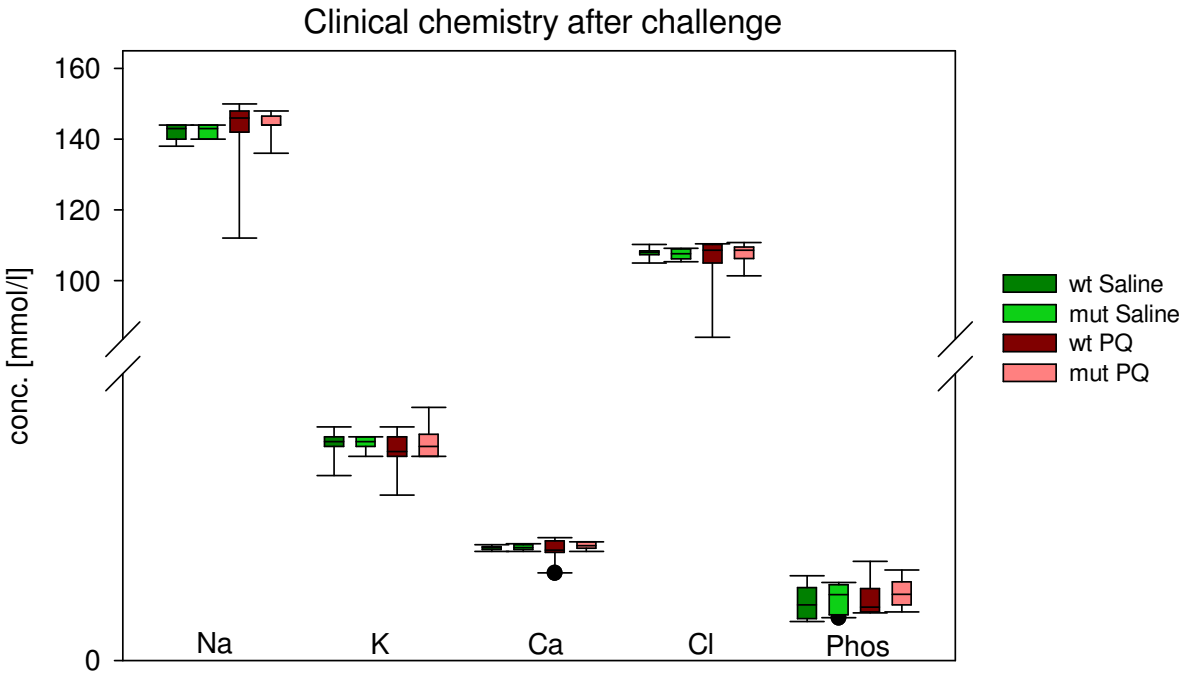

Figure 106: Sodium, potassium, calcium, chloride, phosphate

Sodium (Na), potassium (K), calcium (Ca), chloride (Cl), phosphate (Phos); There were no significant genotype- or treatment-effects.

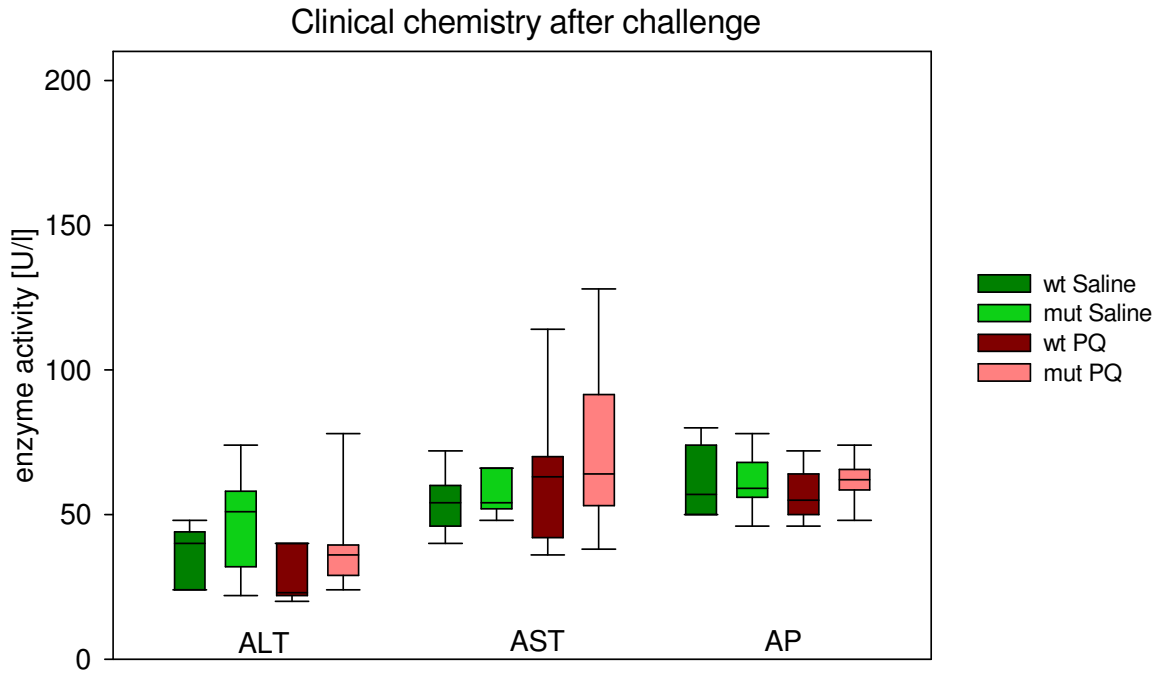

Figure 107: Alanine- and aspartate-amino-transferase, alkaline phosphatase

Alanine-amino-transferase (ALT), aspartate-amino-transferase (AST), alkaline phosphatase (AP); There were no significant genotype- or treatment-effects.

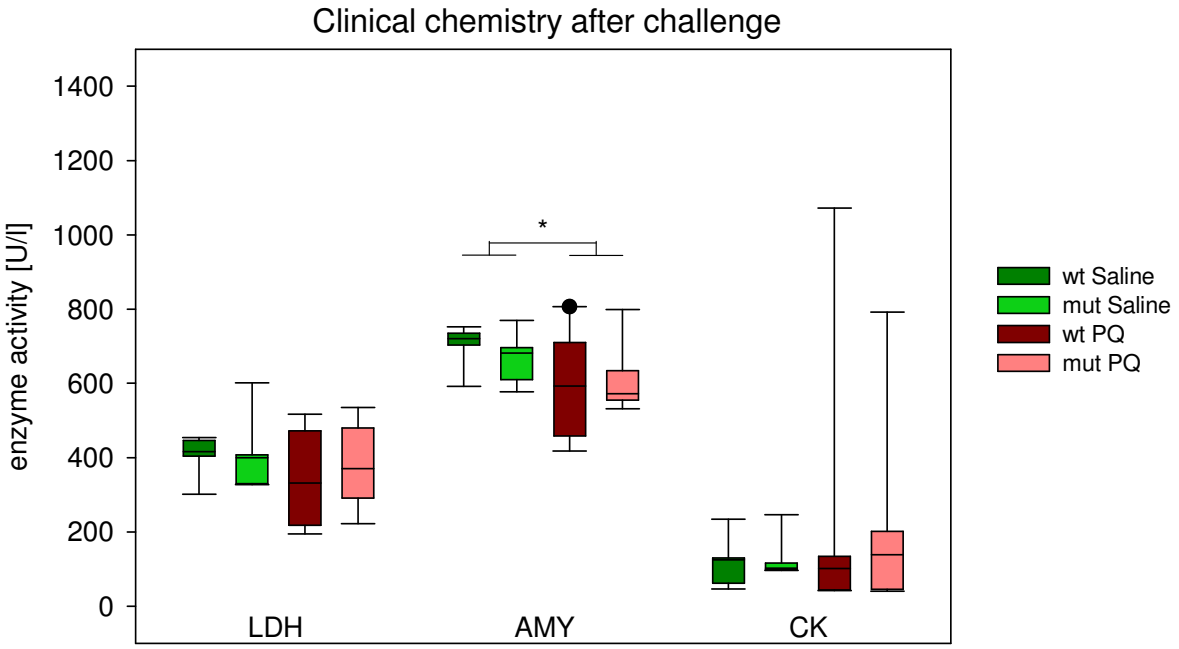

Figure 108: Lactate dehydrogenase (LDH), α-amylase (AMY), creatine kinase (CK)
There was a significant treatment effect in AMY activity (Two Way ANOVA: $p<0.05$, *). LDH and CK activity were not altered in treated animals.

Aconitase and Citrate synthase activity were measured in liver tissue lysates. There was a significant reduction of aconitase activity in treated animals (Fig.109; Two Way ANOVA: $p<0.05$, *). However, treatment with PQ didn't seem to have more influence on mutant mice than on controls. Citrate synthase activity was neither influenced by treatment nor by genotype.

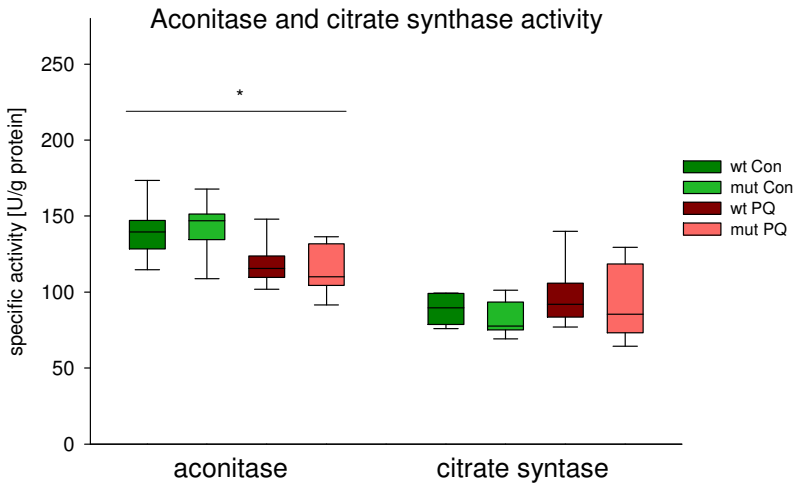

Figure 109: Aconitase and citrate synthase activity (liver tissue)
There was a significant treatment effect in aconitase activity which was lowered in PQ treated animals compared to saline treated (Two Way ANOVA: $p<0.05$, *). Citrate synthase was not altered in treated animals. There were no genotype-specific differences

Citrate synthase is commonly used as marker for mitochondrial activity and therefore the ratio between aconitase and citrate synthase was calculated. There was a highly significant treatment effect afterwards (Fig.110; Two Way ANOVA: $p<0.001$, ***) with treated animals showing a reduced aconitase activity in their liver tissue.

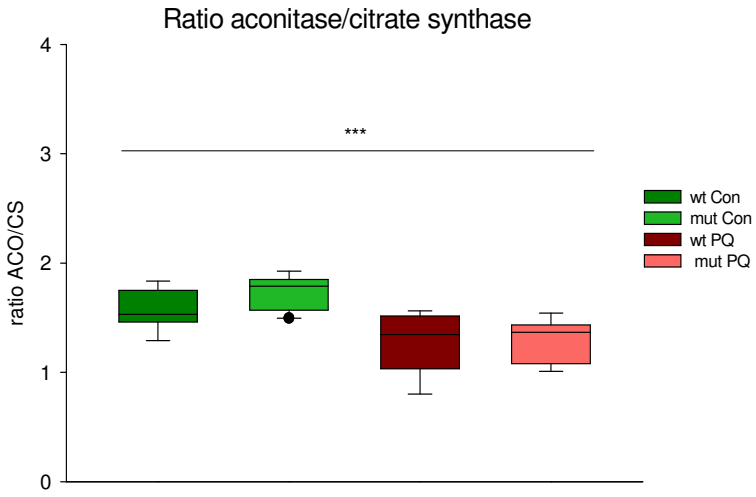

Figure 110: Ratio aconitase / citrate synthase activity (liver tissue)

There was a significant treatment effect in aconitase activity which was lowered in PQ treated animals compared to saline treated (Two Way ANOVA: $p<0.001$, ***).

4.15.2 Cold challenge

The pilot study with only two versu two animals revealed a marked difference between wildtype and mutant animals concerning oxygen consumption rates in response to drop in temperature (Fig.111). Both mutants showed elevated VO_2. Due to the low animal number it was not possible to analyze these data statistically and therefore it was decided that a larger cohort of Tom40 animals should undergo a cold challenge.

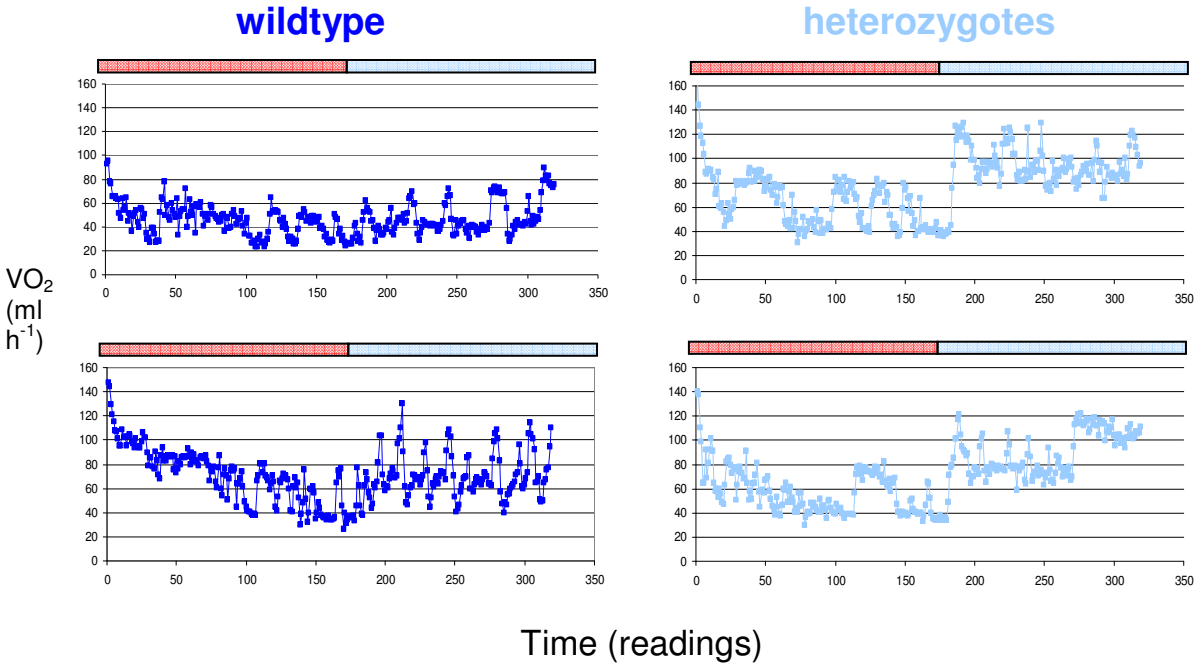

Figure 111: Results of preliminary cold challenge study

The results of this extensive cold challenge, however using a different protocol, are summarized in table 21 (appendix). There was no significant difference in body mass between control and mutant mice before and after the experiment. No significant difference could be detected in body mass loss. Mice of both sexes also showed no significant difference in rectal body temperature prior to the experiment. After the challenge male mutants had a higher body temperature compared to controls resulting in a milder body temperature reduction in response to the cold challenge.

Due to high activity levels and explorative behaviour both control and mutant mice showed elevated energy expenditure immediately after transfer to the respirometric cages. Mice adapted to the experimental conditions and reached stable values during the last 75 minutes of the 2 hours trial. Therefore, the first hour of adaptation was discarded and only the final 15 recordings (75min) before the temperature reduction were chosen for calculations at thermoneutrality. In response to the reduction of ambient temperature to 5°C mutants of both sexes were able to increase oxygen consumption comparable to controls indicating that thermogenesis was not severely impaired. During cold exposure female mice of both genotypes showed a steady reduction in VO_2. The same was found for control males whereas mutant males showed a less pronounced decrease over time. To investigate overall energy turnover at 5°C chamber temperature all data were analyzed.

At thermoneutrality (30°C), no significant genotype effect on absolute and body mass adjusted oxygen consumption could be detected (Fig. 112). Minimum (VO_{2min}) and maximum (VO_{2max}) oxygen consumption were calculated using the highest and the lowest individual data point. There was no difference in VO_{2min} whereas VO_{2max} was slightly but not significantly decreased both in male and female mutants (see table 21). The span in oxygen consumption was calculated as the difference between VO_{2max} and VO_{2min}. The span in VO_2 was smaller in mutant mice ($p = 0.055$, table 21 appendix) especially because, VO_{2max} tended to be lower in mutants. BMR was calculated by averaging gas exchange data during a 15 minutes interval where mice showed lowest oxygen consumption. BMR was only slightly increased in female mutants compared to controls but no difference was found in males.

During cold exposure (5°C) no significant differences could be detected (Fig.121). Mean oxygen consumption in the cold was slightly but not significantly increased in male mutants and slightly decreased in female mutants (table 21). At 5°C male mutants displayed higher VO_{2min} whereas there was no difference in VO_{2max} (table 21). Female mutants showed no difference in VO_{2min} during the cold challenge but slightly decreased VO_{2max} (table 21). Similarly as was found for thermoneutral conditions VO_2 span in mutant mice in cold was significantly lower compared to controls (table 21). Interestingly, in females this was due to reduced VO_{2max} whereas males showed increased VO_{2min}.

The resting metabolic rate (RMR) at 5°C was slightly increased in male and decreased in female mutants (table 22). The capacity in oxygen consumption was calculated as difference between VO_{2max} at 5°C and VO_{2min} at 30°C. No genotype specific difference was found for this parameter (table 21).

Energy metabolism variables strongly depend on body size or body mass. When body mass was included in the statistical models, there was no statistically significant difference in any of the parameters that were calculated from gas exchange data apart from VO_2 span at 5°C (table 21).

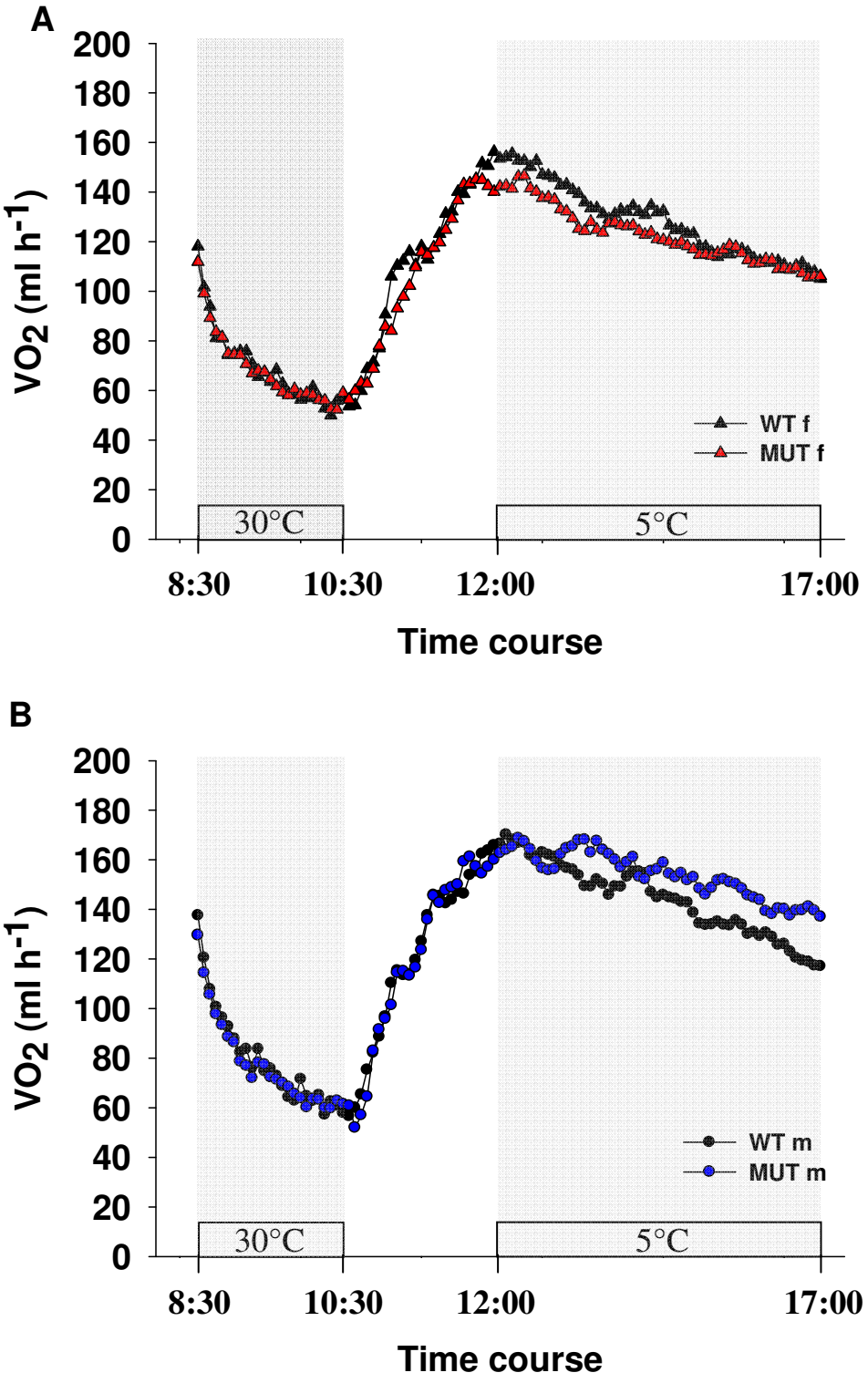

Figure 112: Oxygen consumption (ml h^{-1}) in thermoneutrality (30°C) and cold (5°C)
(A) Females, (B) Males

Respiratory exchange ratio (RER) also did not differ between genotypes both at thermoneutrality and in the cold indicating that mutants were able to switch from carbohydrate oxidation to fat utilization in the cold (table 21; Fig.113).

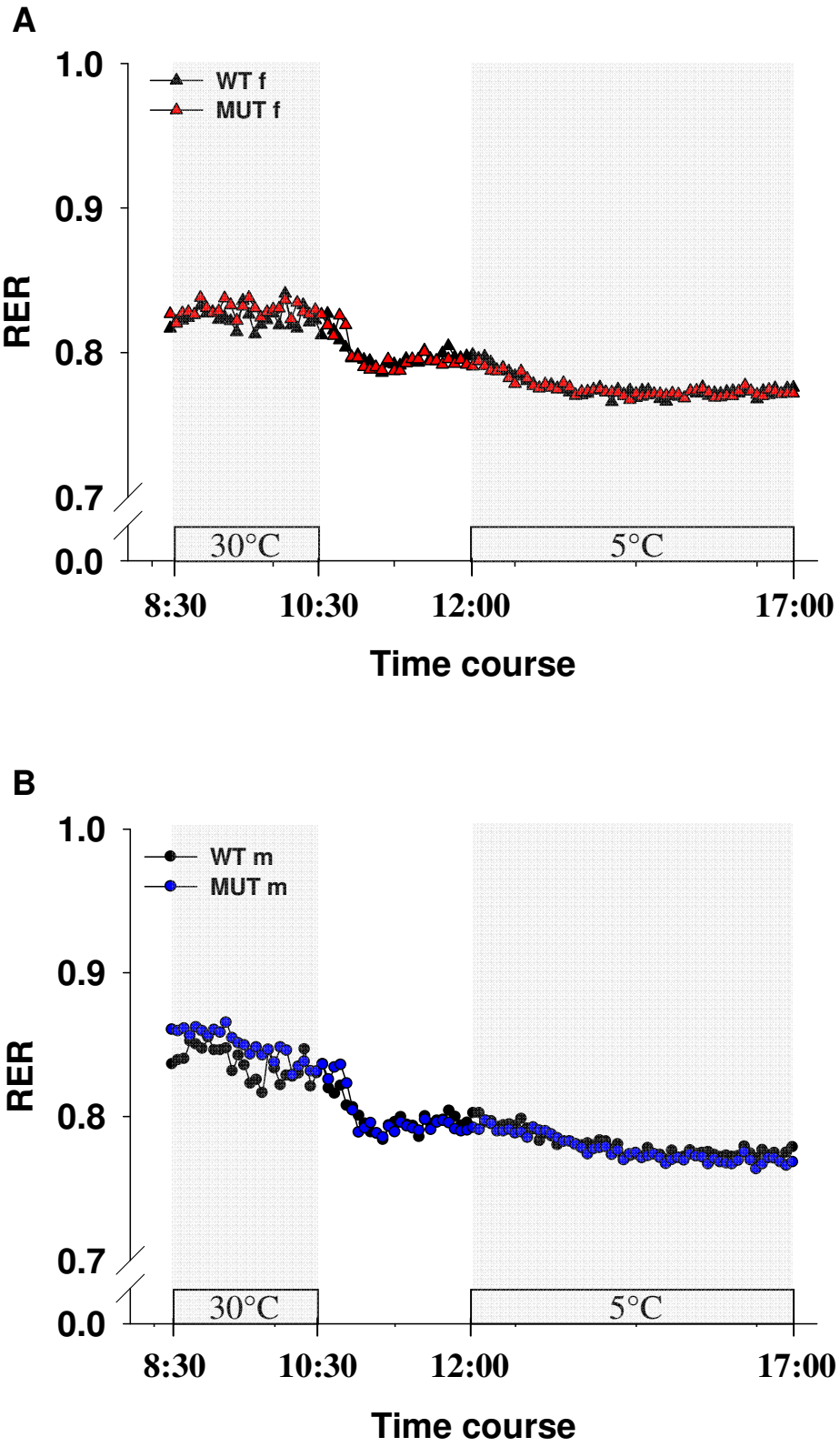

Figure 113: Mean RER in thermoneutrality (30°C) and cold (5°C).
(A) Females, (B) Males

5 Discussion

In the present study, the influence of a mutation in the *Tom40* gene on mammalian development and mitochondrial function was evaluated in a mouse model. Aim of the investigation was to analyze a systemic impairment of the mitochondrial proteome by mutation of the main import channel of the translocase of the outer mitochondrial membrane (TOM) complex. The mutant mouse line was generated via gene trap mutagenesis. Homozygous *Tom40*-/- mice were not viable, while heterozygous *Tom40*+/- mice showed normal development but a reduced life span with a 30% higher mortality after two years. Systematical analysis of the animals at different time points during their life span revealed mild cardiac dysfunction and slowly progressing neurological impairments. Young heterozygous *Tom40* mutants showed a subtle heart phenotype in the ECG analysis and a slight sensorimotor impairment in motor coordination and balance tasks. Motor nerve conduction velocity (NCV) in the sciatic nerve was reduced compared to wildtypes pointing towards a peripheral neuropathy. The morphology of heart mitochondria was widely altered in shape, size and inner structure in these young mutants. Nevertheless, the function and the composition of the respiratory chain in the inner mitochondrial membrane were not affected. In aged mutant mice respirometric analyses of isolated mitochondria revealed a strong genotype-dependant worsening of mitochondrial function in mutants, both in heart and in brain. The same effect could be shown for the motor and the electrophysiological phenotypes. The same effect could be shown for the motor and the electrophysiological phenotypes. AD specific phenotypes like a memory loss were assessed without detecting any alterations in mutant mice, iIrrespective of genome-wideassociation studies (GWAS) which stated a possible association to Alzheimer's diseases (AD) (Grupe A et al., 2007; Takei N et al., 2009). However, given the movement impairments quantitative analysis of dopaminergic neurons was performed. Alterations in the abundance of TH-positive neurons and the consequent impairment of the dopaminergic system in the brain are observed in patients suffering from Parkinson's disease (PD). Tyrosin-Hydroxylase (TH) positive neurons in the substantia nigra of these aged mutants revealed a reduced number compared to age-matched wildtypes. Thus, the Tom40 mouse model could help to understand age-related decline of motor functions associated with respiratory chain inhibition.

The Tom40 mouse model was created by the German Genetrap consortium (Hansen J et al., 2003; Wiles MV et al., 2000). The double-stranded pT1ßgeo gene trap vector integrated in chr.7 at position 2030096, its coding sequence entering the antistrand and its consensus sequence disrupting the *Tom40* promoter region, thereby reducing the *Tom40* expression to approximately 50%. There are no genes annotated to the antistrand insertion site, but the vector must have been under the control of a promoter as the clone was selected due to a vector mediated neomycin resistance. It has been shown that many genomic loci contain transcription units on both strands, with one direction coding for a protein and the other for non-encoding endogenous RNA molecules (reviewed by Lapidot and Piepel (2004)). In many species, mice included, the existence of these natural antisense transcripts (NAT) has been verified (Carninci P et al., 2005; Katayama S et al., 2005; Kiyosawa H et al., 2003; Sun M et al., 2006). They are acting as regulators for either the gene on the opposite strand (cis-NATs with a perfect sequence overlap) or for genes elsewhere in the genome (trans-NATs with imperfect complementarities and therefore the ability to form complex regulation networks) (Li YY et al., 2006). It is likely that the inserted pT1βgeo vector was driven by one of these NAT promoters. The existence of the NATs and their potential role as gene regulators also give rise to an alternative explanation for the impaired *Tom40* transcription in our mouse model. So the reduced *Tom40* expression could be due to a failing regulation by possible NATs from the opposite strand and/or due to the integration of the gene trap vector into the *Tom40* promoter. Another critical issue about the used gene-trap vector is that there is no possibility to excise the inserted neomycin resistance which probably could have an influence on the mouse (Scacheri PC et al., 2001). Additional, the insertion on the antistrand could also have an impact on further genes upstream. Examining the expression of neighboured genes in this region could not detect expression differences between mutant and wildtype animals (i.e. ApoE expression was not altered), pointing towards an exclusive impairment of the *Tom40* gene. To exclude the involvement of other genes than *Tom40* a rescue experiment would have to be performed.

Since the vector used (pT1βgeo) lacks an ATG codon in front of the lacZ reporter gene, the determination of the expression pattern of the gene trap vector in the mouse embryo was not possible. This vector type was generated by the group of Skarnes in the year 1989 (Gossler A et al., 1989; Skarnes WC et al., 1992) and

although it was successfully used in several laboratories, it has the decisive disadvantage that it has to be inserted in frame with the endogenous transcript to maintain β-galactosidase activity (Cecconi F and Meyer BI, 2000; Wurst W and Gossler A, 2000). It is likely that in the Tom40 mouse model either the insertion is not in frame or the promoter on the antistrand which drove the neomycin resistance was not active at the investigated embryonic stages. As mitochondria are present everywhere in the body, the protein should be expressed ubiquitous with an emphasis on tissues with a high energy demand like the brain. However, lacZ expression after mutagenesis is not mandatory for a successful gene knock-out. PCR-genotyping of numerous offspring of *Tom40* +/- intercrosses circumstantiated that no homozygous *Tom40* mutant offspring was born, suggesting that the knock-out was functional and had an immense influence on the developing embryo. The lethality of homozygous embryos is not unexpected considering the results in literature where the function of Tom40 was intensely analyzed and proven to be essential for cell viability in yeast (Vestweber D et al., 1989) and in *Neurospora crassa* (Kiebler M et al., 1990). To establish a timing of the observed complete embryo lethality, embryos of different developmental stages ranging from preimplantation to E11.5 were genotyped. No homozygous embryos or blastocysts were detected. It has been demonstrated previously in mice with an impaired energy metabolism to have difficulties in embryonic stages were the energy demand is high. Studies of early mouse embryos showed that oxygen consumption is relatively constant from zygote to morula stages, followed by a significant increase in the blastocyst and again in E6.5 dpc stages (Houghton FD et al., 1996). As we could not detect homozygous null mutants at E 3.5 dpc it is likely that a complete *Tom40* KO leads to a massive energy deficit as soon as the embryo starts to proliferate and therefore to lethality.

There still remains the question at which time point a complete lack of *Tom40* expression induces the death of the harbouring cell. In most mammalian species, including the mouse, mitochondria are inherited solely through the female germ cell line, whereas the paternal mitochondria are eliminated after fertilization as reviewed by Cummins (2000). In the analyzed mouse model the *Tom40* mutation is transmitted through both germ lines, therefore there must be viable and fertile oocytes and sperms carrying the mutant allele. The zygote is exclusively supplied with energy provided by maternal mitochondria.

Mitochondria in both gametes are derived from the heterozygous parents and apparently supply enough energy. During spermatogenesis there are no major changes in mitochondria shape or number. In the mature sperm there are 22-75 mitochondria arranged end to end in the midpiece (Otani H et al., 1988). This is way different during oogenesis: there is a massive increase in mitochondria number (increase from 10-100 to 100000-200000 copies from progenitor germ cell to mature oocyte (Shoubridge EA and Wai T, 2007)). It seems that the material that is delivered by the heterozygous *Tom40* mother is enough to hold the *Tom40* null allele oocyte alive until fertilization, although *Tom40* expression is no longer possible. After fertilization, there is a reduction of mtDNA copy number per cell with increasing cell number visible, accounting for that mitochondria are just apportioned equally to the daughter cells and not regenerated in the very early embryo (Cao L et al., 2007). In fact, the first mtDNA replication in the developing mouse takes place postimplantational (Piko L and Taylor KD, 1987).

One functional *Tom40* allele is obviously enough to guarantee a quite normal development. Expression analysis on mRNA level demonstrated a 50% reduction of expressed *Tom40.* Relationship between gene expression measured at the mRNA level and the corresponding protein level sometimes only shows a weak correlation or especially in tumour cells even no correlation at all (Chen G et al., 2002; Greenbaum D et al., 2003; Guo Y et al., 2008). Post-translational protein concentration is affected by several parameters such as regulatory processes during transcription and translation (Greenbaum D et al., 2003). Therefore analysis of the expression level of TOM40 protein would have been important to make a conclusion about how much functional active TOM40 is left, although mRNA analysis showed that *Tom40* mRNA is 50% reduced in *Tom40* heterozygous mutants as expected if only one functional allele is left. Unfortunately the outcome of the western blot studies demonstrated that there are no commercial primary anti-TOM40 antibodies available to date that work properly on mouse tissue lysate. Existing antibodies are only predicted to react with mouse TOM40 because of the highly conserved structural properties of human and murine TOM40. There was only one antibody which resulted in a 40kDa band. The antibody proved to be quite unspecific as it produced numerous bands ranging from a size of 10 to 100kDa. Rinsing the membrane with blocking solution was finally successful to get rid of the unspecific bands and at first

glance TOM40 expression seemed to be slightly lowered in mutant animals. This finding was irreproducible, and a final conclusion about the remaining expression could not be drawn because of the insufficient sample size.

Heterozygous *Tom40* +/- animals did not suffer from obvious impairments that could be detected at first glance. As mitochondria are apparent everywhere in the organism, mitochondrial mutations could manifest anywhere. To address the question which organ systems are affected by the mutation, young animals were phenotyped systemically in the GMC. There were no findings in the primary screen of the modules Eye, Nociception, Allergy, Steroid Metabolism, Lung Function, Molecular Phenotyping, and Pathology. Dysmorphology detected in the DEXA test that fat mass and fat content were significantly increased in female mutants compared to female controls. This phenotype was verified by the energy metabolism screen: mutant mice were significantly heavier than controls. They could not determine a shift in body composition by NMR scans. However, screens from pipeline II also detected a difference in body weight, but in the opposite direction. Wildtypes were significantly heavier than mutants. Taken the results from pipeline I and II together it was evident that the found body weight differences were findings by chance and not genotype-related.

Subtle changes were found in immunology, with mutant males showing higher CD4+ and CD8+ T-cell levels than wildtypes. Nevertheless, the changes were very small, only in one sex detectable and no clear cluster segregation could be observed, so they are supposed to be a finding by chance and without physiological relevance. Further investigation would be necessary to clarify if the consequences of the mutation have an impact on the immune system.

There were no clearly genotype-related clinical chemical or haematological phenotypes in *Tom40*-mutant mice. Small genotype-related differences in blood lipid values of fasted (HDL-cholesterol and NEFA) and non fasted (cholesterol and triglycerides) mice as well as slightly lower glucose concentrations in plasma of mutant *ad libitum* fed male mutants, might indicate small effects on fat and energy metabolism. Additionally there were slightly increased ALP levels in plasma of mutant mice. This was more pronounced in male mutants. ALP activity in plasma origins from different sources, for example liver, bone, gut, and small intestine (Moss DW, 1982) and hints on specific defects in one of these organs are missing in young

animals. In the cardiovascular screen animals showed a subtle cardiac phenotype. It has been reported that ALP expression in the heart is largely confined to the right atrium of the heart (Müller E and Pearse AG, 1969). ALP is supposed to contribute to vascular hardening and calcification which could be related to vascular aging and vascular disease (Hui M and Tenenbaum HC, 1998; Schultz-Hector S et al., 1993). However, there were no hints in the primary hematoxylin and eosin stain screen of the pathology that the hearts of mutant animals showed macroscopic changes like vascular hardening. Plus, ALP activity was analyzed after the PQ challenge with the control group showing no genotype specific difference concerning this parameter, although it has to be considered that these animals had another age and another antecedent as the animals from the primary screen, so direct comparison is difficult.

As already mentioned above, one of the few phenotypes already apparent in young mice was found in the cardiovascular screen during ECG analysis. *Tom40* mutant mice showed a mild cardiac phenotype with prolonged QT- and ST-interval and decreased p-wave duration. It is well known from literature that mitochondrial dysfunction in humans is commonly accompanied by cardiac phenotypes (Russell LK et al., 2005). There are several different diseases where patients suffer from cardiac problems i.e. the Kearns-Sayre syndrome that is caused by mtDNA mutations and results in opthalmoplegia, retinal degeneration and a dilated cardiomyopathy (DiMauro S et al., 1985; Kearns TP and Sayre GP, 1958). Not only mtDNA mutations are known to be causative for heart phenotypes, but also mutations in nuclear encoded genes encoding mitochondrial proteins. Complex I deficiency which is characterized by a hypertrophic cardiomyopathy, lactic acidosis, encephalopathy, and vision loss can for example be either caused by mitochondrial or nuclear encoded complex I subunit genes (Loeffen JL et al., 2000; Triepels RH et al., 2001). A prolonged QT-interval like found in the Tom40 mouse model was also found in some LHON patients (Ortiz RG et al., 1992). The findings in GMC primary screen could hint for alterations in the conduction properties of the heart. As aging strongly influences mitochondrial function (Ames BN et al., 1993; Bowling AC et al., 1993; Chan DC, 2006; Shigenaga MK et al., 1994) it would have been interesting to investigate another batch of animals, older than the primary screen animals, in order to replicate the found heart phenotype and moreover to see if aging worsens the cardiac problems. This failed because of an observation made during a preceding study where aged mutant animals have proven to be incompatible to narcosis: while

none of the control animals faced serious problems with anaesthesia all sedated mutant mice died. In the past years there were methods developed which allow measuring of ECG in awake, free moving mice (Jeron A et al., 2000). This technology indeed is currently established in the GMC, but yet not available for usage.

Because of the cardiac phenotype and the known comorbidity of cardiomyopathy and mitochondrial diseases, heart and heart mitochondria of *Tom40* heterozygous mice were analyzed in detail in the pathology screen of the GMC.

In the complete standard morphological analysis with hematoxilin and eosin stain performed in the primary pathology screen, no obvious morphological phenotype had been detected. Nevertheless, morphological changes at the level of the mitochondria are better analyzed with electronic microscopy (Stirling JW et al., 1999). TEM imaging of heart tissue of young mutant mice revealed ultrastructural changes. In some areas of the heart muscle, mitochondria with abnormal shape and size aggregated around distorted myofibrils. This was not generalized as there were completely normal areas in the mutant heart, probably accounting for the present but quite subtle heart phenotype observed in the cardiovascular screen. Results of mtDNA copy number analysis point to the fact, that there is the same mtDNA content in wildtypes like in mutants. Citrate synthase activity as an indicator of mitochondrial mass was also not altered in mutants. It is possible that mitochondria compensate their import defect with a reduction of size and simultaneously an increase in mitochondrial but not mtDNA number. In literature one proposed cause for cardiomyopathy was an impaired protein import from cytoplasm into the mitochondrial matrix. Various studies describe a drastic reduction of mitochondrial carnitine levels in cardiomyopathic patients (Hart Z et al., 1978; Tripp ME et al., 1981; Waber LJ et al., 1982). Carnitine itself is an obligatory cofactor for carnitine palmitoyl transferase (CPT) and is essential for the transport of fatty acids across the inner mitochondrial membrane. In cooperation with the carnitine/acylcarnitine translocase a carnitine palmitoyltransferase system (CPT) consisting of two membrane-bound enzymes (CPT1 in the outer mitochondrial membrane and CPT2 in the inner mitochondrial membrane) permits the transport of long-chain acyl-CoA from the cytosol to the mitochondrial matrix (McGarry JD and Brown NF, 1997; McGarry JD et al., 1989). While carnitine is imported into mitochondria by its own transorter, the components of the carnitine cycle, i.e. CPT1 and CPT2 have to be imported to

mitochondria via the TOM/TIM system located in the mitochondrial membranes (Brown NF et al., 1991; Cohen I et al., 1998).

Interestingly, the electronmicroscopical investigation of heart tissue from carnitine deficient patients revealed an accumulation of aggregated heart mitochondria with bizarre shapes, a finding that was also present in the Tom40 mouse model, harbouring an affected import system. Plasma or muscle carnitine concentrations have not been measured so far in the *Tom40* mutants, but it is entirely conceivable that there is an insufficient carnitine import to the matrix caused by the reduced Tom40 amounts. If so, the lack seems to be not dramatic as animals do not show markedly detracted myocardial function but only a quite subtle phenotype. Anyway, an investigation of metabolic parameters in plasma could perhaps help to get further insights and should be followed up.

Additional, the inner structure of the investigated *Tom40* heterozygous heart mitochondria was altered compared to wildtypes. Mitochondria derived from mutant animals appeared condensed compared to those of wildtypes. There was no clear difference between the compartments, the matrix appeared denser and there were hardly distinct cristae and vacuoles visible. Altered cristae are a condition in a variety of disease. In contrast to the alterations found in the heart mitochondria of Tom40 mutants, pathological findings often involve mitochondrial swelling and breakup of cristae invagination (Baloyannis SJ et al., 2004; Hayashi J-I et al., 1994; Kaido M et al., 1995; McKechnie NM et al., 1985; Suomalainen A, 1997; Swerdlow RH et al., 1997; Swerdlow RH et al., 1998). However there are conditions described which resembles the situation found in *Tom40* +/- heart mitochondria. After acute brain ischemia the most striking ultrastructural phenotype found are swollen mitochondria (Garcia JH et al., 1978). If they exposed rats to transient severe ischemic/reperfusion conditions there were dramatic signs of mitochondrial injury such as condensation, increased matrix density, and deposits of electron-dense material followed by disintegration (Solenski NJ et al., 2002). They conclude that because of the generation of ROS during the reperfusion phase mitochondria are damaged. Tom40 +/- heart mitochondria look condensed with little space in between the cristae and a quite dark matrix. In some areas there is hardly any cristae structure visible. It could be speculated that the mutant mitochondria are always subject to a minimal oxidative stress level, not sufficient to damage aconitase or RCC activity severely but to have an influence on mitochondrial structure. Another study suggests that the absence of

oxidizable substrate results in matrix condensation (Gottlieb E et al., 2003), a cause which also has to be taken in account for mutant *Tom40* mitochondria considering the fact that important substrates have to be imported. Considering the fact that the TOM40 protein is involved in the mitochondrial import system the altered morphology of *Tom40* heterozygous mitochondria also could be related problems with mitochondrial dynamics: fission needs import of various proteins into the resultant daughter mitochondria. Import studies could give information about the efficiency and velocity of the import system in mutant animals.

As consequence of the detected structural alterations the composition of the respiratory chain was assessed especially in the heart. Quantification of the amounts of OXPHOS complexes by BNE showed that a lack of one *Tom40* allele does not affect import of proteins required for the OXPHOS in a dose dependent manner. The results of the analysis of TOM40 +/- tissue indicate that the import machinery works sufficiently and all required proteins needed to assemble wildtype amounts of OXPHOS complexes are imported. Since the first analysis was done with samples from young animals long term effects on the import machinery could not be determined. Therefore the analysis was extended to heart tissues from old mice. However, also in the aged mice there were no differences between mutants and wildtypes. Aging apparently does not impair the import of necessary components of the respiratory chain in mutant animals more than it does in control mice.

Respiratory chain complexes can be isolated as single protein complexes that are catalytically active. Since more than a decade ago the use of mild solubilisation conditions and BNE showed that respiratory chain complexes build larger assemblies within the inner mitochondrial membrane. These macromolecular complexes, also called supercomplexes or respirasomes are stoichiometric assemblies of the complexes I1III2 and IV0-4 (Schägger H and Pfeiffer K, 2000). The function of respirasomes remains elusive. It was proposed that the respirasome could direct the complete electron flow from NADH to oxygen thereby preventing the formation of ROS. The analysis of patients with isolated deficiency of single complexes provided evidence that the formation of respirasomes is essential for the assembly/stability of complex I (Acín-Pérez R et al., 2004; Schägger H et al., 2004).

Evaluation of respirasomes of Tom40 mice showed that there were no genotype-specific differences between the analyzed cohorts. Not only the respiratory chain complexes form larger complex assemblies, also complex V (ATP synthase) is known to form homo-dimers and homo-oligomers (Arnold K et al., 1998; Wittig I and Schaegger H, 2005). Oligomerization of ATP synthase is described to play a role in cristae formation (Paumard P et al., 2002) but since there were no differences between the genotypes there is no evidence that it is involved in the formation of the ultrastructural alterations in *Tom40* mutant mitochondria.

Investigating respirasomes of aged and young Tom40 mutant and wildtype heart tissue lead to some interesting findings: the respirasomes were more stable and of higher abundance in old heart tissue, both in wildtypes and heterozygous deletion mutants. This was also found for the homo-oligomers of ATP synthase. In a contradicting study in isolated rat heart mitochondria found an age dependant decline in respirasome abundance was detected (Gómez LA et al., 2009). Gomez et al. described that the most severe reduction occurred in the supercomplexes with the highest molecular mass and argued that the supercomplex decline was not due to a reduction of the individual ETC complexes whose abundance was not affected by aging at all. They suggest that a supercomplex reduction may account for the age dependent reduction in OXPHOS activity which manifests in decreased complex I, III and IV enzyme activity, with complex I being especially vulnerable to aging possibly due to its high content mtDNA encoded subunits (Castelluccio C et al., 1994; Fannin SW et al., 1999; Genova ML et al., 1995; Lesnefsky EJ et al., 2001). Beyond, a decrease in cardiac respirasomes has been reported in heart failure (Rosca MG et al., 2008) and disorders like the Barth syndrome (McKenzie M et al., 2006) but there are no further studies about supercomplexes and aging. In the present study performed by Dr. Wittigs' lab in Frankfurt/Main, the aged *Tom40* wildtype and mutant heart mitochondria disclosed a markedly increase in the amount of supercomplexes. As there were similar results for fungi and varying results for fish mitochondria (unpublished results) the group of Dr. Wittig is currently following up this issue systematically. One possible explanation for the detected increase in old tissue could be that the dynamic of the inner mitochondrial membrane is reduced. It has been shown that aging significantly decreases mitochondrial fusion and fission activity (Jendrach M et al., 2005). Reduced fission results in a decrease of protein turn-over, but more stable supercomplexes might be built. Additionally, the presence of more

supercomplexes hints towards a slightly increased cellular stress level and respectively an eased mitochondrial quality control. Cell survival depends on essential processes in mitochondria, which contain various proteases regulating mitochondrial biogenesis (Tatsuta T and Langer T, 2008). Membrane-integrated ATP-dependent proteolytic complexes, termed AAA proteases, are responsible for the quality control in the inner membrane and the selective degradation of non-assembled and damaged proteins (Koppen M and Langer T, 2007). The observation, that there is a higher supercomplex abundance points towards a decreased activity of these enzymes. The mitochondrial inner membrane is a prime target of mitochondrial ROS as it harbours the respiratory chain. Loss of the m-AAA isoform of the protease results in an increased sensitivity towards oxidative stress and complex I deficiency (Atorino L et al., 2003). There is evidence that m-AAA proteases act not exclusively as surveillant for quality control but additional as protector of the respiratory chain by mediating the maturation of the ROS scavenger cytochrome c peroxidase (Ccp1) in the intermembrane space (Esser K et al., 2002). If the AAA-protease is not fully active an increased oxidative stress level within the mitochondria isolated from old heart tissue could be a possible consequence. However, there were no indications that this was more pronounced in heterozygous Tom40 mice than in controls, pointing towards a mere effect of aging.

Evaluating the specific OXPHOS enzyme activities in heart tissue of young and aged mice of both sexes revealed no differences at all. Neither genotype nor age seemed to have an influence on the results, although an aging effect had been expected. For analysis, enriched mitochondria isolated from whole hearts were used. Most studies describing the age-dependent reduction of respiratory chain complex activity in the heart divided heart mitochondria into two fractions: Faninn et al. differentiated between subsarcolemmal mitochondria (SSM) that reside beneath the plasma membrane or interfibrillar mitochondria (IFM) located between the myofibrils (Fannin SW et al., 1999). COX activity was significantly reduced in heart IFM of old rats but not in SSM, indicating that only IFM are sensitive for aging-induced alterations. This might be due to of a selective loss of the antioxidant capacity with aging, resulting in a higher level of oxidative stress (Suh JH et al., 2003). Lesnefsky et al. showed the same for complex III and additional they were able to localize the aging defect at the cytochrome c binding site (Lesnefsky EJ et al., 2001). Based on these studies whole

heart lysates with a mixture of both cardiac mitochondria types are not adequate for examining age-dependent differences due to the fact that the mixture contains affected and unaffected mitochondria which could cause a high variance and thereby a loss of the aging phenotype. Another possibility could be that the samples were not sufficiently age matched. Castulluccio et al monitored mitochondrial enzymes over the whole life span in group of rats (Castelluccio C et al., 1994). They could demonstrate that NADH cytochrome c reductase (combined measurement of complex I and III) and cytochrome oxidase (complex IV) activities increase up to an age of 1year followed by a slow decrease until the 18-26month. Succinate - cytochrome c reductase (complex II + III) activity steadily increases from 1-26 month, although absolute values remain quite low. However, measuring these enzyme activities in our animals revealed no effect of aging. Animals from the young cohort were around 160 days old while aged animals died when they were ~700 days old. As the peak activity was found to be around 12 month life time it is possible that the tested animals from the young cohort were just too young. Last but not least it is just possible, that the detected age-dependent increase in respirasome amount resulted in a compensation of the ageing induced decline in the investigated Tom40 hearts. Mitochondrial function was not only studied looking at the enzyme activity but additionally by observing the oxygen consumption of fresh isolated heart mitochondria following a substrate-inhibitor titration protocol developed for the Oroboros Oxygraph.

In respirometry a general age-dependent reduction of oxygen consumption was observed and additional a strong genotype-associated effect indicating that aged mutant mitochondria perform much worse than aged wildtypes. There were no differences in young animals visible. The results of respirometry reflect what has been found in nearly all studies performed with the Tom40 mouse model: there were only subtle phenotypes in young mutants but considerable phenotypes in aged mutant animals. The impairment of mitochondrial function in aged mutants is not restricted to a single enzyme but affects all complexes. In contrast to enzyme activity results, an age-dependent activity reduction concerning complex IV but not complex II-III could be observed. While in the enzymatic assays the maximum capacity of the RCC enzymes was assessed, respirometric assays yield information on the capacities of whole metabolic pathways in intact mitochondria rather than of individual enzymes, thus providing insight into pathological effects on integrated

mitochondrial function (Gnaiger E, 2008). It is well established that various OXPHOS defects can be identified by oxygen consumption studies in fresh sample preparations but not by the more focused enzymatic analysis, the measurement of mitochondrial membrane potential, or electron microscopic analyses of mitochondrial structure (Puchowicz MA et al., 2004). The results of BNE, where no quantitative difference of the OXPHOS complexes could be detected, support the absence of enzyme activity reduction. In *Tom40* heterozygous animals mitochondria are smaller than in wildtypes and appear condensated. The structural alterations in mutant mitochondria could impair the access or availability for substrates. To get information about all proteins located in the mitochondria a detailed analysis of the mitochondrial proteome would be necessary.

Moreover, heart mitochondria of young animals were investigated concerning their uncoupling ability. There were no obvious differences visible between the genotypes.
In the absence of artificial uncoupling agents, uncoupling results from protons leaking back into the mitochondrial matrix, a process that dissipates the proton motive force and reduces the number of protons flowing through the ATP synthase (Krauss S et al., 2005). Uncoupling has been suggested to be involved in thermogenesis. *UCP1* is exclusively expressed in brown fat (BAT), where it plays a key role in facultative thermogenesis in rodents (Argyropoulos G and Harper ME, 2002): activated UCP1 catalyzes a proton leak across the mitochondrial inner membrane leading to thermogenesis. In the last years it has become evident that uncoupling is not exclusively restricted to thermogenesis. Meanwhile there are 5 UCP genes known and investigated (Ježek P and Urbánková E, 2000). *UCP2* is expressed in various tissues, including the nervous system (Fleury C et al., 1997); *UCP3* is expressed only in skeletal and cardiac muscle (Boss O et al., 1997); *UCP4* and *UCP5* (originally described as *BMCP1*) have also been identified and shown to be highly expressed in the CNS.
Due to the so-called respiratory control, uncoupling usually leads to acceleration of respiration, since in many tissues and cell types the capacity of respiratory chain overcomes the capacity of ATP-synthase and other processes consuming the H^+ gradient. This effect could be seen in all investigated heart mitochondria lysates treated with artificial uncoupling agents. However, the maximum oxygen flow did not differ between *Tom40* mutants and wildtypes. Due to the influence on ROS

production, UCP2 and 3 have been proposed to be involved in longevity (Speakman JR et al., 2004). *Tom40* heterozygous mice showed a reduced life-span. It is yet not clear if a defective uncoupling in aging mice accounts to this phenotype but it is at least a possibility. Because the respirometric investigation is in need of fresh tissue and old animals are very rare this could not be tested to date.

To check the animals' ability to switch to thermogenesis, an acute cold challenge was performed. The acute cold challenge revealed only small differences between young *Tom40* mutant and control mice. At thermoneutrality and in the cold, the span in oxygen consumption was decreased in mutants and we found a trend towards increased oxygen consumption and body temperature in male mutants when exposed to low ambient temperature. In males and females no major differences in metabolic rate at thermoneutrality could be detected. The increase in oxygen consumption as immediate response to the cold challenge did not differ between genotypes. Cold exposure of five hours had no obvious genotype related effect on oxygen consumption in females. Male mutants showed increased body temperature and oxygen consumption in the final phase of the measurement. These findings do not contradict results of a pilot study with different design that was conducted after the GMC primary screen. In the pilot mice were exposed to a combination of food deprivation and moderately low ambient temperature. Even though only two male control and mutant mice were tested mutants showed a steeper and more rapid increase in oxygen consumption in response to the temperature drop. The results found in the challenge support the hypothesis that young animals may have some restriction that they are able to compensate. However, the phenotypes are too subtle to exclude that they are not a finding by chance. Maybe evaluating aged animals could give more information about uncoupling, thermogenesis and metabolic issues.

Reduced mitochondrial activity could prove detrimental to tissues that have a high energy demand, such as the brain and it is known that in several neurological disorders mitochondrial dysfunctions are involved (Baron M et al., 2007; Mattson MP et al., 2008; Zeviani M and Carelli V, 2007)

During the GMC primary screen animals also passed the behavioural module. It could be shown that the Tom40 mutation did not produce any significant effects on open field behaviour. In this mildly stressful environment, locomotor activity,

exploratory and anxiety-related behaviours are normal. No change in locomotor activity is consistent with the initial neurological tests that were carried out. The Tom40 mutation did, however, produce a clear increase in prepulse inhibition responses in the female's at all prepulse intensities. A similar pattern was observed in the male mutants but this only reached significance at the 73 dB intensity. Alterations in PPI show a change in sensorimotor integration, hence alterations in brain function, which could be due to transformations in several neurochemical systems (Geyer MA et al., 2001). PPI is largely regulated by neuronal connections between the limbic cortex (including the hippocampus and amygdala), ventral striatum, ventral palladium as well as the pontine tegmentum (Geyer MA and Dulawa SC, 2003; Swerdlow NR et al., 1994). As mitochondria are found in all bodily tissues, mitochondrial dysfunction could manifest anywhere including these brain regions. According to the Allen Brain Atlas however, detectable Tom40 expression levels (presumably indicative of a higher density level) have been found in the cerebellum, olfactory bulbs and the medulla (http://mouse.brain-map.org/brain/Tomm40.html?ispopup=1). These are not areas generally associated with prepulse inhibition responses and so irregularities within these more Tom40 dense regions does not aid in explaining the current observation. The increased prepulse inhibition is also not due to a higher sensitivity to auditory signals, since mutants even show a non-significant decrease in acoustic startle reactivity.

Administration of the mitochondrial toxin, 3-nitropropionic acid, is used to generate a mouse model of Huntington's disease (Kodsi MH and Swerdlow NR, 1997). The resulting mitochondrial dysfunction in rats is associated with decreased prepulse inhibition. It is thus surprising that, the opposite, increased PPI was observed. In healthy humans, elevated PPI reflects enhanced pre-attentive perceptual processing and is associated with improved performance in upstream cognitive functions (measured by 5-choice reaction time tests, problem solving tasks, and a test of spatial working memory (Bitsios P et al., 2006). This is exemplified by enhanced strategy formation and execution times, possibly due to more efficient early information processing. As problem solving is determined by the integrity of the frontal lobe, it could be that increased PPI signifies more effective prefrontal lobe function.

Alterations in acoustic startle and PPI are associated with schizophrenia as it has been proven that schizophrenic individuals show a deficit concerning the PPI

response (Baker N et al., 1987). PPI measures sensorimotor gating which has been shown to be modulated by dopaminergic neurotransmission mainly by the mesostriatal dopaminergic system (Zhang J et al., 2000). Decrease of PPI could be induced by drugs like the dopamine receptor 2 (D”2) -like agonist quinelorane in rats (Ralph RJ and Caine SB, 2005). Dopaminergic antagonists with selectivity for the schizophrenia associated D4 receptor have been shown to have the opposite effect (Mansbach RS et al., 1998). An antagonist blocks the receptor, thereby inhibiting a cellular answer. Considering this it is at least a possibility that the monitored increase in the PPI reaction in *Tom40* heterozygous mice is associated with the alterations found in the dopaminergic system of the animals. This even gets more plausible considering the fact that dopamine levels in schizophrenic patients were elevated (Ashby B, 1990; Stefansson H et al., 2009; Toda M and Abi-Dargham A, 2007). Animals tested in PPI were quite young and the dopaminergic system of young animals was not studied in detail to date but it is feasible that there is already a dopamine deficit in young animals. Results from neurological screening pointed towards a slowly progressing movement disorder in mutant animals. However, altered PPI reaction has not been described in association with motor diseases so far. For instance, in contrast to the *Tom40* mice, in a MPTP induced mouse model of PD no differences were found in PPI reaction (Leng A et al., 2004). The same was true for PARKIN null mutants, which had a significant altered acoustic startle response but no PPI phenotype (Von Coelln R et al., 2004).

Moreover, mitochondrial dysfunction is an early marker of Late Onset Alzheimer’s Disease (LOAD) pathogenesis and associated with neuronal cell death (Atamna H and Frey WH, 2007). *Tom40* is a candidate gene for mitochondrial dysfunction in LOAD. While there is a dearth of information on the prepulse inhibition status of LOAD patients, those patients with standard Alzheimer’s disease (AD) perform normally in this test (Hejl AM et al., 2004). This is despite the fact that the hippocampus and entorhinal cortex is malfunctioning and also involved in prepulse inhibition responses. PPI tends to be altered in psychiatric diseases where there are abnormalities in the glutamergic, dopaminergic and serotonergic systems; AD is largely associated with abnormalities within the cholinergic system (Hejl AM et al., 2004).

Thus changes in cognitive function, for example, those of learning and memory were tested in a second batch of mice. The animals were first tested with an age of three months, what resembles the age of the primary behavioural screen. It was also aimed on a replication of the GMC prepulse inhibition finding in this second batch of animals. PPI results were similar although less pronounced as in the primary screen (data not shown). Determining the influences of age on this measurement was not possible due to the already discussed severe sensorineural hearing loss of the C57BL/6 strain at an early age. Animals' cognitive abilities were tested using the social discrimination task and the object recognition task. The social discrimination test is commonly used to assess the declarative memory in laboratory animals based on the use of olfactory signals for social communication in rodents (Engelmann M et al., 2011). The test relies on the feature of rodents to prefer novel conspecifics rather then familiar ones. Object recognition is very similar to social recognition but without the social component. In young animals no obvious abnormalities could be detected (data not shown). AD is a progressing disease with an age of onset in the second half of life. Therefore, animals were tested again with an age of around two years. It has to be mentioned that both genotypes were very unwilling to move at all and so the exploration times were very low. There was a slight tendency stating that mutant animals performed worse in social discrimination. The investigation time of the novel conspecific for example did not differ at all from the time spent with the familiar animals in female mutants. However, all found differences were too small to consider them as relevant findings. The malfunction of brain mitochondria revealed by respirometry had no significant influence on learning and memory abilities and the underlying structures. In mitochondria isolated from brains of aged *Tom40* mutant mice a reduced oxygen flow was observed for all measured complexes. In post-mortem brains of AD patients a decreased complex IV activity has been reported, while the other RCC remained widely unaffected (Chagnon P et al., 1995; Kish SJ et al., 1992; Maurer I et al., 2000; Mutisya EM et al., 1994). Complex IV inhibition is mediated by the neurotoxic Aβ which likewise opens the mitochondrial transition pore (Parks JK et al., 2001). Brains of AD patients are under massive oxidative stress and it has become clear that Aβ-induced oxidative stress is involved in the pathophysiology of AD (Butterfield DA and Boyd-Kimball D, 2005; Moreira PI et al., 2005; Parks JK et al., 2001) such as the Aβ-induced disruption of mitochondrial integrity through opening of the mitochondrial transition pores being able to initiate

cell death cascades (Parks JK et al., 2001). Taken together, there was no evidence for an AD phenotype in the aged animals.

The aging cohort was not solely bred and kept for two years to perform memory tasks but also for investigating the influence of aging on the genetically predisposed mutant mice in general, although young animals did not suffer from apparent phenotypes. Mitochondrial dysfunction is significantly involved in the development of neurodegenerative diseases, since nerve cells have an extremely high energy demand (Shulman RG et al., 2004). Visual impairment is a common symptom in a variety of neurodegenerative diseases, e.g. PD, where patients also suffer from a variety of non-motor symptoms like retinopathy (Bodis-Wollner I, 2009) or AD where patients show an increase of retinal nerve fiber layer (RNFL) thickness and a decrease of macular volume (Iseri PK et al., 2006). Iseri et al. were also able to show that the macular volume relates to the severity of cognitive impairment. Mitochondrial diseases itself are often accompanied by visual defects, too. For instance in LHON patients a fiber loss in the peripapillary RNFL was observed (Barboni P et al., 2010). The aged *Tom40* mutants with distorted mitochondria and altered mitochondrial function were therefore an ideal target for further studies concerning their vision and also concerning the function of their nerves. OCT is a non-invasive technique that allows imaging of the RNFL as model for neurodegeneration (Galetta KM et al., 2011). There were no indications for abnormal vision in aged mutants. The RCC inhibition induced by the *Tom40* mutation appears to be insufficient to set great damage to the visual system.

Anyhow, measuring the conduction velocity of the sciatic nerve in both young and aged animals uncovered a conspicuous NCV reduction in mutant animals and an effect of age. Reduced NCV in elderly have been reported by various studies (LaFratta CW and Canestrari R, 1966; LaFratta CW and Zalis A, 1973; Mayer RF, 1963; Norris AH et al., 1953; Rivner MH et al., 2001; Wagman IH and Lesse H, 1952). In humans a loss of nerve fibers including their cell bodies plus structural changes in the nerve system were detected long ago as a consequence of aging (Corbin KB and ED, 1937; Cottrell L, 1940; Redex B, 1944). The sciatic nerve that was analyzed in the Tom40 cohort belongs to the peripheral nerve system (PNS), and quite a lot is known about functionally, structurally and biochemically changes

during life time. It has been demonstrated for many species, including humans (Rabben OK, 1995) and mice (Verdú E et al., 1996) that the motoric and sensoric NCV tends to increase until young adulthood, arguing for a long postnatal maturation period, and then stays stable until the last third of life. In mice, NCV started to decline after 12month as indicated by increasing latencies (Verdú E et al., 1996). Degeneration starts with a mild decrease in number and the density of myelinated and unmyelinated nerve fibers, and an increase in present outfolded myelin loops (Ceballos D et al., 1999). Later the investigated nerves showed a general disorganization and a marked fiber loss, plus alterations in the myelinated nerve fiber morphology, including decreased size, circularity and myelin thickness (Ceballos D et al., 1999). There is hardly any information about normal NCV values of mice to be found in literature, but it seems that the values measured in adult Tom40 wildtype mice lie in the normal range one could expect of one year old mice (personal communication with Prof. Kaspar Matiasek and Dr. Jéssica Molín from the Chair of Veterinary Medicine, LMU, Munich). The values of the two years old mice were significantly reduced, reflecting the described aging induced degeneration. In mutant mice, NCV was already relatively low in adult mice; values resembled those of aged wildtypes. Aged mutant mice showed even lower values. The NCV test is commonly used as diagnostic tool to detect nerve injury. Cause for altered NCV values can either be a nerve disorder like peripheral neuropathy (Pascuzzi RM, 2009) or conditions whereby nerves are injured by mechanical compression such as the carpal tunnel syndrome (Bleecker ML et al., 1985; Stevens JC et al., 1999). Peripheral neuropathy means damage to nerves of the peripheral nervous system (PNS) and can be elicited by various reasons like genetic factors, tumours, toxins, autoimmune responses, nutritional deficiencies, alcoholism, and vascular and metabolic disorders (Martyn CN and Hughes RA, 1997). Several neurodegenerative and metabolic diseases are accompanied by peripheral neuropathy, for instance type I diabetes or AD (Jolivalt CG et al., 2012). Mitochondria have also been implicated in the pathogenesis of peripheral neuropathy. There is clear evidence of the emerging role of altered mitochondrial dynamics in peripheral nerve diseases (Baloh RH, 2008). Peripheral neurons possess very long axons for what reason axonal transport of cytoskeletal components, vesicles, and organelles is of high importance for maintenance and development of the neurons (Grafstein B, 1969; Schwartz JH, 1979). As nerves belong to the most energy consuming tissues, mitochondria have to

be transported along the axon to provide enough ATP to maintain the ionic gradients necessary for firing action potentials (Hollenbeck PJ and Saxton WM, 2005). Mitochondria are delivered to areas of the axon where metabolic demand is high, such as synapses (Bogan N and Cabot JB, 1991; Gotow T et al., 1991; Palay SL, 1956), active growth cones and branches (Morris RL and Hollenbeck PJ, 1993; Povlishock JT, 1976; Ruthel G and Hollenbeck PJ, 2003), axonal protein synthesis (Martin R et al., 1998) and regions of demyelination were it has been shown that they accumulate (Mutsaers SE and Carroll WM, 1998). The long-distance transport of mitochondria mainly proceeds via the ATP-dependent motor-proteins kinesin and dynein (Hollenbeck PJ, 1996). In the *Tom40* +/- mice there is an apparent mitochondrial dysfunction, supposedly resulting in a subtle energy deficit. It could be speculated if the axonal transport of mitochondria is impaired in Tom40 mutant mice and the cause for the reduced nerve conduction velocities in the sciatic nerve.
A second explanation for the neuropathy in Tom40 mutants could maybe be found in mitochondrial dynamics itself. It has been suggested for mitochondrial dynamics that mitochondrial movement and fusion/fission are not completely independent from each other (Baloh RH, 2008). A decrease in mitochondrial movement would alter the balance of mitochondrial dynamics toward fission, because for fusion active movement is required while fission just requires Drp1 (Smirnova E et al., 2001a). It has been shown that a defined balance between fusion and fission processes is necessary to maintain mitochondrial function, dysregulated fusion/fission results in neurodegenerative diseases like the inherited Charcot-Marie-Tooth, which is diagnosed by reduced NCV values and nerve biopsy (Züchner S et al., 2004).

The electrophysiological phenotype was among the few alterations already found in young animals. Monitoring the life span of *Tom40* mutant mice revealed a higher mortality in mutants when they were older than 12 month. Several neurodegenerative diseases like AD or PD have progressing phenotype. This was also found in the neurological examination of the *Tom40* heterozygous and wildtype mice. In young animals tested with GMC primary screening methods there were no obvious phenotypes detectable. Additional to the primary screening methods, a test battery of various neurological and motor tasks was performed to get a deeper insight in the mutant mice. Evaluating the mice again when aged revealed strong motor impairments in mutant mice. Additional to the primary screening methods Rotarod

and grip strength, the used test battery consisted of pole test, beam walk, ladder walk, running wheels, and endurance Rotarod. The pole test was developed by Matsuura et al. (1997) to check for bradykinesia (slowed ability to start and continue movements, impairment in body position adjustment). In young animals, there were no genotype-specific differences. Repeating the experiment with aged mice revealed also no significant difference. Pole performance is strongly associated with body weight; heavier animals in general have problems to turn around in this test. Some aged mice of both genotypes showed a quite high body weight, especially within the males, and with this attended an inability to perform correctly on the test apparatus.

The running wheels task was used to assess voluntary running in female mice. There were no differences between mutants and wildtypes for all evaluated parameters as long as the wheels were not restricted. There was a marked training effect, all animals got faster, more persistent and improved their daily running distance. Beyond, all the other evaluated parameters were improved as well: mice got faster and more sustained within the first two weeks. It has been shown for mice that voluntary wheel running results in cardiac hypertrophy, increased skeletal muscle oxidative capacity and changes in muscle consistent with endurance exercise adaption (Allen DL et al., 2001; Houle-Leroy P et al., 2000; Kaplan ML et al., 1994; Vihko V et al., 1979). The training phase proofed that it is still possible to train mutant animals. They show a comparable performance improvement like control mice in answer to the daily running. The situation changed when additional exercise was added by restriction of the wheels. This was achieved using an integrated eddy current brake at two different intensities. While both genotypes showed impairment (reduced total distance, lowered maximum speed, lower maximum and average run duration) when higher brake intensity was used, only the mutants had real problems with the moderate one. The total distance they covered was not significantly changed after restriction, but the maximum and the average run length were significantly affected. While maximal run duration was significantly lowered in both genotypes, more pronounced in mutants, the average run duration only was significant affected in mutant mice. Looking at the speed revealed that maximal speed was not affected by restriction neither in wildtype nor in control mice, only the average speed was lower in mutants. So the endurance phenotype in the mutants was only observed

after workload augmentation; at higher resistance, more energy is needed to run the wheel.

Monitoring the running wheel activity over a long distance also provided information of the circadian rhythm of the mice. Mice are nocturnal animals, and their activity peaks within the first hour of the dark phase. Changes in activity cycle were clearly manifested in a number of transgenic models of disease, such as the R6/2 mouse strain that carries a mutation which is causative for Huntington's disease (Morton AJ et al., 2005). The altered circadian rhythm is reflected in the flattening and progressive disruption of the 24 h activity cycle. In *Tom40* heterozygous mice there is no hint on a disturbance of the light-dark activity rhythm suggesting that a mutation in the *Tom40* gene and the resulting mitochondrial dysfunction has no influence on involved structures like the suprachiasmatic nuclei (SCN), a pair of distinct groups of cells located in the hypothalamus, whose destruction results in the complete absence of a regular sleep–wake rhythm (Hastings MH et al., 2008). Mini Spec analysis, which was done once weekly in the running wheel cohort, detected no obvious differences in body weight, lean and fat mass distribution. Body weight decreased due to a fat mass reduction, especially in the beginning, undermining the training effect and stayed constant afterwards. There were no hints that mutants are in need of using other energy sources than wildtypes or that their metabolism differs strongly from control mice.

In the Tom40 mouse model there was a very subtle motor phenotype in young animals which was slowly progressing with age. Both tests used to analyze the mice, beam walk and Rotarod, are frequently used to assess motor coordination and balance in mouse models for motor diseases (Carter RJ et al., 2001; Fleming SM and Chesselet MF, 2006; Fleming SM et al., 2005; Stanley JL et al., 2005). Aged mutants showed impaired performance in both tasks, with more foot slips while walking over the beam and they had a shorter latency to fall of the rotating rod in the Rotarod task. Interestingly, animals were evaluated just after the females had finished the running wheel study and the phenotype found was more pronounced in male mice. Supposedly the endurance exercise previous to the motor test battery improved the females' motor abilities. In literature, there were numerous studies describing also clear positive effects of training on the motor system, for instance visible adaptions in α-motoneurons like evidence of dendrite restructuring, increased protein synthesis,

increased axon transport of proteins or enhanced neuromuscular transmission dynamics (Gardiner P et al., 2006). In a chronic mouse model of PD which was induced by treating the animals with MPTD it could be shown that training has a neuroprotective effect (Lau YS et al., 2011). After 18 weeks of treadmill exercise the MPTP mice showed reduced impairment in balance and movement coordination and reduced mitochondrial dysfunction. Additional, they were protected against the protein oxidation induced by the applied neurotoxin and the dopaminergic neuron loss previously observed in the striatum.

The observation of a general age-dependant motor worsening also in wildtypes is a common feature of aging, observable in humans as well as in mice (Fahlström A et al., 2011; Kauranen K and Vanharanta H, 1996). Evaluating the young Tom40 cohort revealed no impairments in mutant mice on the Rotarod but a worse performance on the beam walk. It has been proven in drug studies that beam walk is more sensitive than the Rotarod to determine motor coordination defects induced by benzodiazepines (Stanley JL et al., 2005). Probably the motor impairments that are causative for the observed phenotype with more foot slips observed in Tom40 heterozygous mice were only very subtle in young animals. A typical feature for neurodegenerative diseases is that they are progressing with age, a phenotype which was also observed in animal models (Price DL et al., 1998). The progressing motor phenotype in Tom40 mice is in line with the other results found as for example decreasing NCV and decreasing mitochondrial function. The motor phenotype found in the Tom40 mouse model resembles one of the main symptoms found in PD animal models. An increased number of footslips was approved in a mouse model for Parkinson's' disease (PD) in which the alpha-synuclein protein was mutated at position 30 (alanine was replaced with proline; SNCA A30P) and thereby mimicking a familial form of PD in humans (Plaas M et al., 2008). In the study, beam walk and stride length analysis was used to check for nigrostratial function. A significant increase in foot slip number with increasing age was found in mutant SNCA A30P animals, but they could not detect a Rotarod phenotype. In addition, mutant SNCA A30P mice had altered dopamine levels in the different brain regions. The nigrostriatial pathway resembles one of the four major dopaminergic pathways in the brain. It transmits dopamine from the substantia nigra to the striatum (Dahlstrom A and Fuxe K, 1965; Gerfen CR, 1992; Poirier LJ and Sourkes TL, 1964; Sourkes TL and Poirier LJ, 1965). Due to he progressive motor phenotype in the Tom40 mouse

model, the dopaminergic system of aged animals was investigated. It could be shown that the number of TH-positive neurons was reduced in mutant animals. Due to the small sample size results could not reach a significant level. At the moment a second batch of aged mice is investigated to verify these preliminary findings. In addition, investigating the dopaminergic system of young animals could also prove useful.

The motor phenotype found in the Tom40 mouse model was further evaluated using ladder walk which was developed to investigate skilled fore- and hind-limb stepping in mice. In contrast to beam walk, this test assess skilled walking and measure both forelimb and hind limb placing, stepping, and inter-limb co-ordination as it is sensitive to detect specific ipsilateral and contralateral lesions (Cummings BJ et al., 2007; Metz GA and Whishaw IQ, 2002). Ladder beam is frequently used to assess forelimb and hind limb deficits after sensorimotor cortex injury in rats (Farr TD et al., 2006; Soblosky JS et al., 1997). The results of the examination of the Tom40 cohort on the ladder were the same like on the beam: mutant animals showed significantly more foot slippings traversing the ladder than their wildtype littermates, more pronounced in aged animals. There was no difference between forepaws and hind paws, demonstrating that the found phenotype is a generalized motor problem. The gait of the animals was assessed when they where mature and aged on a running belt where animals are forced to run on the belt with different speeds. In adult animals there were no clear defects concerning any gait parameter, suggesting that the animals were able to walk normal. From the aged cohort only a couple of females were available for gait analysis. There were some parameters altered in aged mutants but there was no clear picture and interpretation is not possible. The animals were not willing or able to walk at higher speeds and the variations within the groups were quite high. This was true for both genotypes. Therefore no final conclusion about the gait could be drawn from the obtained data, but it is noteworthy that there are no severe gait impairments. The loss of motor control in patients is strongly correlated with the loss of dopaminergic neurons. The reduction in dopamniergic neurons detected in the brain of aged mice was at least in this first batch not big enough to reach significance. In humans it has been proven that approximately 60-80% of dopaminergic neurons have to be lost before the motor signs of Parkinson disease emerge (Binukumar BK et al., 2010; Lee CS et al., 1996).

Dopaminergic neurons have a reduced antioxidant capacity, demonstrated by low intracellular glutathione (Loeffler DA et al., 1994). This makes them more vulnerable

to oxidative stress. Plus dopaminergic neurons have been shown to be more vulnerable to energy metabolism defects (Zeevalk GD et al., 1997). An impairment of Na^+/K^+ ATPase activity which maintains ionic gradients has been proven to be especially harmful (Calabresi P et al., 1995; Pisani A et al., 2006). Both is possible, a slight increased oxidative stress level in *Tom40* mutants which was, however, not detectable measuring just aconitase activity as it was done in line with the challenge experiments, or a slight impairment of energy metabolism, not detectable in the respiratory measurements in young animals, but progressing damaging the dopaminergic neurons.

The exact mechanisms that are responsible for neural cell death in PD are poorly understood. As possible primary cause mitochondrial dysfunction specifically respiratory chain inhibition has been implicated (Keeney PM et al., 2006; Kitada T et al., 1998; Mizuno Y et al., 1989; Schapira AH et al., 1990). Complex I deficiency in PD patients was the first finding that linked mitochondrial dysfunction to the disorder (Schapira AH et al., 1990). This was found globally in the body (Bindoff LA et al., 1991; Haas RH et al., 1995; Parker WD Jr et al., 2008). Enzymatic assessment of the NADH dehydrogenase activity in mitochondria isolated from the brain of aged Tom40 mice and age matched controls showed that complex I activity in mutant brain mitochondria was slightly reduced compared to wildtypes. However, the results were neither statistically significant before nor after CS normalization. CS activity as a marker for mitochondrial activity itself was not altered. Increasing evidence suggest that it is not only complex I that is affected in PD but also complex III, which goes in line with increased ROS formation (Haas RH et al., 1995; Rana M et al., 2000; Shinde S and Pasupathy K, 2006). Complex I and complex III are the most potent sources for oxidative stress (Turrens JF and Boveris A, 1980). Beyond, complex III is required to maintain complex I in mammalian mitochondria (Acín-Pérez R et al., 2004). Inhibition of this complexes causes increased release of electrons from the transport chain into the mitochondrial matrix and form ROS together with the there located oxygen. The electron leakage is a consequence of an impaired electron movement to the next acceptor molecule (Lambert AJ and Brand MD, 2004). ROS in turn is, as generally known, one of the discussed mechanisms to be responsible for dopaminergic neuron loss.

To date, the brains of Tom40 mice were not checked for increased oxidative stress. In the brain samples cytochrome c oxidase activity was assumed in a second step

and the activity was slightly increased in mutant mice, even though this was only significant without CS normalization. Increased COX activity was previously reported in skeletal muscle of patients with Chronic Obstructive Pulmonary Disease (COPD) and in other chronic inflammatory diseases (such as bronchial asthma and chronic arthritis), the mechanisms and implications of this observation are still unclear (Sauleda J et al., 2000). To check whether the COX increase in Tom40 mice is a compensatory effect, it would be interesting to investigate the composition of the respiratory chain in aged brain tissue mitochondria.

Concerning sporadic PD there were reports about patients with complex IV defects or combinations of all complexes (Barroso N et al., 1993). It occurs that the common feature in all patients was the mitochondrial impairment which can be a result of a variety of defects. Aged *Tom40* mutant mice don't show a specific deficiency of a single complex in respirometry but a generalized inhibition of the respiratory chain.

For a familial form of PD, which has been associated with a mutation in the alpha synuclein gene, an association between α-synuclein and mitochondrial dysfunction has been proposed (Greene JG and Greenamyre JT, 1996; Hsu LJ et al., 2000). It was reported that mutant (A53T) alpha synuclein over expressing transgenic mice developed mitochondrial degeneration as well as reduced complex IV activity (Martin LJ et al., 2006). They did not check for the other complexes, but it has been shown by various studies that overexpression is associated with complex I inhibition (Loeb V et al., 2010). Mutant α-synuclein is targeted to and accumulates in the inner mitochondrial membrane, causes complex I impairment and, again, an increase in ROS (Devi L et al., 2008).

Another symptom frequently observed in PD patients is the loss of foveal contrast sensitivity to patterns. ERG is used to determine the functional deficit of the neural retina and retinal output of PD patients. A lack of ganglion cell receptive field organization seems to be present within the dopamine-deficient retina. OCT can be used to quantify morphology changes, like RNFL thinning what is often but not always observed in PD patients (Bodis-Wollner I, 2009; Galetta KM et al., 2011). However, as already described in 1 ½ years old *Tom40* mutant mice there was no hint of a retinopathy in the tested animals.

Taken together, there are various different mechanisms by which mitochondrial function can be impaired in a way that has the potential to cause neurodegeneration

and PD symptoms. *Tom40* might be one additional risk factor, which contributes to the mitochondrial dysfunction inducing neurodegeneration.

Since oxidative stress has such tremendous influence on neurodegeneration a challenge study for endogenous induced oxidative stress with Tom40 mice was planned. The aim was to set an additional damage using the herbicide Paraquat to the already biased heterozygous *Tom40* mutants. Paraquat treatment led to Isignificant reduction of liver aconitase activity. Aconitase is an enzyme of the TCA cycle which has been demonstrated to be vulnerable towards oxidative stress (Castro L et al., 1994; Hausladen A and Fridovich I, 1994; Murakami K and Yoshino M, 1997). The catalytically active form of this enzyme contains a $[Fe_4S_4]^{2+}$ cluster, of which three iron ions are directly ligated to the cystein residues of the protein, and the fourth is only ligated to inorganic sulfur of the iron-sulfur cluster thereby presenting a free coordination site to bind substrates (Emptage MH et al., 1983; Robbins AH and Stout CD, 1989a, b). Oxidants inactivate the enzyme by removing the labile iron from the cluster, leaving the inactive form $[Fe_3S_4]^{1+}$ (Kennedy MC et al., 1983; Verniquet F et al., 1991). Decreased aconitase activity was reported for a variety of diseases, including progressive supranuclear palsy (Park LC et al., 2001), a degenerative disease involving the brain stem, basal ganglia and cerebellum (Steele JC et al., 1964), Huntington's disease (Tabrizi SJ et al., 1999), and Friedreich's ataxia (Bradley JL et al., 2000), of which all bear relation to mitochondrial dysfunction and oxidative stress.

It has been shown that Paraquat is capable to induce PD-like symptoms in experimental animals (Betarbet R et al., 2000). The concurrent aconitase inactivation was achieved by superoxide and hydroxyl radical formation when oxygen reacts with paraquat (Murakami K and Yoshino M, 1997). This was of special interest for the Tom40 challenge study because of the phenotype in aged animals. Aging studies with a huge cohort of mice is an expensive and capacity consuming, so challenging was a trial to get a phenotype triggered already in young mice. However,the examination of the challenged mice after an eight weeks treatment period revealed only very subtle differences between the groups. Body weight was significantly reduced, which is a known phenotype in PQ challenged mice (Kang MJ et al., 2010; Prasad K et al., 2009) and most findings in the treated Tom40 mice correlated with this body weight reduction. Decreased body weight is an indication for a general toxic

effect and has previously been associated with decreased water intake and food consumption of the treated animals (Prasad K et al., 2009). Body composition of all groups was investigated and could not show treatment or genotype related differences after challenge. Paraquat was used as herbizide in agriculture for quite a long time until it was prohibited in the the European union because of its deleterious toxic effects (Revkin AC (1983); Court of First Instance of the European Communities PRESS RELEASE No° 45/07). In studies with toxified human workers, several symptoms were reported including muscle weakness (Yan AS et al., 2002).

Evaluating grip strength revealed a small but statistically significant effect in treated animals exerting more force in the four paws measurement. However, differences found were very small and might also be a finding by chance.

In literature, much more attention is paid on the influence of PQ on processes involving motor coordination and movement than on PQ related grip force or muscle alterations. The Tom40 challenge cohort was analyzed in several different motor tests before and after the challenge. The deficits seen on beam and ladder after challenge were already apparent before the first PQ injection. This is in accordance with the previous results gained from another cohort of Tom40 mice: mutants have motor deficits, very subtle but present already at a very young age. PQ treated mutants, however, performed not worse than saline treated mutants, suggesting that there was no additional influence on the motor system of the mice. This was also true for the rotarod task. There was no difference in performance between the individual groups before the challenge and there was no influence, neither of treatment nor of genotype, after the challenge. Longterm rotarod, used to get information about the animals endurance, was hard to evaluate since there were differences between the groups already before the challenge and these differences were most likely caused by grouping the animals to the individual cohorts. Taken together, PQ challenge of Tom40 mice had no influence on the motor performance of the mice, arguing that there was only minor damage to critically involved structures like the dopaminergic system. A study using wildtype C57BL/6 mice could show after treatment that the dopaminergic system was significantly impaired, but only if the PQ was combined with a treatment of maneb (Thiruchelvam M et al., 2000). The same was true for motor phenotypes. In contrast, there are various other studies using the same mouse strain that could verify that there was loss of TH-positive neurons solely induced by PQ administration (Brooks AI et al., 1999; Kang MJ et al., 2010; Richardson JR et al.,

2005). Difference between mouse strains were described to have different susceptibility to PQ with DBA/2J showing significant tyrosine hydroxylase negative cell loss and not C57BL/6J (but both showed TH positive neuron loss with B6 more than D2) (but both showed TH positive neuron loss with B6 more than D2) (Yin et al., 2011). A study performed with rats revealed that the administration of PQ alone was competent to induce neuronal loss but not to destroy the striatal fibers (Cicchetti F et al., 2005). To sum up, the findings of the various studies are not consistent. In addition, there might be additional influences on the outcome of the different studies such as animal housing and feeding.

The reduced aconitase activity measured in liver lysates of the treated animals demonstrated that there was enhanced oxidative stress in these mice. However, the activity of the enzyme was measured exclusively in the liver. Thus it is not possible to say if there was oxidative stress in the brain with the potential to damage TH-positive neurons.

Tom40 mutants are able to cope with the oxidative stress just as well as wildtypes. The toxicity of the herbicide is mediated through superoxide generation and subsequent lipid peroxidation (Bus JS et al., 1976). Blood serum of the animals was used to get information about the general health of the animals and if there was a hint that PQ influences an organ system in mutant animals more than in wildtypes. There were only minor findings detected here. Uric acid values of PQ treated wildtypes showed a broad variation with a tendency towards lowered values. Usually hypouricemia is based on an ingestion of drugs and toxic agents, but it also can be caused by diet, genetics or an underlying medical condition such as liver disorders (Ogino K et al., 1991). There was a significant reduction of urea levels in challenged wildtype mice whereas mutant values were in the same range like animals from the saline groups. Lower urea values could indicate liver failure or damage, or malnutrition (Clarkson MR et al., 2008). Common features of PQ intoxication are the development of fibrous tissue in the lungs, leading to asphyxiation (Copland et al., 1974; Smith P et al., 1974), hepatotoxicity (Cagen SZ et al., 1976; Yasaka T et al., 1981) and kidney failure (Yasaka T et al., 1981). The urea levels detected were only slightly reduced. Due to the chronic damage of the Tom40 mutation, mutant mitochondria seem to be somehow more resistent towards oxidative stress than wildtypes.

ALT, AST and ALP were measured as part of standard liver function tests (Limdi JK and Hyde GM, 2003). The aminotransferases ALT and AST are excellent markers of hepatocellular injury. Liver cell damage would lead to a raise of liver specific enzyme ALT because of augmented release into the bloodstream (Pratt DS and Kaplan MM, 2000). AST is found mainly in the liver but also in other parts of the body. AST and ALT are usually measured together and are good indicators of liver disease or damage. ALT in challenged animals is slightly reduced not raised, a finding that is contradicting to liver cell damage. AST however is slightly but not significant increased in the PQ cohorts, but it is less specific to the liver (Limdi JK and Hyde GM, 2003). ALP, mainly secreted by liver and bone (Pratt DS and Kaplan MM, 1999), was similar in all tested groups. In vitro studies have reported that PQ exposure can inhibit the enzyme activities of ALT, AST, LDH, and AChE (El-Demerdash FM et al., 2001). In the Tom40 cohort there were no significant findings concerning these enzymes, so a liver damage could be excluded. Elevated CK and AST levels point towards muscle damage (Van der Meulen JH et al., 1991). The variation of CK activity in the challenged Tom40 cohort was too high to see a difference between the groups. A treatment effect concerning both genotypes could be seen for cholesterol. PQ challenged animals showed much lower values than saline treated ones. The same was found for triglycerides and α-amylase while iron concentrations in serum slightly increased. Paraquat has been shown to remove iron from ferritin (Reif DW, 1992), what could explain the slightly higher iron values in treated animals' serum. The decrease in cholesterol and triglycerides levels point towards an altered liver metabolism in the PQ cohort as the liver is the main production site for these compounds (Dietschy JM, 1997; Hillgartner FB et al., 1995). Cholesterol content in the blood is linked to lipid metabolism and depends on the calorific value of the food (Byers SO, 1964; Olson RE, 1998). A case study in poisoned patients showed that cholesterol and triglyceride levels dropped the first days after ingestion of the herbicide and afterwards a strong increase occurred (Fairshter RD et al., 1976). They argued that the primary decrease might be due to the influx of cholesterol to the lungs. However, in most studies an increase in serum cholesterol and triglyceride levels was seen, for example in the subsequent study using rats (Attia AM and Nasr HM, 2009). They collected blood samples from rats 24h after injection with a single dose of PQ (10 mg.kg-1 body weight). They could show that some blood serum compounds were altered including an increase in cholesterol and triglycerides. It has

to be considered that they used a lower dose and administrated the toxin only once, in contrast to the studies with intoxicated patients and studies using lethal doses. Additional, values are strongly influenced by environmental factors such as food.

Among healthy individuals, the pancreas and the salivary glands account for almost all serum amylase, 40-45% from the pancreas and 55-60% from the salivary glands. (Pieper-Bigelow C et al., 1990). The major isoform which is found in many mammals is the α-amylase, an enzyme that hydrolyses alpha-bonds of large alpha-linked polysaccharides yielding glucose and maltose (Reddy NS et al., 2003). It has been shown that PQ inhibits severely the gibberellic acid induced α-amylase synthesis and activity in weed (Jones DW and Foy CL, 1971). In humans with pancreatitis hypoamylasemia may indicate permanent damage to the amylase-producing cells (Abruzzo JL et al., 1958).

In summary, the results of the challenge implicate that treating animals with PQ injections has not the competence to damage Tom40 mutants more than wildtypes. There have been some effects of the treatment but this was seen in both genotypes, like most of the altered clinical chemistry parameters. The only genotype difference that was found was a impaired urea level in treated wildtypes. However, in routine screening the clinical chemistry is done twice to get rid of false positives so the single findings in Clinical chemistry parameters detected here should not be overinterpreted without confirmation in a second batch.

6 Perspectives

The results of the examination of the Tom40 mouse model points towards a slowly progressing neurodegenerative disease. Mutant aged mice showed several symptoms reminiscent of Parkinsonism. The reduced number of Th-positive neurons in the brain of aged mice gave a hint that there is a reduction, but it was at least in this first batch not big enough to reach significance. In humans it has been proven that approximately 60-80% of dopaminergic neurons have to be lost before the motor signs of Parkinson disease emerge (Binukumar BK et al., 2010; Lee CS et al., 1996). Based on our experiments there was no hint that reduced *Tom40* expression and aging alone are enough to trigger the development of AD, although at least some GWAS suggested an association between *Tom40* and AD (Cervantes S et al., 2011; Grupe A et al., 2007; Hong MG et al., 2010). In contrast other papers discuss that this finding is the result of a known strong linkage disequilibrium in this genomic region containing the genes *PVRL2, TOMM40, APOE* and *APOC1* (Cruchaga C et al., 2011; Takei N et al., 2009; Yu CE et al., 2007). The Aβ-precursor APP has been shown to accumulate in the mitochondrial import pores resulting in mitochondrial dysfunction in LOAD (Anandatheerthavarada HK et al., 2003; Devi L et al., 2006). Aβ itself is also imported into the organelle and the import requires interaction with the TOM complex and also Tom40 (Hansson Petersen CA et al., 2008; Sirk D et al., 2007; Yamaguchi H et al., 1992). It has been reported that the import is independent of membrane potential and that the protein is located to the cristae after import (Hansson Petersen CA et al., 2008). It could be speculated whether reduced *Tom40* expression resulting in less import channels would enhance severity of the found symptoms due to the fact that all available import pores are arrested earlier than in controls. Otherwise it would also be possible that reduced Tom40 import pores could slow down the progress of the disease as APP and Aβ are not arrested in the mitochondrial matrix in such big amounts than in wildtypes. One possibility therefore would be to cross Tom40 heterozygous animals with an APP overexpressing mouse line such as APP23 mice expressing human APP (Van Dam D et al., 2003). APP23 have a clear and quite early phenotype with includes the development of amyloid plaques after 6month lifetime accompanied by inflammatory reactions (Van Dam D et al., 2005). If one of the above mentioned hypotheses is correct, there should be more

or respectively less amyloid deposits in the brain of the double-mutant Tom40-APP mice visible. Interestingly APP23 mice develop cognitive impairments already at an age of three months (Kelly PH et al., 2003). It would be interesting to analyze this and also the other phenotypes found in this mouse model i.e. pathological limb reflexes, myoclonic jumping, seizure activity, and tail malformation as well as body weight reduction (Lalonde R et al., 2005) with an additional *Tom40* mutation. Studies on this issue could help to improve the understanding of AD, the involvement of mitochondria, the mitochondrial import system and mitochondrial trafficking of APP and Aβ.

Mutant mitochondria were evaluated in various different tests. However, there are still many questions unanswered. Besides the composition of the respiratory chain less is known about the mitochondrial proteome of mutant animals. Deeper insights would be provided by 'Difference gel electrophoresis' (DIGE), a technique which allows two independent samples to be run in one gel simultaneously by implicating two different fluorescent dyes, cyanine-3 (Cy3) and cyanine-5 (Cy5), which label lysines in proteins (Unlü M et al., 1997). DIGE was frequently used to get information on the mitochondrial proteome of for example mutant mouse lines like the Double-knockout Creatine Kinase (DbKO-CK) mice who suffered from a cardiac phenotype (Kernec F et al., 2001) or to study the effects of aging on rat muscle mitochondria (O'Connell K and Ohlendieck K, 2009) and could be an useful tool to get further insights into the structure and composition of Tom40-deficient mitochondria. Additional metabolomic investigation using blood serum of mutant and wildtypes as well as PQ treated an untreated animals would help to get a better understanding about the influences of the mutation itself and additional about the influence of the treatment.

Beyond, investigation of ATP production and import studies would be interesting to get a deeper understanding about how *Tom40* and the import pathway itself influence the respiratory chain, the energy production and how these alterations could be compensated to guarantee quite normal function.

7 References

Abruzzo JL, Homa M, Houck JC, and Coffey RJ (1958). Significance of the serum amylase determination. Annals of surgery *147*, 921-930.
Acín-Pérez R, Bayona-Bafaluy MP, Fernández-Silva P, Moreno-Loshuertos R, Pérez-Martos A, Bruno C, Moraes CT, and Enríquez JA (2004). Respiratory complex III is required to maintain complex I in mammalian mitochondria. Molecular Cell *13*.
Ackrell BAC (2000). Progress in understanding structure–function relationships in respiratory chain complex II. FEBS letters *466*, 1-5.
Ackrell BAC, Johnson MK, Gunsalus RP, and Cecchini G (1992). Structure and function of succinate dehydrogenase and fumarate reductase, Vol 3 (Boca Raton, FL: CRC Press).
Ahting U, Floss T, Uez N, Schneider-Lohmar I, Becker L, Kling E, Iuso A, Bender A, de Angelis MH, Gailus-Durner V*, et al.* (2009). Neurological phenotype and reduced lifespan in heterozygous Tim23 knockout mice, the first mouse model of defective mitochondrial import. Biochimica et Biophysica Acta *1787*, 371-376.
Alconada A, Kübrich M, Moczko M, Hönlinger A, and Pfanner N (1995). The Mitochondrial Receptor Complex: the Small Subunit Mom8b/Isp6 Supports Association of Receptors with the General Insertion Pore and Transfer of Preproteins. Molecular and cellular biology *15*, 6196-6205.
Alessandrini F, Jakob T, Wolf A, Wolf E, Balling R, Hrabě de Angelis M, Ring J, and Behrendt H (2001). ENU mouse mutagenesis: Generation of mouse mutants with aberrant plasma IgE levels. International archives of allergy and immunology *124*, 25-28.
Alexis NE, Dietrich WD, Green EJ, Prado R, and Watson BD (1995). Nonocclusive Common Carotid Artery Thrombosis in the Rat Results in Reversible Sensorimotor and Cognitive Behavioral Deficits Stroke *26*, 2338-2346.
Allen DL, Harrison BC, Maass A, Bell ML, Byrnes WC, and Leinwand LA (2001). Cardiac and skeletal muscle adaptations to voluntary wheel running in the mouse. Journal of Applied Physiology *90*, 1900-1908.
Altmann R (1890). Die Elementarorganismen Und Ihre Beziehungen Zu Den Zellen, Vol 145 (Leipzig: Veit & comp.).
Amende I, Kale A, McCue S, Glazier S, Morgan JP, and Hampton TG (2005). Gait dynamics in mouse models of Parkinson's disease and Huntington's disease. Journal of neuroengineering and rehabilitation [electronic resource] *25*, 20.
Ames BN, Shigenaga MK, and Hagen TM (1993). Oxidants, antioxidants, and the degenerative diseases of aging. Proceedings of the National Academy of Sciences of the United States of America *90*, 7915-7922.
Anandatheerthavarada HK, Biswas G, Robin MA, and Avadhani NG (2003). Mitochondrial targeting and a novel transmembrane arrest of Alzheimer's amyloid precursor protein impairs mitochondrial function in neuronal cells. The Journal of cell biology *161*, 41-54.
Anderson S, Bankier AT, Barrell BG, de Bruijn MH, Coulson AR, Drouin J, Eperon IC, Nierlich DP, Roe BA, and F, S. (1981). Sequence and organization of the human mitochondrial genome. Nature *290*, 457-465.
Antoch MP, Song EJ, Chang AM, Vitaterna MH, Zhao Y, Wilsbacher LD, Sangoram AM, King DP, Pinto LH, and Takahashi JS (1997). Functional identification of the mouse circadian Clock gene by transgenic BAC rescue. Cell *89*, 655-667.
Archer J (1973). Tests for emotionality in rats and mice: A review. . Animal Behaviour *21*, 205-236.
Argyropoulos G, and Harper ME (2002). Uncoupling proteins and thermoregulation. Journal of applied physiology *92*, 2187-2198.
Arnold K, Pfeiffer AK, Neupert W, Stuart RA, and Schägger H (1998). Yeast mitochondrial F_1F_O-ATP synthase exists as a dimer: identification of three dimer-specific subunits. The EMBO Journal *17*, 7170-7178.
Ashby B (1990). Dopamine and schizophrenia. Nature *348*, 493.

Astuti D, Latif F, Dallol A, Dahia PL, Douglas F, George E, Sköldberg F, Husebye ES, Eng C, and Maher ER (2001). Gene mutations in the succinate dehydrogenase subunit SDHB cause susceptibility to familial pheochromocytoma and to familial paraganglioma. American Society of Human Genetics *69*, 49-54.
Atamna H, and Frey WH (2007). Mechanisms of mitochondrial dysfunction and energy deficiency in Alzheimer's disease. Mitochondrion *7*, 297-310.
Atorino L, Silvestri L, Koppen M, Cassina L, Ballabio A, Marconi R, Langer T, and Casari G (2003). Loss of m-AAA protease in mitochondria causes complex I deficiency and increased sensitivity to oxidative stress in hereditary spastic paraplegia. Journal of Cell Biology *163*, 777-787.
Attia AM, and Nasr HM (2009). Evaluation of protective effect of omega- 3 fatty acids and selenium on paraquat intoxicated rats. Slovak Journal of Animal Science *42*, 180-187.
Babcock GT, and Wikström M (1992). Oxygen activation and the conservation of energy in cell respiration. Nature *356*, 301-309.
Baker KP, Schaniel A, Vestweber D, and Schatz G (1990). A yeast mitochondrial outer membrane protein essential for protein import and cell viability. Nature *348*, 605-609.
Baker N, Adler LE, Franks RD, Waldo M, Berry S, Nagamoto H, Muckle A, and Freedman R (1987). Neurophysiological assessment of sensory gating in psychiatric inpatients: comparison between schizophrenia and other diagnoses. Biological psychiatry *22*, 603-617.
Balling R (2001). ENU mutagenesis: analyzing gene function in mice. Annual Review of Genomics and Human Genetics *2*, 463-492.
Baloh RH (2008). Mitochondrial dynamics and peripheral neuropathy. The Neuroscientist : a review journal bringing neurobiology, neurology and psychiatry *14*, 12-18.
Baloyannis SJ, Costa V, and Michmizos D (2004). Mitochondrial alterations in Alzheimer's disease. American Journal of Alzheimer's disease and Other Dementias *19*, 89-93.
Banci L, Bertini I, Cefaro C, Ciofi-Baffoni S, Gallo A, Martinelli M, Sideris DP, Katrakili N, and Tokatlidis K (2009). Nat Struct Mol Biol. 2009 Feb;16(2):198-206. Epub 2009 Feb 1.
MIA40 is an oxidoreductase that catalyzes oxidative protein folding in mitochondria.
Banci L, Bertini I, Cefaro C, Ciofi-Baffoni S, Gallo A, Martinelli M, Sideris DP, Katrakili N, Tokatlidis K. Nature Structural & Molecular Biology *16*, 198-206.
Barboni P, Carbonelli M, Savini G, Ramos Cdo V, Carta A, Berezovsky A, Salomao SR, Carelli V, and Sadun AA (2010). Natural history of Leber's hereditary optic neuropathy: longitudinal analysis of the retinal nerve fiber layer by optical coherence tomography. Ophthalmology *117*, 623-627.
Baron M, Kudin AP, and Kunz WS (2007). Mitochondrial dysfunction in neurodegenerative disorders. Biochemical Society Transactions *35*, 1228-1231.
Barroso N, Campos Y, Huertas R, Esteban J, Molina JA, Alonso A, Gutierrez-Rivas E, and Arenas J (1993). Respiratory chain enzyme activities in lymphocytes from untreated patients with Parkinson disease. Clinical Chemistry *39*, 667-669.
Bauer MF, Gempel K, Hofmann S, Jaksch M, Philbrook C, and Gerbitz K-D (1999). Mitochondrial Disorders. A Diagnostic Challenge in Clinical Chemistry. Clinical Chemistry and Laboratory Medicine *37*, 855-876.
Bauer MF, Hofmann S, Neupert W, and Brunner M (2000). Protein translocation into mitochondria: the role of TIM complexes. Trends in Cell Biology *10*, 25-31.
Baysal BE, Ferrell RE, Willett-Brozick JE, Lawrence EC, Myssiorek D, Bosch A, van der Mey A, Taschner PE, Rubinstein WS, Myers EN*, et al.* (2000). Mutations in SDHD, a mitochondrial complex II gene, in hereditary paraganglioma. Science *287*, 848-851.
Baysal BE, Rubinstein WS, and Taschner PE (2001). Phenotypic dichotomy in mitochondrial complex II genetic disorders. Journal of molecular medicine (Berlin, Germany) *79*, 495-503.
Becker T, Pfannschmidt S, Guiard B, Stojanovski D, Milenkovic D, Kutik S, Pfanner N, Meisinger C, and Wiedemann N (2008a). Biogenesis of the mitochondrial TOM complex: Mim1 promotes insertion and assembly of signal-anchored receptors. The Journal of Biological Chemistry *283*, 120-127.
Becker T, Vögtle FN, Stojanovski D, and Meisinger C (2008b). Sorting and assembly of mitochondrial outer membrane proteins. Biochimica et Biophysica Acta *1777*, 557-563.

Beckers J, Behrendt H, Daniel H, Esposito I, Favor J, Graw J, Heldmaier G, Höfler H, Ivandic B, Katus H*, et al.* (2009). The German Mouse Clinic: a platform for systemic phenotype analysis of mouse models. Current Pharmaceutical Biotechnology *10*, 236-243.
Bedell MA, Jenkins NA, and Copeland NC (1996). Good genes in bad neighborhoods. Nature Genetics *12*, 229-232.
Bender A, Krishnan KJ, Morris CM, Taylor GA, Reeve AK, Perry RH, Jaros E, Hersheson JS, Betts J, Klopstock T*, et al.* (2006). High levels of mitochondrial DNA deletions in substantia nigra neurons in aging and Parkinson disease. Nature Genetics *38*, 515-517.
Bereiter-Hahn J, and Vöth M (1994). Dynamics of mitochondria in living cells: shape changes, dislocations, fusion, and fission of mitochondria. Microscopy Research and Technique *27*, 198-219.
Betarbet R, Sherer TB, MacKenzie G, Garcia-Osuna M, Panov AV, and Greenamyre JT (2000). Chronic systemic pesticide exposure reproduces features of Parkinson's disease. Nature Neuroscience *3*, 1301-1306.
Bindoff LA, Birch-Machin MA, Cartlidge NE, Parker WD Jr, and Turnbull DM (1991). Respiratory chain abnormalities in skeletal muscle from patients with Parkinson's disease. Journal of the neurological sciences *104*, 203-208.
Binukumar BK, Bal A, Kandimalla RJ, and Gill KD (2010). Nigrostriatal neuronal death following chronic dichlorvos exposure: crosstalk between mitochondrial impairments, α synuclein aggregation, oxidative damage and behavioral changes. Molecular brain [electronic resource] *3*, 35.
Bischoff C, Dengler R, and Hopf HC (2008). EMG. NLG: Elektromyographie, Nervenleitungsuntersuchungen (Georg Thieme Verlag).
Bit-Avragim N, Perrot A, Schöls L, Hardt C, Kreuz FR, Zühlke C, Bubel S, Laccone F, Vogel HP, Dietz R, and Osterziel KJ (2001). The GAA repeat expansion in intron 1 of the frataxin gene is related to the severity of cardiac manifestation in patients with Friedreich's ataxia. Journal of molecular medicine (Berlin, Germany) *78*, 626-632.
Bitsios P, Giakoumaki SG, Theou K, and Frangou S (2006). Increased prepulse inhibition of the acoustic startle response is associated with better strategy formation and execution times in healthy males. Neuropsychologia *44*, 2494-2499.
Bleecker ML, Bohlman M, Moreland R, and Tipton A (1985). Carpal tunnel syndrome: role of carpal canal size. Neurology *35*, 1599-1604.
Bodis-Wollner I (2009). Retinopathy in Parkinson Disease. Journal of neural transmisson *116*, 1493-1501.
Bogan N, and Cabot JB (1991). Light and electron microscopic analyses of intraspinal axon collaterals of sympathetic preganglionic neurons. Brain Research *541*, 241-251.
Bonnefoy N, Fiumera HL, Dujardin G, and Fox TD (2009). Roles of Oxa1-related inner-membrane translocases in assembly of respiratory chain complexes. Biochimica et Biophysica Acta *1793*, 60-70.
Boss O, Samec S, Paoloni-Giacobino A, Rossier C, Dulloo A, Seydoux J, Muzzin P, and Giacobino JP (1997). Uncoupling protein-3: a new member of the mitochondrial carrier family with tissue-specific expression. FEBS Letters *408*, 39-42.
Bourgeron T, Rustin P, Chretien D, Birch-Machin M, Bourgeois M, Viegas-Péquignot E, Munnich A, and Rötig A (1995). Mutation of a nuclear succinate dehydrogenase gene results in mitochondrial respiratory chain deficiency. Nature Genetics *11*, 144-149.
Bowling AC, Mutisya EM, Walker LC, Price DL, Cork LC, and Beal MF (1993). Age-dependent impairment of mitochondrial function in primate brain. Journal of neurochemistry *60*, 1964-1967.
Bradley JL, Blake JC, Chamberlain S, Thomas PK, Cooper JM, and Schapira AH (2000). Clinical, biochemical and molecular genetic correlations in Friedreich's ataxia. Human Molecular Genetics *9*, 275-282.
Branden G, Gennis RB, and Brzezinski P (2006). Transmembrane proton translocation by cytochrome c oxidase. Biochimica et Biophysica Acta *1751*.
Brenner C, and Kroemer G (2000). Apoptosis. Mitochondria--the death signal integrators. Science *289*, 1150-1151.

Brielmeier M, Fuchs H, Przemeck G, Gailus-Durner V, Hrabě de Angelis M, and Schmidt J (2002). The GSF-Phenotype Analysis Center (German Mouse Clinic, GMC): A sentinel-based health-monitoring concept in a multi-user unit for standardized characterization of mouse mutants. J.-L. Guenet and C. Herweg (eds.) Laboratory Animals Science - Basis and Strategy for Animal Experimentation *11*, 19-22.

Brooks AI, Chadwick CA, Gelbard HA, Cory-Slechta DA, and Federoff HJ (1999). Paraquat elicited neurobehavioral syndrome caused by dopaminergic neuron loss. Brain Research *823*, 1-10.

Brown MD, Torroni A, Shoffner JM, and Wallace DC (1992). Mitochondrial tRNA(Thr) mutations and lethal infantile mitochondrial myopathy. The American Journal of Human Genetics *51*, 446-447.

Brown NF, Esser V, Gonzalez AD, Evans CT, Slaughter CA, Foster DW, and McGarry JD (1991). Mitochondrial import and processing of rat liver carnitine palmitoyltransferase II defines the amino terminus of the mature protein. Possibility of differential modification of the rat and human isoforms. The Journal of Biological Chemistry *266*, 15446-15449.

Brown SD, Chambon P, MH;, d.A., and Consortium, E. (2005). EMPReSS: standardized phenotype screens for functional annotation of the mouse genome. Nature Genetics *37*, 1155.

Bus JS, Cagen SZ, Olgaard M, and Gibson JE (1976). A mechanism of paraquat toxicity in mice and rats, Toxicology and. Toxicology and Applied Pharmacology *35*, 501-513.

Butterfield DA, and Boyd-Kimball D (2005). The critical role of methionine 35 in Alzheimer's amyloid beta-peptide (1-42)-induced oxidative stress and neurotoxicity. Biochimica et Biophysica Acta *1703*, 149-156.

Byers SO (1964). Liver regulation of plasma cholesterol. Biochemical clinics *4*, 157-168.

Cagen SZ, Janoff AS, Bus JS, and Gibson JE (1976). Effect of paraquat (methyl viologen) on liver function in mice. Journal of Pharmacology and Experimental Therapeutics *198*, 222-228.

Calabresi P, De Murtas M, Pisani A, Stefani A, Sancesario G, Mercuri NB, and Bernardi G (1995). Vulnerability of medium spiny striatal neurons to glutamate: role of Na+/K+ ATPase. European Journal of Neuroscience *7*, 1674-1683.

Campanella M, Parker N, Tan CH, Hall AM, and Duchen MR (2009). IF(1): setting the pace of the F(1)F(o)-ATP synthase. Trends in biochemical sciences *34*, 343-335.

Campuzano V, Montermini L, Moltò MD, Pianese L, Cossée M, Cavalcanti F, Monros E, Rodius F, Duclos F, Monticelli A*, et al.* (1996). Friedreich' s ataxia: autosomal recessive disease caused by an intronic GAA triplet repeat expansion. Science *271*, 1423-1427.

Cao L, Shitara H, Horii T, Nagao Y, Imai H, Abe K, Hara T, Hayashi J, and Yonekawa H (2007). The mitochondrial bottleneck occurs without reduction of mtDNA content in female mouse germ cells. Nature Genetics *39*, 386-390.

Capecchi MR (1989). The new mouse genetics: altering the genome by gene targeting. Trends in Genetics *5*, 70-76.

Carninci P, Kasukawa T, Katayama S, Gough J, Frith MC, Maeda N, Oyama R, Ravasi T, Lenhard B, Wells C*, et al.* (2005). The transcriptional landscape of the mammalian genome. Science. *309*, 1559-1563.

Carroll J, Fearnley IM, Shannon RJ, Hirst J, and Walker JE (2003). Analysis of the subunit composition of complex I from bovine heart mitochondria. Molecular & Cellular Proteomics *2*, 117-126.

Carroll J, Shannon RJ, Fearnley IM, Walker JE, and Hirst J (2002). Definition of the nuclear-encoded protein composition of bovine heart mitochondrial complex I. Identification of two newsubunits. Journal of Biological Chemistry *277*, 50311-50317.

Carter RJ, Morton J, and Dunnett SB (2001). Motor Coordination and Balance in Rodents. Current Protocols in Neuroscience *Chapter 8*, Unit 8.12.

Castello PR, Drechsel DA, and Patel M (2007). Mitochondria are a major source of paraquat-induced reactive oxygen species production in the brain. The Journal of Biological Chemistry *282*, 14186-14193.

Castelluccio C, Baracca A, Fato R, Pallotti F, Maranesi M, Barzanti V, Gorini A, Villa RF, Parenti Castelli G, Marchetti M, and et al. (1994). Mitochondrial activities of rat heart during ageing. Mechanisms of ageing and development *76*, 73-88.
Castro L, Rodriguez M, and Radi R (1994). Aconitase is readily inactivated by peroxynitrite, but not by its precursor, nitric oxide. The Journal of Biological Chemistry *269*, 29409-29415.
Ceballos D, Cuadras J, Verdú E, and Navarro X (1999). Morphometric and ultrastructural changes with ageing in mouse peripheral nerve. Journal of Anatomy *195*.
Cecconi F, and Meyer BI (2000). Gene trap: a way to identify novel genes and unravel their biological function. FEBS Letters *480*, 63-71.
Cervantes S, Samaranch L, Vidal-Taboada JM, Lamet I, Bullido MJ, Frank-García A, Coria F, Lleó A, Clarimón J, Lorenzo E*, et al.* (2011). Genetic variation in APOE cluster region and Alzheimer's disease risk. Neurobiology of aging *32*, 2107.e2107-2117.
Chacinska A, Lind M, Frazier AE, Dudek J, Meisinger C, Geissler A, Sickmann A, Meyer HE, Truscott KN, Guiard B*, et al.* (2005). Mitochondrial Presequence Translocase: Switching between TOM Tethering and Motor Recruitment Involves Tim21 and Tim17. Cell *120*, 817-829.
Chacinska A, Pfannschmidt S, Wiedemann N, Kozjak V, Sanjuán Szklarz LK, Schulze-Specking A, Truscott KN, Guiard B, Meisinger C, and Pfanner N (2004). Essential role of Mia40 in import and assembly of mitochondrial intermembrane space proteins. The EMBO Journal *23*, 37.
Chagnon P, Bétard C, Robitaille Y, Cholette A, and Gauvreau D (1995). Distribution of brain cytochrome oxidase activity in various neurodegenerative diseases. Neuroreport *6*, 711-715.
Chan DC (2006). Mitochondrial Fusion and Fission in Mammals. Annual Review of Cell and Developmental Biology *22*, 79-99.
Chen G, Gharib TG, Huang CC, Taylor JM, Misek DE, Kardia SL, Giordano TJ, Iannettoni MD, Orringer MB, Hanash SM, and Beer DG (2002). Discordant protein and mRNA expression in lung adenocarcinomas. Molecular & Cellular Proteomics *1*, 304-313.
Choleris E, Thomas AW, Kavaliers M, and Prato FS (2001). A detailed ethological analysis of the mouse open field test: effects of diazepam, chlordi-azepoxide and an extremely low frequency pulsed magnetic field. Neuroscience and biobehavioral reviews *25*, 235-260.
Church DM, Goodstadt L, Hillier LW, Zody MC, Goldstein S, et al., She X, Bult CJ, AgarwalaR, Cherry JL, DiCuccio M*, et al.* (2009). Lineage-Specific Biology Revealed by a Finished Genome Assembly of the Mouse. PLoS Biology *7*, e1000112.
Cicchetti F, Lapointe N, Roberge-Tremblay A, Saint-Pierre M, Jimenez L, Ficke BW, and Gross RE (2005). Systemic exposure to paraquat and maneb models early Parkinson's disease in young adult rats. Neurobiology of disease *20*, 360-371.
Clarkson MR, Friedewald JJ, Eustace JA, and Rabb H (2008). Acute kidney injury. In Brenner and Rector's The Kidney, 8, ed. (Philadelphia: Saunders).
Cohen I, Kohl C, McGarry JD, Girard J, and Prip-Buus C (1998). The N-terminal Domain of Rat Liver Carnitine Palmitoyltransferase 1 Mediates Import into the Outer Mitochondrial Membrane and Is Essential for Activity and Malonyl-CoA Sensitivity. The Journal of Biological Chemistry *273*, 29896-29904.
Copland GM, Kolin A, and Shulman HS (1974). Fatal Pulmonary Intra-Alveolar Fibrosis after Paraquat Ingestion. New England Journal of Medicine *291*, 290-292.
Corbin KB, and Gardner ED(1937). Decrease in number of myelinated fibers in human spinal roots with age. The Anatomical record *68*.
Cottrell L (1940). Histologic variations with age in apparently normal peripheral nerve trunks. Archieves of Neurology and Psychiatry *43*, 1138-1150.
Crawley JN (2008). Behavioral phenotyping strategies for mutant mice. Neuron *57*, 809-818.
Crofts AR (2004). THE CYTOCHROME BC1 COMPLEX: Function in the Context of Structure Annual Review of Physiology. Annual Review of Physiology *66*, 689-733.
Crofts AR, Hong S, Ugulava N, Barquera B, Gennis R, Guergova-Kuras M, and Berry EA (1999). Pathways for proton release during ubihydroquinone oxidation by the bc(1) complex. Proceedings of the National Academy of Sciences of the United States of America *96*, 10021-10026.

Cruchaga C, Nowotny P, Kauwe JS, Ridge PG, Mayo K, Bertelsen S, Hinrichs A, Fagan AM, Holtzman DM, Morris JC, and Goate AM (2011). Association and Expression Analyses With Single-Nucleotide Polymorphisms in TOMM40 in Alzheimer Disease. Archieves of Neurology *68*, 1013-1019.
Cummings BJ, Engesser-Cesar C, Cadena G, and Anderson AJ (2007). Adaptation of a ladder beam walking task to assess locomotor recovery in mice following spinal cord injury. Behavioural Brain Research *177*, 232-241.
Cummins JM (2000). Fertilization and elimination of the paternal mitochondrial genome. Human Reproduction *15*, 92-101.
Dahlstrom A, and Fuxe K (1965). Evidence for the existence of monoamine-containing neurons in the central nervous system. I. Demonstration of monoamines in the cell bodies of brain stem neurons. Acta physiologica Scandinavica Supplementum *62*, 1-55.
Danik S, Cabo C, Chiello C, Kang S, Wit AL, and Coromilas J (2002). Correlation of repolarization of ventricular monophasic action potential with ECG in the murine heart. American journal of physiology. Heart and circulatory physiology *283*, H372-381.
Delettre C, Lenaers G, Griffoin JM, Gigarel N, Lorenzo C, Belenguer P, Pelloquin L, Grosgeorge J, Turc-Carel C, Perret E, A.-D.C., *, et al.* (2000). Nuclear gene OPA1, encoding a mitochondrial dynamin-related protein, is mutated in dominant optic atrophy. Nature Genetics *26*, 207-210.
Dembowski M, Künkele K-P, Nargang FE, Neupert W, and Rapaport D (2001). Assembly of Tom6 and Tom7 into the TOM Core Complex of Neurospora crassa. The Journal of Biological Chemistry *276*, 17679-17685.
Dennis G Jr, Sherman BT, Hosack DA, Yang J, Gao W, Lane HC, and Lempicki RA (2003). DAVID: Database for Annotation, Visualization, and Inte-grated Discovery. Genome Biology *4*, P3.
Devi L, Prabhu BM, Galati DF, Avadhani NG, and Anandatheerthavarada HK (2006). Accumulation of amyloid precursor protein in the mitochondrial import channels of human Alzheimer's disease brain is associated with mitochondrial dysfunction. The Journal of Neuroscience *26*, 9057-9068.
Devi L, Raghavendran V, Prabhu BM, Avadhani NG, and Anandatheerthavarada HK (2008). Mitochondrial import and accumulation of alpha-synuclein impair complex I in human dopaminergic neuronal cultures and Parkinson disease brain. The Journal of Biological Chemistry *283*, 9089-9100.
Dietschy JM (1997). Overview of cholesterol and lipoprotein metabolism in the brain, liver and extrahepatic organs. Nutrition, Metabolism & Cardiovascular diseases *7*, 162-168.
DiMauro S, Bonilla E, Zeviani M, Nakagawa M, and DeVivo DC (1985). Mitochondrial myopathies. Annals of Neurology *17*, 521-538.
Drapier JC, and Hibbs JB Jr (1996). Aconitases: a class of metalloproteins highly sensitive to nitric oxide synthesis. Methods in Enzymology *269*, 26-36.
Drorbaugh JE, and Fenn WO (1955). A barometric method for measuring ventila-tion in newborn infants. Pediatrics *16*, 81-87.
Dyall SD, Brown MT, and Johnson PJ (2004). Ancient Invasions: From Endosymbionts to Organelles Science *304*, 253-257.
Eddy NB, and Leimbach D (1953). Synthetic analgesics II. Diethienylbutenyl and dithienylbutylamines. The Journal of pharmacology and experimental therapeutics. *107*, 385-393.
El-Demerdash FM, Yousef MI, and Elagamy EI (2001). Influence of paraquat, glyphosate, and cadmium on the activity of some serum enzymes and protein electrophoretic behavior (in vitro). Journal of Environmental Science and Health, Part B *36*.
Ellrich J, and Wesselak M (2003). Electrophysiology of sensory and sensorimotor processing in mice under general anaesthesia. Brain research Brain research Protocols *11*.
Elmore S (2007). Apoptosis: a review of programmed cell death. Toxicologic pathology *35*, 495-516.
Emptage MH, Dreyers JL, Kennedy MC, and Beinert H (1983). Optical and EPR characterization of different species of active and inactive aconitase. The Journal of Biological Chemistry *258*, 11106-11111.

Endo T, and Yamano K (2009). Multiple pathways for mitochondrial protein traffic. Biological chemistry *390*, 723-730.
Engelmann M, Hädicke J, and Noack J (2011). Testing declarative memory in laboratory rats and mice using the nonconditioned social discrimination procedure. Nature Protocols *6*, 1152-1162.
Esposito LA, Melov S, Panov A, Cottrell BA, and Wallace DC (1999). Mitochondrial disease in mouse results in increased oxidative stress. Proceedings of the National Academy of Sciences of the United States of America *96*, 4820-4825.
Esser K, Tursun B, Ingenhoven M, Michaelis G, and Pratje E (2002). A novel two-step mechanism for removal of a mitochondrial signal sequence involves the m-AAA complex and the putative rhomboid protease Pcp1. Journal of Molecular Biology *323*, 835-843.
Fahlström A, Yu Q, and Ulfhake B (2011). Behavioral changes in aging female C57BL/6 mice. Neurobiology of aging *32*, 1868-1880.
Fairshter RD, Rosen SM, Smith WR, Glauser FL, Morae DM, and Wilson AF (1976). Paraquat Poisoning: New Aspects of Therapy. Quarterly Journal of Medicine, New Series *XLV*, 551-585.
Fannin SW, Lesnefsky EJ, Slabe TJ, Hassan MO, and Hoppel CL (1999). Aging selectively decreases oxidative capacity in rat heart interfibrillar mitochondria. Archieves of Biochemistry and Biophysik *372*, 399-407.
Farr TD, Liu L, Colwell KL, Whishaw IQ, and Metz GA (2006). Bilateral alteration in stepping pattern after unilateral motor cortex injury: a new test strategy for analysis of skilled limb movements in neurological mouse models. Journal of neuroscience methods *153*, 104-113.
Farrer LA, Cupples LA, Haines JL, Hyman B, Kukull WA, Mayeux R, Myers RH, Pericak-Vance MA, Risch N, and van Duijn CM (1997). Effects of age, sex, and ethnicity on the association between apolipoprotein E genotype and Alzheimer disease. A meta-analysis. APOE and Alzheimer Disease Meta Analysis Consortium. JAMA : the journal of the American Medical Association *278*, 1349-1356.
Favor J (1983). A comparison of the dominant cataract and recessive spe-cific-locus mutation rates induced by treatment of male mice with ethyl-nitrosourea. Mutation Research *110*, 367-382.
Feil R, Holter SM, Weindl K, Wurst W, Langmesser S, Gerling A, Feil S, and Albrecht U (2009). cGMP-dependent protein kinase I, the circadian clock, sleep and learning. Commun Integr Biol *2*, 298-301.
Ferguson-Miller S, and Babcock GT (1996). Heme/Copper Terminal Oxidases. Chemical reviews *96*, 2889-2908.
Fernagut PO, Chalon S, Diguet E, Guilloteau D, Tison F, and Jaber M (2003). Motor behaviour deficits and their histopathological and functional correlates in the nigrostriatal system of dopamine transporter knockout mice. Neuroscience *116*, 1123-1130.
Fischer MD, Huber G, Beck SC, Tanimoto N, Muehlfriedel R, Fahl E, Grimm C, Wenzel A, Remé CE, van de Pavert SA*, et al.* (2009). Noninvasive, *In Vivo* Assessment of Mouse Retinal Structure Using Optical Coherence Tomography. PLoS One *4*, e7507.
Flavell RA, Sabo DL, Bandle EF, and Weissmann C (1975). Site-directed mutagenesis: effect of an extracistronic mutation on the in vitro propagation of bacteriophage Qbeta RNA. Proceedings of the National Academy of Sciences of the United States of America *72*, 367-371.
Fleming SM, and Chesselet MF (2006). Behavioral phenotypes and pharmacology in genetic mouse models of Parkinsonism. Behavioural pharmacology *17*, 383-391.
Fleming SM, Fernagut PO, and Chesselet MF (2005). Genetic mouse models of parkinsonism: strengths and limitations. NeuroRx : the journal of the American Society for Experimental NeuroTherapeutics *2*, 495-503.
Fleury C, Neverova M, Collins S, Raimbault S, Champigny O, Levi-Meyrueis C, Bouillaud F, Seldin MF, Surwit RS, Ricquier D, and Warden CH (1997). Uncoupling protein-2: a novel gene linked to obesity and hyperinsulinemia. Nature genetics *15*.
Fornai F, Schlüter OM, Lenzi P, Gesi M, Ruffoli R, Ferrucci M, Lazzeri G, Busceti CL, Pontarelli F, Battaglia G*, et al.* (2005). Parkinson-like syndrome induced by continuous MPTP infusion: convergent roles of the ubiquitin-proteasome system and alpha-synuclein.

Proceedings of the National Academy of Sciences of the United States of America *102*, 3413-3418.
Fowler RE, and Edwards RG (1957). Induction of superovulation and pregnancy in mature mice by gonadotrophins. Journal of Endocrinology *15*, 374-384.
Freitag S, Schachner M, and Morelli F (2003). Behavioral alterations in mice deficient for the extracellular matrix glycoprotein tenascin-R Behavioural Brain Research *145*, 189-207.
Friedrich G, and Soriano P (1991). Promoter traps in embryonic stem cells: a genetic screen to identify and mutate developmental genes in mice. Genes & Development *5*, 1413-1523.
Fuchs H, Gailus-Durner V, Adler T, Aguilar-Pimentel JA, Becker L, Calzada-Wack J, Da Silva-Buttkus P, Neff F, Götz A, Hans W*, et al.* (2011). Mouse phenotyping. Methods *53*, 120-135.
Fuchs H, Gailus-Durner V, Adler T, Pimentel JA, Becker L, Bolle I, Brielmeier M, Calzada-Wack J, Dalke C, Ehrhardt N*, et al.* (2009). The German Mouse Clinic: a platform for systemic phenotype analysis of mouse models. Current Pharmaceutical Biotechnology *10*, 236-243.
Fuchs H, Lisse T, Abe K, and Hrabě de Angelis M (2006). Screening for bone and cartilage phenotypes in mice. In: Phenotyping of the Laboratory Mouse. Eds.: Hrabě de Angelis M., Chambon P. and Browns S. Wiley-VCH, Weinheim, 35-86.
Fuchs H, Schughart K, Wolf E, Balling R, and Hrabě de Angelis M (2000). Screening for dysmorphological abnormalities - a powerful tool to isolate new mouse mutants. Mammalian Genome *11*, 528-530.
Gabriel K, Egan B, and Lithgow T (2003). Tom40, the import channel of the mitochondrial outer membrane, plays an active role in sorting imported proteins. The EMBO journal *22*, 2380-2386.
Gailus-Durner V, Fuchs H, Adler T, Aguilar Pimentel A, Becker L, Bolle I, Calzada-Wack J, Dalke C, Ehrhardt N, Ferwagner B*, et al.* (2009). Systemic first-line phenotyping. Methods in Molecular Biology *530*, 463-509.
Gailus-Durner V, Fuchs H, Becker L, Bolle I, Brielmeier M, Calzada-Wack J, Elvert R, Ehrhardt N, Dalke C, Franz TJ*, et al.* (2005). Introducing the German Mouse Clinic: open access platform for standardized phenotyping. Nature Methods *2*, 403-404.
Galante YM, Wong SY, and Hatefi Y (1979). Composition of complex V of the mitochondrial oxidative phosphorylation system. Journal of Biological Chemistry *254*, 12372-12378.
Galetta KM, Calabresi PA, Frohman EM, and Balcer LJ (2011). Optical coherence tomography (OCT): imaging the visual pathway as a model for neurodegeneration. Neurotherapeutics *8*, 117-132.
Garcia JH, Lossinsky AS, Kauffman FC, and Conger KA (1978). Neuronal ischemic injury: light microscopy, ultrastructure and biochemistry. Acta neuropathologia (Berl) *43*, 85-95.
Gardiner P, Dai Y, and Heckman CJ (2006). Effects of exercise training on alpha-motoneurons. Journal of Applied Physiology *101*, 1228-1236.
Gardner PR (2002). Aconitase: sensitive target and measure of superoxide. Methods in Enzymology *349*, 9-23.
Geissler A, Chacinska A, Truscott KN, Wiedemann N, Brandner K, Sickmann A, Meyer HE, Meisinger C, Pfanner N, and Rehling P (2002). The mitochondrial presequence translocase: an essential role of Tim50 in directing preproteins to the import channel. Cell *111*, 507-518.
Genova ML, Castelluccio C, Fato R, Parenti Castelli G, Merlo Pich M, Formiggini G, Bovina C, Marchetti M, and Lenaz G (1995). Major changes in complex I activity in mitochondria from aged rats may not be detected by direct assay of NADH:coenzyme Q reductase. The Biochemical journal *311*, 105-109.
Gerfen CR (1992). The neostriatal mosaic: multiple levels of compartmental organization. Trends in Neurosciences *15*.
Geyer MA, and Dulawa SC (2003). Assessment of murine startle reactivity, pre-pulse inhibition and habituation. Current Protocols in Neuroscience *8*, 8-17.
Geyer MA, Krebs-Thomson K, Braff DL, and Swerdlow NR (2001). Pharmacological studies of prepulse inhibition models of sensorimotor gating deficits in schizophrenia: a decade in review. Psychopharmacology *156*, 117-154.

Gibson GE, Haroutunian V, Zhang H, Park LC, Shi Q, Lesser M, Mohs RC, Sheu RK, and Blass JP (2000). Mitochondrial damage in Alzheimer's disease varies with apolipoprotein E genotype. Annals of neurology *48*, 297-303.
Glenner GG, and Wong CW (1984). Alzheimer's disease: Initial report of the purification and characterization of a novel cerebrovascular amyloid protein Biochemical and Biophysical Research Communications *120*, 885-890.
Gnaiger E (2008). Polarographic oxygen sensor, the oxygraph, and high-resolution respirometry to assess mitochondrial function. In Drug-Induced Mitochondrial Dysfunction Will JADaY (John Wiley & Sons Inc), pp. 327-352.
Gnaiger E (2010). The Oxygraph for High-Resolution Respirometry (HRR) Mitochondrial Physiology Network *06.01*, 1-18.
Gnaiger E, Mendez G, and Hand SC (2000). High phosphorylation efficiency and depression of uncoupled respiration in mitochondria under hypoxia. Proceedings of the National Academy of Sciences of the United States of America *97*, 11080-11085
Gómez LA, Monette JS, Chavez JD, Maier CS, and Hagen TM (2009). Supercomplexes of the mitochondrial electron transport chain decline in the aging rat heart. Archieves of Biochemistry and Biophysik *490*, 30-35.
Gossler A, Joyner AL, Rossant J, and Skarnes WC (1989). Mouse embryonic stem cells and reporter constructs to detect developmentally regulated genes. Science *244*, 463-465.
Gotow T, Miyaguchi K, and Hashimoto PH (1991). Cytoplasmic architecture of the axon terminal: filamentous strands specifically associated with synaptic vesicles. Neuroscience *40*, 587-598.
Gottlieb E, Armour SM, Harris MH, and Thompson CB (2003). Mitochondrial membrane potential regulates matrix configuration and cytochrome c release during apoptosis. Cell death and differentiation *10*, 709-717.
Grafstein B (1969). Axonal transport: communication between soma and synapse. Advances in biochemical psychopharmacology *1*.
Graham BH, Waymire KG, Cottrell B, Trounce IA, MacGregor GR, and Wallace DC (1997). A mouse model for mitochondrial myopathy and cardiomyopathy resulting from a deficiency in the heart/muscle isoform of the adenine nucleotide translocator. Nature Genetics *16*, 226-234.
Graßhoff G, and May M (2003). Hans Krebs' and Kurt Henseleit's Laboratory Notebooks and Their Discovery of the Urea Cycle-Reconstructed with Computer Models. Archimedes *7*, 269-294.
Green MC (1989). Catalog of mutant genes and polymorphic loci (Oxford: Oxford University Press).
Greenbaum D, Colangelo C, Williams K, and Gerstein M (2003). Comparing protein abundance and mRNA expression levels on a genomic scale. Genome Biology *4*, 117.
Greene JG, and Greenamyre JT (1996). Bioenergetics and glutamate excitotoxicity. Progress in Neurobiology *48*, 613-634.
Gresser MJ, Myers JA, and Boyer PD (1982). Catalytic site cooperativity of beef heart mitochondrial F1 adenosine triphosphatase. Correlations of initial velocity, bound intermediate, and oxygen exchange measurements with an alternating three-site model. Journal of Biological Chemistry *257*, 12030-12038.
Grossman LI, and Lomax MI (1997). Nuclear genes for cytochrome c oxidase. Biochimica et Biophysica Acta *1352*, 174-192.
Grundke-Iqbal I, Iqbal K, Quinlan M, Tung Y-C, Zaidi MS, and Wisniewski HM (1986). Microtubule-associated Protein Tau. A component of Alzheimer paired helical filaments. The Journal of Biological Chemistry *261*, 6084-6089.
Grupe A, Abraham R, Li Y, Rowland C, Hollingworth P, Morgan A, Jehu L, Segurado R, Stone D, Schadt E*, et al.* (2007). Evidence for novel susceptibility genes for late-onset Alzheimer's disease from a genome-wide association study of putative functional variants. Human Molecular Genetics *16*, 865-873.
Guo Y, Xiao P, Lei S, Deng F, Xiao GG, Liu Y, Chen X, Li L, Wu S, Chen Y*, et al.* (2008). How is mRNA expression predictive for protein expression? A correlation study on human circulating monocytes. Acta biochimica et biophysica Sinica (Shanghai) *40*, 426-436.

Haas RH, Nasirian F, Nakano K, Ward D, Pay M, Hill R, and Shults CW (1995). Low platelet mitochondrial complex I and complex II/III activity in early untreated Parkinson's disease. Annals of Neurology *37*, 714-722.
Habib SJ, Waizenegger T, Lech M, Neupert W, and Rapaport D (2005). Assembly of the TOB complex of mitochondria. Journal of Biological Chemistry *280*, 6434-6440.
Hägerhäll C (1997). Succinate: quinone oxidoreductases - Variations on a conserved theme. Biochimica et Biophysica Acta *1320*, 107-141.
Hansen J, Floss T, Van Sloun P, Fuchtbauer EM, Vauti F, Arnold HH, Schnutgen F, Wurst W, von Melchner H, and Ruiz P (2003). A large-scale, gene-driven mutagenesis approach for the functional analysis of the mouse genome. Proceedings of the National Academy of Sciences of the United States of America *100*, 9918-9922.
Hansson Petersen CA, Alikhani N, Behbahani H, Wiehager B, Pavlov PF, Alafuzoff I, Leinonen V, Ito A, Winblad B, Glaser E, and Ankarcrona M (2008). The amyloid beta-peptide is imported into mitochondria via the TOM import machinery and localized to mitochondrial cristae. Proceedings of the National Academy of Sciences of the United States of America *105*, 13145-13150.
Hart Z, Chang C, DiMauro S, Farooki Q, and Ayyar R (1978). Muscle carnitine deficiency and fatal cardiomyopathy. Neurology *28*, 147-151.
Hastings MH, Maywood ES, and Reddy AB (2008). Two decades of circadian time. Journal of Neuroendocrinology *20*, 812-819.
Hatefi Y (1985). The mitochondrial electron transport and oxidative phosphorylation system. Annual review of biochemistry *54*, 1015-1069.
Hatefi Y, Haavik AG, and Griffiths DE (1962). Studies on the electron transfer system. XL. Preparation and properties of mitochondrial DPNH-coenzyme Q reductase. The Journal of Biological Chemistry *237*, 1676-1680.
Hausladen A, and Fridovich I (1994). Superoxide and peroxynitrite inactivate aconitases, but nitric oxide does not. The Journal of Biological Chemistry *269*, 29405-29408.
Hausladen A, and Fridovich I (1996). Measuring nitric oxide and superoxide: rate constants for aconitase reactivity. Methods in Enzymology *269*, 37-41.
Hayashi J-I, Ohta S, Kagawa Y, Takai D, Miyabayashi S, Tada K, Fukushima H, Inui K, Okada S, Goto Y-I, and Nonaka I (1994). Functional and morphological abnormalities of mitochondria in human cells containing mitochondrial DNA with pathogenic point mutations in tRNA genes. Journal of Biological Chemistry *269*, 19060-19066.
He L, Chinnery PF, Durham SE, Blakely EL, Wardell TM, Borthwick GM, Taylor RW, and Turnbull DM (2002). Detection and quantification of mitochondrial DNA deletions in individual cells by real-time PCR. Nucleic Acids Research *30*, e68.
Hegde P, Qi R, Abernathy K, Gay C, Dharap S, Gaspard R, Hughes JE, Snesrud E, Lee N, and Quackenbush J (2000). A concise guide to cDNA mi-croarray analysis-II. Biotechniques *29*, 548-556.
Hejl AM, Glenthøj B, Mackeprang T, Hemmingsen R, and Waldemar G (2004). Prepulse inhibition in patients with Alzheimer's disease. Neurobiology of aging *25*, 1045-1050.
Hermann JM, and Neupert W (2000). Protein transport into mitochondria Current Opinion in Microbiology *3*, 210-214.
Hill K, Model K, Ryan MT, Dietmeier K, Martin F, Wagner R, and Pfanner N (1998). Tom40 forms the hydrophilic channel of the mitochondrial import pore for preproteins Nature *395*, 516-521.
Hillgartner FB, Salati LM, and Goodridge AG (1995). Physiological and molecular mechanisms involved in nutritional regulation of fatty acid synthesis. Physiological Reviews *75*, 47-76.
Hines V, Brandt A, Griffiths G, Horstmann H, Brütsch H, and Schatz G (1990). Protein import into yeast mitochondria is accelerated by the outer membrane protein MAS70. The EMBO Journal *9*, 3191-3200.
Hirst J, Carroll J, Fearnley IM, Shannon RJ, and Walker JE (2003). The nuclear encoded subunits of complex I from bovine heart mitochondria. Biochimica et Biophysica Acta *1604*, 135-160.

Hogeboom GH, Claude A, and Hotch-kiss RD (1946). The distribution of cytochrome oxidase and succinoxidase in the cytoplasm of the mammalian liver cell. The Journal of biological chemistry *165*, 615-629.
Hollenbeck PJ (1996). The pattern and mechanism of mitochondrial transport in axons. Frontiers in bioscience : a journal and virtual library. *1*, d91-102.
Hollenbeck PJ, and Saxton WM (2005). The axonal transport of mitochondria. Journal of cell science *118*, 5411-5419.
Holt IJ, Harding AE, and Morgan-Hughes JA (1988). Deletions of muscle mitochondrial DNA in patients with mitochondrial myopathies. Nature
Deletions of muscle mitochondrial DNA in patients with mitochondrial myopathies.
Hong MG, Alexeyenko A, Lambert JC, Amouyel P, and Prince JA (2010). Genome-wide pathway analysis implicates intracellular transmembrane protein transport in Alzheimer disease. Journal of Human Genetics *55*, 707-709.
Hönlinger A, Bömer U, Alconada A, Eckerskorn C, Lottspeich F, Dietmeier K, and Pfanner N (1996). Tom7 modulates the dynamics of the mitochondrial outer membrane translocase and plays a pathway-related role in protein import. The EMBO Journal *15*, 2125-2137.
Horsch M, Schädler S, Gailus-Durner V, Fuchs H, M.H., ,, Hrabě de Angelis M, and Beckers J (2008). Systematic gene expression profiling of mouse model series reveals coexpressed genes. Proteomics *8*, 1248-1256.
Hosler JP, Ferguson-Miller S, and Mills DA (2006). Energy transduction: proton transfer through the respiratory complexes. Annual review of biochemistry *75*.
Houghton FD, Thompson JG, Kennedy CJ, and Leese HJ (1996). Oxygen consumption and energy metabolism of the early mouse embryo. Molecular reproduction and development *44*, 476-485.
Houle-Leroy P, Garland T Jr, Swallow JG, and Guderley H (2000). Effects of voluntary activity and genetic selection on muscle metabolic capacities in house mice Mus domesticus. Journal of Applied Physiology *89*, 1608-1616.
Hrabé de Angelis MH, Flaswinkel H, Fuchs H, Rathkolb B, Soewarto D, Marschall S, Heffner S, Pargent W, Wuensch K, Jung M*, et al.* (2000). Genome-wide, large-scale production of mutant mice by ENU mutagenesis. Nature Genetics *25*.
Hsu LJ, Sagara Y, Arroyo A, Rockenstein E, Sisk A, Mallory M, Wong J, Takenouchi T, Hashimoto M, and Masliah E (2000). Alpha-synuclein promotes mitochondrial deficit and oxidative stress. The American journal of pathology *157*, 401-410.
Hui M, and Tenenbaum HC (1998). New face of an old enzyme: alkaline phosphatase may contribute to human tissue aging by inducing tissue hardening and calcification. The Anatomical record *253*, 91-94.
Ide T, Tsutsui H, Kinugawa S, Utsumi H, Kang D, Hattori N, Uchida K, Arimura K, Egashira K, and Takeshita A (1999). Mitochondrial electron transport complex I is a potential source of oxygen free radicals in the failing myocardium. Circulation Research *85*, 357-363.
Igney FH, and Krammer PH (2002). Death and anti-death: tumour resistance to apoptosis. Nature Reviews. Cancer *2*, 277-288.
Inoue K, Nakada K, Ogura A, Isobe K, Goto Y, Nonaka I, and Hayashi JI (2000). Generation of mice with mitochondrial dysfunction by introducing mouse mtDNA carrying a deletion into zygotes. Nature Genetics *26*, 176-181.
Iseri PK, Altinaş O, Tokay T, and Yüksel N (2006). Relationship between cognitive impairment and retinal morphological and visual functional abnormalities in Alzheimer disease. Journal of neuro-ophthalmology : the official journal of the North American Neuro-Ophthalmology Society *26*, 18-24.
Ishikawa D, Yamamoto H, Tamura Y, Moritoh K, and Endo T (2004). Two novel proteins in the mitochondrial outer membrane mediate β-barrel protein assembly. The Journal of Cell Biology *166*, 621-627.
Iwata S, Lee JW, Okada K, Lee JK, Iwata M, Rasmussen B, Link TA, Ramaswamy S, and Jap BK (1998). Complete structure of the 11-subunit bovine mitochondrial cytochrome bc1 complex. Science *281*, 64-71.
James DI, Parone PA, Mattenberger Y, and Martinou JC (2003). hFis1, a novel component of the mammalian mitochondrial fission machinery. The Journal of Biological Chemistry *278*.

Janssen RJ, Nijtmans LG, van den Heuvel LP, and Smeitink JAM (2006). Mitochondrial complex I: Structure, function and pathology. Journal of Inherited Metabolic Disease *29*, 499-515.
Jendrach M, Pohl S, Vöth M, Kowald A, Hammerstein P, and Bereiter-Hahn J (2005). Morpho-dynamic changes of mitochondria during ageing of human endothelial cells. Mechanisms of ageing and development *126*, 813-821.
Jensen RE, and Dunn CD (2002). Protein import into and across the mitochondrial inner membrane: role of the TIM23 and TIM22 translocons. Biochimica et Biophysica Acta *1592*, 25-34.
Jeron A, Mitchell GF, Zhou J, Murata M, London B, Buckett P, Wiviott SD, and Koren G (2000). Inducible polymorphic ventricular tachyarrhythmias in a transgenic mouse model with a long Q-T phenotype. American journal of physiology. Heart and circulatory physiology *278*, 1891-1898.
Ježek P, and Urbánková E (2000). Specific sequence of motifs of mitochondrial uncoupling proteins. IUBMB life *49*, 63-70.
Jolivalt CG, Calcutt NA, and Masliah E (2012). Similar pattern of peripheral neuropathy in mouse models of type 1 diabetes and Alzheimer's disease. Neuroscience *202*, 405-412.
Jonckheere AI, Smeitink JA, and Rodenburg RJ (2011). Mitochondrial ATP synthase: architecture, function and pathology. Journal of Inherited Metabolic Disease *[Epub ahead of print]*.
Jones BJ, and Roberts DJ (1968). The quantitative measurement of motor incoor-dination in naive mice using an accelerating Rota-Rod. Naunyn-Schmiedeberg's Archives of Pharmacology *259*, 211.
Jones DW, and Foy CL (1971). Herbicidal Inhibition of GA-Induced Synthesis of α-Amylase. Weed Science *19*, 595-597.
Kadenbach B, Jarausch J, Hartmann R, and Merle P (1983). Separation of mammalian cytochrome c oxidase into 13 polypeptides by a sodium dodecyl sulfate-gel electrophoretic procedure. Analytical biochemistry *192*, 517-521.
Kaido M, Fujimura H, Taniike M, Yoshikawa H, Toyooka K, Yorifuji S, Inui K, Okada S, Sparaco M, and Yanagihara T (1995). Focal cytochrome c oxidase deficiency in the brain and dorsal root ganglia in a case with mitochondrial encephalomyopathy (tRNA(Ile) 4269 mutation): histochemical, immunohistochemical, and ultrastructural study. Journal of the neurological sciences *131*, 170-176.
Kamboh MI (2004). Molecular Genetics of Late-Onset Alzheimer' s Disease. Annals of Human Genetics *68*, 381-404.
Kang MJ, Gil SJ, Lee JE, and Koh HC (2010). Selective vulnerability of the striatal subregions of C57BL/6 mice to paraquat. Toxicology Letters *195*, 127-134.
Kaplan ML, Cheslow Y, Vikstrom K, Malhotra A, Geenen DL, Nakouzi A, Leinwand LA, and Buttrick PM (1994). Cardiac adaptations to chronic exercise in mice. The American journal of physiology. *267*, H1167-1173.
Karl T, Pabst R, and von Hörsten S (2003). Behavioral phenotyping of mice in pharmacological and toxicological research. Experimental and toxicologic pathology *55*, 69-83.
Kassenbrock CK, Cao W, and Douglas MG (1993). Genetic and biochemical characterization of ISP6, a small mitochondrial outer membrane protein associated with the protein translocation complex. The EMBO Journal *12*, 3023-3034.
Katayama S, Tomaru Y, Kasukawa T, Waki K, Nakanishi M, Nakamura M, Nishida H, Yap CC, Suzuki M, Kawai J*, et al.* (2005). Antisense transcription in the mammalian transcriptome. Science *309*, 1564-1566.
Kauranen K, and Vanharanta H (1996). Influences of aging, gender, and handedness on motor performance of upper and lower extremities. Perceptual and motor skills *82*, 515-525.
Keaney JF Jr (1999). Oxidative Stress and Vascular Disease (Developments in Cardiovascular Medicine), Vol 1 (Springer US).
Kearns TP, and Sayre GP (1958). Retinitis pigmentosa, external ophthalmoplegia, and complete heart block: Unusual syndrome with histologic study in one of two cases. A.M.A Archives of Ophthalmology *60*, 280-289.

Keeney PM, Xie J, Capaldi RA, and Bennett JP Jr (2006). Parkinson's disease brain mitochondrial complex I has oxidatively damaged subunits and is functionally impaired and misassembled. The Journal of Neuroscience *26*, 5256-5264.
Kelly PH, Bondolfi L, Hunziker D, Schlecht HP, Carver K, Maguire E, Abramowski D, Wiederhold KH, Sturchler-Pierrat C, Jucker M*, et al.* (2003). Progressive age-related impairment of cognitive behavior in APP23 transgenic mice. Neurobiology of aging *24*, 365-378.
Kennedy EP, and Lehninger AL (1949). Oxidation of fatty acids and tricarboxylic acid cycle intermediates by isolated rat liver mitochondria. The Journal of Biological Chemistry *179*.
Kennedy MC, Emptage MH, Dreyer JL, and Beinert H (1983). The role of iron in the activation-inactivation of aconitase. The Journal of Biological Chemistry *258*, 11098-11105.
Kernec F, Unlü M, Labeikovsky W, Minden JS, and Koretsky AP (2001). Changes in the mitochondrial proteome from mouse hearts deficient in creatine kinase. Physiological genomics *6*, 117-128.
Kiebler M, Keil P, Schneider H, van der Klei IJ, Pfanner N, and Neupert W (1993). The mitochondrial receptor complex: a central role of MOM22 in mediating preprotein transfer from receptors to the general insertion pore. Cell *74*, 483-492.
Kiebler M, Pfaller R, Söllner T, Griffiths G, Horstmann H, Pfanner N, and Neupert W (1990). Identification of a mitochondrial receptor complex required for recognition and membrane insertion of precursor proteins. Nature *348*, 610-616.
Kish SJ, Bergeron C, Rajput A, Dozic S, Mastrogiacomo F, Chang LJ, Wilson JM, DiStefano LM, and Nobrega JN (1992). Brain cytochrome oxidase in Alzheimer's disease. Journal of Neurochemistry *59*, 776-779.
Kita K, Oya H, Cennis RB, Ackrelltt BAC, and Kasaharatt M (1990). Human complex II (succinate-ubiquinone oxidoreductase): cDNA cloning of Iron sulfur (Ip) subunit of liver mitochondria. Biochemical and Biophysical Research Communications *166*, 101-108.
Kitada T, Asakawa S, Hattori N, Matsumine H, Yamamura Y, Minoshima S, Yokochi M, Mizuno Y, and Shimizu N (1998). Mutations in the parkin gene cause autosomal recessive juvenile parkinsonism. Nature *392*, 605-608.
Kiyosawa H, Yamanaka I, Osato N, Kondo S, and Members., H.Y.R.G.G.G. (2003). Antisense transcripts with FANTOM2 clone set and their implications for gene regulation. Genome Research *13*, 1324-1334.
Kodsi MH, and Swerdlow NR (1997). Mitochondrial toxin 3-nitropropionic acid pro-duces startle reflex abnormalities and striatal damage in rats that model some features of Huntinton's disease. Neuroscience Letters *231*, 103-107.
Koppen M, and Langer T (2007). Protein degradation within mitochondria: versatile activities of AAA proteases and other peptidases. Critical reviews in biochemistry *42*, 221-242.
Korpi ER, Koikkalainen P, Vekovischeva OY, Makela R, Kleinz R, Uusi-Oukari M, and Wisden W (1999). Cerebellar granule-cell-specific GABAA receptors attenuate benzodiazepine-induced ataxia. European Journal of Neuroscience *11*, 233-240.
Kovermann P, Truscott KN, Guiard B, Rehling P, Sepuri NB, Müller H, Jensen RE, Wagner R, and Pfanner N (2002). Tim22, the essential core of the mitochondrial protein insertion complex, forms a voltage-activated and signal-gated channel. Molecular Cell *9*, 363-373.
Kozjak V, Wiedemann N, Milenkovic D, Lohaus C, Meyer HE, Guiard B, Meisinger C, and Pfanner N (2003). An essential role of Sam50 in the protein sorting and assembly machinery of the mitochondrial outer membrane. Journal of Biological Chemistry *278*, 48520-48523.
Krauss S, Zhang CY, and Lowell BB (2005). The mitochondrialuncoupling-protein homologues. An up-to-date review on the biochemical regulationof UCPs. Nature Reviews Molecular Cell Biology *6*, 248-261.
Krebs HA, and Weitzman PDJ (1987). Krebs' citric acid cycle: half a century and still turning (London: Biochemical Society).
Kroemer G, Galluzzi L, and Brenner C (2007). Mitochondrial membrane permeabilization in cell death. Physiological reviews *87*, 99-163.
Kunkel-Bagden E, Dai HN, and Bregman BS (1993). Methods to assess the development and recovery of locomotor function after spinal cord injury in rats. Experimental neurology *119*, 153-164.

Künkele K, Heins S, Dembowski M, Nargang F, Benz R, Thieffry M, Walz J, Lill R, Nussberger S, and Neupert W (1998). The Preprotein Translocation Channel of the Outer Membrane of Mitochondria Cell *93*, 1009-1019.
Kutik S, Stojanovski D, Becker L, Becker T, Meinecke M, Krüger V, Prinz C, Meisinger C, Guiard B, Wagner R*, et al.* (2008). Dissecting membrane insertion of mitochondrial b-barrel proteins. Cell *132*.
Kuznetsov AV, Strobl D, Ruttmann E, Königsrainer A, Margreiter R, and Gnaiger E (2002). Evaluation of Mitochondrial Respiratory Function in Small Biopsies of Liver. Anal Biochem. *305*, 186-194.
Labrie F, Belanger A, Simard J, Van L-T, and Labrie C (1995). DHEA and peripheral androgen and estrogen formation: intracrinology. Annals of the New York Academy of Sciences *774*.
LaFratta CW, and Canestrari R (1966). A comparison of sensory and motor nerve conduction velocities as related to age. Archives of physical medicine and rehabilitation *47*, 286-290.
LaFratta CW, and Zalis A (1973). Age effects on sural nerve conduction velocity. Archives of physical medicine and rehabilitation *54*, 475-477.
Lalonde R, Dumont M, Staufenbiel M, and Strazielle C (2005). Neurobehavioral characterization of APP23 transgenic mice with the SHIRPA primary screen. Behavioural Brain Research *157*, 91-98.
Lambert AJ, and Brand MD (2004). Inhibitors of the quinone-binding site allow rapid superoxide production from mitochondrial NADH:ubiquinone oxidoreductase (complex I). The Journal of biological chemistry *279*, 39414-39420.
Lapidot M, and Pilpel Y (2004). Genome-wide natural antisense transcription: coupling its regulation to its different regulatory mechanisms. EMBO Reports *7*, 1216-1222.
Lapointe J, and Hekimi S (2010). When a theory of aging ages badly. Cellular and Molecular Life Sciences *67*, 1-8.
Larsson NG, Wang J, Wilhelmsson H, Oldfors A, Rustin P, Lewandoski M, Barsh GS, and Clayton DA (1998). Mitochondrial transcription factor A is necessary for mtDNA maintenance and embryogenesis in mice. Nature Genetics *18*, 231-236.
Lau YS, Patki G, Das-Panja K, Le WD, and Ahmad SO (2011). Neuroprotective effects and mechanisms of exercise in a chronic mouse model of Parkinson's disease with moderate neurodegeneration. The European journal of neuroscience. *33*, 1264-1274.
Leber T (1871). Uber hereditare und congenital-angelegte Sehnervenleiden. Graefe's Archive for Clinical and Experimental Ophthalmology *17*, 249-291.
Lee CS, Sauer H, and Bjorklund A (1996). Dopaminergic neuronal degeneration and motor impairments following axon terminal lesion by instrastriatal 6-hydroxydopamine in the rat. Neuroscience *72*, 641-653.
Lee HJ, and DeLisa J (2004). Manual of Nerve Conduction Study and Surface Anatomy for Needle Electromyography 4.th edn (Lippincott Williams & Wilkins).
Leeuwenburgh C, Pamplona R, and Sanz A (2011). Mitochondria and Ageing. Journal of Aging Research *2011*, 3 pages.
Leng A, Yee BK, Feldon J, and Ferger B (2004). Acoustic startle response, prepulse inhibition, and spontaneous locomotor activity in MPTP-treated mice. Behavioural Brain Research *154*, 449-456.
Lesnefsky EJ, Gudzc TI, Moghaddas S, Migita CT, Ikeda-Saito M, Turkaly PJ, and Hoppel CL (2001). Aging Decreases Electron Transport Complex III Activity in Heart Interfibrillar Mitochondria by Alteration of the Cytochrome c Binding Site. Journal of Molecular and Cellular Cardiology *33*, 37-47.
Li F, Calingasan NY, Yu F, Mauck WM, Toidze M, Almeida CG, Takahashi RH, Carlson GA, Flint Beal M, Lin MT, and Gouras GK (2004). Increased plaque burden in brains of APP mutant MnSOD heterozygous knockout mice. Journal of Neurochemistry *89*, 1308-1312.
Li YY, Qin L, Guo ZM, Liu L, Xu H, Hao P, Su J, Shi Y, He WZ, and Li YX (2006). In silico discovery of human natural antisense transcripts. BMC Bioinformatics *7*, 18.
Limdi JK, and Hyde GM (2003). Evaluation of abnormal liver function tests. Postgraduate medical journal *79*, 307-312.

Little PFR (2005). Structure and function of the human genome. Genome Research *15*, 1759-1766.
Livaka KJ, and Schmittgen TD (2001). Analysis of Relative Gene Expression Data Using Real-Time Quantitative PCR and the 2−ΔΔCT Method. Methods *25*, 402-408.
Loeb V, Yakunin E, Saada A, and Sharon R (2010). The transgenic overexpression of alpha-synuclein and not its related pathology associates with complex I inhibition. The Journal of Biological Chemistry *285*, 7334-7343.
Loeffen JL, Smeitink JA, Trijbels JM, Janssen AJ, Triepels RH, Sengers RC, and van den Heuvel LP (2000). Isolated complex I deficiency in children: clinical, biochemical and genetic aspects. Human Mutation *15*, 123-134.
Loeffler DA, DeMaggio AJ, Juneau PL, Havaich MK, and LeWitt PA (1994). Effects of enhanced striatal dopamine turnover in vivo on glutathione oxidation. Clinical neuropharmacology *17*, 370-379.
Lowell BB, and Shulman GI (2005). Mitochondrial Dysfunction and Type 2 Diabetes. Science *307*, 384-387.
Lowenstein JM (1969). Methods in Enzymology, Vol 13: Citric Acid Cycle (Boston: Academic Press).
MacLennan DH, and Tzagoloff A (1968). Studies on the mitochondrial adenosine triphosphatase system. IV. Purification and characterization of the oligomycin sensitivity conferring protein. Biochemistry *7*, 1603-1610.
Manis JP (2007). Knock Out, Knock In, Knock Down - Genetically Manipulated Mice and the Nobel Prize. The New England Journal of Medicine *357*, 2426-2429.
Mansbach RS, Brooks EW, Sanner MA, and Zorn SH (1998). Selective dopamine D4 receptor antagonists reverse apomorphine-induced blockade of prepulse inhibition. Psychopharmacology *135*, 194-200.
Marmolino D (2011). Friedreich's ataxia: Past, present and future. Brain Research Reviews *67*, 311-330.
Martin LJ, Pan Y, Price AC, Sterling W, Copeland NG, Jenkins NA, Price DL, and Lee MK (2006). Parkinson's disease alpha-synuclein transgenic mice develop neuronal mitochondrial degeneration and cell death. The Journal of Neuroscience *16*, 41-50.
Martin R, Vaida B, Bleher R, Crispino M, and Giuditta A (1998). Protein synthesizing units in presynaptic and postsynaptic domains of squid neurons. Journal of Cell Science *111*, 3157-3166.
Martyn CN, and Hughes RA (1997). Epidemiology of peripheral neuropathy. Journal of neurology, neurosurgery, and psychiatry *62*, 310-318.
Masters CL, Simms G, Weinman NA, Multhaup G, McDonald BL, and Beyreuther K (1985). Amyloid plaque core protein in Alzheimer disease and Down syndrome. Proceedings of the National Academy of Sciences of the United States of America *82*, 4245-4249.
Matsuura K, Kabuto H, Makino H, and Ogawa N (1997). Pole test is a useful method for evaluating the mouse movement disorder caused by striatal dopamine depletion. Journal of Neuroscience Methods *73*, 45-48.
Mattson MP, Gleichmann M, and Cheng A (2008). Mitochondria in Neuroplasticity and Neurological Disorders. Neuron *60*, 748-766.
Maurer I, Zierz S, and Möller HJ (2000). A selective defect of cytochrome c oxidase is present in brain of Alzheimer disease patients. Neurobiology of aging *21*, 455-462.
Mayer A, Nargang FE, Neupert W, and Lill R (1995a). MOM22 is a receptor for mitochondrial targeting sequences and cooperates with MOM19. EMBO J. *14*, 4204-4211.
Mayer A, Neupert W, and Lill R (1995b). Mitochondrial protein import: reversible binding of the presequence at the trans side of the outer membrane drives partial translocation and unfolding. Cell *80*, 127-137.
Mayer RF (1963). Nerve conduction studies in man. Neurology *13*, 1021-1030.
McGarry JD, and Brown NF (1997). The mitochondrial carnitine palmitoyltransferase system. From concept to molecular analysis. European Journal of Biochemistry *244*, 1-14.
McGarry JD, Woeltje KF, Kuwajima M, and Foster DW (1989). Regulation of ketogenesis and the renaissance of carnitine palmitoyltransferase. Diabetes/metabolism reviews *5*, 271-284.

McGregor A, Temperley R, Chrzanowska-Lightowlers ZM, and Lightowlers RN (2001). Absence of expression from RNA internalised into electroporated mammalian mitochondria. Molecular Genetics & Genomica *265*, 751-729.
McKechnie NM, King M, and Lee WR (1985). Retinal pathology in the Kearns-Sayre syndrome. The British journal of ophthalmology *69*, 63-75.
McKenzie M, Lazarou M, Thorburn DR, and Ryan MT (2006). Mitochondrial respiratory chain supercomplexes are destabilized in Barth Syndrome patients. Journal of molecular biology *361*, 462-469.
Meisinger C, Rissler M, Chacinska A, Szklarz LK, Milenkovic D, Kozjak V, Schönfisch B, Lohaus C, Meyer HE, Yaffe MP*, et al.* (2004). The mitochondrial morphology protein Mdm10 functions in assembly of the preprotein translocase of the outer membrane. Developmental Cell *7*, 61-71.
Méndez G, and Gnaiger E (1994). How does oxygen pressure control oxygen flux in isolated mitochondria? A methodological approach by high-resolution respirometry and digital data analysis. Modern Trends in BioThermo-Kinetics 3. Innsbruck Univ. Press, 191-194.
Mesecke N, Terziyska N, Kozany C, Baumann F, Neupert W, Hell K, and Herrmann JM (2005). A disulfide relay system in the intermembrane space of mitochondria that mediates protein import. Cell *121*, 1059-1069.
Metz GA, and Whishaw IQ (2002). Cortical and subcortical lesions impair skilled walking in the ladder rung walking test: a new task to evaluate fore- and hindlimb stepping, placing, and co-ordination. Journal of Neuroscience Methods 115 *115*, 169-179.
Metz GA, and Whishaw IQ (2009). The Ladder Rung Walking Task: A Scoring System and its Practical Application. Journal of Visualized Experiments *http://www.jove.com/details.php?id=1204*
Meyer CW, Klingenspor M, Rozman J, and Heldmaier G (2004). Gene or size: metabolic rate and body temperature in obese growth hormone-deficient dwarf mice. Obesity Research *12*, 1509.
Mitchell P (1961). Coupling of Phosphorylation to Electron and Hydrogen Transfer by a Chemi-Osmotic type of Mechanism. Nature 191, 144 - 148 *191*, 144-148.
Mitchell P (1975). The protonmotive Q cycle: a general formulation. FEBS Letters *59*, 137-139.
Mizuno Y, Ohta S, Tanaka M, Takamiya S, Suzuki K, Sato T, Oya H, Ozawa T, and Kagawa Y (1989). Deficiencies in complex I subunits of the respiratory chain in Parkinson's disease. Biochemical and biophysical research communications *163*, 1450-1455.
Moczko M, Dietmeier K, Söllner T, Segui B, Steger HF, Neupert W, and Pfanner N (1992). Identification of the mitochondrial receptor complex in Saccharomyces cerevisiae. FEBS Letters *310*, 265-268.
Moczko M, Gärtner F, and Pfanner N (1993). The protein import receptor MOM19 of yeast mitochondria. FEBS Letters *326*, 251-254.
Mokranjac D, and Neupert W (2005). Protein import into mitochondria. Biochemical Society transactions *33*, 1019-1023.
Mokranjac D, Paschen SA, Kozany C, Prokisch H, Hoppins SC, Nargang FE, Neupert W, and Hell K (2003). Tim50, a novel component of the TIM23 preprotein translocase of mitochondria. The EMBO Journal *22*, 816-825.
Mokranjac D, Sichting M, Popov-Celeketic D, Mapa K, Gevorkyan-Airapetov L, Zohary K, Hell K, Azem A, and Neupert W (2009). Role of Tim50 in the transfer of precursor proteins from the outer to the inner membrane in mitochondria. Molecular Biology of the Cell *20*, 1400-1407.
Mootha VK, Lindgren CM, Eriksson KF, Subramanian A, Sihag S, Lehar J, Puigserver P, Carlsson E, Ridderstråle M, Laurila E*, et al.* (2003). PGC-1alpha-responsive genes involved in oxidative phosphorylation are coordinately downregulated in human diabetes. Nature Genetics *34*, 267-273.
Moreira PI, Honda K, Liu Q, Santos MS, Oliveira CR, Aliev G, Nunomura A, Zhu X, Smith MA, and Perry G (2005). Oxidative stress: the old enemy in Alzheimer's disease pathophysiology. Current Alzheimer Research *2*, 403-408.

Morris RL, and Hollenbeck PJ (1993). The regulation of bidirectional mitochondrial transport is coordinated with axonal outgrowth. Journal of cell science *104*, 917-927.
Morton AJ, Wood NI, Hastings MH, Hurelbrink C, Barker RA, and Maywood ES (2005). Disintegration of the sleep-wake cycle and circadian timing in Huntington's disease. The Journal of Neuroscience *25*, 157-163.
Moss DW (1982). Alkaline phosphatase isoenzymes. Clinical Chemistry *28*, 2007-2016.
Müller E, and Pearse AG (1969). The effect of catecholamines on alkaline phosphatase activity in rat heart. Cardiovascular Research *3*, 391-395.
Muller FL, Liu Y, and Van Remmen H (2004). Complex III releases superoxide to both sides of the inner mitochondrial membrane. Journal of Biological Chemistry *279*, 49064-49073.
Müller W, Weber H, Meyer F, and Weissmann C (1978). Site-directed mutagenesis in DNA: Generation of point mutations in cloned β globin complementary DNA at the positions corresponding to amino acids 121 to 123. Journal of Molecular Biology *124*, 343-358.
Murakami K, and Yoshino M (1997). Inactivation of aconitase in yeast exposed to oxidative stress. Biochemistry and molecular biology international *41*, 481-486.
Mutisya EM, Bowling AC, and Beal MF (1994). Cortical Cytochrome Oxidase Activity Is Reduced in Alzheimer's Disease. Journal of Neurochemistry *63*, 2179-2184.
Mutsaers SE, and Carroll WM (1998). Focal accumulation of intra-axonal mitochondria in demyelination of the cat optic nerve. Acta neuropathologica *96*, 139-143.
Nakada K, Inoue K, and Hayashi JI (2001). Mito-mice: animal models for mitochondrial DNA-based diseases. Seminars in Cell & Developmental Biology *12*, 459-465.
Nakada K, Sato A, Sone H, Kasahara A, Ikeda K, Kagawa Y, Yonekawa H, and Hayashi J (2004). Accumulation of pathogenic DeltamtDNA induced deafness but not diabetic phenotypes in mito-mice. Biochemical and Biophysical Research Communications *323*, 175-184
Nakamoto RK, Ketchum CJ, and al-Shawi MK (1999). Rotational coupling in the F0F1 ATP synthase. Annual review of biophysics and biomolecular structure. *28*, 205-234.
Nass S, and Nass MMK (1963). Ultramitochondrial fibers with DNA characteristics. The Journal of Cell Biology *19*, 593-629.
Nelson DL, and Cox MM (2008). Lehninger Principles of Biochemistry 5edn (W. H. Freeman).
Neupert W (1997). Protein import into mitochondria. Annual review of biochemistry *66*, 863-917.
Neupert W, and Herrmann JM (2007). Translocation of Proteins into Mitochondria. Annual review of biochemistry *76*, 723-749.
Niemann S, and Müller U (2000). Mutations in SDHC cause autosomal dominant paraganglioma, type 3. Nature Genetics *26*, 268-270.
Norris AH, Shock NW, and Wagman IH (1953). Age Changes in the Maximum Conduction Velocity of Motor Fibers of Human Ulnar Nerves. Journal of Applied Physiology *5*, 589-593.
O'Connell K, and Ohlendieck K (2009). Proteomic DIGE analysis of the mitochondria-enriched fraction from aged rat skeletal muscle Proteomics *9*, 5509-5524.
O'Brien TP, and Frankel WN (2004). Moving forward with chemical mutagenesis in the mouse. The Journal of Physiology *554*, 13-21.
Ogino K, Hisatome I, Saitoh M, Miyamoto J, Ishiko R, Hasegawa J, Kotake H, and Mashiba H (1991). Clinical significance of hypouricemia in hospitalized patients. Journal of Medicine *22*, 76-82.
Olson RE (1998). Discovery of the Lipoproteins, Their Role in Fat Transport and Their Significance as Risk Factors1. Journal of Nutrition *128*, 439S-443S.
Ortiz RG, Newman NJ, Manoukian SV, Diesenhouse MC, Lott MT, and Wallace DC (1992). Optic disk cupping and electrocardiographic abnormalities in an American pedigree with Leber's hereditary optic neuropathy. American journal of ophthalmology *113*, 561-566.
Otani H, Tanaka O, Kasai K, and Yoshioka T (1988). Development of mitochondrial helical sheath in the middle piece of the mouse spermatid tail: regular dispositions and synchronized changes. The Anatomical record *222*, 26-33.
Palade GE (1956). Electron microscopy of mitochondria and other cytoplasmic structures (New York: Academic).

Palay SL (1956). Synapses in the central nervous system. The Journal of biophysical and biochemical cytology *2*, 193-202.
Palsdottir H, Lojero CG, Trumpower BL, and Hunte C (2003). Structure of the yeast cytochrome bc1 complex with a hydroxyquinone anion Qo site inhibitor bound. Journal of Biological Chemistry *278*, 31303-31311.
Parfait B, Chretien D, Rötig A, Marsac C, Munnich A, and Rustin P (2000). Compound heterozygous mutations in the flavoprotein gene of the respiratory chain complex II in a patient with Leigh syndrome. Human Genetics *106*, 236-243.
Park LC, Albers DS, Xu H, Lindsay JG, Beal MF, and Gibson GE (2001). Mitochondrial impairment in the cerebellum of the patients with progressive supranuclear palsy. Journal of Neuroscience Research *66*, 1028-1034.
Parker WD Jr, Parks JK, and Swerdlow RH (2008). Complex I deficiency in Parkinson's disease frontal cortex. Brain Research *1189*, 215-218.
Parks JK, Smith TS, Trimmer PA, Bennett JP Jr, and Parker WD Jr (2001). Neurotoxic Abeta peptides increase oxidative stress in vivo through NMDA-receptor and nitric-oxide-synthase mechanisms, and inhibit complex IV activity and induce a mitochondrial permeability transition in vitro. Journal of Neurochemistry *76*, 1050-1056.
Paschen SA, Neupert W, and Rapaport D (2005). Biogenesis of b-barrel membrane proteins of mitochondria. Trends in biochemical sciences *30*, 575-582.
Paschen SA, Waizenegger T, Stan T, Preuss M, Cyrklaff M, Hell K, Rapaport D, and Neupert W (2003). Evolutionary conservation of biogenesis of beta-barrel membrane proteins. Nature *426*, 862-866.
Pascuzzi RM (2009). Peripheral neuropathy. The Medical clinics of North America *93*, 317-342, vii-viii.
Patti M-E, and Corvera S (2010). The Role of Mitochondria in the Pathogenesis of Type 2 Diabetes. Endocrine Reviews *31*, 364-395.
Paumard P, Vaillier J, Coulary B, Schaeffer J, Soubannier V, Mueller DM, Brèthes D, di Rago JP, and Velours J (2002). The ATP synthase is involved in generating mitochondrial cristae morphology. The EMBO Journal *21*, 221-230.
Petkova SB, Yuan R, Tsaih S-W, Schott W, Roopenian DC, and Paigen B (2008). Genetic influence on immune phenotype revealed strain-specific varia-tions in peripheral blood lineages. Physiological genomics *34*, 304-314.
Petrozzi L, Ricci G, Giglioli NJ, Siciliano G, and Mancuso M (2007). Mitochondria and Neurodegeneration. Biocscience reports *27*, 87-104.
Pfanner N, Craig EA, and Hönlinger A (1997). Mitochondrial Preprotein Translocase. Annual Review of Cell and Developmental Biology *13*, 25-51.
Pham TT, Giesert F, Rothig A, Floss T, Kallnik M, Weindl K, Holter SM, Ahting U, Prokisch H, Becker L*, et al.* (2010). DJ-1-deficient mice show less TH-positive neurons in the ventral tegmental area and exhibit non-motoric behavioural impairments. Genes, Brain and Behaviour *9*, 305-317.
Pieper-Bigelow C, Strocchi A, and Levitt MD (1990). Where does serum amylase come from and where does it go? Gastroenterology clinics of North America *19*, 793-810.
Piko L, and Taylor KD (1987). Amounts of mitochondrial DNA and abundance of some mitochondrial gene transcripts in early mouse embryos. Developmental biology *123*, 364-374.
Pinheiro JC, and Bates DM (2000). Mixed-effects models in s and s-plus.
Pisani A, Martella G, Tscherter A, Costa C, Mercuri NB, Bernardi G, Shen J, and Calabresi P (2006). Enhanced sensitivity of DJ-1-deficient dopaminergic neurons to energy metabolism impairment: role of Na+/K+ ATPase. Neurobiology of disease *23*, 54-60.
Plaas M, Karis A, Innos J, Rebane E, Baekelandt V, Vaarmann A, Luuk H, Vasar E, and Koks S (2008). Alpha-synuclein A30P point-mutation generates age-dependent nigrostriatal deficiency in mice. Journal of physiology and pharmacology *59*, 205-216.
Poirier LJ, and Sourkes TL (1964). Influence du locus niger sur la concentration des catécholamines du striatum. Journal de physiologie (Paris) *56*, 426-427
Potkin SG, Guffanti G, Lakatos A, Turner JA, Kruggel F, Fallon JH, Saykin AJ, Orro A, Lupoli S, Salvi E*, et al.* (2009). Hippocampal atrophy as a quantitative trait in a genome-wide

association study identifying novel susceptibility genes for Alzheimer's disease. Plos Online *4*, e6501.
Povlishock JT (1976). The fine structure of the axons and growth cones of the human fetal cerebral cortex. Brain Research *114*, 379-399.
Prasad K, Tarasewicz E, Mathew J, Strickland PA, Buckley B, Richardson JR, and Richfield EK (2009). Toxicokinetics and toxicodynamics of paraquat accumulation in mouse brain. Experimental Neurology *215*, 358-367.
Pratt DS, and Kaplan MM (1999). Laboratory tests. In Schiff's diseases of the liver, Schiff ER, Sorrell MF, and Maddrey WC, eds. (Philadelphia: Lippencott-Raven), pp. 205-244.
Pratt DS, and Kaplan MM (2000). Evaluation of abnormal liver-enzyme results in asymptomatic patients. The New England journal of medicine *342*, 1266-1271.
Price DL, and Sisodia SS (1998). Mutant genes in familial Alzheimer's disease and transgenic models. Annual review of neuroscience *21*, 479-505.
Price DL, Sisodia SS, and Borchelt DR (1998). Genetic neurodegenerative diseases: the human illness and transgenic models. Science *282*, 1079-1083.
Puchowicz MA, Varnes ME, Cohen BH, Frieman NR, Kerr DS, and Hoppel CL (2004). Oxidative phosphorylation analysis: assessing the integrated functional activity of human skeletal muscle mitochondria - case studies. Mitochondrion *4*, 377-385.
Puk O, Dalke C, Calzada-Wack J, Ahmad N, Klaften M, Wagner S, Hrabe´ de Angelis M, and Graw J (2009). Reduced Corneal Thickness and Enlarged Anterior Chamber in a Novel ColVIIIa2G257D Mutant Mouse. Investigative Ophthalmology & Visual Science *50*, 5653-5661.
Quackenbush J (2002). Microarray data normalization and transformation. Nature Genetics *32*, 496-501.
Rabben OK (1995). Sensory nerve conduction studies in children. Age-related changes of conduction velocities. Neuropediatrics *26*, 26-32.
Ralph RJ, and Caine SB (2005). Dopamine D1 and D2 agonist effects on prepulse inhibition and locomotion: comparison of Sprague-Dawley rats to Swiss-Webster, 129X1/SvJ, C57BL/6J, and DBA/2J mice. The Journal of pharmacology and experimental therapeutics *312*, 733-741.
Ramage L, Junne T, Hahne K, Lithgow T, and G Schatz (1993). Functional cooperation of mitochondrial protein import receptors in yeast. The EMBO Journal *12*, 4115-4123.
Rana M, de Coo I, Diaz F, Smeets H, and Moraes CT (2000). An out-of-frame cytochrome b gene deletion from a patient with parkinsonism is associated with impaired complex III assembly and an increase in free radical production. Annals of Neurology *48*, 774-781.
Rapaport D (2002). Biogenesis of the mitochondrial TOM complex. Trends in biochemical sciences *27*, 191-197.
Reddy NS, Nimmagadda A, and Sambasiva Rao KRS (2003). An overview of the microbial α-amylase family. African Journal of Biotechnology *2*, 645-648.
Reddy S, DeGregori JV, von Melchner H, and Ruley HE (1991). Retrovirus promoter-trap vector to induce lacZ gene fusions in mammalian cells. Journal of virology *65*, 1507-1515.
Redex B (1944). Contributions to the knowledge of the post natal development of the peripheral nervous system in man. Acta Psychiatry and Neurology *33*.
Rehling P, Brandner K, and Pfanner N (2004). Mitochondrial import and the twin-pore translocase. Nature Reviews Molecular Cell Biology *5*, 519-530.
Reif DW (1992). Ferritin as a source of iron for oxidative damage. Free radical biology & medicine *12*, 417-427.
Revkin AC (1983). Paraquat: A potent weed killer is killing people. Science Digest *91*, 36-38.
Richardson JR, Quan Y, Sherer TB, Greenamyre JT, and Miller GW (2005). Paraquat neurotoxicity is distinct from that of MPTP and rotenone. Toxicological sciences : an official journal of the Society of Toxicology *88*, 193-201.
Rieske JS (1976). Composition, structure, and function of complex III of the respiratory chain. Biochimica et Biophysica Acta 456(2):195-247]
Rivera IL, Shore GC, and Schleiff E (2000). Cloning and characterization of a 35-kDa mouse mitochondrial outer membrane protein MOM35 with high homology to Tom40. Journal of Bioenergetics and Biomembranes *32*, 111-121.

Rivner MH, Swift TR, and Malik K (2001). Influence of age and height on nerve conduction. Muscle & Nerve *24*, 1134-1141.
Robbins AH, and Stout CD (1989a). The structure of aconitase. Proteins *5*, 289-312.
Robbins AH, and Stout CD (1989b). Structure of activated aconitase: formation of the [4Fe-4S] cluster in the crystal. Proceedings of the National Academy of Sciences of the United States of America *86*, 3639-3643.
Rogers DC, Fisher EM, Brown SD, Peters J, Hunter AJ, and Martin JE (1997). Behavioral and functional analysis of mouse phenotype: SHIRPA, a proposed protocol for comprehensive phenotype assessment. Mammalian Genome *8*, 711-713.
Rosca MG, Vazquez EJ, Kerner J, Parland W, Chandler MP, Stanley W, Sabbah HN, and Hoppel CL (2008). Cardiac mitochondria in heart failure: decrease in respirasomes and oxidative phosphorylation. Cardiovascular Research *80*, 30-39.
Rose IA, and O'Connell EL (1967). Mechanism of aconitase action. The hydrogen transfer reaction. The Journal of Biological Chemistry *242*, 1870-1879.
Russell LK, Finck BN, and Kelly DP (2005). Mouse models of mitochondrial dysfunction and heart failure. Journal of Molecular and Cellular Cardiology *38*, 81-91.
Russell WL, Kelly EM, Hunsicker PR, Bangham JW, Maddux SC, and Phipps EL (1979). Specific-locus test shows ethylnitrosourea to be the most potent mutagen in the mouse. Proceedings of the National Academy of Sciences of the United States of America *76*, 5818-5819.
Rustin P, Munnich A, and Rötig A (2002). Succinate dehydrogenase and human diseases: new insights into a well-known enzyme. European Journal of human genetics *10*, 289-291.
Ruthel G, and Hollenbeck PJ (2003). Response of mitochondrial traffic to axon determination and differential branch growth. The Journal of neuroscience : the official journal of the Society for Neuroscience *23*, 8618-8624.
Ryan MT, Wagner R, and Pfanner N (2000). The transport machinery for the import of preproteins across the outer mitochondrial membrane. The International Journal of Biochemistry & Cell Biology *32*, 13-21.
Saeed AI, Sharov V, White J, Li J, Lioang W, Bhagabati N, Braisted J, Klapa M, Currier T, Thiagarajan M*, et al.* (2003). TM´4: a free, open-source system for microar-ray data management and analysis. Biotechniques *34*, 374-378.
Santel A, and Fuller MT (2001). Control of mitochondrial morphology by a human mitofusin. Journal of Cell Science *114*, 857-874.
Sauleda J, García-Palmer FJ, González G, Palou A, and Agustí AG (2000). The activity of cytochrome oxidase is increased in circulating lymphocytes of patients with chronic obstructive pulmonary disease, asthma, and chronic arthritis. American journal of respiratory and critical care medicine *161*, 32-35.
Scacheri PC, Crabtree JS, Novotny EA, Garrett-Beal L, Chen A, Edgemon KA, Marx SJ, Spiegel AM, Chandrasekharappa SC, and Collins FS (2001). Bidirectional transcriptional activity of PGK-neomycin and unexpected embryonic lethality in heterozygote chimeric knockout mice. Genesis *30*, 259-263.
Schägger H, de Coo R, Bauer MF, Hofmann S, Godinot C, and Brandt U (2004). Significance of respirasomes for the assembly/stability of human respiratory chain complex I. Journal of Biological Chemistry *279*, 36349 - 36353.
Schägger H, Link TA, Engel WD, and von Jagow G (1986). Isolation of the eleven protein subunits of the bc1 complex from beef heart. Methods in Enzymology *126*, 224-237.
Schägger H, and Pfeiffer K (2000). Supercomplexes in the respiratory chains of yeast and mammalian mitochondria. The EMBO journal *19*, 1777-1783.
Schägger H, and von Jagow G (1987). Tricine-sodium dodecyl sulfate-polyacrylamide gel electrophoresis for the separation of proteins in the range from 1 to 100 kDa. Analytical Biochemistry *166*, 368-437.
Schapira AH, Cooper JM, Dexter D, Clark JB, Jenner P, and Marsden CD (1990). Mitochondrial Complex I Deficiency in Parkinson's Disease. Journal of Neurochemistry *54*, 823-827.
Schapira AH, Cooper JM, Dexter D, Jenner P, Clark JB, and Marsden CD (1989). Mitochondrial Complex I Deficiency in Parkinson's disease. Lancet *1*, 1269.

Schatz G (1996). The Protein Import System of Mitochondria. The Journal of Biological Chemistry *271*, 31763-31766.
Scheffler IE (2007). Mitochondria, 2 edn (Wiley-Liss).
Schmucker C, and Schaeffel F (2004). In vivo biometry in the mouse eye with low coherence interferometry. Vision Research *44*, 2445-2456.
Schneider H, Söllner T, Dietmeier K, Eckerskorn C, Lottspeich F, Trülzsch B, Neupert W, and Pfanner N (1991). Targeting of the master receptor MOM19 to mitochondria. Science *254*, 1659-1662.
Schultz-Hector S, Balz K, Böhm M, Ikehara Y, and Rieke L (1993). Cellular localization of endothelial alkaline phosphatase reaction product and enzyme protein in the myocardium. The journal of histochemistry and cytochemistry : official journal of the Histochemistry Society. *41*, 1813-1821.
Schwartz JH (1979). Axonal transport: components, mechanisms, and specificity. Annual review of neuroscience *2*, 467-504.
Selkoe DJ, Bell DS, Podlisny MB, Price DL, and Cork LC (1987). Conservation of brain amyloid proteins in aged mammals and humans with Alzheimer's disease. Science *235*, 873-877.
Sgobbo P, Pacelli C, Grattagliano I, Villani G, and Cocco T (2007). Carvedilol inhibits mitochondrial complex I and induces resistance to H2O2-mediated oxidative insult in H9C2 myocardial cells Biochimica et Biophysica Acta (BBA) - Bioenergetics *1767*, 222-232
Sherer TB, Betarbet R, Testa CM, Seo BB, Richardson JR, Kim JH, Miller GW, Yagi T, Matsuno-Yagi A, and Greenamyre JT (2003). Mechanism of toxicity in rotenone models of Parkinson's disease. Journal of Neuroscience *23*, 10756-10764.
Shigenaga MK, Hagen TM, and Ames BN (1994). Oxidative damage and mitochondrial decay in aging. Proceedings of the National Academy of Sciences of the United States of America *91*, 10771-10778.
Shin J Oh (2002). Clinical Electromyography: Nerve Conduction Studies, 3rd edn (Lippincott Williams and Wilkins).
Shinde S, and Pasupathy K (2006). Respiratory-chain enzyme activities in isolated mitochondria of lymphocytes from patients with Parkinson's disease: preliminary study. Neurology India *54*, 390-393.
Shoubridge EA, and Wai T (2007). Mitochondrial DNA and the mammalian oocyte. Current topics in developmental biology *77*, 87-111.
Shulman RG, Rothman DL, Behar KL, and Hyder F (2004). Energetic basis of brain activity: implications for neuroimaging. Trends in Neurosciences *27*, 489-495.
Sirk D, Zhu Z, Wadia JS, Shulyakova N, Phan N, Fong J, and Mills LR (2007). Chronic exposure to sub-lethal beta-amyloid (Abeta) inhibits the import of nuclear-encoded proteins to mitochondria in differentiated PC12 cells. Journal of neurochemistry *103*, 1989-2003.
Sirrenberg C, Bauer MF, Guiard B, Neupert W, and Brunner M (1996). Import of carrier proteins into the mitochondrial inner membrane mediated by Tim22. Nature *384*, 582-585.
Sisodia SS, and Price DL (1995). Role of the beta-amyloid protein in Alzheimer's disease. The FASEB Journal *9*, 366-370.
Sjöstranda FS, and Hanzon V (1954). Membrane structures of cytoplasm and mitochondria in exocrine cells of mouse pancreas as revealed by high resolution electron microscopy. Experimental Cell Research *7*, 393-414.
Skarnes WC, Auerbach BA, and Joyner AL (1992). A gene trap approach in mouse embryonic stem cells: the lacZ reported is activated by splicing, reflects endogenous gene expression, and is mutagenic in mice. Genes & Development *6*, 903-918.
Smirnova E, Griparic L, Shurland DL, and van der Bliek AM (2001a). Dynamin-related protein Drp1 is required for mitochondrial division in mammalian cells. Molecular biology of the cell *12*, 2245-2256.
Smirnova E, Griparic L, Shurland DL, and van Der Bliek AM (2001b). Dynamin-related protein drp1 is required for mitochondrial division in mammalian cells. Molecular Biology of the Cell *12*, 2245-2256.
Smith P, Heath D, and Kày JM (1974). The pathogenesis and structure of paraquat-induced pulmonary fibrosis in rats. The Journal of Pathology *114*, 57-67.

Smithies O (1993). Animal models of human genetic diseases. Trends in Genetics *9*, 112-116.
Soblosky JS, Colgin LL, Chorney-Lane D, Davidson JF, and Carey ME (1997). Ladder beam and camera video recording system for evaluating forelimb and hindlimb deficits after sensorimotor cortex injury in rats. Journal of neuroscience methods *78*, 75-83.
Sogo LF, and Yaffe MP (1994). Regulation of mitochondrial morphology and inheritance by Mdm10p, a protein of the mitochondrial outer membrane. Journal of Cell Biology *126*, 1361-1373.
Sohal RS, Kamzalov S, Sumien N, Ferguson M, Rebrin I, Heinrich KR, and Forster MJ (2006). Effect of coenzyme Q10 intake on endogenous coenzyme Q content, mitochondrial electron transport chain, antioxidative defenses, and life span of mice. Free radical biology & medicine *40*, 480-487.
Solenski NJ, diPierro CG, Trimmer PA, Kwan AL, and Helm GA (2002). Ultrastructural changes of neuronal mitochondria after transient and permanent cerebral ischemia. Stroke *33*, 816-824.
Söllner T, Pfaller R, Griffiths G, Pfanner N, and Neupert W (1989). MOM19, an import receptor for mitochondrial precursor proteins. Cell *59*, 1061-1070.
Söllner T, Pfaller R, Griffiths G, Pfanner N, and Neupert W (1990). A mitochondrial import receptor for the ADP/ATP carrier. Cell *62*, 107-115.
Söllner T, Rassow J, Wiedemann M, Schlossmann J, Keil P, Neupert W, and Pfanner N (1992). Mapping of the protein import machinery in the mitochondrial outer membrane by crosslinking of translocation intermediates. Nature *355*, 84-87.
Sourkes TL, and Poirier LJ (1965). Influence of the substantia nigra on the concentration of 5-hydroxytryptarnine and dopamine of the striatum. Nature *207*, 202-203.
Speakman JR, Talbot DA, Selman C, Snart S, McLaren JS, Redman P, Krol E, Jackson DM, Johnson MS, and Brand MD (2004). Uncoupled and surviving: individual mice with high metabolism have greater mitochondrial uncoupling and live longer. Aging cell *3*, 87-95.
Spraul CW, Lang GE, and Lang GK (1998). Value of optical coherence tomography in diagnosis of age-related macular degeneration. Correlation of fluorescein angiography and OCT findings. Klinische Monatsblätter für Augenheilkunde *212*, 141-148.
Stanford WL, Cohn JB, and Cordes SP (2001). Gene-trap mutagenesis: past, present and beyond. Nature reviews. Genetics. *2*, 756-768.
Stanley JL, Lincoln RJ, Brown TA, McDonald LM, Dawson GR, and Reynolds DS (2005). The mouse beam walking assay offers improved sensitivity over the mouse rotarod in determining motor coordination deficits induced by benzodiazepines Journal of Psychopharmacology *19*, 221–227.
Steele JC, Richardson JC, and Olszewski J (1964). A heterogeneous degeneration involving the brain stem, basal ganglia and cerebellum with vertical gaze and pseudobulbar palsy, nuchal dystonia and dementia. Archieves of Neurology *10*, 333-359.
Stefansson H, Ophoff RA, Steinberg S, Andreassen OA, Cichon S, Rujescu D, Werge T, Pietiläinen OP, Mors O, Mortensen PB*, et al.* (2009). Common variants conferring risk of schizophrenia. Nature *460*, 744-747.
Steger HF, Söllner T, Kiebler M, Dietmeier KA, Pfaller R, Trülzsch KS, Tropschug M, Neupert W, and Pfanner N (1990). Import of ADP/ATP carrier into mitochondria: two receptors act in parallel. The Journal of Cell Biology *111*, 2353-2363.
Stevens JC, Smith BE, Weaver AL, Bosch EP, Deen HG Jr, and Wilkens JA (1999). Symptoms of 100 patients with electromyographically verified carpal tunnel syndrome. Muscle & Nerve *22*, 1448-1456.
Stirling JW, Coleman M, Thomas A, and Woods AE (1999). Role of transmission electron microscopy in tissue diagnosis: diseases of the kidney, skeletal muscle and myocardium. Journal of Cell Pathology *4*, 223-243.
Suh JH, Heath SH, and Hagen TM (2003). Two subpopulations of mitochondria in the aging rat heart display heterogenous levels of oxidative stress. Free radical biology & medicine *35*, 1064-1072.

Sun M, Hurst LD, Carmichael GG, and Chen J (2006). Evidence for variation in abundance of antisense transcripts between multicellular animals but no relationship between antisense transcriptionand organismic complexity. Genome Research *16*, 922-933.
Suomalainen A (1997). Mitochondrial DNA and disease. Annals of Medicine *29*, 235-246.
Swerdlow NR, Braff DL, Taaid N, and Geyer MA (1994). Assessing the validity of an animal model of deficient sensorimotor gating in schizophrenic patients. Archives of general psychiatry *51*, 139-154.
Swerdlow RH, Parks JK, Cassarino DS, Maguire DJ, Maguire RS, Bennett JP, Davis RE, and Parker WD (1997). Cybrids in Alzheimer's disease: A cellular model of the disease? Neurology *49*, 918-925.
Swerdlow RH, Parks JK, Cassarino DS, Trimmer PA, Miller SW, Maguire DJ, Sheehan JP, Maguire RS, Pattee G, Juel VC*, et al.* (1998). Mitochondria in sporadic amyotrophic lateral sclerosis. Experimental neurology *153*, 135-142.
Tabrizi SJ, Cleeter MW, Xuereb J, Taanman JW, Cooper JM, and Schapira AH (1999). Biochemical abnormalities and excitotoxicity in Huntington's disease brain. Annals of neurology *45*, 25-32.
Takei N, Miyashita A, Tsukie T, Arai H, Asada T, Imagawa M, Shoji M, Higuchi S, Urakami K, Kimura H*, et al.* (2009). Genetic association study on in and around the APOE in late-onset Alzheimer disease in Japanese. Genomics *93*, 441-448.
Tamura Y, Harada Y, Shiota T, Yamano K, Watanabe K, Mihoko Y, Yamamoto H, Sesaki H, and Endo T (2009). Tim23-Tim50 pair coordinates functions of translocators and motor proteins in mitochondrial protein import. The Journal of Cell Biology *184*, 129-141.
Tatsuta T, and Langer T (2008). Quality control of mitochondria: protection against neurodegeneration and ageing. The EMBO Journal *27*, 306-314.
Taylor RD, McHale BJ, and Nargang FE (2003). Characterization of Neurospora crassa Tom40-deficient mutants and effect of specific mutations on Tom40 assembly. The Journal of Biological Chemistry *278*, 765-775.
Thiruchelvam M, Richfield EK, Baggs RB, Tank AW, and Cory-Slechta DA (2000). The nigrostriatal dopaminergic system as a preferential target of repeated exposures to combined paraquat and maneb: implications for Parkinson's disease. The Journal of Neuroscience *20*, 9207-9214.
Toda M, and Abi-Dargham A (2007). Dopamine hypothesis of schizophrenia: making sense of it all. Current psychiatry reports *9*, 329-336.
Triepels RH, Van Den Heuvel LP, Trijbels JM, and JA, S. (2001). Respiratory chain complex I deficiency. American Journal of Medical Genetics (Semin. Med. Genet.) *106*, 37-45.
Tripp ME, Katcher ML, Peters HA, Gilbert EF, Arya S, Hodach RJ, and Shug AL (1981). Systemic carnitine deficiency presenting a familial endocardia1 fibroelastosis. A treatable cardiomyopathy. The New England journal of medicine *305*, 385-390.
Truscott KN, Kovermann P, Geissler A, Merlin A, Meijer M, Driessen AJ, Rassow J, Pfanner N, and Wagner R (2001). A presequence- and voltage-sensitive channel of the mitochondrial preprotein translocase formed by Tim23. Nature Structural & Molecular Biology *8*, 1074-1082.
Turrens JF, and Boveris A (1980). Generation of superoxide anion by the NADH dehydrogenase of bovine heart mitochondria. The Biochemical journal *191*, 421-427.
Tusher VG, Tibshirani R, and Chu G (2001). Significance analysis of microarrays applied to the ionizing radiation response. Proceedings of the National Academy of Sciences of the United States of America *98*, 5116-5121.
Tyynismaa H, and Suomalainen A (2009). Mouse models of mitochondrial DNA defects and their relevance for human disease. EMBO Reports *10*, 137-143.
Tzagoloff A, Byington KH, and MacLennan DH (1968). Studies on the mitochondrial adenosine triphosphatase system. II. The isolation and characterization of an oligomycin-sensitive adenosine triphosphatase from bovine heart mitochondria. Journal of Biological Chemistry *243*, 2405-2412.
Unlü M, Morgan ME, and Minden JS (1997). Difference gel electrophoresis: a single gel method for detecting changes in protein extracts. Electrophoresis *18*, 2071-2077.

Van Dam D, D'Hooge R, Staufenbiel M, Van Ginneken C, Van Meir F, and De Deyn PP (2003). Age-dependent cognitive decline in the APP23 model precedes amyloid deposition. European Journal of Neuroscience *17*, 388-396.
Van Dam D, Vloeberghs E, Abramowski D, Staufenbiel M, and De Deyn PP (2005). APP23 mice as a model of Alzheimer's disease: an example of a transgenic approach to modeling a CNS disorder. CNS spectrums *10*, 207-222.
Van der Meulen JH, Kuipers H, and Drukker J (1991). Relationship between exercise-induced muscle damage and enzyme release in rats. Journal of Applied Physiology *71*, 999-1004.
Velliquette RA, O'Connor T, and Vassar R (2005). Energy inhibition elevates -secretase levels and activity and is potentially amyloidogenic in APP transgenic mice: possible early events in Alzheimer's disease pathogenesis. Journal of Neuroscience *25:* 10874-10883
Verdú E, Butí M, and Navarro X (1996). Functional changes of the peripheral nervous system with aging in the mouse. Neurobiology of Aging *17*, 73-77.
Verniquet F, Gaillard J, Neuburger M, and Douce R (1991). Rapid inactivation of plant aconitase by hydrogen peroxide. The Biochemical journal *276*, 643-648.
Vestweber D, Brunner J, Baker A, and Schatz G (1989). A 42K outer-membrane protein is a component of the yeast mitochondrial protein import site. Nature *341*, 205-209.
Vihko V, Salminen A, and Rantamäki J (1979). Exhaustive exercise, endurance training, and acid hydrolase activity in skeletal muscle. Journal of Applied Physiology *47*, 43-50.
Von Coelln R, Thomas B, Savitt JM, Lim KL, Sasaki M, Hess EJ, Dawson VL, and Dawson TM (2004). Loss of locus coeruleus neurons and reduced startle in parkin null mice. Proceedings of the National Academy of Sciences of the United States of America *101*, 10744-10749.
Von Kölliker (1856). Zeitschrift für wissenschaftliche Zoologie VIII, 311-318.
von Melchner H, Rayburn H, Reddy S, Friedel C, and Ruley HE (1992). Selective disruption of genes expressed in totipotent embryonal stem cells. Genes & Development *6*: 919-927
von Melchner H, and Ruley HE (1989). Identification of cellular promoters by using a retrovirus promoter trap. Journal of Virology *63*.
Waber LJ, Valle D, Neill C, DiMauro S, and Shug A (1982). Camitine deficiency presenting as familial cardiomypathy: a treatable defect in camitine transport. The Journal of pediatrics *101*, 700-705.
Wagman IH, and Lesse H (1952). Maximum conduction velocities of motor fibers of ulnar nerve in human subjects of various ages and sizes. Journal of Neurophysiology *15*, 235-244.
Waizenegger T, Habib SJ, Lech M, Mokranjac D, Paschen SA, Hell K, Neupert W, and **Rapaport D** (2004). Tob38, a novel essential component in the biogenesis of beta-barrel proteins of mitochondria. EMBO reports *5*, 704-709.
Waizenegger T, Schmitt S, Zivkovic J, Neupert W, and Rapaport D (2004b). Mim1, a protein required for the assembly of the TOM complex of mitochondria. EMBO reports *6*.
Walker JE, Arizmendi JM, Dupuis A, Fearnley IM, Finel M, Medd SM, Pilkington SJ, Runswick MJ, and Skehel JM (1992). Sequences of 20 subunits of NADH: ubiquinone oxidoreductase from bovine heart mitochondria. Application of a novel strategy for sequencing proteins using the polymerase chain reaction. Journal of Molecular Biology *226*, 1051-1072.
Walker JE, Skehel JM, and Buchanan SK (1995). Structural analysis of NADH: ubiquinone oxidoreductase from bovine heart mitochondria. Methods in Enzymology *260*, 14-34.
Wallace DC (1994). Mitochondrial DNA sequence variation in human evolutionand disease. PNAS *91*, 8739-8746.
Wallace DC (1999). Mitochondrial Diseases in Man and Mouse. Science *283*, 1482-1488.
Wallace DC, Lott MT, Shoffner JM, and Brown MD (1992). Diseases resulting from mitochondrial DNA point mutations. Journal of inherited metabolic disease. *15*, 472-479.
Wallace DC, Singh G, Lott MT, Hodge JA, Schurr TG, Lezza AM, Elsas 2nd LJ, and Nikoskelainen EK (1988). Mitochondrial DNA mutation associated with Leber's hereditary optic neuropathy. Science *242*, 1427-1430.
Wang J, Wilhelmsson H, Graff C, Li H, Oldfors A, Rustin P, Brüning JC, Kahn CR, Clayton DA, Barsh GS*, et al.* (1999). Dilated cardiomyopathy and atrioventricular conduction blocks

induced by heart-specific inactivation of mitochondrial DNA gene expression. Nature Genetics *21*, 133-137.
Weaver JL, and Broud D (2002). Serial phenotypical analysis of mouse peripheral blood leukocytes. Toxicology Mechanisms and Methods *12*.
Webb C, Gorman MA, Lazarou, M., ,, Ryan MT, and Gulbis JM (2006). Crystal structure of the mitochondrial chaperone Tim9•10 reveals a six-bladed a-propeller. Molecular Cell *21*, 123-133.
Weiss H, and Friedrich T (1991). Redox-linked proton translocation by NADH-ubiquinone reductase (complex I). Journal of Bioenergetics and Biomembranes *23*, 743-754.
Weiss H, Friedrich T, Hofhaus G, and Preis D (1991). The respiratory-chain NADH dehydrogenase (complex I) of mitochondria. European Journal of Biochemistry *197*, 563-576.
Weiss SM, Lightowler S, Stanhope KJ, Kennett GA, and Dourish CT (2000). Measurement of anxiety in transgenic mice. Reviews in the Neurosciences *11*, 59-74.
Wenz T (2011). Mitochondria and PGC-1α in Aging and Age-Associated Diseases. Journal of Aging Research *2011*, 12 pages.
Wiedemann N, Kozjak V, Chacinska A, Schonfisch B, Rospert S, Ryan MT, Pfanner N, and Meisinger C (2003). Machinery for protein sorting and assembly in the mitochondrial outer membrane. Nature *424*, 565-571.
Wiesner RJ, Ruegg JC, and Morano I (1992). Counting target molecules by exponential polymerase chain reaction: copy number of mitochondrial DNA in rat tissues. Biochemical and Biophysical Research Communications *183*, 553-559.
Wiles MV, Vauti F, Otte J, Füchtbauer EM, Ruiz P, Füchtbauer A, Arnold HH, Lehrach H, Metz T, von Melchner H, and Wurst W (2000). Establishment of a gene-trap sequence tag library to generate mutant mice from embryonic stem cells. Nat Genet. *24*, 13-14.
Williams RW (1999). A targeted screen to detect recessive mutations that have quantitative effects. Mammalian Genome *10*, 734-738.
Wittig I, and Schaegger H (2005). Advantages and limitations of clear native polyacrylamide gel electrophoresis. Proteomics *5*, 4338-4346.
Wooley CM, Sher RB, Kale A, Frankel WN, Cox GA, and Seburn KL (2005). Gait analysis detects early changes in transgenic SOD1(G93A) mice. Muscle & Nerve *32*, 43-50.
Wurst W, and Gossler A (2000). Gene trap strategies in ES cells.
Yamaguchi H, Yamazaki T, Ishiguro K, Shoji M, Nakazato Y, and Hirai S (1992). Ultrastructural localization of Alzheimer amyloid beta/A4 protein precursor in the cytoplasm of neurons and senile plaque-associated astrocytes. Acta neuropathologia *85*, 15-22.
Yamamoto H, Esaki M, Kanamori T, Tamura Y, Nishikawa S, and Endo T (2002). Tim50 is a subunit of the TIM23 complex that links protein translocation across the outer and inner mitochondrial membranes. Cell *111*, 519-528.
Yan AS, Keuk K, and San S (2002). A survey of the health effects of Pesticides Survey as part of a farmer field school exercise in Cambodia. In Murphy HH, Summary of farmer health studies Conference on Health Effects of Pesticides (Penang, Malaysia, FAO Programme for Community IPM (CIPM) in Asia).
Yasaka T, Ohya I, Matsumoto J, Shiramizu T, and Sasaguri Y (1981). Acceleration of Lipid Peroxidation in Human Paraquat Poisoning. Archieves of internal medicine *141*, 1169-1171.
Yu CE, Seltman H, Peskind ER, Galloway N, Zhou PX, Rosenthal E, Wijsman EM, Tsuang DW, Devlin B, and Schellenberg GD (2007). Comprehensive analysis of APOE and selected proximate markers for late-onset Alzheimer's disease: patterns of linkage disequilibrium and disease/marker association. Genomics *89*, 655-665.
Zamai L, Falcieri E, Marhefka G, and Viatle M (1996). Supravital exposure to propidium iodide identifies apoptotic cells in the absence of nucleosomal DNA fragmentation. Cytometry *2223*.
Zeevalk GD, Manzino L, Hoppe J, and Sonsalla P (1997). In vivo vulnerability of dopamine neurons to inhibition of energy metabolism. European journal of pharmacology *320*, 111-119.
Zeviani M, and Carelli V (2007). Mitochondrial disorders. Current Opinion in Neurology *20*, 564-571.
Zeviani M, and Di Donato S (2004). Mitochondrial disorders Brain *127*, 2153-2173.

Zhang J, Forkstam C, Engel JA, and Svensson L (2000). Role of dopamine in prepulse inhibition of acoustic startle. Psychopharmacology *149*, 181-188.
Zhang Z, Huang L, Schulmeister VM, Chi YI, Kim KK, Hung LW, Crofts AR, Berry EA, and Kim S-H (1998). Electron transfer by domain movement in cytochrome bc1. Nature *392*, 677-684.
Züchner S, Mersiyanova IV, Muglia M, Bissar-Tadmouri N, Rochelle J, Dadali EL, Zappia M, Nelis E, Patitucci A, Senderek J*, et al.* (2004). Mutations in the mitochondrial GTPase mitofusin 2 cause Charcot-Marie-Tooth neuropathy type 2A. Nature Genetics *36*, 449-451.

8 Appendix

8.1 Clinical chemistry screen – additional data

Table 16: Blood lipid and glucose values of fasted mice.
Data are presented as mean ± standard error of mean.

Parameter	Control (A)		Mutant (B)		A~B	A~B	ANOVA		
	Male	Fe-male	Male	Fe-male	Male	Fe-male	Geno-type	sex	inter.
	(n=9)	(n=10)	(n=10)	(n=10)	*p*	*p*	*p*	*p*	*p*
Choleste-rol [mg/dl]	102.2 ±4.52	88.6 ± 2.67	111.6 ± 3.34	89 ± 2.46	n.s.	n.s.	n.s.	P <0.001	n.s.
HDL-Chol. [mg/dl]	78.4 ±3.93	65.8 ± 2.05	87.5 ± 2.7	68.2 ± 1.96	n.s.	n.s.	p<0.05	P <0.001	n.s.
non-HDL Chol. [mg/dl]	23.8 ±0.97	22.8 ± 0.92	24.1 ± 0.77	20.8 ± 0.66	n.s.	n.s.	n.s.	p<0.05	n.s.
Triglycerides [mg/dl]	135 ± 6.6	106 ± 11.8	123 ± 12.6	85 ± 7.8	n.s.	n.s.	n.s.	p<0.05	n.s.
NEFA [mmol/l]	1.08 ± 0.071	0.84 ± 0.072	0.94 ± 0.068	0.7 ± 0.04	n.s.	n.s.	p<0.05	P <0.001	n.s.
Glycerol [mmol/l]	0.26 ± 0.017	0.27 ± 0.009	0.26 ± 0.012	0.27 ± 0.017	n.s.	n.s.	n.s.	n.s.	n.s.
Glucose [mg/dl]	120.5 ± 4.9	146.8 ± 9	139.1 ± 8.8	155.7 ± 7.3	n.s.	n.s.	n.s.	p<0.01	n.s.

Table 17: Clinical-chemical parameters, 2nd sample.
Data are presented as mean ± standard error of mean.

Parameter	Control (A)		Mutant (B)		A~B	A~B	ANOVA		
	Male	Fe-male	Male	Fe-male	Male	Fe-male	Geno-type	sex	inter.
	(n=10)	(n=10)	(n=10)	(n=9)	*p*	*p*	*p*	*p*	*p*
Calcium [mmol/l]	2.27 ± 0.01	2.24 ± 0.02	2.24 ± 0.02	2.28 ± 0.02	n.s.	n.s.	p=0.073	n.s.	p<0.05
inorg. phos. [mmol/l]	1.38 ± 0.09	1.38 ± 0.14	1.54 ± 0.16	1.2 ± 0.11	n.s.	n.s.	n.s.	n.s.	n.s.
Total Protein [g/dl]	5.26 ± 0.08	5.2 ± 0.09	5.28 ± 0.09	5.07 ± 0.09	n.s.	n.s.	n.s.	n.s.	n.s.
Albumin [g/dl]	2.5 ± 0.033	2.48 ± 0.061	2.4 ± 0.03	2.489 ±0.05	p<0.05	n.s.	n.s.	n.s.	n.s.
Cholesterol [mg/dl]	113.6 ± 3.06	85.6 ± 2.13	106.5 ± 5.21	78.2 ± 4.72	n.s.	n.s.	p=0.070	P <0.001	n.s.
Triglyceri-des [mg/dl]	173 ± 13.4	91 ± 9.9	141 ± 12.5	90 ± 9.2	n.s.	n.s.	n.s.	P <0.001	n.s.
LDH [U/l]	267.5 ±14.19	269.9 ±31.59	247.9 ±13.9	229.8 ±13.9	n.s.	n.s.	n.s.	n.s.	n.s.
ALP [U/l]	90 ± 1.98	125 ± 3.14	98.4 ± 2.9	130.9 ± 4.15	p<0.05	n.s.	p<0.05	P <0.001	n.s.
Glucose [mg/dl]	216.8 ± 6	187.5 ± 13.5	191.5 ± 9	197.1 ± 14.7	p<0.05	n.s.	n.s.	n.s.	n.s.
Transferrin [mg/dl]	135.4 ± 1.1	138.9 ± 1.5	136.1 ± 1.24	136.2 ± 1.63	n.s.	n.s.	n.s.	n.s.	n.s.
Iron [µg/dl]	91.9 ± 3.88	131.8 ±12.01	90.5 ± 3.52	126.4 ± 6.48	n.s.	n.s.	n.s.	P <0.001	n.s.

8.2 Neurology screen – additional data

Table 18: SHIRPA Parameters I: young animals
Statistical analysis: chi-squared test; significance p<0.05

Parameter	*Male*			*Female*			
	Control (n=10)	**Mutant (n=10)**	**p-value**	**Control (n=10)**	**Mutant (n=10)**	**p-value**	**p-value**
Body position							
Inactive	0	0		0	0		
Active	10	10		10	10		
Excessive	0	0	**n.s.**	0	0	**n.s.**	**n.s.**
Tremor							
Absent	10	10		10	10		
Present	0	0	**n.s.**	0	0	**n.s.**	**n.s.**
Palpebral closure							
Eyes open	10	10		10	10		
Eyes closed	0	0	**n.s.**	0	0	**n.s.**	**n.s.**
Lacrimation							
Absent	10	10		10	10		
Present	0	0	**n.s.**	0	0	**n.s.**	**n.s.**
Defecation							
Absent	6	6		5	6		
Present	4	4	**n.s.**	5	4	**n.s.**	**n.s.**
Urination							
Absent	8	5		4	7		
Present	2	5	**n.s.**	6	3	**n.s.**	**n.s.**
Transfer arousal							
Extended freeze	0	0		0	0		
Brief freeze	8	7		9	6		
Immediate movement	2	3	**n.s.**	1	4	**n.s.**	**n.s.**
Gait							
Fluid movement	10	10		10	10		
Lack fluidity	0	0	**n.s.**	0	0	**n.s.**	**n.s.**
Pelvic elevation							
Less than 5mm	2	4		1	1		
More than 5mm	8	6	**n.s.**	9	9	**n.s.**	**n.s.**
Tail elevation							
Dragging	0	0		0	0		
Horizontally extension	0	3		5	2		
Elevated/Straub tail	10	7	**n.s.**	5	8	**n.s.**	**n.s.**
Touch escape							
No response	0	0		0	0		
Response to touch	4	7		7	6		
Flees prior to touch	6	3	**n.s.**	3	4	**n.s.**	**n.s.**
Positional pasivity							
Struggles (held by tail)	10	10		10	10		
No struggle	0	0	**n.s.**	0	0	**n.s.**	**n.s.**
Trunk curl							
Absent	10	10		10	10		
Present	0	0	**n.s.**	0	0	**n.s.**	**n.s.**
Limb grasping							
Absent	10	10		10	10		
Present	0	0	**n.s.**	0	0	**n.s.**	**n.s.**
Pinna reflex							
Present	10	10		10	10		
Absent	0	0	**n.s.**	0	0	**n.s.**	**n.s.**

Table 19: SHIRPA Parameters II: young animals
Statistical analysis: chi-squared test; significance p<0.05

Parameter	*Male*			*Female*			
	Control (n=10)	**Mutant (n=10)**	**p-value**	**Control (n=10)**	**Mutant (n=10)**	**p-value**	**p-value**
Corneal reflex							
Present	10	10		10	10		
Absent	0	0	**n.s.**	0	0	**n.s.**	**n.s.**
Startle response							
None	0	0		1	0		
Preyer reflex	7	6		5	7		
Jumping	3	4	**n.s.**	4	3	**n.s.**	**n.s.**
Contact Righting							
Present	10	10		10	10		
Absent	0	0	**n.s.**	0	0	**n.s.**	**n.s.**
Evidence of biting							
None	4	5		6	5		
Biting	6	5	**n.s.**	4	5	**n.s.**	**n.s.**
Vocalisation							
None	2	4		5	6		
Vocal	8	6	**n.s.**	5	4	**n.s.**	**n.s.**

Table 20: SHIRPA Parameters I: aged animals
Statistical analysis: chi-squared test; significance p<0.05

Parameter	*Male*			*Female*			
	Control (n=19)	**Mutant (n=13)**	**p-value**	**Control (n=17)**	**Mutant (n=24)**	**p-value**	**p-value**
Body position							
Inactive	2	3		4	3		
Active	15	7		13	21		
Excessive	2	3	**n.s.**	0	0	**n.s.**	**n.s.**
Tremor							
Absent	19	13		17	24		
Present	0	0	**n.s.**	0	0	**n.s.**	**n.s.**
Palpebral closure							
Eyes open	19	13		17	24		
Eyes closed	0	0	**n.s.**	0	0	**n.s.**	**n.s.**
Lacrimation							
Absent	19	12		17	23		
Present	0	1	**n.s.**	0	1	**n.s.**	**n.s.**
Defecation							
Absent	3	5		5	11		
Present	16	8	**n.s.**	12	13	**n.s.**	**n.s.**
Urination							
Absent	2	3		0	7		
Present	17	10	**n.s.**	17	17	**n.s.**	**n.s.**
Transfer arousal							
Extended freeze	0	0		0	0		
Brief freeze	18	12		17	24		
Immediate movement	1	1	**n.s.**	0	0	**n.s.**	**n.s.**
Gait							
Fluid movement	17	9		17	24		
Lack fluidity	2	4	**n.s.**	0	0	**n.s.**	**n.s.**
Pelvic elevation							
Less than 5mm	12	11		9	14		
More than 5mm	7	2	**n.s.**	8	10	**n.s.**	**n.s.**

Table 21: SHIRPA Parameters II: aged animals
Statistical analysis: chi-squared test; significance p<0.05

Parameter	*Male*			*Female*			
	Control (n=10)	**Mutant (n=10)**	**p-value**	**Control (n=10)**	**Mutant (n=10)**	**p-value**	**p-value**
Tail elevation							
Dragging	1	0		0	1		
Horizontally extension	8	6		6	11		
Elevated/Straub tail	10	7	**n.s.**	11	12	**n.s.**	**n.s.**
Touch escape							
No response	0	0		0	0		
Response to touch	15	10		17	22		
Flees prior to touch	4	3	**n.s.**	0	2	**n.s.**	**n.s.**
Positional pasivity							
Struggles (held by tail)	19	13		17	24		
No struggle	0	0	**n.s.**	0	0	**n.s.**	**n.s.**
Trunk curl							
Absent	19	13		17	24		
Present	0	0	**n.s.**	0	0	**n.s.**	**n.s.**
Limb grasping							
Absent	19	13		17	24		
Present	0	0	**n.s.**	0	0	**n.s.**	**n.s.**
Pinna reflex							
Absent	19	13		17	24		
Present	0	0	**n.s.**	0	0	**n.s.**	**n.s.**
Corneal reflex							
Present	19	13		17	24		
Absent	0	0	**n.s.**	0	0	**n.s.**	**n.s.**
Startle response							
None	16	13		17	19		
Preyer reflex	3	0		0	2		
Jumping	0	0	**n.s.**	0	3	**n.s.**	**n.s.**
Contact Righting							
Present	19	13		17	24		
Absent	0	0	**n.s.**	0	0	**n.s.**	**n.s.**
Evidence of biting							
None	17	13		17	24		
Biting	2	0	**n.s.**	0	0	**n.s.**	**n.s.**
Vocalisation							
None	14	7		12	17		
Vocals	5	6	**n.s.**	5	7	**n.s.**	**n.s.**

8.3 Cold challenge – metabolic data

Table 22: Metabolic Parameters recorded during the cold challenge experiment
Data are presented as mean ± standard error.

Parameter	*Control*		*Mutants*		2– Way – ANOVA *LM (genotype + sex + BM)			
	Male (n=10)	**Female (n=9)**	**Male (n=10)**	**Female (n=10)**	***P geno***	***P sex***	***P inter***	***P BM***
Bw before [g]	30.5 ± 1.3	23.8 ± 1.8	30.5 ± 2.1	23.2 ± 1.9	n.s.	**<0.001**	n.s.	
Bw after [g]	27.5 ± 1.0	21.5 ± 1.7	27.6 ± 1.9	21.0 ± 1.8	n.s.	**<0.001**	n.s.	
Bw mean [g]	29.0 ± 1.2	22.6 ± 1.7	29.1 ± 2.0	22.1 ± 1.8	n.s.	**<0.001**	n.s.	
Body weight loss [g]	-3.0 ± 0.4	-2.3 ± 0.3	-3.0 ± 0.4	-2.2 ± 0.3	n.s. n.s.	**<0.001** n.s.	n.s. n.s.	**<0.001**
T_{re} **before [°C]**	37.59 ± 0.72	37.41 ± 0.52	37.28 ± 0.73	37.31 ± 0.45	n.s.	n.s.	n.s.	
T_{re} **after [°C]**	31.58 ± 3.00	32.26 ± 3.12	34.03 ± 2.00	32.41 ± 2.55	n.s.	n.s.	n.s.	
T_{re} **loss [°C]**	-6.01 ± 3.03	-5.15 ± 3.11	-3.25 ± 1.95	-4.90 ± 2.77	n.s.	n.s.	n.s.	
***VO_2, mean 30 °C [ml h^{-1}]**	66.97 ± 9.00	59.51 ±13.59	66.46 ± 5.53	59.42 ± 7.97	n.s. n.s.	**<0.05** **<0.05**	n.s. n.s.	**<0.001**
***VO_2, min 30 °C [ml h^{-1}]**	47.53 ± 10.05	41.24 ± 13.39	46.65 ± 7.39	43.46 ± 10.74	n.s. n.s.	n.s. n.s.	n.s. n.s.	**<0.05**
***VO_2, max 30 °C [ml h^{-1}]**	87.11 ± 8.55	79.25 ± 13.91	81.98 ± 5.48	73.96 ± 9.57	n.s. n.s.	**<0.05** **<0.01**	n.s. n.s.	**<0.001**
***(BMR) 30 °C [ml h^{-1}]**	61.04 ± 13.33	52.16 ± 19.63	60.46 ± 10.37	56.76 ± 10.75	n.s. n.s.	n.s. n.s.	n.s. n.s.	**<0.05**
***VO_2 mean 5 °C [ml h^{-1}]**	144.36 ± 7.62	128.78 ± 12.60	153.88 ± 16.98	123.03 ± 11.27	n.s. n.s.	**<0.001** n.s.	n.s. n.s.	**<0.001**
***VO_2, min 5 °C [ml h^{-1}]**	112.89 ± 18.10	103.56 ± 18.90	127.31 ± 20.49	101.47 ± 12.75	n.s. n.s.	**<0.01** n.s.	n.s. n.s.	**<0.001**
***VO_2 max 5 °C [ml h^{-1}]**	184.61 ± 8.57	165.16 ± 10.29	185.49 ± 15.75	154.82 ± 13.88	n.s. n.s.	**<0.001** n.s.	n.s. n.s.	**<0.001**
***RMR 5 °C [ml h^{-1}]**	137.10 ± 16.40	130.94 ± 12.77	148.52 ± 21.18	123.70 ± 14.12	n.s. n.s.	**<0.01** n.s.	n.s. n.s.	n.s
***VO_2 Range at 30 °C**	39.57 ± 9.05	38.01 ± 4.44	35.33 ± 9.51	30.51 ± 11.87	**0.055** n.s.	n.s. n.s.	n.s. n.s.	n.s
***VO_2 Range at 5 °C (min to max) [ml h^{-1}]**	71.72 ± 21.53	61.60 ± 15.10	58.19 ± 11.52	53.35 ± 12.56	**<0.05** **<0.05**	n.s. n.s.	n.s. n.s.	n.s.
VO_2 Capacity [ml h^{-1}]	137.08 ± 15.85	123.91 ± 9.72	138.84 ± 16.82	111.36 ± 19.35	n.s. n.s.	**<0.001** **<0.001**	n.s. n.s.	**<0.05**
RER mean 30 °C	0.83 ± 0.01	0.82 ± 0.02	0.84 ± 0.02	0.83 ± 0.02	n.s.	n.s.	n.s.	
RER mean 5 °C	0.78	0.78	0.78	0.78	n.s.	n.s.	n.s.	
RER during RMR 30 °C	0.83 ± 0.01	0.82 ± 0.02	0.84 ± 0.03	0.83 ± 0.03	n.s.	n.s.	n.s.	
RER during RMR 5 °C	0.78 ± 0.01	0.77 ± 0.01	0.77 ± 0.01	0.77 ± 0.01	n.s.	n.s.	n.s.	

8.4 Paraquat challenge – clinical chemistry data

Table 23: Clinical-chemical parameters, 1st sample.
Data are presented as mean ± standard error of mean.

Parameter	Control (A)		Mutant (B)		A~B	A~B	ANOVA		
	Saline	PQ	Saline	PQ	Sa-line	PQ	Geno-type	treat	inter.
	(n=6)	(n=6)	(n=6)	(n=9)	*p-value*	*p-value*	*p-value*	*p-value*	*p-value*
Sodium [mmol/l]	142 ± 1.003	140.7 ±5.858	142.3 ±0.803	144.4 ±1.192	n.s.	n.s.	n.s.	n.s.	n.s.
Potassium [mmol/l]	4.43 ± 0.803	4.267 ±0.198	4.467 ±0.067	4.467 ±0.115	n.s.	n.s.	n.s.	n.s.	n.s.
Calcium [mmol/l]	2.313 ± 0.02	2.257 ±0.103	2.323 ±0.025	2.356 ±0.024	n.s.	n.s.	n.s.	n.s.	n.s.
Chloride [mmol/l]	108 ± 0.69	104 ± 4.17	108 ± 0.63	108 ± 0.97	n.s.	n.s.	n.s.	n.s.	n.s.
Phosph. [mmol/l]	1.197 ± 0.11	1.283 ±0.168	1.28 ± 0.125	1.382 ±0.104	n.s.	n.s.	n.s.	n.s.	n.s.
TP [g/dl]	5.16 ± 0.07	5.06 ± 0.3	5.32 ± 0.08	5.37 ± 0.06	n.s.	n.s.	n.s.	n.s.	n.s.
Albumin [g/dl]	2.51 ± 0.045	2.493 ± 0.162	2.57 ± 0.074	2.629 ±0.055	n.s.	n.s.	n.s.	n.s.	n.s.
Creatinine [mg/dl]	0.33 ± 0.01	0.31 ± 0.02	0.33 ± 0.01	0.31 ± 0.01	n.s.	n.s.	n.s.	n.s.	n.s.
Urea (HST) [mg/dl]	70.8 ± 3.66	67.6 ± 2.85	55.8± 5.11	72.1 ± 2.58	n.s.	<0.01	0.08	n.s.	<0.05
Cholesterol [mg/dl]	107 ± 4.24	84.7 ± 9.46	106 ± 6.56	91.6 ± 2.17	n.s.	n.s.	n.s.	<0.01	n.s.
Triglyceri-des [mg/dl]	162.1 ±19.55	98.13 ±15.09	131 ± 16.45	111.4 ±9.038	n.s.	n.s.	n.s.	<0.01	n.s.
LDH [U/l]	406.37 ±22.46	344.27 ± 54.45	410.84 ± 40.91	383.1 ± 38.711	n.s.	n.s.	n.s.	n.s.	n.s.
ALT [U/l]	36.7 ± 4.22	28 ± 3.83	48 ± 7.59	38 ± 5.42	n.s.	n.s.	n.s.	n.s.	n.s.
AST [U/l]	54.333 ±4.801	64.667 ±11.333	56.667 ±3.084	73.778 ±11.325	n.s.	n.s.	n.s.	n.s.	n.s.
ALP [U/l]	61.33 ± .333	57 ± 3.89	61 ±4.524	61.78 ± 2.57	n.s.	n.s.	n.s.	n.s.	n.s.
α-Amylase [U/l]	703.58 ± 3.46	596.17 ± 60.05	669.54 ± 27.98	608.26 ± 28.72	n.s.	n.s.	n.s.	<0.05	n.s.
Glucose [mg/dl]	235 ± 17.22	202.7± 21.81	200.5 ±13.38	187.8 ± 13.87	n.s.	n.s.	n.s.	n.s.	n.s.
E-Krea [mg/dl]	0.114 ± .005	0.111 ± 0.011	0.109 ± 0.005	0.118± 0.003	n.s.	n.s.	n.s.	n.s.	n.s.
Transferrin [mg/dl]	155.1 ±1.651	153.967 ±3.705	156.33 ±1.654	157.756 ±1.442	n.s.	n.s.	n.s.	n.s.	n.s.
Iron [µg/dl]	98.67 ± .173	123.7± 12.09	95.13 ± 8.502	114.7 ± 5.487	n.s.	n.s.	n.s.	<0.05	n.s.
HS [mg/dl]	1.653 ±0.078	1.66 ± 0.214	1.66 ± 0.094	1.836 ± 0.071	n.s.	n.s.	n.s.	n.s.	n.s.
CK [U/l]	120 ±27.1	249 ±165	127±24	202 ±78.9	n.s.	n.s.	n.s.	n.s.	n.s.

9 Acknowledgements

First of all, I thank Prof. Martin Hrabě de Angelis, the supervisor of my doctoral thesis, for the opportunity to work in his research facility at the Helmholtz Zentrum München. I also want to thank Prof. Thomas Klopstock, the head of the neurological screen within the German Mouse Clinic, for his support through all of the different problems I had while working on my dissertation and for his faith in my work and my abilities. An additional thank to Prof. Martin Klingenspor who agreed in chairing the examination committee.

I especially want to express my gratitude to Dr. Lore Becker whose support and knowledge was always available to me, whenever I needed and her critical judgment of my work, which helped me to see things from another perspective. Furthermore, I thank all the past and present members of the group who accompanied and supported me during the past four years. Many thanks also to Dr. Alexandra Vernaleken from the vestibular group for her willingness to help me establishing the electrophysiological methods and for the additional ideas and notes concerning my work. Thanks to Eva Kling, who teached me about everything important and necessary right at the beginning of my phD time at the centre. Special thanks to Evelyn Schiller, who helped me a lot establishing the biochemical protocols and for the fruitful discussions. Thanks to Tobias Hopfner and Ingrid Lilliana Vargas Panesso for their practical and theoretical support, ranging from discussing my results to assistance during various experiments.

I want to highlight the importance of the support of our technical assistants Yvonne Sonntag and Waldtraud Stettinger, who did all the background work, the breeding and the routine genotyping, and who also helped phenotyping and challenging the animals. Our work would also be harder - if not impossible – without their assistance.

Of course I am deeply indepted to all my cooperation partners: Dr. Holger Prokisch, Birgit Haberberger, Katharina Danhauser and Anne Löschner from the Genetics of Mitochondrial Disorders/ Institute of Human Genetics; Dr. Julia Calzada-Wack, Dr. Frauke Neff and Elenore Samson from the Institute of Pathology. Thanks to Dr. Thomas Floss and Dr. Claudia Seisenberger from the GGTC. Thanks to Dr. Gerhard Przemeck for helping me isolating embryos at various developmental stages, thanks to Dr. Susan Marshal and her technicians Stefanie Dunst and Stefanie Steegmüller for helping me with the blastocyst isolation, and thanks to Dr. Dominika Peters for her useful advices concerning the blastocyst genotyping. Thanks to Dr. Jan Rozman, Monja Willershäuser and Ann-Elisabeth Schwarz from the metabolic screen. Thanks to Dr. Birgit Rathkolb and Kataryna Micklich for helping us with the clinical chemistry. Thanks to Prof. Jochen Graw and Dr. Oliver Puk from the eye screen. Thanks to Dr. Sabine Hölter-Koch and Dr. Lillian Garrett for doing the behavioural and cognitive analysis of the mouse model. Thanks to Dr. Daniela Vogt-Weisenhorn and Dr. Andreas Hofmann from the Institute of Developmental Genetics, who helped us analysing the brains of the aged mice. Thanks to Dr. Andreas Bender and Lena Bruns from the Department of Neurology/University of Munich. Thanks to Prof. Kaspar Matiasek and Dr. Jéssica Molín from the Chair of Veterinary Medicine, LMU, Munich. Special thanks to our cooperation partners Dr. Ilka Wittig and Valentina Strecker from the University of Frankfurt/Main, who spent a great effort to help us analysing the composition of the respiratory chain.

And to give all those helpful hands a name, who assisted me in various different ways I say thank you to Dr. Helmut Fuchs, Dr. Valerie Gailus-Durner, Dr. Beatrix Naton, Reinhard Seeliger, and Barbara Ferwagner from the GMC management; Dr. Anja Schrewe, Dr. András Frankó, Dr. Susanne Neschen, Melanie Kahle, Dr. Gabriele Möller, Dr. Jerzy Adamski, Dr. Cornelia Prehn, Dr. Christoph Lengger, Dr. Holger Maier, Dr. Karlheinz Schäble, Tonia

Ludwig, Martin Kistler, Nina Schieven, Sandra Hoffmann, Ferdinand Haller, Christian Cohrs, Frank Thiele, the whole team of the GMC and all whom I might have forgotten.

Insbesondere bedanke ich mich bei meinem Freund Clot, meinen Eltern und meiner Schwester Marion sowie meinen Freunden, die mich über all die Jahre tatkräftig unterstützten (besonderer Dank an Anne für ihr immer offenes Ohr und freies Sofa!), mich von der Arbeit auch ablenkten und mir geholfen haben, diesen Weg erfolgreich zu beschreiten.